CRANFIELD UNIVERSITY

JOANNA EWA ZAWADZKA

THE IMPORTANCE OF SPATIAL CONFIGURATION OF URBAN LAND COVER IN GOVERNING THERMAL RESPONSE OF URBAN FORM STRUCTURE AT DESIGN AND MASTERPLAN LEVELS

SCHOOL OF WATER, ENERGY AND ENVIRONMENT

PhD THESIS

PhD

Academic Year: 2014 - 2020

Supervisor: Professor Ron Corstanje

Associate Supervisor: Professor Jim Harris

Sep 2020

CRANFIELD UNIVERSITY

SCHOOL OF WATER, ENERGY AND ENVIRONMENT

PhD Thesis

Academic Year 2014 - 2020

JOANNA EWA ZAWADZKA

The importance of spatial configuration of urban land cover in governing thermal response of urban form structure at design and masterplan levels

Supervisor: Professor Ron Corstanje
Associate Supervisor: Professor Jim Harris
Sep 2020

ABSTRACT

Urban areas worldwide are affected by the urban heat island (UHI) effect whereby towns and cities are warmer than their rural backgrounds, having a negative impact on human health and well-being, energy use, and ecology. Appropriately distributed and spatially configured urban greenspaces can be used to mitigate the UHI, however, their efficacy so far has been investigated from either sparse air temperature measurements, micro-scale model simulations or coarse-resolution remotely sensed land surface temperature (LST), resulting in outcomes specific to particular urban fragments or averaged over areas relevant to masterplan and not urban design level. Additionally, the effect of the non-vegetated portion of land cover (LC) on the capacity of urban greenspaces to alleviate excess heat has largely been ignored. In this work, these gaps are addressed by using fine spatial resolution LST and LC data over the entire extents of three British towns to elucidate the relationship between LST and spatial configuration of urban form, taking into account both the spatial properties of greenspaces and their built-up neighbours. Spatial configuration of urban form was defined by aggregation of individual LC patches, size, elevation, and distance to LC patches of other types. Elucidation of the urban form-LST relationships required downscaling of available coarse resolution imagery with the use of high resolution ancillary data, and sub-division of main LC types into classes with distinct spatial aggregation and thermal properties. Random Forest regression allowed for determination of specific spatial configuration conditions leading to the formation of the hottest and coldest LC patches of a given type and highlighted the importance of neighbouring LC in their formation. Subsequently, the requirement for sophisticated spatial analyses for UHI-mitigating urban design was verified through assessment of the heat mitigation index generated by the InVEST 3.8.7 Urban Cooling model, which performed better at scales relevant to masterplans.

Keywords:

Land surface temperature, downscaling, Landsat 8, Fragstats, LSI, COHESION, PLADJ, InVEST 3.8.7 Urban Cooling model

ACKNOWLEDGEMENTS

First and foremost, big thanks go to my supervisors, Professor Ron Corstanje and Professor Jim A. Harris, for their guidance, support and patience throughout the past six years. I would also like to thank my subject advisor, Dr Anil Graves, and my review committee chair, Dr Ip-Shing Fan, for their additional guidance with respect to this project. Special thanks go to Professor Phil Warren, Dr Karl Evans and Dr Briony Norton, who as part of the F^{3}UES project (Grant Number NE/J015067/1) initiated the idea for mapping temperature within the "Cranfield Triangle" in an ecological context, after which the research acquired a very different direction. Further thanks go to Dr Darren Grafius and Dr Steve Hancock, both associated with the F^{3}UES project, for compiling the very high resolution land cover maps and generating digital elevation models for Bedford, Luton and Milton Keynes, respectively, – two datasets that made this work possible. Much of the results presented in this thesis were derived with the use of the R statistical programming software and I would like to acknowledge all users of various online technical help forums, who remain anonymous, for posting solutions to problems that proved of great assistance to this work.

I would also like to thank all my colleagues from the Centre of Environmental and Agricultural Informatics at Cranfield, who have given me much needed space in the final few months, as well as good company throughout the duration of the project.

Special thanks go to all my friends, based in the UK, Poland, rest of Europe, Asia, Australia, and the Vincent Building, and especially my housemate and friend Dr Leigh Kirkwood as well as my very dear friend Dr Catia Sousa, with her Girls, and a perfect adventure companion, Dr Kate Panikowska, for their patience with my less-sociable self but also for their companionship and encouragement, especially towards the submission date.

I express my great gratitude to my Mom, Dad and Aunts for their hospitability during my visits back home, giving me much needed refuge, as well as encouragement throughout these challenging six years.

Last but not least, this achievement would not have been possible without my University friend, Iwona Kemp, who back in 2006 initiated the idea to study at Cranfield, and my very much loved Grandad, Mieczysław “Jurek” Zawadzki, whose generous support put this idea into practice.

TABLE OF CONTENTS

LIST OF FIGURES

LIST OF TABLES

LIST OF EQUATIONS

LIST OF ABBREVIATIONS

A	Albedo
ANOVA	Analysis of variance
ASTER	Advanced Spaceborne Thermal Emission and Reflection Radiometer
B/b	Buildings
BD	Bedford
BUAEI	Built-up area extraction index
°C	Degrees Celsius
C	Coldest
CC	Cooling capacity
CL	Cluster
CLUMPY	Clumpiness index
CMR	Clay minerals ratio
COH	Cohesion index
COHESION	Cohesion index
CONTIG_MN	Mean of contiguity index
db	Distance to buildings
d_{cool}	Cooling distance of greenspaces
dg	Distance to grass
dp	Distance to paved
DSM	Digital surface model
dt	Distance to trees
dw	Distance to water
ET_0	Potential evapotranspiration
ET_a	Actual evapotranspiration
ETI	Evapotranspiration index
ET_{max}	Maximum evapotranspiration
Exp	Exponential function
FEB	2nd February 2014
FMR	Ferrous minerals ratio
FRAC_MN	Mean of fractal dimension index
G/g	Grass
GA	Area of greenspace
H_S	Hypothesis
H	Hottest
HM	Heat Mitigation
IJI	Interspersion and juxtaposition index
InVEST	Integrated Valuation of Ecosystem Services and Tradeoffs
IOR	Iron oxide ratio
JAN	19th January 2015

JUL	8th July 2013
JUN	6th June 2013
K	Degrees Kelvin
Kc	Crop coefficient
LA	Least aggregated
Landsat	Land Remote-Sensing Satellite
LC	Land cover
LiDAR	Light Detection And Ranging
LSI	Landscape shape index
LST	Land surface temperature
LT	Luton
MA	Most aggregated
MARS	Multivariate Adaptive Regression Splines
M-C	Medium-cold
MD	Median
M-H	Medium-hot
MK	Milton Keynes
MN	Mean
MNMD	Manmade
MODIS	Moderate Resolution Imaging Spectroradiometer
MR	Multiple regression
NA	Not available/applicable
NDBI	Normalised difference built-up index
NDVI	Normalised difference vegetation index
NERC-ARSF	Natural Environment Research Centre Airborne Research Facility
NIR	Near infra-red
NLSI	Normalised landscape shape
ns	Not significant
O	Objective
P/p	Paved
P	Precipitation
PARA_MN	Mean of parameter to area ratio
PLADJ	Percentage of like adjacencies index
r	Correlation coefficient
R^2	Regression coefficient
RA	Extra-terrestrial radiation
RF	Random Forests
RLA	Relatively less aggregated
RMA	Relatively more aggregated
RMSE	Root mean square error
S	Shading by trees

SD	Standard Deviation
SGH	Short trees, tall grass, hedge
SHAPE_MN	Mean of shape index
SUHI	Surface urban heat island
SWIR	Shortwave infra-red
T/t	Trees
T1	Tier 1
T2	Tier 2
T_{avg}	Average daily minimum and maximum air temperature
Tb	Broadleaf trees
Tc	Coniferous trees
TD	Difference between daily maximum and mean daily minimum temperatures
TIR	Thermal infra-red
UHI	Urban heat island
USGS	United States Geological Survey
V	Vegetation
VIS	Visible
W/w	Water
WTR	Water

1 CHAPTER ONE

Introduction

1.1 Background

1.1.1 Overview of the implications and causes of urban heat islands

Urban areas often suffer from the urban heat island (UHI) effect which manifests in air temperature within towns and cities being higher than in their rural surroundings (Oke, 1976). The UHI effect is associated with various negative implications that include human mortality and morbidity (Heaviside, Macintyre and Vardoulakis, 2017; Heaviside, Vardoulakis and Cai, 2016), changes to ecological cycles (Shochat et al., 2006; Yow, 2007), and increased energy demand (Santamouris et al. 2015). Consideration of these impacts is becoming increasingly important due to the progressing urbanisation, with over 68% of global population being forecast to inhabit cities by year 2050 (United Nations, Department of Economic and Social Affairs, 2019), as well as concerns over the climate change-driven increased incidence of heatwaves (Perkins, Alexander and Nairn, 2012; Wouters et al., 2017) that pose particular threats to human survival. There is therefore an urgent need for actions aiming at the mitigation of excess heat within urban areas.

Before mitigation measures of the UHIs are discussed, it is necessary to describe the factors contributing to the warmer thermal responses of towns and cities. The UHIs are phenomena originally conceived as occurring at night when longwave heat fluxes from urban fabric materials, characterised with a high capacity to store heat absorbed from short-wave solar radiation during the day, are released into the atmosphere (Oke, 1988) causing warming of air. In this context, the UHI can be separated into warming of air within the urban canopy layer, i.e. the most immediate layer of air between ground surface and rooftops and the urban boundary layer extending beyond the canopy layer into the atmosphere until urban surface influences are no longer perceptible (Oke, 1976). The urban heat island effect, termed the surface urban heat island (SUHI), relates to the temperature of urban land surface and is associated with the UHI through

modulation of air temperature at the lowest layers of the atmosphere (Voogt and Oke, 2003), however, with differences induced through air advection (Wang, Yao and Shu, 2020), and being more prominent during the day (Roth, Oke and Emery, 1989). Whilst warming of the urban surface and canopy layers is directly concerned with human thermal comfort, increased air temperatures in the boundary layer have broader implications on wind systems and air pollution dispersion, amongst others (Oke, 1995).

The UHI is created due to the radiative fluxes of sensible and latent heat, the former characteristic of the urban built environment and associated with increased air temperatures and the latter – of vegetated surfaces, associated with cooling properties (Lin et al., 2017). The formation and intensity of the UHI effect is governed by complex interactions between multiple factors (Oke et al., 1991) that include decreased long-wave radiation loss from and multiple reflections of short-wave radiation between buildings, increased storage of sensible heat in urban fabric materials, decreased evapotranspiration due to the reduction of vegetation coverage as compared to rural areas, anthropogenic heat sources, and air pollution, with aerosols trapping reflected and re-emitting long-wave radiation towards the surface (Li et al., 2018). The occurrence and intensity of the UHI (Mohajerani et al. 2017; Manoli et al. 2019) are determined by the geographical location that drives specific climatic conditions governing air temperatures, precipitation as well as dominant wind patterns to which a city is exposed to.

1.1.2 UHI quantification

The UHI can be quantified through air temperature measurements, collected either at point locations in cities or over transects (Lin et al., 2019; Schwarz et al., 2012), street- or site-scale computer simulations (Tsoka et al., 2020) or through analysis of remotely captured aerial or satellite land surface temperature (LST) imagery (Voogt and Oke, 2003, 1998), directly related to the SUHI. Air temperature measurements taken at fixed locations within a city allow for long-term, high temporal resolution monitoring within the canopy layer, however, they do not allow for concurrent assessments of all locations within an entire city,

typically due to the sparsity of sampling sites. Transects are helpful in assessments of changes in air temperature across gradients of different urban forms, however, are affected by low spatial coverage and lack of concurrence of measurements (Romero Rodríguez et al., 2020). Model simulations utilise principles of computational fluid dynamics to accurately represent diurnal changes in temperature with considerations of all factors, including air flow, contributing to the formation of specific thermal effects in cities, however, due to substantial computational requirements, their use is limited to micro-scales. LST imagery, on the other hand, offers city-wide coverage, with observations, due to varied spatial resolutions of raster datasets, applicable to a variety of spatial scales explored in urban temperature studies. Despite LST being only indirectly related to air temperature, its use has been widespread in investigations of the SUHI at spatial scales ranging from local to global (Zhou et al., 2018), with a possibility for multi-temporal coverage as well, subject to cloud cover.

1.1.3 UHI mitigation

In the urban planning community, UHI mitigation is largely concerned with regulation of microclimates at the pedestrian or building scales (Erell, 2008; Norton et al., 2015). Whilst pedestrian scales are mostly related to the creation of outdoor spaces providing thermal comfort to humans, building scales focus on measures leading to both thermal comfort and energy conservation in buildings. Multiple typologies of UHI mitigation strategies exist (Gago et al., 2013; Kleerekoper, van Esch and Salcedo, 2012; Nuruzzaman, 2015). For example the typology developed by Aleksandrowicz et al. (2017) distinguishes between measures than can be implemented towards specific features of urban environment, i.e. building envelope, urban landscaping, pavement, and street geometry. Building envelope approaches are intended at reducing the exposure to solar irradiation of buildings through covering them with green roofs or facades as well as use of high-albedo construction materials, reflecting a high proportion of incoming solar radiation to prevent heat absorption. Approaches related to urban landscaping involve introduction of strategically placed trees, green vegetation and water bodies into the landscape, which reduce surface and

ambient temperature through shading, evapotranspiration and evaporation. Interventions related to pavements involve the use of high-albedo or water retentive materials to reduce heat absorption at street level. Street geometry modifications include appropriate street orientation with relation to direction of sunlight to ensure shading, prevailing wind direction for adequate ventilation as well as optimisation of the street canyons' geometry to balance trade-offs between shading, air flow and heat trapping (Oke, 1988). Measures for mitigation of SUHI are largely similar and involve the use of vegetation, irrigation, and albedo reduction (Meng, 2017; Sung, 2013).

1.1.4 Links between urban form and urban thermal environment

UHI mitigation measures point to strong links between urban thermal environment and the way urban space is designed. Appropriate urban design, however, requires that these links are described and quantified. There is a large body of research investigating these relationships (Wu and Ren, 2019), which are often explored from LST imagery and spatial configuration descriptors of urban form derived from land cover (LC) maps. Spatial configuration descriptors used in urban thermal studies often include landscape metrics – indicators of two-dimensional landscape structure describing area, shape, proximity of individual land cover patches, as well as spatial aggregation of land cover classes enclosed within a variously defined space or entire landscapes viewed as composites of all land cover classes pertinent to a given area (McGarigal, 2015; McGarigal and Marks, 1995). Some authors also include the third dimension through specification of feature heights, buildings and trees in particular (Berger et al., 2017).

Given relatively coarse spatial resolution of widely available satellite thermal imagery, ranging from 30-100m for Landsat, 90m for ASTER and 250m for MODIS sensors, studies relating spatial configuration of urban form to LST were carried out over larger and variously defined sub-divisions of land, such as artificially superimposed grids (e.g. Berger et al. 2017; Chen et al. 2014), city districts (e.g. Li et al. 2012), or city functional zones (e.g. Li et al. 2020). Consequently, findings of such studies can only identify trends in thermal effects

of spatial configuration of urban form enclosed within them, relying on its homogeneity to enable recommendations relevant to urban design operating at micro-scales rather than overviews applicable to masterplans. Whilst the broader scale studies have contributed to the wider understanding of the role of urban form, and the size and spatial distribution of urban greenspaces in particular, to (S)UHI mitigation, studies carried out with computer simulations highlighted the importance of the interactions between built-up and greenspaces in excess heat mitigation at scales pertaining to fine-tuning of urban design (Chen and Wong, 2006; Perini et al., 2017; Sodoudi et al., 2018).

There are, however, other methods for assessment of UHI mitigation measures that do not involve sophisticated analyses requiring academic expertise that may not be available to all urban planners (Bherwani, Singh and Kumar, 2020; Norton et al., 2015). Such methods, an example of which is given by the assessment framework developed by Zardo et al. (2017) and recently operationalised in the form of the InVEST Urban Cooling Model (Sharp et al. 2020), use simplified assumptions regarding factors contributing the formation and mitigation of the UHI to arrive at conclusions regarding the cooling capacity of cities, towns or districts characterised with specific spatial arrangement of land cover (Ronchi, Salata and Arcidiacono, 2020). Such approaches, despite being well-grounded in theory, need to be validated, both in terms of accuracy of representation of urban thermal environment as well as operational spatial scale, determining their applicability at various stages of urban planning. Specifically, two stages in urban planning are considered in this project – fine-tuning of urban design, when the size, shape and spatial arrangement of built-up and green features are determined at a site scale, referred to as the micro-scale, or master-planning when decisions regarding strategic locations of various urban structures and functions are made.

1.2 Research question

The overarching research question of this thesis was to determine the feasibility of elucidation of specific conditions of spatial configuration of urban form conducive to the formation of cooler or hotter spaces in towns at micro-

scales, and at the same time, to verify the need for sophisticated spatial analyses of urban thermal environment requiring expertise that is rarely present in the urban planning community. The novelty of the approach taken in this thesis was substantiated in investigation of the relationships between land surface temperature, serving as a proxy for air temperature, and spatial configuration urban form with special focus on thermal response of individual land cover patches rather than larger tracts of land, enabled by the availability of very fine spatial resolution land surface temperature and land cover data. This allowed for the expectation of this project to provide recommendations as to the spatial arrangement of land cover patches contributing to the formation of thermal cold and hot spots within urban areas. Given the large complexity of analyses required to arrive at specific conclusions, the utility of a recent simplified urban cooling model in the context of urban design relevant to thermal comfort at micro-scales was verified, providing the first formal validation of its outputs and insights into the model applicability towards fine-tuning or master planning of urban design.

1.3 Aims and Objectives

The specific hypotheses (HS) and objectives (O) in the context of this thesis were as follows:

HS1: Urban form, through the existence of specific spatial configuration conditions contributing to the formation of cool- and hot spots within urban areas, has the capacity to regulate land surface temperature of individual land cover patches and that capacity is dependent on properties of target and neighbouring land cover patches.

O1-1: Evaluate the performance of multiple adaptive regression spline method and ancillary data in downscaling of coarse resolution land surface temperature imagery to a very fine spatial resolution suitable for microscale temperature studies.

O1-2: Develop a fine-resolution urban land cover typology and evaluate its relevance to urban temperature studies at microscales.

O1-3: Determine and evaluate the zone of influence of urban form on land surface temperature of individual land cover patches.

O1-4: Evaluate the impact of spatial configuration properties of urban form on the formation of the coldest and hottest land cover patches of different types.

O1-5: Evaluate the impact of spatial resolution of land surface temperature imagery on the outcome of temperature regulation studies at microscales.

HS2: Urban form's capacity to regulate land surface temperature of individual LC patches is resilient throughout a warming summer.

O2-1: Evaluate the capacity of spatial configuration of urban form to continuously deliver a regulatory function for land surface temperature of individual land cover patches.

HS3: Simplified urban cooling models can substitute sophisticated spatial analyses in assessment of the land surface temperature regulation capacity of urban form at microscales.

O3-1: Validate the performance of the heat mitigation index generated by the InVEST 3.8.7 Urban Cooling model in estimation of land surface temperature at microscales

O3-2: Evaluate the capacity of the heat mitigation index, generated by the InVEST 3.8.7 Urban Cooling model, to accurately represent land surface temperature of different land cover types at microscales.

Figure 1-1 shows a conceptual diagram representing the hypotheses to be verified as part of this research project.

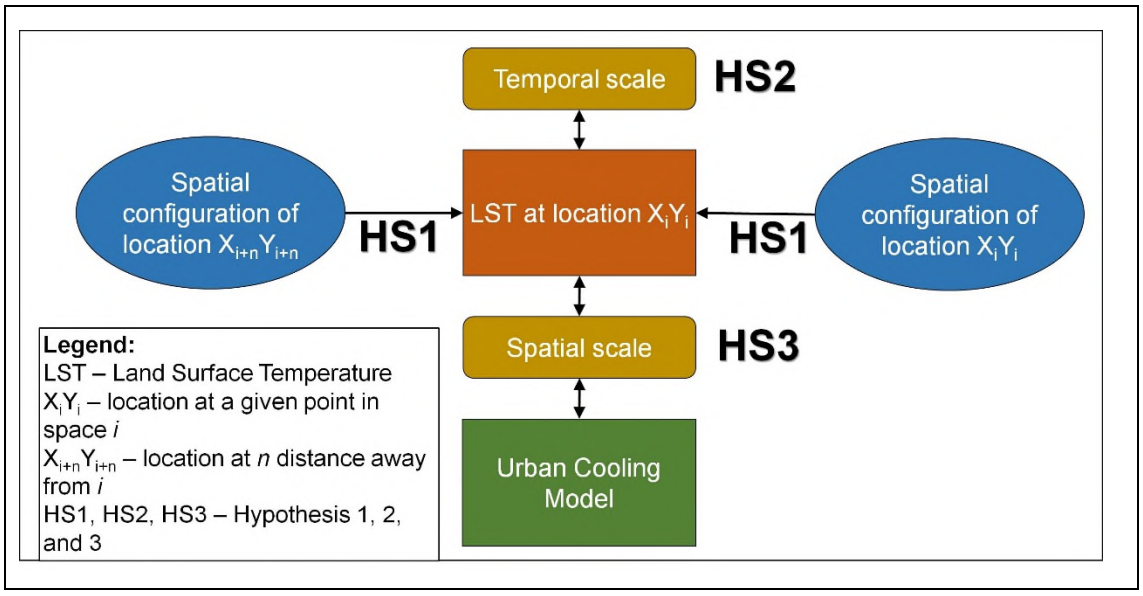

Figure 1-1 Conceptual diagram of the hypotheses posed in this project.

1.4 Thesis structure

The main body of this thesis is formed by a series of four chapters formatted as journal papers, all of which were written by the primary author Joanna E. Zawadzka and edited by thesis supervisors: Professor Ron Corstanje and Professor Jim A. Harris. All technical work was carried out by Joanna Zawadzka with help from Ian Truckell, a geospatial analyst at Cranfield University, whose contributions are acknowledged through a co-authorship on the first journal paper (Chapter 2) presented here. Additional acknowledgments go to Dr Darren Grafius (Cranfield University) and Dr Steven Hancock (University of Exeter), who, through their contributions to the NERC-funded Biodiversity and Ecosystem Service Sustainability programme (Grant Number NE/J015067/1) developed high-resolution land cover and elevation maps, respectively, for the study area, without which research presented in this thesis would not be possible.

The thesis opens with a literature review highlighting key concepts and research gaps needed to be addressed in studies related to urban heat mitigation. Work described in Chapter 2 (published, refer to Table 1-1 for details) of this thesis focused on the development of a new methodology for downscaling coarse-resolution satellite thermal imagery to a very fine resolution relevant to micro-scales presumed in this study. The resultant summertime LST temperature maps

for two time steps a month apart were instrumental to findings presented in the following three chapters of this thesis. This Chapter 3 (published, with comments from three anonymous reviewers incorporated into the text) was dedicated to the sub-division of urban land cover classes into subtypes based on spatial aggregation level and surface temperature of individual land cover patches, resulting in the generation of a new urban land cover typology suitable to urban temperature studies at micro-scales. Its applicability in this context was confirmed in Chapter 4 (paper in preparation) whereby spatial configuration of all land cover types and subtypes were proven to have a an impact on LST of different land covers, with formation of the coldest and hottest patches of each type being associated with different spatial configuration properties of neighbouring patches. Research presented in Chapter 4 offers a city-wide bottom-up perspective on the role of spatial configuration of urban form in excess heat mitigation, appropriate to urban form design at scales relevant to the thermal comfort of individuals indoors and outdoors. Chapter 5 (paper in preparation), on the other hand, presented a top-down view on the matter of urban heat island mitigation through an appropriate urban form design, and highlighted the need for incorporation of non-spatial properties of land cover in studies of urban thermal environment. Here, a user-friendly tool for the quantification of the role of greenspaces in urban heat mitigation was validated through a comparison between the main output of the tool and the available fine and coarse resolution LST data with conclusions pointing to the need for detailed assessments to yield urban design recommendations at scales finer than masterplans. Chapter 6 provides a discussion and implications of the findings presented in Chapters 2 to 5. Chapter 7 summarises the key conclusions and provides recommendations for future research.

Table 1-1 Thesis structure and status of paper submissions with links to specific hypotheses (H) and objectives (O).

Chapter	Paper	Link to H and O	Title	Journal	Status
1	-		Introduction	-	-
2	1	HS1: O1-1	Downscaling Landsat-8 land surface temperature maps in diverse urban landscapes using multivariate adaptive regression splines and very high resolution auxiliary data	International Journal of Digital Earth	International Journal of digital Earth 2020, Vol. 13, no. 8, 899–914 **Received** 28 Aug 2018 **Accepted** 6 Mar 2019
3	2	HS1: O1-2	A simple method for determination of fine resolution urban form patterns with distinct thermal properties using class-level landscape metrics	Landscape Ecology	Landscape Ecology **Received** 28 May 2020 **Accepted** 7 November 2020
4	3	HS1: O1-3, O1-4, O1-5 HS2: O2-1	Unravelling the relationship between land surface temperature of individual land cover patches and spatial configuration of urban form	Landscape Ecology	In preparation
5	4	HS3: O3-1	Assessment of heat mitigation capacity of urban greenspaces with the use of InVEST Urban Cooling model, verified with day-time land surface temperature data	Landscape and Urban Planning	In preparation
6	-		Discussion	-	-
7	-		Conclusions and future work	-	-

1.5 References

Aleksandrowicz, O., Vuckovic, M., Kiesel, K. and Mahdavi, A. (2017) ‘Current trends in urban heat island mitigation research: Observations based on a comprehensive research repository’, *Urban Climate*, 21 Elsevier B.V., pp. 1–26. Available at: 10.1016/j.uclim.2017.04.002 (Accessed: 3 May 2020).

Berger, C., Rosentreter, J., Voltersen, M., Baumgart, C., Schmullius, C. and Hese, S. (2017) ‘Spatio-temporal analysis of the relationship between 2D/3D urban site characteristics and land surface temperature’, *Remote Sensing of Environment*, 193, pp. 225–243. Available at: 10.1016/j.rse.2017.02.020 (Accessed: 6 September 2017).

Bherwani, H., Singh, A. and Kumar, R. (2020) ‘Assessment methods of urban microclimate and its parameters: A critical review to take the research from lab to land’, *Urban Climate*, 34 Elsevier B.V., p. 100690. Available at: 10.1016/j.uclim.2020.100690 (Accessed: 14 September 2020).

Chen, A., Yao, L., Sun, R. and Chen, L. (2014) ‘How many metrics are required to identify the effects of the landscape pattern on land surface temperature?’, *Ecological Indicators*, 45 Elsevier, pp. 424–433. Available at: 10.1016/j.ecolind.2014.05.002 (Accessed: 22 June 2018).

Chen, Y. and Wong, N.H. (2006) ‘Thermal benefits of city parks’, *Energy and Buildings*, 38(2) Elsevier, pp. 105–120. Available at: 10.1016/j.enbuild.2005.04.003 (Accessed: 3 July 2018).

Erell, E. (2008) ‘The Application of Urban Climate Research in the Design of Cities’, *Advances in Building Energy Research*, 2(1), pp. 95–121. Available at: 10.3763/aber.2008.0204 (Accessed: 31 August 2020).

Gago, E.J., Roldan, J., Pacheco-Torres, R. and Ordóñez, J. (2013) ‘The city and urban heat islands: A review of strategies to mitigate adverse effects’, *Renewable and Sustainable Energy Reviews*, 25 Pergamon, pp. 749–758. Available at: 10.1016/j.rser.2013.05.057 (Accessed: 4 September 2020).

Heaviside, C., Macintyre, H. and Vardoulakis, S. (2017) ‘The Urban Heat Island: Implications for Health in a Changing Environment’, *Current Environmental Health Reports*, 4(3) Springer, pp. 296–305. Available at: 10.1007/s40572-017-0150-3 (Accessed: 30 April 2020).

Heaviside, C., Vardoulakis, S. and Cai, X.-M. (2016) ‘Attribution of mortality to the urban heat island during heatwaves in the West Midlands, UK’, *Environmental Health*, 15(S1) BioMed Central Ltd., p. S27. Available at: 10.1186/s12940-016-0100-9 (Accessed: 30 April 2020).

Kleerekoper, L., van Esch, M. and Salcedo, T.B. (2012) ‘How to make a city climate-proof, addressing the urban heat island effect’, *Resources, Conservation and Recycling*, 64 Elsevier B.V., pp. 30–38. Available at: 10.1016/j.resconrec.2011.06.004 (Accessed: 30 April 2020).

Li, H., Meier, F., Lee, X., Chakraborty, T., Liu, J., Schaap, M. and Sodoudi, S. (2018) ‘Interaction between urban heat island and urban pollution island during summer in Berlin’, *Science of the Total Environment*, 636, pp. 818–828. Available at: 10.1016/j.scitotenv.2018.04.254 (Accessed: 24 September 2020).

Li, T., Cao, J., Xu, M., Wu, Q. and Yao, L. (2020) ‘The influence of urban spatial pattern on land surface temperature for different functional zones’, *Landscape and Ecological Engineering*, 16(3) Springer, pp. 249–262. Available at: 10.1007/s11355-020-00417-8 (Accessed: 8 May 2020).

Li, X., Zhou, W., Ouyang, Z., Xu, W. and Zheng, H. (2012) ‘Spatial pattern of greenspace affects land surface temperature: evidence from the heavily urbanized Beijing metropolitan area, China’, *Landscape Ecology*, 27(6), pp. 887–898. Available at: 10.1007/s10980-012-9731-6 (Accessed: 15 March 2016).

Lin, F.-Y., Huang, K.-T., Lin, T.-P. and Hwang, R.-L. (2019) ‘Generating hourly local weather data with high spatially resolution and the applications in bioclimatic performance’, *Science of The Total Environment*, 653 Elsevier B.V., pp. 1262–1271. Available at: 10.1016/j.scitotenv.2018.10.433 (Accessed: 3 May 2020).

Lin, P., Gou, Z., Lau, S. and Qin, H. (2017) ‘The Impact of Urban Design Descriptors on Outdoor Thermal Environment: A Literature Review’, *Energies*, 10(12) MDPI AG, p. 2151. Available at: 10.3390/en10122151 (Accessed: 2 September 2020).

Manoli, G., Fatichi, S., Schläpfer, M., Yu, K., Crowther, T.W., Meili, N., Burlando, P., Katul, G.G. and Bou-Zeid, E. (2019) ‘Magnitude of urban heat islands largely explained by climate and population’, *Nature*, 573(7772) Nature Publishing Group, pp. 55–60. Available at: 10.1038/s41586-019-1512-9 (Accessed: 2 September 2020).

McGarigal, K. (2015) Fragstats help version 4.2 http://www.umass.edu/landeco/research/fragstats/documents/fragstats.help.4.2.pdf, Available at: 10.1016/S0022-3913(12)00047-9 (Accessed: 10 September 2020).

McGarigal, K. and Marks, B.J. (1995) FRAGSTATS: spatial pattern analysis program for quantifying landscape structure. Available at: 10.2737/PNW-GTR-351 (Accessed: 4 May 2020).

Meng, C. (2017) ‘Mitigating the surface urban heat island: Mechanism study and sensitivity analysis’, *Asia-Pacific Journal of Atmospheric Sciences*, 53(3) Korean Meteorological Society, pp. 327–338. Available at: 10.1007/s13143-017-0036-1 (Accessed: 3 September 2020).

Mohajerani, A., Bakaric, J. and Jeffrey-Bailey, T. (2017) ‘The urban heat island effect, its causes, and mitigation, with reference to the thermal properties of asphalt concrete’, *Journal of Environmental Management*, 197 Academic Press, pp. 522–538. Available at: 10.1016/j.jenvman.2017.03.095 (Accessed: 30 April 2020).

Norton, B.A., Coutts, A.M., Livesley, S.J., Harris, R.J., Hunter, A.M. and Williams, N.S.G. (2015) ‘Planning for cooler cities: A framework to prioritise green infrastructure to mitigate high temperatures in urban landscapes’, *Landscape and Urban Planning*, 134 Elsevier, pp. 127–138. Available at: 10.1016/j.landurbplan.2014.10.018 (Accessed: 29 August 2020).

Nuruzzaman, M. (2015) ‘Urban Heat Island: Causes, Effects and Mitigation Measures - A Review’*, International Journal of Environmental Monitoring and Analysis*, 3(2) Science Publishing Group, p. 67. Available at: 10.11648/j.ijema.20150302.15 (Accessed: 31 August 2020).

Oke, T.R. (1976) ‘The distinction between canopy and boundary-layer urban heat islands’, *Atmosphere,* 14(4) Taylor & Francis Group, pp. 268–277. Available at: 10.1080/00046973.1976.9648422 (Accessed: 30 April 2020).

Oke, T.R. (1988) ‘The urban energy balance’, *Progress in Physical Geography*, 12(4) Sage PublicationsSage CA: Thousand Oaks, CA, pp. 471–508. Available at: 10.1177/030913338801200401 (Accessed: 31 August 2020).

Oke, T.R. (1995) ‘The Heat Island of the Urban Boundary Layer: Characteristics, Causes and Effects’, in *Wind Climate in Cities*. Springer Netherlands, pp. 81–107. Available at: 10.1007/978-94-017-3686-2_5 (Accessed: 25 September 2020).

Oke, T.R., Johnson, G.T., Steyn, D.G. and Watson, I.D. (1991) ‘Simulation of surface urban heat islands under “ideal” conditions at night part 2: Diagnosis of causation’, *Boundary-Layer Meteorology*, 56(4) Kluwer Academic Publishers, pp. 339–358. Available at: 10.1007/BF00119211 (Accessed: 29 August 2020).

Perini, K., Chokhachian, A., Dong, S. and Auer, T. (2017) ‘Modeling and simulating urban outdoor comfort: Coupling ENVI-Met and TRNSYS by grasshopper’, *Energy and Buildings*, 152 Elsevier Ltd, pp. 373–384. Available at: 10.1016/j.enbuild.2017.07.061 (Accessed: 7 September 2020).

Perkins, S.E., Alexander, L. V. and Nairn, J.R. (2012) ‘Increasing frequency, intensity and duration of observed global heatwaves and warm spells’, *Geophysical Research Letters*, 39(20) Blackwell Publishing Ltd, p. 2012GL053361. Available at: 10.1029/2012GL053361 (Accessed: 30 April 2020).

Romero Rodríguez, L., Sánchez Ramos, J., Sánchez de la Flor, F.J. and Álvarez Domínguez, S. (2020) ‘Analyzing the urban heat Island: Comprehensive

methodology for data gathering and optimal design of mobile transects', *Sustainable Cities and Society*, 55 Elsevier Ltd, p. 102027. Available at: 10.1016/j.scs.2020.102027 (Accessed: 3 May 2020).

Ronchi, S., Salata, S. and Arcidiacono, A. (2020) 'Which urban design parameters provide climate-proof cities? An application of the Urban Cooling InVEST Model in the city of Milan comparing historical planning morphologies', *Sustainable Cities and Society*, 63, p. 102459.

Roth, M., Oke, T.R. and Emery, W.J. (1989) 'Satellite-derived urban heat islands from three coastal cities and the utilization of such data in urban climatology', *International Journal of Remote Sensing*, 10(11) Taylor & Francis Group , pp. 1699–1720. Available at: 10.1080/01431168908904002 (Accessed: 3 September 2020).

Santamouris, M., Cartalis, C., Synnefa, A. and Kolokotsa, D. (2015) 'On the impact of urban heat island and global warming on the power demand and electricity consumption of buildings—A review', *Energy and Buildings*, 98 Elsevier Ltd, pp. 119–124. Available at: 10.1016/j.enbuild.2014.09.052 (Accessed: 29 August 2020).

Schwarz, N., Schlink, U., Franck, U. and Großmann, K. (2012) 'Relationship of land surface and air temperatures and its implications for quantifying urban heat island indicators - An application for the city of Leipzig (Germany)', *Ecological Indicators*, 18, pp. 693–704. Available at: 10.1016/j.ecolind.2012.01.001 (Accessed: 14 November 2017).

Sharp, R., Douglass, J., Wolny, S., Arkema, K., Bernhardt, J., Bierbower, W., Chaumont, N., Denu, D., Fisher, D., Glowinski, K., Griffin, R., Guannel, G., Guerry, A., Johnson, J., Hamel, P., Kennedy, C., Kim, C.K., Lacayo, M., Lonsdorf, E., Mandle, L., Rogers, L., Silver, J., Toft, J., Verutes, G., Vogl, A. L., Wood, S, and Wyatt, K. 2020, InVEST 3.8.7.post12+ug.gbcad34f User's Guide. The Natural Capital Project, Stanford University, University of Minnesota, The Nature Conservancy, and World Wildlife Fund.

Shochat, E., Warren, P.S., Faeth, S.H., McIntyre, N.E. and Hope, D. (2006) 'From patterns to emerging processes in mechanistic urban ecology', *Trends in Ecology and Evolution*, 21(4) Elsevier, pp. 186–191. Available at: 10.1016/j.tree.2005.11.019 (Accessed: 18 April 2018).

Sodoudi, S., Zhang, H., Chi, X., Müller, F. and Li, H. (2018) 'The influence of spatial configuration of green areas on microclimate and thermal comfort', *Urban Forestry & Urban Greening*, 34 Elsevier GmbH, pp. 85–96. Available at: 10.1016/j.ufug.2018.06.002 (Accessed: 3 May 2020).

Sung, C.Y. (2013) 'Mitigating surface urban heat island by a tree protection policy: A case study of The Woodland, Texas, USA', *Urban Forestry & Urban Greening*, 12(4) Urban & Fischer, pp. 474–480. Available at: 10.1016/j.ufug.2013.05.009 (Accessed: 3 September 2020).

Tsoka, S., Tsikaloudaki, K., Theodosiou, T. and Bikas, D. (2020) 'Urban warming and cities' microclimates: Investigation methods and mitigation strategies—A review', *Energies*, 13(6) MDPI AG, p. 1414. Available at: 10.3390/en13061414 (Accessed: 14 September 2020).

United Nations, Department of Economic and Social Affairs, P.D. (2019) World Urbanization Prospects The 2018 Revision.

Voogt, J.. and Oke, T.. (2003) 'Thermal remote sensing of urban climates', *Remote Sensing of Environment*, 86(3) Elsevier, pp. 370–384. Available at: 10.1016/S0034-4257(03)00079-8 (Accessed: 3 July 2018).

Voogt, J.A. and Oke, T.R. (1998) 'Effects of urban surface geometry on remotely-sensed surface temperature', *International Journal of Remote Sensing*, 19(5) Taylor & Francis Group, pp. 895–920. Available at: 10.1080/014311698215784 (Accessed: 29 August 2020).

Wang, W., Yao, X. and Shu, J. (2020) 'Air advection induced differences between canopy and surface heat islands', *Science of The Total Environment*, 725, p. 138120. Available at: 10.1016/j.scitotenv.2020.138120.

Wouters, H., De Ridder, K., Poelmans, L., Willems, P., Brouwers, J., Hosseinzadehtalaei, P., Tabari, H., Vanden Broucke, S., van Lipzig, N.P.M. and Demuzere, M. (2017) ‘Heat stress increase under climate change twice as large in cities as in rural areas: A study for a densely populated midlatitude maritime region’, *Geophysical Research Letters*, 44(17) Blackwell Publishing Ltd, pp. 8997–9007. Available at: 10.1002/2017GL074889 (Accessed: 30 April 2020).

Wu, Z. and Ren, Y. (2019) ‘A bibliometric review of past trends and future prospects in urban heat island research from 1990 to 2017’, *Environmental Reviews*, 27(2) Canadian Science Publishing, pp. 241–251. Available at: 10.1139/er-2018-0029 (Accessed: 30 April 2020).

Yow, D.M. (2007) ‘Urban Heat Islands: Observations, Impacts, and Adaptation’, *Geography Compass*, 1(6) Wiley, pp. 1227–1251. Available at: 10.1111/j.1749-8198.2007.00063.x (Accessed: 31 August 2020).

Zardo, L., Geneletti, D., Pérez-Soba, M. and Van Eupen, M. (2017) ‘Estimating the cooling capacity of green infrastructures to support urban planning’, *Ecosystem Services*, 26 Elsevier B.V., pp. 225–235. Available at: 10.1016/j.ecoser.2017.06.016 (Accessed: 24 July 2020).

Zhou, D., Xiao, J., Bonafoni, S., Berger, C., Deilami, K., Zhou, Y., Frolking, S., Yao, R., Qiao, Z. and Sobrino, J. (2018) ‘Satellite Remote Sensing of Surface Urban Heat Islands: Progress, Challenges, and Perspectives’, *Remote Sensing*, 11(1) MDPI AG, p. 48. Available at: 10.3390/rs11010048 (Accessed: 14 September 2020).

2 CHAPTER TWO

Downscaling Landsat-8 land surface temperature maps in diverse urban landscapes using multivariate adaptive regression splines and very high resolution auxiliary data.

Joanna Zawadzka[a*], Ron Corstanje[a], Jim Harris[a], Ian Truckell[a]

[a]*Centre for Environmental and Agricultural Informatics, School of Water, Energy and Environment, Cranfield University, Bedfordshire, UK*

[*]joanna.zawadzka@cranfield.ac.uk, Centre for Environmental and Agricultural Informatics, School of Water, Energy and Environment, Cranfield University, Cranfield, Bedfordshire, MK43 0AL, UK

Abstract

We propose a method for spatial downscaling of Landsat-8 derived LST maps from 100(30)m resolution down to 2-4m with the use of the Multiple Adaptive Regression Splines (MARS) models coupled with very high resolution auxiliary data derived from hyperspectral aerial imagery and large-scale topographic maps. We applied the method to four Landsat 8 scenes, two collected in summer and two in winter, for three British towns collectively representing a variety of urban form. We used several spectral indices as well as fractional coverage of water and paved surfaces as LST predictors, and applied a novel method for the correction of temporal mismatch between spectral indices derived from aerial and satellite imagery captured at different dates, allowing for the application of the downscaling method for multiple dates without the need for repeating the aerial survey. Our results suggest that the method performed well for the summer dates, achieving RMSE of 1.40-1.83K prior to and 0.76-1.21K after correction for residuals. We conclude that the MARS models, by addressing the non-linear relationship of LST at coarse and fine spatial resolutions, can be successfully

applied to produce high resolution LST maps suitable for studies of urban thermal environment at local scales.

Keywords: land surface temperature, downscaling, urban, multivariate adaptive regression splines, remote sensing

2.1 Introduction

Urban environments are becoming an increasingly important habitat for humans, with over 68% of global population being forecast to inhabit cities by year 2050 (United Nations, 2019). Urbanisation and associated changes to land cover and urban structure (Oke, 2004) has been linked to significant thermal changes to the environment, termed the urban heat island effect, where the air and surface temperatures of cities are typically much higher than surrounding landscapes (Bornstein, 1968; Pitman et al., 2015), with implications to both ecological status of populations (Shochat et al., 2006) as well as human health and well-being (Kalkstein and Smoyer, 1993; Lee et al., 2003). There is therefore a need for regulation of air temperatures in the cities, and this role can be fulfilled by urban greenspaces, which have been shown to reduce the intensity of urban heat islands subject to appropriate size and configuration in studies relying on coarser-resolution satellite-derived land surface temperature (LST) observations (Asgarian et al., 2015; Kong et al., 2014; Zhou et al., 2017) and studies utilising on-the-ground-measurements of air temperature associated with paved-vegetated area gradient (Schwarz et al., 2012; Takebayashi and Hideki, 2017; Yu and Hien, 2006).

Although the air-temperature studies provide an accurate picture of thermal gradients over the boundary between contrasting urban land covers, these are often limited to a relatively small study area for which air temperatures can be measured simultaneously across its full extent. Remotely sensed LST data offer an alternative to capture data for relatively large areas, however, the spatial resolution of such datasets, typically ranging from 60m to 1km, is insufficient to capture local interactions of LST in relation to the heterogeneous character of land cover in the cities (Lo, Quattrochi and Luvall, 1997). Very high spatial resolution thermal imagery (5-10m or higher) can be acquired from aerial or UAV

surveys, however, these are typically costly, especially for large areas or monitoring purposes, requiring repeated data acquisition.

We propose that the study of interactions between LST and urban form could be enhanced by the implementation of very high spatial resolution LST maps obtained in the process of LST downscaling whereby high resolution LST maps are derived from lower resolution thermal data based on the existing statistical relationship between LST and spectral indices or land cover information (Zhan et al., 2013). As so far, LST downscaling studies carried out for urban areas have targeted relatively coarse spatial resolutions, with final downscaled spatial resolutions comprising 1 km (Weng and Fu, 2014), 480-120m (Bonafoni, 2016), 90m (Yang et al., 2010; Zhan et al., 2012; Yang et al., 2017), 60m (Zhan et al., 2012), 50m (Feng et al., 2015), and 30m (Bonafoni et al., 2016), with downscaling factors, defined as the ratio between the observed and downscaled spatial resolution (Zhou et al., 2016; Bonafoni and Tosi, 2017), rarely exceeding 10m. Only one recent study, Bonafoni and Tosi (2017), attempted the downscaling process to 2m spatial resolution.

In this work, we set out to generate very high resolution LST images (2 to 4m) for urban areas based on the relationship between Landsat 8 coarse resolution LST data and auxiliary data comprising very high resolution spectral indices derived from an aerial survey at 2 and 4m spatial resolution as well as 2m resolution fractional cover of paved and water-covered areas derived from topographic maps, for both summer and winter conditions. Given the complex relationship between LSTs and the auxiliary datasets, and the possibility that simple regression models (e.g. ordinary least squares linear regression) may not be able to reveal the causes of the spatial variation in LST (Weng and Fu, 2014), we decided to test our methodology with the use of the Multiple Adaptive Regression Splines (MARS) capable of fitting different regression functions into different regions of n-dimensional data (Friedman, 1991). As so far, very few environmental studies have used the MARS method to predict spatial distribution of environmental phenomena, limited mostly to the fields of digital soil mapping (Piikki et al. 2015; Piikki and Söderström 2019) and landslide detection (Wang et

al., 2015), and this is the first study known to the authors that uses MARS in LST downscaling. Further novelty of our approach consists in adjustments of spectral indices derived from very high resolution aerial imagery for the values of equivalent spectral indices derived from coarser resolution satellite imagery acquired together with the thermal data – a method aiming at mitigation of the temporal mismatch between acquisition dates of aerial and satellite imagery. Such adjustments can potentially allow for multi-temporal assessments of LST at very high spatial resolution without the need of repeated acquisition of very high resolution multispectral data, limited only by the availability of cloud-free satellite data.

The specific objectives of this study are therefore to (1) present an LST downscaling method at rarely explored spatial resolutions for both summer and winter conditions, (2) suggest a method for enhancing the accuracy of the downscaled maps when there is a temporal mismatch between the acquisition dates of coarse resolution LST data and the fine resolution auxiliary imagery from which scaling factors are derived, facilitating multi-temporal downscaling of the LST maps without the need of re-occurring aerial surveys, and (3) evaluate the potential of Multivariate Adaptive Regression Splines method to accurately downscale LST in urban environments.

We envisage that the resulting very fine resolution LST images could provide much-needed evidence for the relationship between the structure of urban fabric and thermal environment at microscales (Jenerette et al., 2016; Norton et al., 2015; Sanusi et al., 2016), essential for an improved design of urban areas that is set to address challenges imposed by urban expansion, potentially exacerbated by the effects of climate change.

2.2 Materials and methods

2.2.1 Study area

The study area (Figure 2-1) comprises the extents of the hyperspectral aerial imagery available for three English towns: Milton Keynes (MK) (52°0′N, 0°47′W, appr. 122 km^2), Bedford (BD) (52°8′N, 0°27′W, appr. 60 km^2), and Luton/Dunstable (LT) (51°52′N, 0°25′W, appr. 86 km^2), characterised with contrasting histories that influenced collective diversity of urban form within the three towns, making them representative of small- to medium sized British towns' structure. Milton Keynes is a recently designed garden city abundant in parks and greenspaces, characterised by a grid of dual-carriageways dissecting the town into clearly defined neighbourhoods. Bedford is a medieval market town characterised with densely built-up city centre with several parks and residential areas located at the outskirts. Luton, on the other hand, is an industrial-era town characterised with a modern densely built-up city centre and residential areas composed of terraced housing. Further information on land cover in the three towns is available in Grafius et al. (2017, 2016). From climatic perspective, the three towns are located within temperate oceanic climate (Köppen–Geiger climate classification system) with the highest monthly average air temperatures of approximately 22 °C in July and lowest temperatures of approximately 1 °C observed in February, and the average annual precipitation of 597.6, 657.4 , and 712.3 mm for BD, MK and LT respectively.

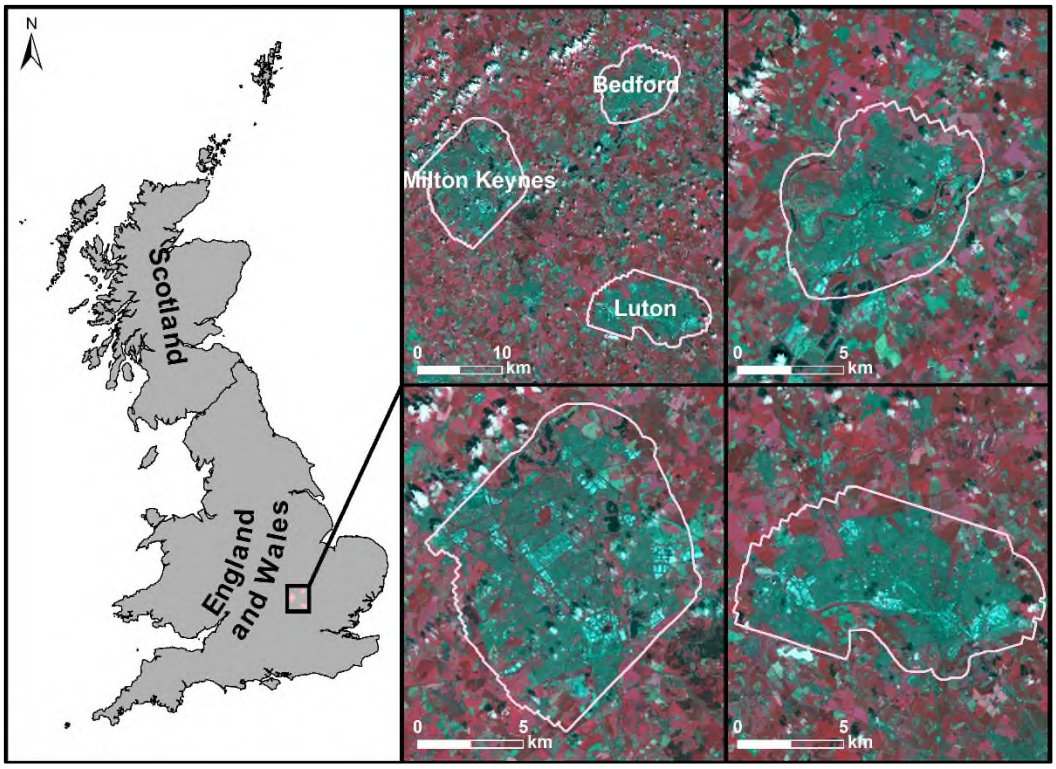

Figure 2-1 Location of the study area displayed over a backdrop of the NIR-Red-Green band composite image of the Landsat 8 dataset acquired on 8 Jul 2013. The outlines shown correspond to the extent of the high-resolution hyperspectral aerial imagery available for the three towns limiting the area to which the downscaling procedure could be applied. Bedford, Luton and Milton Keynes close-ups are shown to scale.

2.2.2 Data used in LST mapping and downscaling

LST maps at medium spatial resolution were derived from TIR bands of Landsat 8 scenes (WRS path 202 row 24) comprising Milton Keynes, Bedford and Luton, acquired from USGS Earth Explorer for two winter and two summer dates (Table 2-1), which allowed for testing of the downscaling methodology under various thermal and phenological conditions. Selection of the dates was restricted by the availability of cloudless images for all three towns captured in a single scene. Total atmospheric water content required for the conversion of the thermal bands of satellite imagery to land surface temperature was estimated from the Near Infrared Total Precipitable Water Vapour Test Result (MOD05_L2) dataset derived from Terra MODIS satellite at 1km spatial resolution (Table Apx A-1).

Emissivity values required for the conversion of thermal radiances to land surface temperature were estimated from the MODIS UCSB Emissivity Library that stores emissivity values of common land cover materials for a high range of spectral bands. LST downscaling was carried out based on high resolution auxiliary datasets, referred here to as LST predictors, acquired from two different sources. Firstly, hyperspectral aerial imagery covering the visible (VIS), near infrared (NIR) and short wave (SWIR) infrared spectra was acquired in July and September 2012 with the Eagle (253 bands in the range of 0.4–1 µm) and Hawk (233 bands in the range of 1–2.5 µm) sensors mounted on the NERC Airborne Research and Survey Facility (ARSF) Data Analysis Node airplane. Spatial resolutions of the data ranged from 2m for the Eagle (4m in Luton) and 4m for the Hawk sensors. Secondly, the Ordnance Survey MasterMap topographic map was used to map the locations of paved urban surfaces and buildings as well as surface water within the three towns at 2m spatial resolution.

Table 2-1 Spatial datasets used in land surface temperature mapping and downscaling for Milton Keynes, Bedford and Luton.

Dataset	Spatial coverage	Date of acquisition	Time of acquisition	Spatial resolution
Hyperspectral aerial imagery	Milton Keynes	24 Jul 2012	14:00–16:03	2 m VIS and NIR (BD and MK)
		26 Jul 2012	09:39–11:52	
	Luton	05 Sep 2012	10:47–12:19	4m VIS and NIR (LT)
	Bedford	06 Sep 2012	13:18–15:43	4 m SWIR
Landsat 8	Milton Keynes, Bedford and Luton	06 Jun 2013	11:00	30m VIS-NIR-SWIR 30 (100) m TIR
		08 Jul 2013	11:00	
		02 Feb 2014	10:59	
		19 Jan 2015	10:58	
MODIS NIR water vapour (MOD05_L2)	Milton Keynes, Bedford, Luton	06 Jun 2013	12:00	1 km
		08 Jul 2013	12:00	
		02 Feb 2014	12:00	
		19 Jan 2015	12:05	
OS MasterMap	Milton Keynes, Bedford, Luton	2006	Not applicable	1:1,250– 1:10,000 scale

2.2.3 Methodology for land surface temperature mapping at medium spatial resolution

Availability of two TIR bands in Landsat-8 imagery allowed for the implementation of the split window algorithm as described in Jimenez-Munoz et al. (2014) to this case study (Figure 2-2). Emissivity for bands 10 and 11 of Landsat 8 sensor was

estimated with the simplified NDVI thresholds method, as presented in Sobrino et al. (2008), with a modification to allow for the assignment of emissivity values for pixels occupied by water as well as built-up areas rather than soil (refer to Section 1 in Appendix A for the detailed description of the undertaken approach).

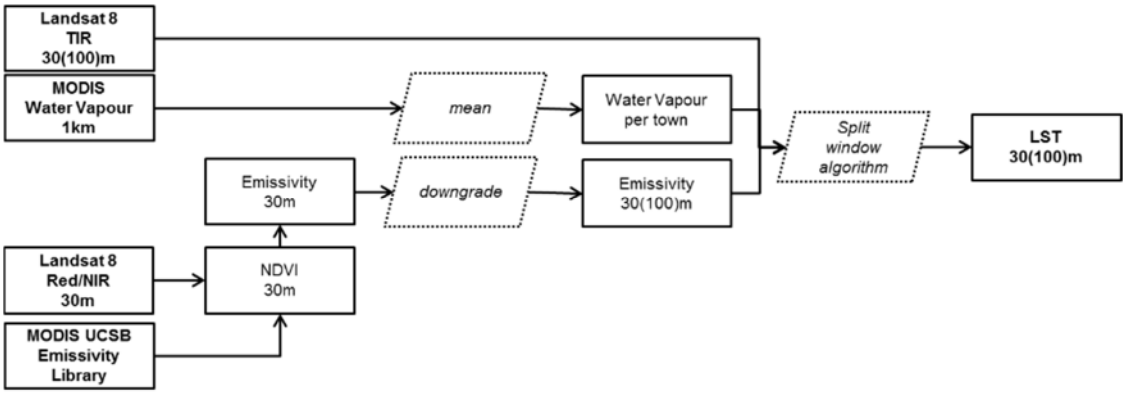

Figure 2-2 Schematic of LST mapping from satellite imagery implemented in this study for each town and date of Landsat 8 images.

2.2.4 Methodology for land surface temperature downscaling

2.2.4.1 Preparation of LST predictors

2.2.4.1.1 Spectral indices

We selected several spectral indices describing the distribution of paved vs vegetated areas (NDVI, NDBI, BUAEI) as well as type of surface materials (CMR, FMR, IOR) potentially distinguishing between built-up areas and bare soil (Table Apx A-2) as proxies for the distribution of LST values across our three towns, and derived them both from satellite and the hyperspectral aerial imagery available for the three towns. For consistency with the satellite data, pixel values of the multiple hyperspectral bands of the aerial imagery equivalent to the spectral ranges of individual bands in the Landsat 8 data were summed prior to the calculations of spectral indices.

As a result of different acquisition dates, there was a temporal mismatch, both in terms of months and years, between the Landsat 8-derived LST maps and spectral indices derived from the very high resolution aerial imagery, which we

considered as a potential limiting factor for the accuracy of our downscaled maps, especially important for the winter scenes, due to different ground conditions in terms of vegetation development stages and paved area extent. We therefore devised a procedure whereby the spectral indices derived from aerial imagery were adjusted to the values of equivalent Landsat-8 indices for each date and town, addressing the differences in spectral indices due to the different phenological stages of vegetation in different seasons of the year represented by the satellite imagery.

The adjusting procedure for the very high resolution spectral indices was similar to the regression kriging method (model B in Odeh et al. (1995)) whereby (1) the aerial-based spectral indices were aggregated to the spatial resolution of corresponding Landsat 8-based indices (30m) with the use of a mean function within corresponding 30x30m blocks of pixels, (2) differences, i.e. residuals, between the Landsat 8-based indices and aggregated aerial-based indices were calculated, (3) the residuals were kriged with the ordinary kriging method (Cressie, 1988) and saved as raster layers at a spatial resolution of the aerial imagery-based indices (2m), and (4) the kriged residuals were added to the aerial imagery-based indices at their native very high resolution. Kriging of the residuals ensured the distribution of the differences in spectral indices values was based on their spatial dependency, avoiding the introduction of box-shaped artefacts sourced from the Landsat 8-derived spectral indices (Mukherjee, Joshi and Garg, 2015a), whilst retaining the expected “crisp” character of the indices at the higher resolution, provided that the variogram parameters (nugget, sill and range) were set to minimise the error of the fitted model. The adjusting procedure was applied individually for each index, town and date, yielding 24 (6 indices x 4 dates) raster maps for each town. Since the kriged residual layer was saved at 2m resolution, any indices that included SWIR wavebands captured at 4m resolution by the Hawk sensor, acquired an intermediary resolution of 2 to 4m. The performance of the adjusting procedure was evaluated based on the comparison of correlation coefficients derived between pairs of Landsat 8-derived spectral indices and the upscaled to 30m resolution (mean of very high resolution pixels within

corresponding 30m pixels) adjusted or original (unadjusted) spectral indices sourced from the aerial imagery.

2.2.4.1.2 Maps of water and manmade surfaces

Manmade and water percent cover raster maps at a 2m spatial resolution were derived from the OS MasterMap topographic maps available in a vector format for the three towns. The generation of these maps involved a series of GIS operations whereby the percentage coverage of land cover classes generally perceived as impervious (buildings, roads, paths, railways and structures) or as water (inland water) were calculated within 2x2m polygons corresponding to pixel locations in the aerial hyperspectral imagery, and subsequently converted to raster maps representing the percentages at the scale of 0 to 1. This method of map production, as opposed to a simpler method of vector to raster conversion, ensured accountability for mixed pixels as well as continuity of narrow linear features such as paths, narrow roads and streams.

2.2.4.2 Land surface temperature downscaling using regression methods

In our downscaling methodology, we assessed the performance of multivariate regression adaptive splines (MARS), to produce LST maps at high spatial resolution (2-4m) from LST maps at medium (30(100)m) spatial resolution. We refer to the medium resolution as 30(100)m due to the fact that the Landsat 8 TIR bands used to map LST in this study are captured at 100m resolution and are subsequently resampled to 30m by data supplier with the bilinear convolution method to match the resolution of the remaining spectral bands. The downscaling procedure comprised three stages: (1) model development (Figure 2-3), (2) model deployment and downscaled map generation, and (3) post-processing of the downscaled maps.

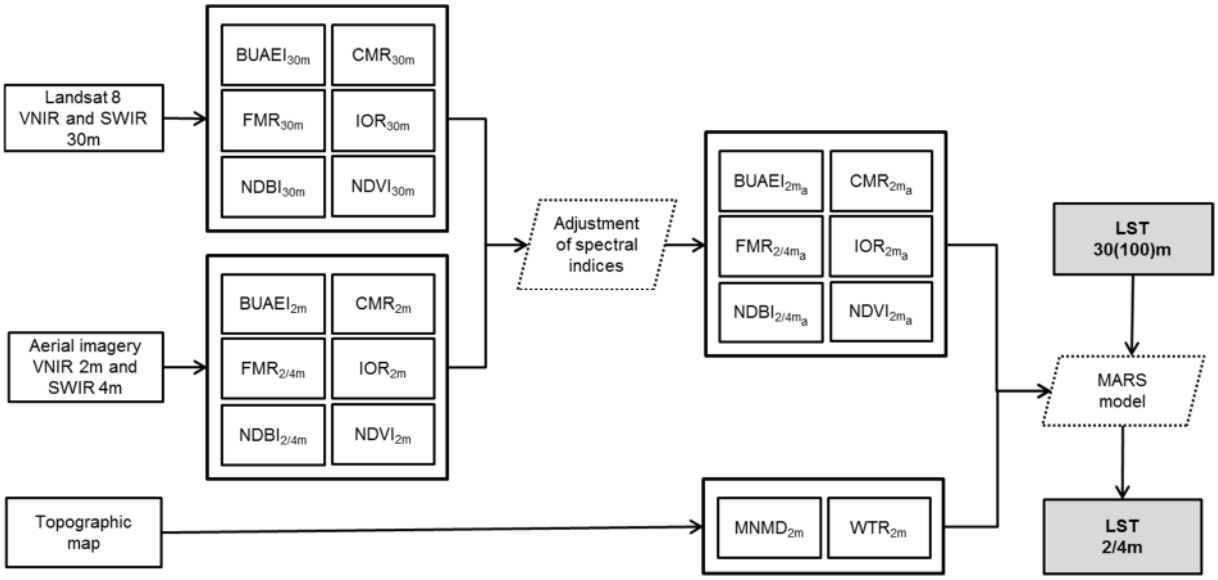

Figure 2-3 Schematic of the LST downscaling model.

In the first stage, model development, the relationship $f()_{MARS}$ between $LST_{30(100)m}$ and LST scaling factors were established MARS regression methods (Equation 2-1). Models for the two summer and two winter dates were implemented in the Statistica 64 software separately for each town. It has to be noted that we used all data pixels to develop the models, which increased the processing time to up to several days per town on a 64GB RAM 12 Core-processor PC. The processing time was increased due to the fact that very high resolution, rather than upscaled to the LST data resolution, ancillary datasets were used in model development, which constitutes a marked methodological difference to numerous published methods (Kustas et al. (2003); Agam et al. (2007); Mukherjee et al. (2014); Bonafoni et al. (2016)).

Equation 2-1

$$LST_{30(100)m} = f_{MARS}(BUAEI_{2/4m_a}, CMR_{2/4m_a}, FMR_{2/4m_a}, IOR_{2m_a}, MNMD_{2m}, NDBI_{2/4m_a}, NDVI_{2m_a}, WTR_{2m})$$

, where:

$LST_{30(100)m}$ – Landsat 8-derived land surface temperature at its native coarse spatial resolution,

$BUAEI_{2/4ma}$ – built-up area extraction spectral index at 2/4m spatial resolution,

$CMR_{2/4ma}$ – clay minerals ratio spectral index at 2-4m spatial resolution,

$FMR_{2/4ma}$ – ferrous minerals spectral ratio index at 2-4m spatial resolution,

$IOR_{2/4ma}$ – iron oxide ratio spectral index at 2-4m spatial resolution,

$MNMD_{2m}$ – percentage of impervious “manmade” surfaces within a 2m resolution pixel,

$NDBI_{2/4ma}$ – normalised difference built-up spectral index at 2-4m spatial resolution,

$NDVI_{2ma}$ – normalised difference vegetation spectral index at 2m spatial resolution,

WTR_{2m} – percentage of water within a 2m resolution pixel.

All the above spectral indices at 2 or 2 to 4 m spatial resolution were extracted from hyperspectral aerial imagery and adjusted for on-the-ground conditions at dates of interest adding the kriged difference between these and equivalent Landsat8-derived indices.

In the second stage, model deployment and map generation, the downscaled $\widehat{\mathrm{LST}}_{\mathrm{MARS2/4ma}}$ values were predicted in Statistica Software using equations listed in Appendix A Tables A-4 – Apx A-6 and mapped as 2m resolution raster maps, using the ‘raster’ and ‘sp’ packages in R software.

In the post-processing stage, the core $\widehat{\boldsymbol{LST}}_{\mathbf{MARS2/4}\boldsymbol{ma}}$ downscaled maps were adjusted for residuals $\Delta\boldsymbol{LST}_{\mathbf{30(100)}\boldsymbol{m}}$ calculated between the Landsat 8 derived maps $\boldsymbol{LST}_{\mathbf{30(100)}\boldsymbol{m}}$ and upscaled predicted maps $\widehat{\boldsymbol{LST}}_{\mathbf{30(100)}\boldsymbol{m}}$ to match the spatial resolution of the Landsat 8 – derived LST maps, to generate the $\widehat{\boldsymbol{LST}'}_{\mathbf{MARS2/4}\boldsymbol{m}}$ map (Equation 2-2 and 2-3).

Equation 2-2

$$\Delta\mathrm{LST}_{30(100)\mathrm{m}} = \mathrm{LST}_{30(100)\mathrm{m}} - \widehat{\mathrm{LST}}_{30(100)\mathrm{m}}$$

Equation 2-3

$$\widehat{LST}'_{\mathrm{MARS2/4}m} = \widehat{LST}_{\mathrm{MARS2/4}m} + \Delta LST_{30(100)m}$$

The predicted $\widehat{LST}_{\mathrm{MARS2/4}m}$ maps were upscaled to $\widehat{LST}_{30(100)m}$ by first resampling to 100m spatial resolution at which the Landsat 8 TIR data are captured, and subsequently resampling to 30m resolution to generate $\widehat{LST}_{30(100)m}$ using the bilinear convolution method, consistent with the resampling method of the TIR bands carried out by the Landsat 8 data provider. These $\widehat{LST}_{30(100)m}$maps were then resampled to 2m spatial resolution with the nearest neighbour method, which maintained the pixel values at 30m spatial resolution, to enable the calculation presented in Equation 2-3.

For method comparison purposes, we also developed MARS models using scaling factors at 30m spatial resolution, and multiple regression (MR) models developed with very high resolution scaling factors that were or were not adjusted for the temporal mismatch between acquisition dates of aerial and satellite imagery.

2.2.5 Verification of the results

Due to the unavailability of alternative land surface temperature datasets, other than the Landsat 8-derived LST maps, that could have been used to independently validate the downscaled LST maps, the performance of the MARS models was verified by the adjusted R squared metric returned at the stage of model development as well as the calculation of the root mean square error (RMSE) between the Landsat 8-derived and downscaled maps. RMSE was calculated in two modes. Firstly, $\mathrm{RMSE}_{2/4\mathrm{m}}$ was calculated from differences between the observed $LST_{30(100)m}$, resampled to 2m spatial resolution with the nearest neighbour method to enable the calculations presented in equations 2-4 and 2-5, and downscaled maps $\widehat{LST}_{\mathrm{MARS2/4}m}$ (Equation 2-4).

Equation 2-4

$$RMSE_{2/4m} = \sqrt{\frac{1}{N}\sum_{i=1}^{N}(LST_{30(100)m} - \widehat{LST}_{\mathrm{MARS2/4}m})^2}$$

Secondly, $RMSE'_{2/4m}$ was calculated as a comparison between the Landsat 8-derived maps and downscaled and adjusted for residuals ($\Delta LST_{30(100)m}$) maps $\widehat{LST'}_{\mathrm{MARS2/4}m}$ (Equation 2-5).

Equation 2-5

$$RMSE'_{2/4m} = \sqrt{\frac{1}{N}\sum_{i=1}^{N}(LST_{30(100)m} - \widehat{LST'}_{\mathrm{MARS2/4}m})^2}$$

2.3 Results and analysis

2.3.1 LST predictors

Prior to inclusion in the LST downscaling models, spectral indices derived from hyperspectral imagery at 2 to 4 m spatial resolution were adjusted for the values of equivalent spectral indices derived from available satellite images to correct for temporal mismatch caused by different years and seasons of data acquisition. We analysed correlation coefficients calculated between pairs of the satellite-derived indices and the aggregated adjusted or original spectral indices derived from the very high resolution hyperspectral data to find that the adjusting procedure was highly successful achieving correlation coefficients as high as 0.80-0.99 for multiple spectral indices, especially in the summer (Table Apx A-3), with some improvement observed in winter. Scatterplots constructed between pairs of equivalent Landsat 8 and aerial imagery-derived spectral indices, both before and after application of the adjustment procedure (Figures Apx A1-4), confirm that in many cases, and especially for the summer dates, the ranges of values of the latter set of indices were satisfactorily matched to the ranges of the satellite-derived indices, achieving a nearly one-to-one relationship in the case of IOR, FMR and NDBI, with NDVI achieving strong, albeit slightly weaker, agreement. The improved predictive power of the adjusted spectral indices was confirmed by adjusted R^2 values obtained by multiple regression models

constructed with both adjusted and non-adjusted spectral indices, which doubled from circa 0.35 to 0.6-0.8 for summer conditions (Figure Apx A-5).

The importance of all predictors in the MARS LST downscaling models was indicated by the frequency of use of each predictor in the basic functions forming model equations (Table Apx A-4) in $MARS_{2/4ma}$ models. All input predictors were consistently used 0 to 5 times in each model developed for each town and each date considered, which highlighted the importance of consideration of multiple predictors in LST downscaling models as each factor may carry useful information in different areas of the data feature space.

2.3.2 Performance of LST downscaling models

The performance of $MARS_{2/4ma}$ models used to downscale LST from a medium spatial resolution (100(30)m) to very high spatial resolution (2 to 4m) was assessed by the adjusted R^2 metric returned by the models at the model development stage as well as root mean square errors calculated between the downscaled and observed values. Adjusted R^2 values (Figure Apx A-5) reveal that models developed for summer months had a stronger predictive power than models developed for winter months, with the adjusted R^2 ranging between 0.64 to 0.84 for summer and 0.06 to 0.21 for winter, depending on town and date. In the summer, the highest model performance was obtained for Luton, for which the effective spatial resolution of all high resolution spectral indices was 4m, which decreased the scale effect between the observed and target resolutions (Zhou et al., 2016) from 50 to 25. Otherwise, it could be assumed that the $MARS_{2/4ma}$ models can explain 65 to 70% of the variance in LST when the majority of predictors is derived at 2m resolution. Poor model performance in winter, however, could be explained by lower dependence of LST on the differences in land cover due to reduced development of foliage as well as potential importance of anthropogenic sources of heat, such as heating of buildings, that were not captured by spectral response of imagery in visible to shortwave infrared regions of the light spectra, from which the spectral indices used in this study were derived. The satellite-derived LST images for the winter dates were also affected by striping, caused by the stray light error of the Landsat

8 thermal bands (Montanaro et al., 2014), and these artefacts likely weakened the relationship between LST and LST predictors used in this study, making the model performance results obtained for winter inconclusive.

Root mean square errors (RMSE) calculated for the unprocessed downscaled maps (Table 2-2) confirmed the observations based on the adjusted R^2 values that, in the summer, $MARS_{2/4ma}$ models had the highest performance, and that adjusting procedure of the high-resolution spectral indices for the values of equivalent satellite-derived indices to correct for the temporal mismatch between collection dates of the aerial and satellite imagery was highly effective in enhancing the accuracy of the downscaled LST maps, yielding an improvement in the range of 0.62 to 1.27K depending on town and date. In winter, the RMSE ranged between 0.44-0.63K across all three towns and did not vary with the modelling approach, confirming poor predictive power of these models.

Table 2-2 RMSE calculated for the pairs of observed and downscaled LST values: A) unprocessed downscaled maps obtained with the $MARS_{2/4ma}$ models and B) downscaled maps obtained with the $MARS_{2/4ma}$ models with added residuals. The Ratio columns specify the value of the ratio calculated between the RMSE and standard deviation of the observed LST values for each town and date.

A	Unprocessed downscaled maps					
Town	Bedford		Luton		Milton Keynes	
Method	MARSadj	Ratio	MARSadj	Ratio	MARSadj	Ratio
FEB	0.44	0.88	0.52	1.04	0.57	0.95
JAN	0.45	0.90	0.61	1.02	0.62	1.03
JUN	1.83	0.52	1.44	0.42	1.78	0.59
JUL	1.72	0.59	1.40	0.39	1.54	0.59

B	Downscaled maps adjusted for residuals					
Town	Bedford		Luton		Milton Keynes	
Method	MARSadj	Ratio	MARSadj	Ratio	MARSadj	Ratio
FEB	0.13	0.26	0.08	0.16	0.13	0.22
JAN	0.07	0.14	0.17	0.28	0.09	0.15
JUN	1.21	0.35	0.76	0.22	1.08	0.36
JUL	1.18	0.41	0.84	0.23	0.96	0.37

Interpretation of the RMSE values can be facilitated by comparison of ratios between RMSE and standard derivation of reference LST data (in our case the

satellite-derived LST), for which values close to 1 indicate low model performance (Bonafoni and Tosi, 2017). These confirmed low model performance for winter images, and indicated that models derived for summer had fair performance. After correction for the residuals, both the RMSE and the RMSE to LST standard deviation ratios dropped considerably, especially for winter images. In the summer, a degree of error persisted somewhat even after the correction, indicating that the downscaling approach did not capture all of the underlying variability of LST at the very high resolution.

Further insight into the performance of the downscaling models is offered by LST density plots (Figure Apx A-6) that allow for comparisons of the distributions of the observed and modelled LST values across the entire range of possible values. These plots indicated that the RMSE values in the unprocessed $MARS_{2/4ma}$ maps derived for summer are largely driven by misrepresentation of the extreme observed LST values and that this method yielded good resemblance of the distributions of the most frequent values in the observed LST images. These plots also confirmed the superiority of the $MARS_{2/4ma}$ method over multiple regression models, derived with the same set of LST predictors, which misrepresented the distribution of both the mid-range and extreme LST values, as well as the importance of the correction of temporal mismatch between the capture dates of the aerial and satellite imagery affecting the fine resolution spectral indices used in LST downscaling. The plots also confirmed that all models derived for winter predicted values close to the mean of observed LST values and did not capture the range of variation in the observed LST.

2.3.3 LST mapping at medium and very high spatial resolution

Visual assessment of the downscaled maps (Figure 2-4Figure 2-5) reveals that the main LST patterns as seen in the satellite-derived images were well reflected in the downscaled images, especially in the summer, and that these corresponded well with the locations of the main types of land cover, with vegetated areas being typically cooler than paved. In winter, the LST variation of the downscaled maps did not match the observed patterns just as well and only major differences due to the occurrence of water bodies or built-up areas were

marked in the modelled maps. Another difference between the observed and downscaled LST images is that the latter appear not to have represented the warmest and coolest areas of the satellite-derived maps correctly. These findings are reflected in standard deviations of the downscaled LST maps (Tables Apx A-8 and 9), which are lower than in the observed images, especially for winter (0.1-0.2K as opposed to 0.5-0.6K), whereas for the summer are closer in magnitude to the observed values (2.1 – 3.3K as compared to 2.6 – 3.6K). The downscaled maps, however, have an advantage over the satellite-derived images in that they do pick out the detail of urban fabric, including the outlines of individual buildings, paved and green spaces (refer to Figure Apx A-7)), making them suitable for urban thermal environment studies at much needed local scales

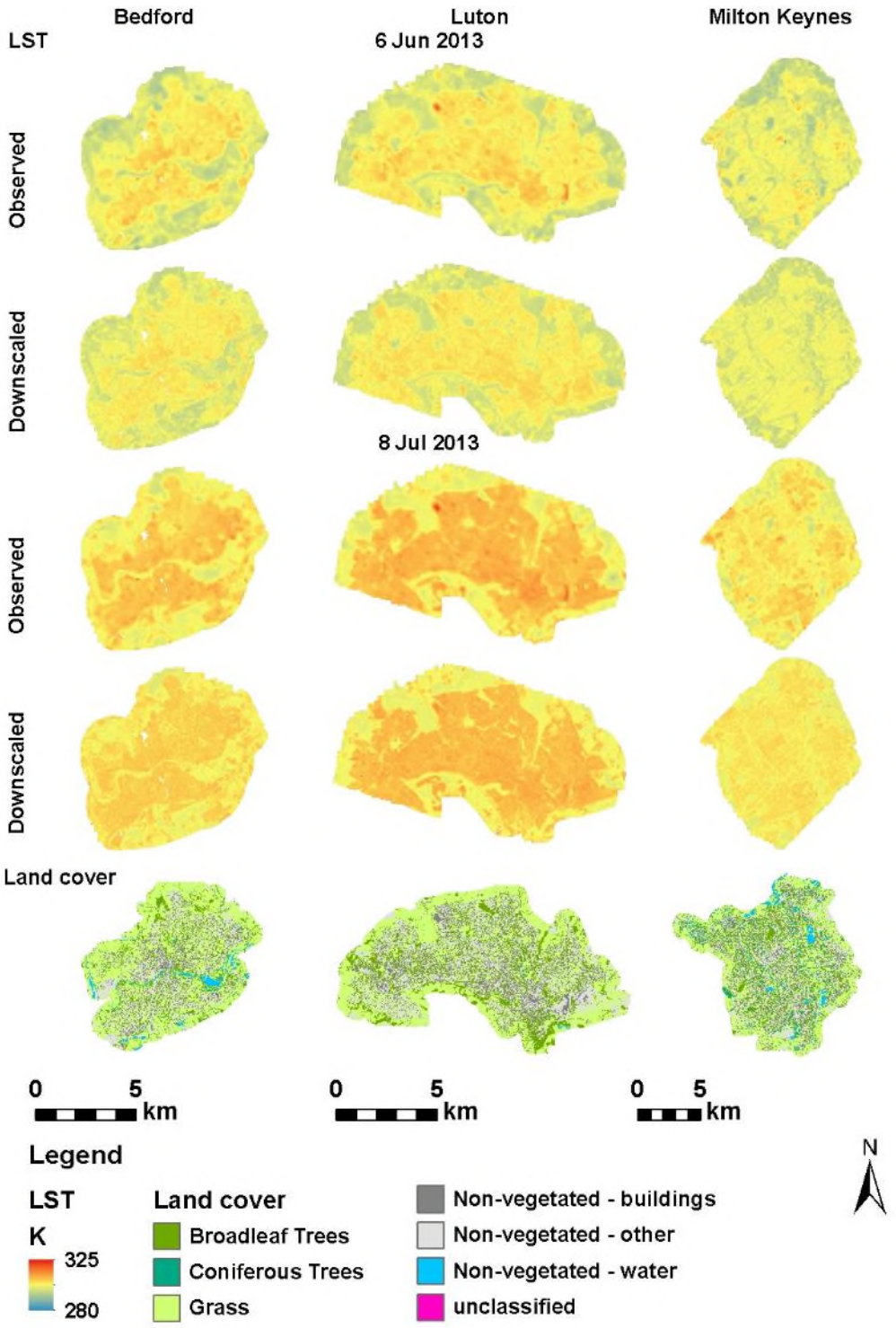

Figure 2-4 Comparison of satellite-derived (observed) and downscaled LST images derived with the $MARS_{2/4ma}$ models constructed with adjusted spectral indices at 2 to 4m spatial resolution for Bedford, Luton and Milton Keynes derived for summer dates. Land cover maps are shown for comparison of LST with the patterns of urban fabric.

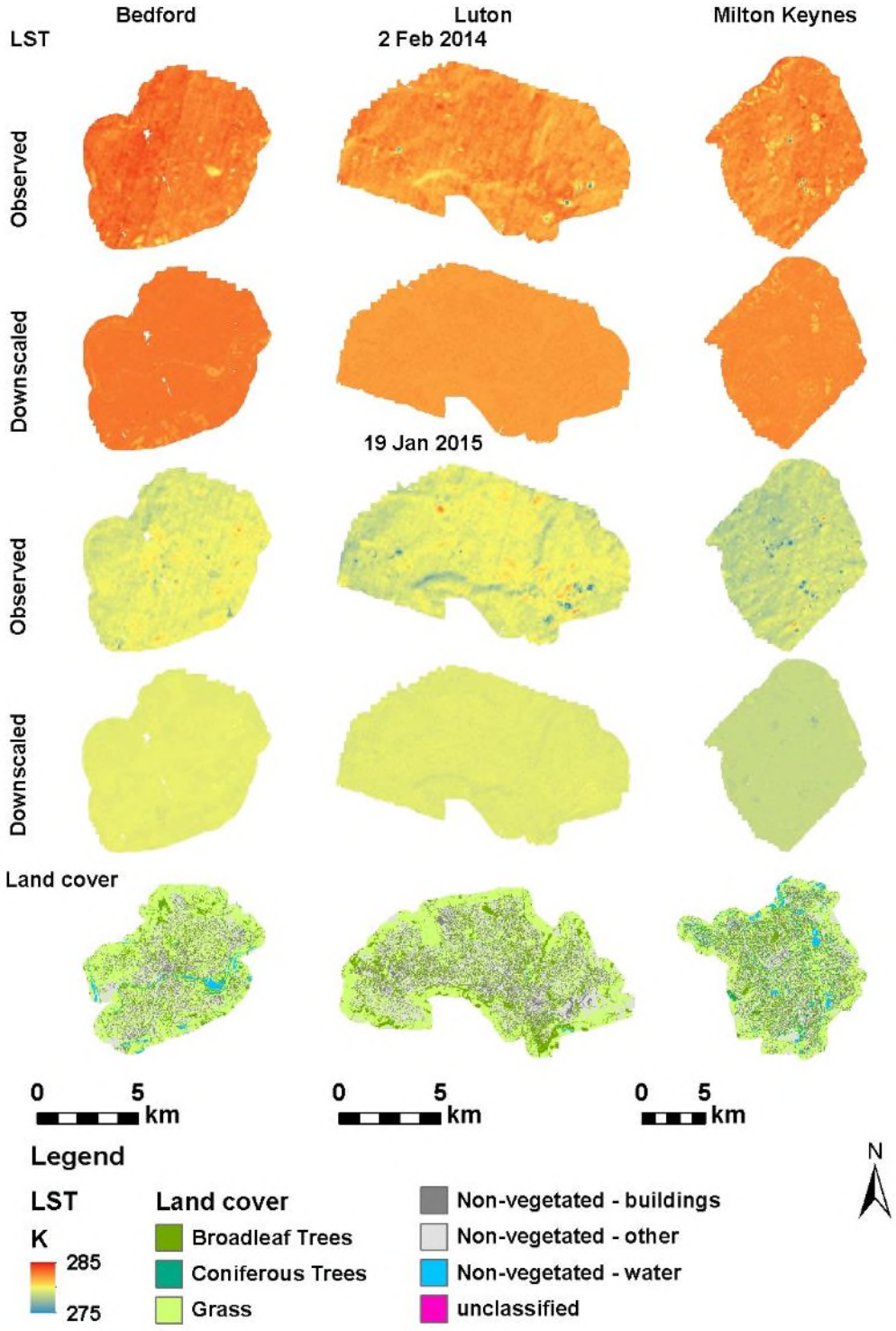

Figure 2-5 Comparison of satellite-derived (observed) and downscaled LST images derived with the $MARS_{2/4ma}$ models constructed with adjusted spectral indices at 2 to 4m spatial resolution for Bedford, Luton and Milton Keynes derived for winter dates. Land cover maps are shown for comparison of LST with the patterns of urban fabric.

2.4 Discussion

2.4.1 Downscaling factor

The primary goal of this study was to generate very high spatial resolution LST maps for urban areas based on medium spatial resolution satellite observations and very high resolution auxiliary data. Our target spatial resolution of 2 to 4m was driven by the spatial resolution of the available ancillary hyperspectral aerial imagery, which was 2m for the visible and near infrared, and 4m for the short wave infrared spectra. Given that our LST downscaling approach was based on observed LST at 100m resolution, the downscaling factor, defined as the ratio between the observed and downscaled spatial resolution (Zhou et al., 2016; Bonafoni and Tosi, 2017), was at an unprecedented 25/50. The downscaling factor has its implications on the accuracy of the downscaled maps, measured by RMSE, with larger differences between the source and target resolutions resulting in lower accuracies of the downscaled images. This could be partially explained by the scale effect and the assumption of conditionality of the scale-invariant relationship between LST and its descriptors (Zhou et al., 2016). Temperatures over the land surface can vary strongly and abruptly over space (Prata, Casellescoll, Sobrino, & Ottle, 1995), and this variation can be lost at spatial resolution of satellite TIR sensors. Indeed, Agam et al. (2007) attributed the increasing RMSE of downscaled LST maps with the increasing downscaling factor due to the increased variability of LST values at higher as compared to lower spatial resolutions. This poses a practical difficulty for the development of downscaling models in the extreme LST ranges of fine resolution LST values due to the lack or low availability of data pixels characterised with such values at coarser resolutions (Liu and Pu, 2008; Mukherjee et al., 2015b; Hutengs and Vohland, 2016) regardless of the implemented downscaling method.

2.4.2 Accuracy of the downscaling approach

Despite the high downscaling factor, the RMSE resulting from our approach for the summer dates was comparable or lower than RMSEs found in the other published urban studies, although it has to be noted that all studies listed below either used independent LST maps to validate their downscaling results or

developed their downscaling models on upscaled LST data and verified the result with the original dataset, which limits comparability of our assessments. For example, spectral unmixing method applied by Deng and Wu (2013) to downscale a Landsat TM image down to 4m spatial resolution yielded with RMSE of 2K, and Bonafoni and Tosi (2017), achieved RMSE of 2.96, 2.85, and 2.71K when using the same principle to downscale LST at 40m, 30m, and 20m to 2m in an urban environment. Other urban LST studies, pertaining to coarser resolutions of output LST maps and scaling factors ranging from 2 to 12 as well as application of various LST downscaling methods, achieved RMSE ranging between 1.28 and 3.9K (Yang et al., 2010; Zhan et al., 2012; Keramitsoglou and Kiranoudis, 2013; Weng and Fu, 2014; Bonafoni, 2016; Yang et al., 2017). In winter, however, the low effectiveness of the downscaling method could have resulted from poor correlation between spectral indices and the reduced ranges of observed LST as compared to summer. This is consistent with lower correlations between the Urban Impervious Surface index in winter than summer LST observed in a selection of Chinese urban areas (Ma et al., 2016) as well as lower performance of LST downscaling procedure observed by Yang et al. (2017) explained by worse performance of such methods when LST magnitudes are lower or when the values of LST are altered by ice and snow cover. Another explanation for poor performance of our downscaling approach in winter could be the previously mentioned stray light error affecting the Landsat 8 thermal sensors and resulting with discernible ghosting within LST maps generated from the TIR bands. In our data this problem was especially visible in the winter-time LST maps, which in turn would have introduced noise into MARS models constructed for the winter scenes, lowering their overall accuracy.

The accuracy of the downscaled LST maps can also depend on the downscaling process (Zhou et al., 2016) which includes the type and number of selected LST descriptors and the applied regression method (Zhan et al., 2013). We chose to use a combination of previously utilised spectral indices, such as NDVI and NDBI as well as land cover fraction within pixels coupled with indices not utilised in previous studies (CMR, FMR and IOR). Our results suggested that in urban areas dominated by a mosaic of vegetated, paved and built-up spaces, NDBI and FMR

next to NDVI can be important as LST predictors in downscaling studies, especially in the summer. This finding is consistent with other studies that used NDBI alongside NDVI and other spectral indices as a downscaling factor and obtained reduced RMSE as compared to methods using solely NDVI (Bonafoni et al., 2016). Good performance of FMR can be explained by the fact that, similarly to NDBI, it is composed of a ratio between short-wave and near-infrared bands, that have been shown to contribute to higher performance of LST downscaling procedure using random forests presented in Hutengs and Vohland (2016). Combination of multiple LST predictors contributed to lowering of RMSE, which is consistent with many other LST downscaling studies (Yang et al., 2010; Hutengs and Vohland, 2016; Bonafoni and Tosi, 2017) where the use of several LST predictors showed an improvement over the standard methods of DisTrad (Kustas et al., 2003) or TsHARP (Agam et al., 2007) utilising NDVI as the sole input. In our case study, the MARS method confirmed findings of other LST downscaling studies that using non-linear regression methods such as artificial neural networks (Kolios, Georgoulas and Stylios, 2013) or random forests (Hutengs and Vohland, 2016) can reduce the RMSE of the downscaled map as compared to multiple regression methods, when coupled with multiple LST predictors.

2.4.3 Adjustment for temporal mismatch between satellite and ancillary data

We also implemented a novel method for making adjustments for the temporal mismatch between available LST data at a coarse spatial resolution and very high resolution LST downscaling factors by adjusting the values of very high spatial resolution spectral indices for the values of equivalent coarse resolution spectral indices derived for the target dates by means of spatial interpolation of differences between images in question. Typically, in LST downscaling studies, spectral indices used as downscaling factors and LST data are derived from temporally matching datasets (Kustas et al., 2003; Agam et al., 2007; Yang et al., 2010; Mukherjee et al., 2014). As so far, Bonafoni et al. (2016) addressed the temporal mismatch between Landsat-derived and airborne LST maps by averaging the Landsat-derived LST captured on the closest possible dates before and after the

acquisition date of the airborne LST image. This, however, was carried out for validation rather than LST-downscaling purposes and was only possible due to seasonal similarity of all the images. Using spectral information captured at various dates to fill in missing spectral information at a date of interest is not uncommon in remote sensing and can be, for instance, implemented for the purpose of cloud cover and cloud shadow correction. This can be done by replacing the missing information within one image with spectral information of another with the application of image fusion within transition zones to account for differences in image colour (Tseng, Tseng and Chien, 2008), information cloning whereby temporal correlation of multitemporal images is utilised to fill in the gaps (Lin, Tsai, Lai, & Chen, 2013), or by contextual reconstruction of cloud-contaminated multitemporal images by reproduction of local spectro-temporal relationships between the considered image and a opportunely selected subset of remaining temporal images (Melgani, 2006). Our method of spectral indices adjustment allows for application of LST downscaling for multiple dates without the necessity of repeated acquisition of very high resolution multispectral imagery, at least for seasons with developed green vegetation.

2.5 Conclusions

The main objective of this study was to generate very high resolution land surface temperature maps for three English towns, Milton Keynes, Bedford and Luton, suitable for determination of the local temperature regulation ecosystem service of urban greenspaces. We applied the multivariate adaptive regression splines method to downscale LST derived from 100m resolution satellite thermal images down to 2 to 4m spatial resolution, with the use of spectral indices derived from high resolution aerial imagery as well as fractional cover of paved and water surfaces, achieving satisfactory results for images captured in the summer and poor performance for winter-time images. The proposed novel technique for addressing non-matching dates of satellite and aerial imagery used in LST downscaling, consisting of adjusting the spectral indices derived from aerial imagery for kriged residuals calculated from the comparison to equivalent spectral indices derived from the reference satellite imagery, performed

satisfactorily and contributed to increased model performance statistics for months with developed vegetation cover. We confirmed that inclusion of multiple spectral indices, and especially ones that are composed of the NIR and SWIR wavebands, can improve the accuracy of the downscaled LST maps. Further improvements to the proposed methodology could involve enhancements to the adjusting procedure of very high resolution spectral indices for the values of equivalent coarse resolution indices derived for the dates of interest as well as incorporation of additional land surface temperature indicators capable of explaining portions of the spatial variation of LST that cannot be represented by spectral indices, such as maps of anthropogenic sources of high or low heat areas.

Acknowledgements

This research (Grant Number NE/ J015067/1) was conducted as part of the Fragments, Functions and Flows in Urban Ecosystem Services (F3UES) project as part of the larger Biodiversity and Ecosystem Service Sustainability (BESS) framework. BESS is a six-year programme (2011–2017) funded by the UK Natural Environment Research Council (NERC) and the Biotechnology and Biological Sciences Research Council (BBSRC) as part of the UK's Living with Environmental Change (LWEC) programme. This work presents the outcomes of independent research funded by NERC and the BESS programme, and the views expressed are those of the authors and not necessarily those of the BESS Directorate or NERC.

We would also like to thank Professor Phil Warren, Dr Karl Evans and Dr Briony Norton for initiating the idea of the presented work as well as invaluable discussions shaping the form of this manuscript; and Dr Steven Hancock for his support in processing of the aerial imagery.

2.6 References

Agam, N., Kustas, W.P., Anderson, M.C., Li, F. and Neale, C.M.U. (2007) 'A vegetation index based technique for spatial sharpening of thermal imagery', *Remote Sensing of Environment*, 107(4), pp. 545–558. Available at: 10.1016/j.rse.2006.10.006 (Accessed: 11 September 2017).

Asgarian, A., Amiri, B.J. and Sakieh, Y. (2015) 'Assessing the effect of green cover spatial patterns on urban land surface temperature using landscape metrics approach', *Urban Ecosystems*, 18(1) Springer US, pp. 209–222. Available at: 10.1007/s11252-014-0387-7 (Accessed: 14 June 2018).

Bonafoni, S. (2016) 'Downscaling of Landsat and MODIS Land Surface Temperature over the Heterogeneous Urban Area of Milan', *IEEE Journal of Selected Topics in Applied Earth Observations and Remote Sensing*, 9(5), pp. 2019–2027. Available at: 10.1109/JSTARS.2016.2514367 (Accessed: 6 September 2017).

Bonafoni, S., Anniballe, R., Gioli, B. and Toscano, P. (2016) 'Downscaling Landsat Land Surface Temperature over the urban area of Florence', *European Journal of Remote Sensing*, 49(1) Taylor & Francis, pp. 553–569. Available at: 10.5721/EuJRS20164929 (Accessed: 6 September 2017).

Bonafoni, S. and Tosi, G. (2017) 'Downscaling of Land Surface Temperature Using Airborne High-Resolution Data: A Case Study on Aprilia, Italy', *IEEE Geoscience and Remote Sensing Letters*, 14(1), pp. 107–111. Available at: 10.1109/LGRS.2016.2630798 (Accessed: 6 September 2017).

Bornstein, R.D. and Bornstein, R.D. (1968) 'Observations of the Urban Heat Island Effect in New York City', *Journal of Applied Meteorology*, 7(4), pp. 575–582. Available at: 10.1175/1520-0450(1968)007<0575:OOTUHI>2.0.CO;2 (Accessed: 18 March 2019).

Chen, Y. and Wong, N.H. (2006) 'Thermal benefits of city parks', *Energy and Buildings*, 38(2) Elsevier, pp. 105–120. Available at: 10.1016/j.enbuild.2005.04.003 (Accessed: 22 July 2020).

Cressie, N. (1988) ‘Spatial prediction and ordinary kriging’, *Mathematical Geology*, 20(4) Kluwer Academic Publishers-Plenum Publishers, pp. 405–421. Available at: 10.1007/BF00892986 (Accessed: 2 July 2018).

Deng, C. and Wu, C. (2013) ‘Estimating very high resolution urban surface temperature using a spectral unmixing and thermal mixing approach’, *International Journal of Applied Earth Observation and Geoinformation*, 23(1), pp. 155–164. Available at: 10.1016/j.jag.2013.01.001 (Accessed: 20 November 2015).

Feng, X., Foody, G., Aplin, P. and Gosling, S.N. (2015) ‘Enhancing the spatial resolution of satellite-derived land surface temperature mapping for urban areas’, *Sustainable Cities and Society*, 19, pp. 341–348. Available at: 10.1016/j.scs.2015.04.007 (Accessed: 6 September 2017).

Friedman, J.H. (1991) ‘Multivariate Adaptive Regression Splines’, *The Annals of Statistics*, 19(1) Institute of Mathematical Statistics, pp. 1–67. Available at: 10.1214/aos/1176347963 (Accessed: 31 August 2017).

Grafius, D.R., Corstanje, R., Siriwardena, G.M., Plummer, K.E. and Harris, J.A. (2017) ‘A bird’s eye view: using circuit theory to study urban landscape connectivity for birds’, *Landscape Ecology*, 32(9) Springer Netherlands, pp. 1771–1787. Available at: 10.1007/s10980-017-0548-1 (Accessed: 3 September 2017).

Grafius, D.R., Corstanje, R., Warren, P.H., Evans, K.L., Hancock, S. and Harris, J.A. (2016) ‘The impact of land use/land cover scale on modelling urban ecosystem services’, *Landscape Ecology*, 31(7) Springer Netherlands, pp. 1509–1522. Available at: 10.1007/s10980-015-0337-7 (Accessed: 3 September 2017).

Hutengs, C. and Vohland, M. (2016) ‘Downscaling land surface temperatures at regional scales with random forest regression’, *Remote Sensing of Environment*, 178, pp. 127–141. Available at: 10.1016/j.rse.2016.03.006 (Accessed: 17 February 2017).

Jenerette, G.D., Harlan, S.L., Buyantuev, A., Stefanov, W.L., Declet-Barreto, J., Ruddell, B.L., Myint, S.W., Kaplan, S. and Li, X. (2016) 'Micro-scale urban surface temperatures are related to land-cover features and residential heat related health impacts in Phoenix, AZ USA', *Landscape Ecology*, 31(4) Kluwer Academic Publishers, pp. 745–760. Available at: 10.1007/s10980-015-0284-3 (Accessed: 1 November 2015).

Jimenez-Munoz, J.C., Sobrino, J.A., Skokovic, D., Mattar, C. and Cristobal, J. (2014) 'Land surface temperature retrieval methods from landsat-8 thermal infrared sensor data', *IEEE Geoscience and Remote Sensing Letters*, 11(10) IEEE, pp. 1840–1843. Available at: 10.1109/LGRS.2014.2312032 (Accessed: 29 February 2016).

Kalkstein, L.S. and Smoyer, K.E. (1993) The impact of climate change on human health: Some international implications *Experientia*. Available at: 10.1007/BF02125644 (Accessed: 3 July 2018).

Keramitsoglou, I., Kiranoudis, C.T. and Weng, Q. (2013) 'Downscaling Geostationary Land Surface Temperature Imagery for Urban Analysis', *IEEE Geoscience and Remote Sensing Letters*, 10(5), pp. 1253–1257. Available at: 10.1109/LGRS.2013.2257668 (Accessed: 20 November 2015).

Kolios, S., Georgoulas, G. and Stylios, C. (2013) 'Achieving downscaling of Meteosat thermal infrared imagery using artificial neural networks', *International Journal of Remote Sensing*, 34(21), pp. 7706–7722. Available at: 10.1080/01431161.2013.825384 (Accessed: 17 November 2015).

Kong, F., Yin, H., James, P., Hutyra, L.R. and He, H.S. (2014) 'Effects of spatial pattern of greenspace on urban cooling in a large metropolitan area of eastern China', *Landscape and Urban Planning*, 128, pp. 35–47. Available at: 10.1016/j.landurbplan.2014.04.018 (Accessed: 27 September 2015).

Kustas, W.P., Norman, J.M., Anderson, M.C. and French, A.N. (2003) 'Estimating subpixel surface temperatures and energy fluxes from the vegetation index–radiometric temperature relationship', *Remote Sensing of Environment*, 85(4),

pp. 429–440. Available at: 10.1016/S0034-4257(03)00036-1 (Accessed: 28 February 2017).

Lee, S.-M., Fernando, H.J.S., Princevac, M., Zajic, D., Sinesi, M., McCulley, J.L. and Anderson, J. (2003) 'Transport and Diffusion of Ozone in the Nocturnal and Morning Planetary Boundary Layer of the Phoenix Valley', *Environmental Fluid Mechanics*, 3(4) Kluwer Academic Publishers, pp. 331–362. Available at: 10.1023/A:1023680216173 (Accessed: 3 July 2018).

Lin, C.H., Tsai, P.H., Lai, K.H. and Chen, J.Y. (2013) 'Cloud removal from multitemporal satellite images using information cloning', *IEEE Transactions on Geoscience and Remote Sensing*, 51(1), pp. 232–241. Available at: 10.1109/TGRS.2012.2197682 (Accessed: 12 April 2018).

Liu, D. and Pu, R. (2008) 'Downscaling Thermal Infrared Radiance for Subpixel Land Surface Temperature Retrieval', *Sensors*, 8(4), pp. 2695–2706. Available at: 10.3390/s8042695 (Accessed: 20 November 2015).

Lo, C.P., Quattrochi, D.A. and Luvall, J.C. (1997) 'Application of high-resolution thermal infrared remote sensing and GIS to assess the urban heat island effect', *International Journal of Remote Sensing*, 18(2) Taylor & Francis Group, pp. 287–304. Available at: 10.1080/014311697219079 (Accessed: 27 January 2018).

Ma, Q., Wu, J. and He, C. (2016) 'A hierarchical analysis of the relationship between urban impervious surfaces and land surface temperatures: spatial scale dependence, temporal variations, and bioclimatic modulation', *Landscape Ecology*, 31(5) Springer Netherlands, pp. 1139–1153. Available at: 10.1007/s10980-016-0356-z (Accessed: 28 February 2018).

Melgani, F. (2006) 'Contextual reconstruction of cloud-contaminated multitemporal multispectral images', *IEEE Transactions on Geoscience and Remote Sensing*, 44(2), pp. 442–455. Available at: 10.1109/TGRS.2005.861929 (Accessed: 12 April 2018).

Montanaro, M., Gerace, A., Lunsford, A., Reuter, D., Montanaro, M., Gerace, A., Lunsford, A. and Reuter, D. (2014) 'Stray Light Artifacts in Imagery from the

Landsat 8 Thermal Infrared Sensor', *Remote Sensing*, 6(11) Multidisciplinary Digital Publishing Institute, pp. 10435–10456. Available at: 10.3390/rs61110435 (Accessed: 4 February 2019).

Mukherjee, S., Joshi, P.K. and Garg, R.D. (2015a) 'Regression-Kriging Technique to Downscale Satellite-Derived Land Surface Temperature in Heterogeneous Agricultural Landscape', *IEEE Journal of Selected Topics in Applied Earth Observations and Remote Sensing*, 8(3), pp. 1–1. Available at: 10.1109/JSTARS.2015.2396032 (Accessed: 10 November 2015).

Mukherjee, S., Joshi, P.K. and Garg, R.D. (2014) 'A comparison of different regression models for downscaling Landsat and MODIS land surface temperature images over heterogeneous landscape', *Advances in Space Research*, 54(4), pp. 655–669. Available at: 10.1016/j.asr.2014.04.013 (Accessed: 10 November 2015).

Mukherjee, S., Joshi, P.K. and Garg, R.D. (2015b) 'Evaluation of LST downscaling algorithms on seasonal thermal data in humid subtropical regions of India', *International Journal of Remote Sensing*, Taylor & Francis Available at: http://www.tandfonline.com/doi/abs/10.1080/01431161.2015.1041175 (Accessed: 10 November 2015).

Norton, B.A., Coutts, A.M., Livesley, S.J., Harris, R.J., Hunter, A.M. and Williams, N.S.G. (2015) 'Planning for cooler cities: A framework to prioritise green infrastructure to mitigate high temperatures in urban landscapes', *Landscape and Urban Planning*, 134 Elsevier, pp. 127–138. Available at: 10.1016/j.landurbplan.2014.10.018 (Accessed: 29 August 2020).

Odeh, I.O.A., McBratney, A.B. and Chittleborough, D.J. (1995) 'Further results on prediction of soil properties from terrain attributes: heterotopic cokriging and regression-kriging', *Geoderma*, 67(3–4) Elsevier, pp. 215–226. Available at: 10.1016/0016-7061(95)00007-B (Accessed: 2 July 2018).

Odeha, I.O.A., McBratney, A.B. and Chittleborough, D.J. (1994) 'Spatial prediction of soil properties from landform attributes derived from a digital

elevation model', *Geoderma*, 63(3–4), pp. 197–214. Available at: 10.1016/0016-7061(94)90063-9 (Accessed: 14 November 2017).

Oke, T.R. (2004) 'Initial guidance to obtain representative meteorological observations at urban sites', *World Meteorological Organization*, (81) Geneva: WMO, p. 51. Available at: http://www.geog.ubc.ca/~toke/IOM-81-UrbanMetObs.pdf (Accessed: 24 January 2021).

Piikki, K. and Söderström, M. (2019) 'Digital soil mapping of arable land in Sweden – Validation of performance at multiple scales', *Geoderma*, 352 Elsevier, pp. 342–350. Available at: 10.1016/j.geoderma.2017.10.049 (Accessed: 2 March 2018).

Piikki, K., Wetterlind, J., Söderström, M. and Stenberg, B. (2015) 'Three-dimensional digital soil mapping of agricultural fields by integration of multiple proximal sensor data obtained from different sensing methods', *Precision Agriculture*, 16(1) Springer US, pp. 29–45. Available at: 10.1007/s11119-014-9381-6 (Accessed: 2 March 2018).

Pitman, S.D., Daniels, C.B. and Ely, M.E. (2015) 'Green infrastructure as life support: Urban nature and climate change', *Transactions of the Royal Society of South Australia*, 139(1) Taylor & Francis, pp. 97–112. Available at: 10.1080/03721426.2015.1035219 (Accessed: 18 March 2019).

Prata, A.J., V. Casellescoll, C., Sobrino, J.A. and Ottle, C. (1995) 'Thermal remote sensing of land surface temperature from satellites: current status and future prospects', *Remote Sensing Reviews*, 12(3–4) Taylor & Francis Group, pp. 175–224. Available at: 10.1080/02757259509532285 (Accessed: 15 February 2018).

Sanusi, R., Johnstone, D., May, P. and Livesley, S.J. (2016) 'Street Orientation and Side of the Street Greatly Influence the Microclimatic Benefits Street Trees Can Provide in Summer.', *Journal of environmental quality*, 45(1) The American Society of Agronomy, Crop Science Society of America, and Soil Science Society of America, Inc., pp. 167–74. Available at: 10.2134/jeq2015.01.0039 (Accessed: 11 April 2016).

Schwarz, N., Schlink, U., Franck, U. and Großmann, K. (2012) ‘Relationship of land surface and air temperatures and its implications for quantifying urban heat island indicators - An application for the city of Leipzig (Germany)’, *Ecological Indicators*, 18, pp. 693–704. Available at: 10.1016/j.ecolind.2012.01.001 (Accessed: 14 November 2017).

Shochat, E., Warren, P.S., Faeth, S.H., McIntyre, N.E. and Hope, D. (2006) ‘From patterns to emerging processes in mechanistic urban ecology’, *Trends in Ecology and Evolution*, 21(4) Elsevier, pp. 186–191. Available at: 10.1016/j.tree.2005.11.019 (Accessed: 18 April 2018).

Sobrino, J.A., Jiménez-Muñoz, J.C., Sòria, G., Romaguera, M., Guanter, L., Moreno, J., Plaza, A. and Martínez, P. (2008) ‘Land surface emissivity retrieval from different VNIR and TIR sensors’, *IEEE Transactions on Geoscience and Remote Sensing*, Vol.46, pp. 316–327. Available at: 10.1109/TGRS.2007.904834 (Accessed: 29 August 2017).

Takebayashi, H. (2017) ‘Influence of Urban Green Area on Air Temperature of Surrounding Built-Up Area’, *Climate*, 5(3) Multidisciplinary Digital Publishing Institute, p. 60. Available at: 10.3390/cli5030060 (Accessed: 14 November 2017).

Tseng, D.C., Tseng, H.T. and Chien, C.L. (2008) ‘Automatic cloud removal from multi-temporal SPOT images’, *Applied Mathematics and Computation*, 205(2) Elsevier, pp. 584–600. Available at: 10.1016/j.amc.2008.05.050 (Accessed: 12 April 2018).

United Nations, Department of Economic and Social Affairs, P.D. (2019) World Urbanization Prospects The 2018 Revision.

Wang, L.-J., Guo, M., Sawada, K., Lin, J. and Zhang, J. (2015) ‘Landslide susceptibility mapping in Mizunami City, Japan: A comparison between logistic regression, bivariate statistical analysis and multivariate adaptive regression spline models’, *CATENA*, 135 Elsevier, pp. 271–282. Available at: 10.1016/J.CATENA.2015.08.007 (Accessed: 2 March 2018).

Weng, Q. and Fu, P. (2014) ‘Modeling diurnal land temperature cycles over Los Angeles using downscaled GOES imagery’, *ISPRS Journal of Photogrammetry and Remote Sensing*, 97, pp. 78–88. Available at: 10.1016/j.isprsjprs.2014.08.009 (Accessed: 10 November 2015).

Yang, G., Pu, R., Huang, W., Wang, J. and Zhao, C. (2010) ‘A Novel Method to Estimate Subpixel Temperature by Fusing Solar-Reflective and Thermal-Infrared Remote-Sensing Data With an Artificial Neural Network’, *IEEE Transactions on Geoscience and Remote Sensing*, 48(4), pp. 2170–2178. Available at: 10.1109/TGRS.2009.2033180 (Accessed: 20 November 2015).

Yang, Y., Li, X., Pan, X., Zhang, Y. and Cao, C. (2017) ‘Downscaling Land Surface Temperature in Complex Regions by Using Multiple Scale Factors with Adaptive Thresholds’, *Sensors*, 17(4) Multidisciplinary Digital Publishing Institute, p. 744. Available at: 10.3390/s17040744 (Accessed: 6 September 2017).

Yu, C. and Hien, W.N. (2006) ‘Thermal benefits of city parks’, *Energy and Buildings*, 38(2) Elsevier, pp. 105–120. Available at: 10.1016/j.enbuild.2005.04.003 (Accessed: 22 July 2020).

Zhan, W., Chen, Y., Wang, J., Zhou, J., Quan, J., Liu, W. and Li, J. (2012) ‘Downscaling land surface temperatures with multi-spectral and multi-resolution images’, *International Journal of Applied Earth Observation and Geoinformation*, 18(1), pp. 23–36. Available at: 10.1016/j.jag.2012.01.003 (Accessed: 20 November 2015).

Zhan, W., Chen, Y., Zhou, J., Wang, J., Liu, W., Voogt, J., Zhu, X., Quan, J. and Li, J. (2013) ‘Disaggregation of remotely sensed land surface temperature: Literature survey, taxonomy, issues, and caveats’, *Remote Sensing of Environment*, 131, pp. 119–139. Available at: 10.1016/j.rse.2012.12.014.

Zhou, J., Liu, S., Li, M., Zhan, W., Xu, Z. and Xu, T. (2016) ‘Quantification of the Scale Effect in Downscaling Remotely Sensed Land Surface Temperature’, *Remote Sensing*, 8(12) Multidisciplinary Digital Publishing Institute, p. 975. Available at: 10.3390/rs8120975 (Accessed: 6 September 2017).

Zhou, W., Wang, J. and Cadenasso, M.L. (2017) ‘Effects of the spatial configuration of trees on urban heat mitigation: A comparative study’, *Remote Sensing of Environment*, 195 Elsevier, pp. 1–12. Available at: 10.1016/j.rse.2017.03.043 (Accessed: 18 November 2017).

3 CHAPTER THREE

A simple method for determination of fine resolution urban form patterns with distinct thermal properties using class-level landscape metrics

J.E. Zawadzka[1]*, R. Corstanje[1], J.A. Harris[1]

[1]*Centre for Environmental and Agricultural Informatics, School of Water, Energy and Environment, Cranfield University, Bedfordshire, UK*

*Corresponding author: joanna.zawadzka@cranfield.ac.uk

Accepted for publication by the Landscape Ecology journal

Abstract

Context

Relationships between land surface temperature (LST) and spatial configuration of urban form described by landscape metrics so far have been investigated with coarse resolution LST imagery within artificially superimposed land divisions. Citywide micro-scale observations are needed to better inform urban design and help mitigate urban heat island effects in warming climates.

Objectives

The primary objective was to sub-divide an existing high-resolution land cover (LC) map into groups of patches with distinct spatial and thermal properties suitable for urban LST studies relevant to micro-scales. The secondary objective was to provide insights into the optimal analytical unit size to calculate class-level landscape metrics strongly correlated with LST at 2m spatial resolution.

Methods

A two-tiered unsupervised k-means clustering analysis was deployed to derive spatially distinct groups of patches of each major LC class followed by further

subdivisions into the hottest, coldest and intermediary sub-classes, making use of high resolution class-level landscape metrics strongly correlated with LST.

Results

Aggregation class-level landscape metrics (LSI, PLADJ and COHESION) were consistently correlated with LST for green and grey LC classes and the optimal search window size for their calculations was 100m for LST at 2m resolution. ANOVA indicated that all Tier 1 and the majority of Tier 2 subdivisions had statistically different spatial and thermal properties.

Conclusions

The two-tiered k-means clustering approach was successful at depicting subdivisions of major LC classes with distinct spatial configuration and thermal properties, especially at a broader Tier 1 level. Further research into spatial configuration of the neighbourhoods of LC patches with similar spatial but different thermal properties is required.

Keywords: land surface temperature, urban land cover classification, class-level landscape metrics, K-means clustering

3.1 Introduction

Recent decades have seen a rise in research (Wu and Ren, 2019) regarding spatial configuration of urban form and its relationship to the urban heat island (UHI) (Oke, 1976) or surface urban heat island (SUHI) (Bärring, Mattsson and Lindqvist, 1985) effects, deriving from concerns over climate change impacts on increased incidence of heatwaves (Perkins, Alexander and Nairn, 2012; Wouters et al., 2017) and related negative impacts on human health (Basara et al., 2010; Heaviside, Macintyre and Vardoulakis, 2017; Heaviside, Vardoulakis and Cai, 2016; Lin et al., 2009; Milojevic et al., 2011), among others., These concerns are substantiated by an accelerating rate of urban growth (Chapman et al. 2017; United Nations, 2019), resulting in an increasing exposure of populations to heat stress.

The impact of urban form on urban heat island is often described through direct measurements of air temperature across different urban gradients (Lin et al., 2019; Schwarz et al., 2012) or through street-scale simulations (Ramyar, Zarghami and Bryant, 2019; Sodoudi et al., 2018) allowing for micro-scale assessments. Such studies, however, take into account only a relatively small sample of observations and may not fully capture specific site effects elsewhere (Romero Rodríguez et al., 2020). On the contrary, the relationship of urban form and the SUHI effect is typically investigated from remotely sensed land surface temperature (LST) imagery at medium (30m) to very coarse (1km) spatial resolutions, offering an opportunity for city-wide assessments, however, compromising applicability of the results to micro-scales by summarising the results over larger subdivisions of land (Kong, Yin, James, Hutyra, & He, 2014; Liu et al., 2016; Masoudi, Tan, & Liew, 2019; Simwanda, Ranagalage, Estoque, & Murayama, 2019; Zhou et al., 2020; Zhou, Huang, & Cadenasso, 2011). These studies commonly use landscape metrics (McGarigal, 2015), pertaining to the field of landscape ecology, to elucidate the relationships between urban form and LST, and recommend deriving them from fine resolution land cover (LC) maps when the relationships are the strongest (Li, Zhou, & Ouyang, 2013). The use of medium to coarse resolution LST imagery within artificially superimposed land divisions allows for neighbourhood to district-scale assessments whose

aggregated character may lack in detail specific to urban design conducive to thermal comfort outdoors (Li et al., 2020; Perini et al., 2017) or within building interiors (Futcher, Kershaw and Mills, 2013; Garshasbi et al., 2020).

We present a methodology that utilises very fine spatial resolution land cover maps and selected class-level landscape metrics to generate a land cover patch typology suitable for accurately depicting LST at a fine spatial resolution in three British towns. The land cover patch typology is intended at facilitating urban design process by determining likely thermal responses of individual land cover patches with specific spatial properties as well as support studies of urban thermal patterns associated with urban form. We verify the distinctiveness of the obtained land cover patch typology by comparison to fine and medium resolution LST maps representative of two summer days a month apart as well as independent spatial configuration descriptors.

3.2 Materials and Methods

3.2.1 Study area

The study area comprises three towns located in a relatively close proximity in England: Milton Keynes (52°0′N, 0°47′W, appr. 122 km^2), Bedford (52°8′N, 0°27′W, appr. 60 km^2), and Luton/Dunstable (51°52′N, 0°25′W, appr. 86 km^2) (Figure 3-1) with population of 229,941, 106,940, and 258,018 (Office for National Statistics (2013) respectively and a temperate oceanic climate according to the Köppen–Geiger climate classification system. The three towns are characterised with contrasting histories: modern-day garden-city, medieval, and industrial, respectively, collectively representing a wide range of urban form patterns (Grafius et al., 2016; Zawadzka et al., 2020).

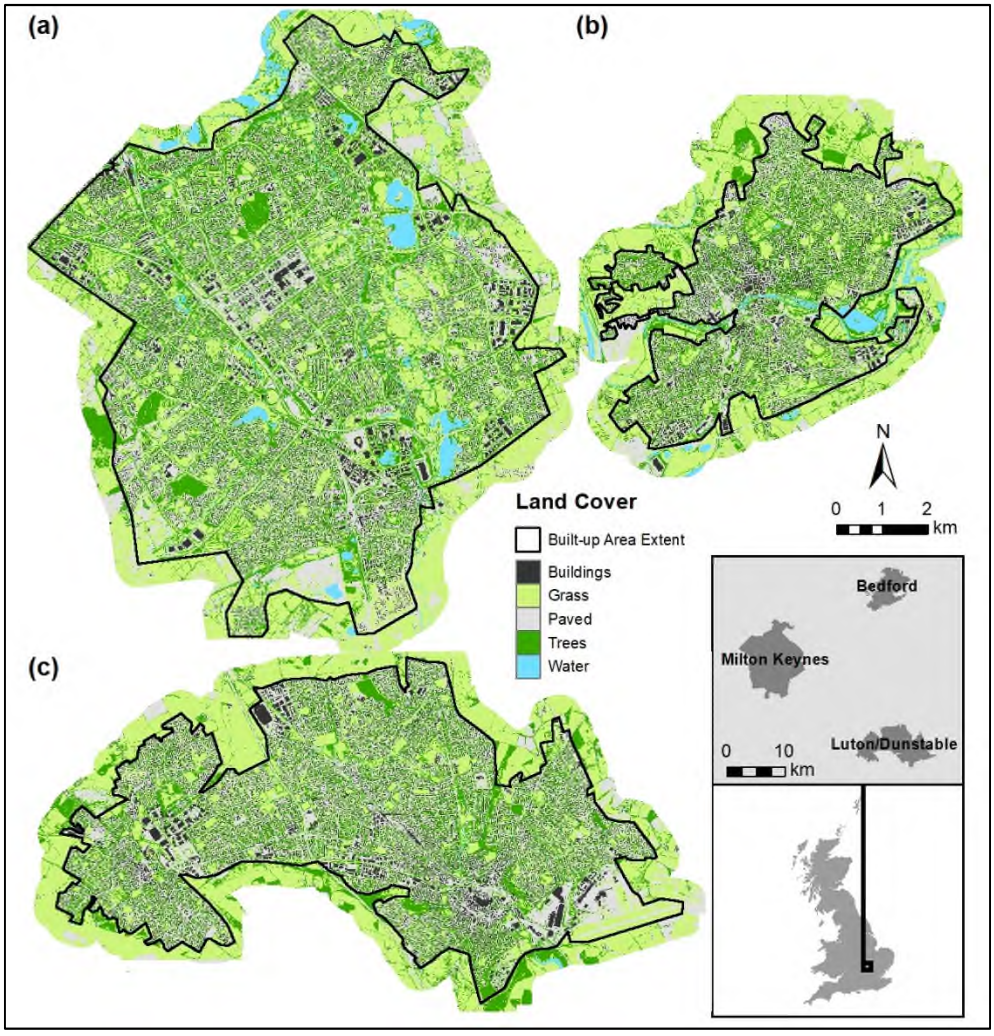

Figure 3-1 Land cover in A – Milton Keynes, B – Bedford, C – Luton/Dunstable. The insert depicts location of the towns within Great Britain. Analyses were carried out for areas within the 'Built-up Area Extent' boundary.

3.2.2 Data

This study required the use of land surface temperature, land cover and feature height data for the three study areas. The LST images were derived from Landsat 8 TIR bands using the split window algorithm as described in Jimenez-Munoz et al.(2014) for two summer dates: 6 June and 8 July 2013. Availability of cloudless images captured a month apart allowed for the assessment of the relationship between urban form patterns and LST over the course of a warming summer.

The land cover map was derived from NDVI generated from Colour-Infrared aerial imagery obtained from LandMap Spatial Discovery (http://landmap.mimas.ac.uk/) and British Ordnance Survey MasterMap, originally at 0.5m spatial resolution (Grafius et al., 2016) and resampled with the nearest neighbour method to 2m spatial resolution to reduce the data volume as well as match spatial resolution with available elevation and LST datasets. Five types of land cover are shown: grass, trees, paved, buildings and water (Figure 3-1). Importantly, the use of a detailed topographic map during land cover map production process allowed for an accurate depiction of the building footprints and road layouts, which are oftentimes obscured by overhanging tree canopies in cases where maps are generated solely from NDVI.

Finally, feature heights were available at 2m resolution. These were created based on a NERC-ARSF Leica ALS50-II LiDAR survey conducted over the three towns (Grafius et al., 2016).

3.2.3 Methods

The primary goal of this study was to develop a simple method for generation of sub-divisions of land cover patches suitable for studies of urban thermal environments at very local scales, comparable to individual or small groups of patches, with the use of the k-means clustering approach. This section describes the steps required to develop and verify the refined land cover maps, which are summarised in Figure 3-2.

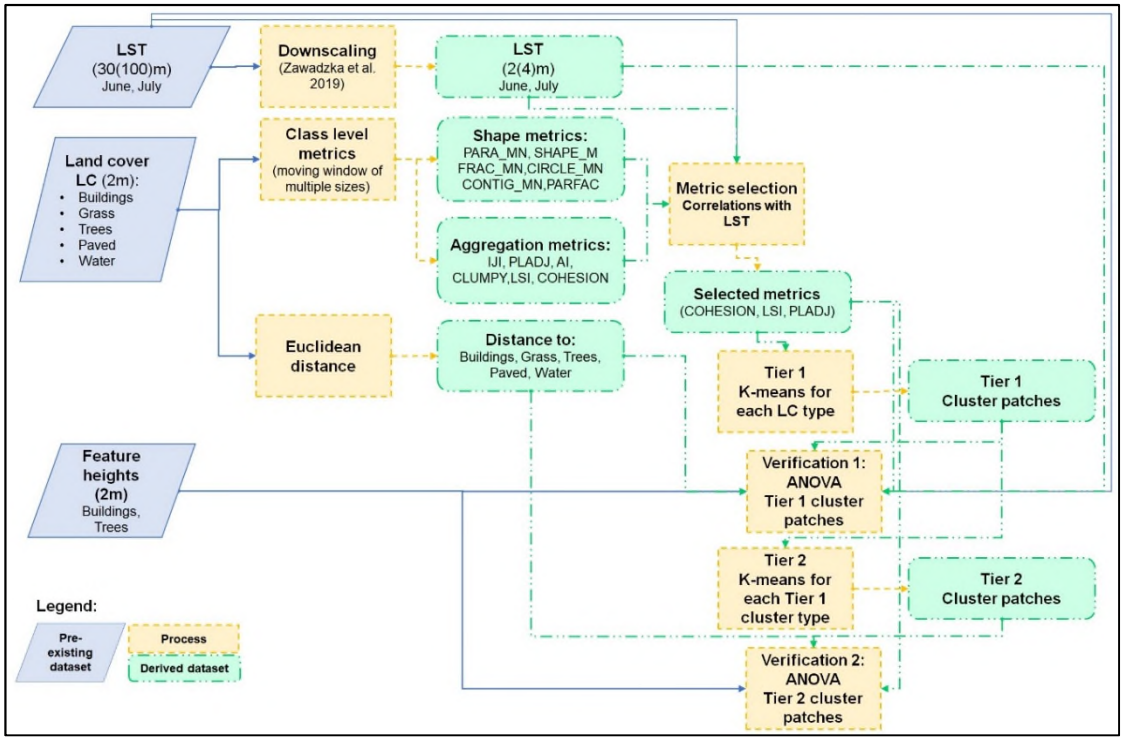

Figure 3-2 Methodological approach for determination of urban fabric patterns with distinct spatial and thermal properties.

3.2.4 LST Downscaling

Landsat 8 LST maps for the three towns at the original 30(100)m spatial resolution were downscaled to 2(4)m resolution using Multiresolution Adaptive Regression Splines method and ancillary data including spectral indices and green-grey infrastructure footprints, described in detail in Zawadzka et al., 2020. The mixed spatial resolution of the coarse LST imagery stems from the fact that Landsat 8 TIR bands are captured at 100m and are subsequently resampled, using the bilinear convolution method, by data provider (USGS – United States Geological Survey). The spectral indices used in LST downscaling were derived from visible and near-infrared bands at 2m and short-wave infrared bands at 4m resolution, resulting in an intermediate information footprint.

3.2.4.1 Spatial configuration metrics

Spatial configuration metrics used in this study included class-level landscape metrics and distances of land cover patches to other patches of

different type. A range of class-level patch aggregation and shape metrics (Table Apx B-1) was derived with the use of the Fragstats 4.2 software (McGarigal et al. 2015) from 2m spatial resolution land cover maps available for Bedford, Luton and Milton Keynes. The choice to use class-level landscape metrics, which describe spatial properties of all patches belonging to a given land cover type within a particular landscape, was justified by a couple of considerations. Firstly, patch-level metrics were discarded due to one of the fundamental reasons for conducting this study, i.e. the tendency of individual patches derived from raster maps of land cover to comprise land cover fragments of contrasting spatial properties, especially when land cover classes are well or appear to be well connected across the landscape. Examples of such land cover types within urban areas include roads and other paved areas, water, and to certain extent – trees or grass. Secondly, landscape-level metrics were inadequate for the purpose of this study looking at the refinement of existing land cover patches, as they return results pertaining to the entire landscape that cannot be attributed to an individual land cover type.

Each metric was calculated over a landscape represented by moving windows of varied sizes (10m to 100m every 10m and 100m to 200m every 20m) using the 4-cell neighbourhood rule indicating that, as opposed to the 8-cell neighbourhood rule, two adjacent grid cells in the raster map are treated as connected when they share a side but not a corner (Figure 3-3). Excluding grid cell corners from the connectivity rule allowed for discernment between small patches, such as individual trees, or other patches separated by very narrow strips of land not depicted at 2m resolution of the land cover map. Window-based analysis, by focusing on a small portion of the study area at a time, allowed for calculation of metrics for individual sections of land cover features, making the analysis relevant to microscales presumed in this study. Given considerable computation times at the very fine spatial resolution used in this study, the entire set of metrics listed was derived for Bedford, characterised with the smallest extent and somewhat intermediary spatial properties of urban form patterns when compared to Milton Keynes or Luton, and only the metrics with the strongest

relationships to LST at both 2m and 100m spatial resolutions were generated for the remaining towns.

Distances of a given LC patch to other LC patch types were derived in ArcGIS 10.5 using the Euclidean distance tool, and were stored as raster layers covering the extents of the three towns.

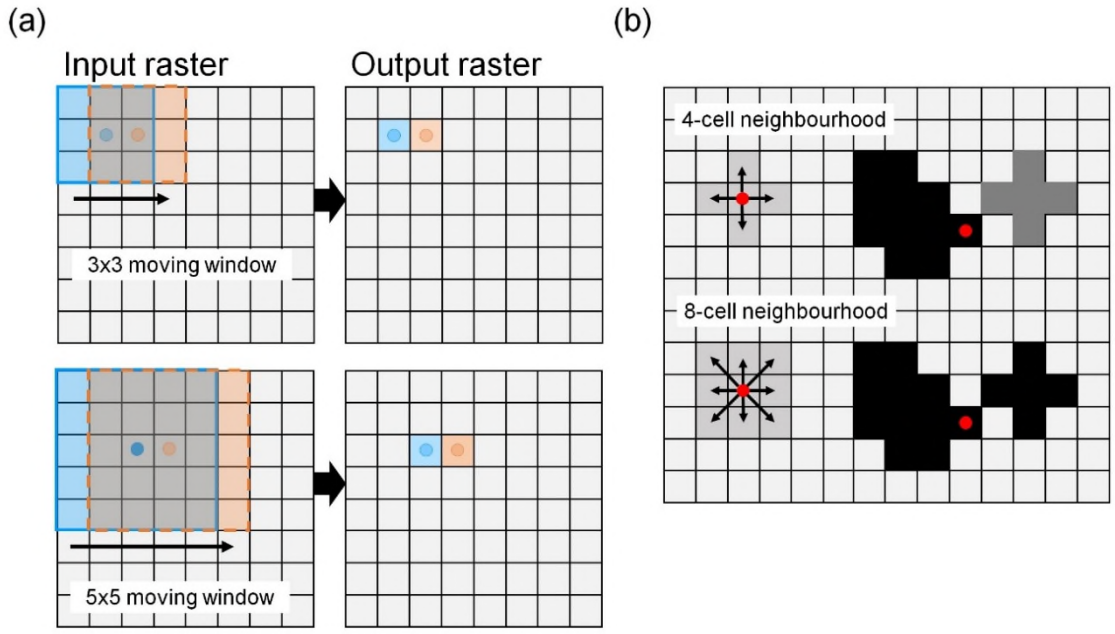

Figure 3-3 Demonstration of the (a) moving window and (b) cell neighbourhood concepts used in generation of landscape metrics from input LC maps. In moving window analysis, each cell of the output raster is assigned a result of a function calculated from all cells located within a moving window sliding across the input raster. The cell neighbourhood rule determines whether LC patches sharing a corner will be viewed as two separate patches (4-cell rule) or as a single patch (8-cell rule) by the Fragstats software.

3.2.4.2 Metrics selection

Shape or aggregation class-level landscape metrics for each land cover type calculated within moving windows of varied sizes in Bedford were compared to LST at 2(4)m and 30(100)m resolutions on a pixel-by-pixel basis using the Spearman rank correlation coefficient (Spearman, 1904) *rho*. *Rho* compares data ranks rather than actual values of two continuous variables and is therefore less

sensitive to outliers or non-normal distributions in either of the variables (Puth, Neuhäuser and Ruxton, 2015), as was the case for class-level metrics computed within small moving windows. Due to pixel-by-pixel comparisons between values of the landscape metrics, assigned to each 2m grid cell of the land cover map, and LST we did not deem it necessary to average LST over equivalent window sizes under an assumption of spatial autocorrelation of LST values (Yin et al., 2018) that would capture any effects of spatial configuration of land cover on LST. Despite the expectation that the associations between landscape metrics calculated within smaller window sizes (10 to 100m) and LST at 2(4)m resolution would be more appropriate than with the coarser LST data, the inclusion of the latter in the correlation analysis allowed for the verification of the observed relationship patterns obtained for the downscaled LST images in different land cover classes, especially in search windows over 100m in size, indirectly assuring validity of the results at the finer resolution.

3.2.4.3 Determination of two-tiered urban fabric patterns

Patterns of urban form were determined separately for each major land cover class (buildings, paved, grass, trees, and water) based on a two-tiered unsupervised k-means clustering analysis. This approach ensured a) independence from LST depiction of land cover sub-divisions and b) unbiased determination of fragments of each urban form type with specific thermal properties. The unsupervised, data-driven approach not only helped avoid bias in the estimation of spatial and thermal properties of the new land cover patches, but also had practical connotations by minimising the chance for potential omission of important or overestimation of unimportant land cover sub-divisions when a supervised method is used.

In Tier 1, class-level landscape metrics with the strongest association to LST in each land cover class were clustered with the k-means method implemented in R statistical software and scree plots representing the within-groups sum of squares (WSS) were used to determine the optimal number of clusters for each land cover class, resulting in maximally homogenous patches in terms of their spatial properties.

In Tier 2, another k-means run was carried out to determine land cover patches located within each of Tier 1 clusters with distinct LST. This required that individual land cover patches belonging to each Tier 1 cluster were attributed with the mean value of LST in June at 2m resolution using the Zonal Statistics as Table tool in ArcGIS 10.5. Again, the optimal number of clusters was determined from inspection of scree plots of WSS. The use of the mean LST rather than a range of values within each Tier 1 patch prevented splitting of individual Tier 1 patches into two or more Tier 2 clusters.

3.2.4.4 Verification

Distinctiveness of clusters obtained in both tiers of the analysis was verified with pairwise Wilcoxon ANOVA analysis (R software) based on LST, selected class-level landscape metrics, elevations, feature heights (buildings and trees only) and distances to other land cover classes.

3.3 Results

3.3.1 Associations between LST and class-level landscape metrics

Inspection of Spearman correlation values ($p<0.05$) for selected class shape and aggregation metrics with LST within different land cover classes revealed that aggregation (Figure 3-4) and not shape metrics were consistently and more strongly correlated with LST, depending on land cover and search window size used to calculate the metrics.

Class aggregation metrics with the strongest correlations to LST included COHESION and PLADJ for all LC classes, except for water, and LSI for grass and trees. The correlations were stronger in June than July and comparable in magnitude between respective months at both spatial resolutions – 2 and 100m. Correlations tended to rise with increasing search window size, achieving the strongest constant value at approximately 100m for 2m and continuing to rise slowly beyond that size for 100m resolution LST data.

At 100m window size for 2m LST in June, the strongest correlations were observed for greenspaces, with grass and trees being positively correlated with

LSI (0.57 and 0.53) and negatively correlated with COHESION (-0.59 and -0.60) and PLADJ (-0.62 and -0.66). Correlations between COHESION and PLADJ and LST for built-up spaces and water were weaker: 0.42 and 0.36 for buildings, 0.36 and 0.31 for paved, and 0.17 and 0.1 for water, respectively.

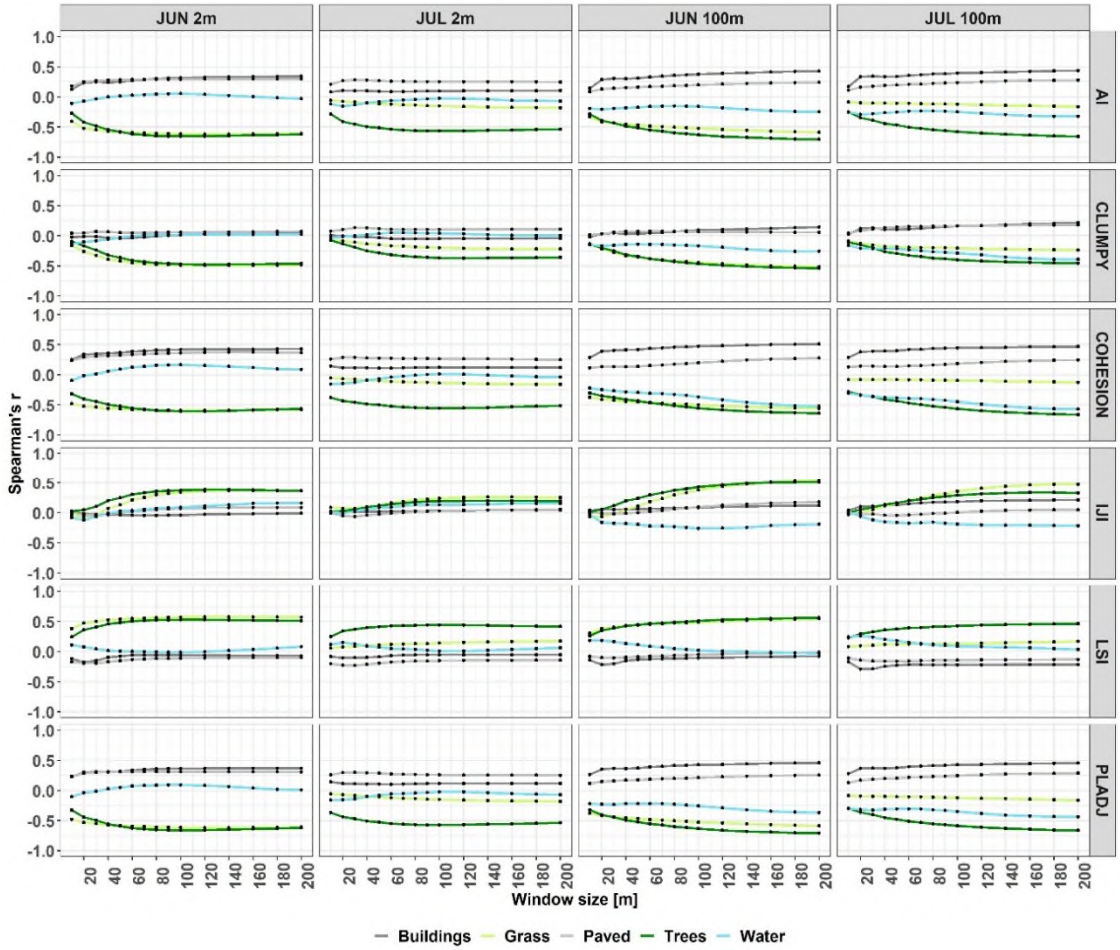

Figure 3-4 Spearman correlations between selected class aggregation metrics and LST for 6th June and 8th July at 2m and 100m spatial resolutions in various land cover types for Bedford.

The strongest correlations within class shape metrics were observed for CONTIG_MN, PARA_MN and SHAPE_MN (Figure Apx B-1), however, here the window size with the strongest relationship was relatively small (~40m) for greenspaces and large for built-up areas (~100m). This inconsistency coupled

with strong search window artefacts visible in the raster layers for shape metrics lead to their rejection as candidates in this study.

3.3.2 Spatial and thermal patterns of urban form

K-means clustering of three class aggregation metrics (COHESION, PLADJ, LSI) for grass and trees, and two class aggregation metrics (COHESION and PLADJ) for paved, buildings and water yielded spatially distinct patterns of urban form within each land cover type (Figure 3-5 and Figure Apx B-2). Each Tier 1 cluster could be attributed with distinct values of the class aggregation metrics, average distance to other land cover classes, elevation, feature heights, and LST (Table 3-1, also Tables Apx B-2 and B-3, and Tables Apx B-4 to B-16). ANOVA has shown that means of COHESION, LSI, PLADJ, and LST (except for one pair of T1 clusters in water) were significantly different ($p<0.001$) for each pair of T1 cluster within each land cover class. A great majority of cluster pairs had also significantly different distances to other land cover types, with well-justified exemptions of distances of residential patches of trees to grass, and few others for water.

Tier 2 clustering sub-divided each Tier 1 cluster into four thermal categories – coldest, hottest, and two intermediary classes: medium-cold and medium-hot, with statistically different June and July (2m) LST means (Figure Apx B-3 and Tables Apx B-17 to B-64). ANOVA carried out on all other diagnostic variables implied that resulting Tier 2 clusters have largely been distinct not only thermally but also spatially, with exceptions that were most common in water and also occurring in buildings, and very rarely in the remaining land cover types. Overall, the two-tiered unsupervised k-means clustering procedure was capable of generating a representation of urban fabric composed of five major land cover types subdivided into clusters with distinct spatial and thermal properties.

Table 3-1 Properties of Tier 1 clusters. LC – Land Cover, T1CL – Tier one cluster number. Thermal properties based on LST means in June and July at 2m and 100m resolution sorted according to decreasing aggregation level: MA – most aggregated, RMA – relatively more aggregated, RLA – relatively less aggregated, LA – least aggregated.

LC	Tier 1 Cluster	Aggregation level	Description – spatial properties including use	Thermal properties
Buildings	T1CL1	MA	Typically in industrial, commercial and other non-residential use. Largest size, most aggregated, located farthest away from grass or trees. Located primarily in city centres and on industrial estates.	Warmest
	T1CL2	RLA	Intermediary in size and other descriptors, representative of terraced housing, flats or smaller non-residential use. Due to height and proximity to vegetation more similar to CL3 than CL1. Typically located closer to city centres than buildings in CL3.	Medium-cold
	T1CL3	LA	Smallest, most fragmented and lowest buildings typically in residential use (detached and semi-detached housing associated with gardens). Located in close proximity to vegetation, typically farthest away from city centres.	Coldest
Paved	T1CL1	MA	Most aggregated, typical of squares, paved areas in commercial or industrial estates or wider roads with low amounts of scattered greenspaces or housing. Located distinctly farthest away from buildings, but not from grass or trees.	Warmest
	T1CL3	RMA	Wider roads as well as crossroads in areas where roads are relatively narrow	Warmest
	T1CL4	RLA	Mostly residential or narrower parts of main roads, less aggregated than CL3	Medium-cold
	T1CL2	LA	Distinctly least aggregated and located in close proximity to grass or trees. Typically narrow patches of footpaths, rarely roads, scattered in residential areas or crossing larger greenspaces.	Coldest
Grass	T1CL4	MA	Very large stretches of grass typical of parks and recreation areas, and occasionally larger strips of grass at roadsides. Located farthest away from buildings.	Coldest
	T1CL2	RMA	Wider strips of grass located next to roads or in parkland in between rows of trees, relatively far from buildings	Medium-cold
	T1CL3	RLA	Patches of grass that were larger than in CL 1 and located either next to residential housing or on industrial estates. Also includes elongated, narrow strips of grass next to roads.	Medium-warm
	T1CL1	LA	Small patches of grass located in residential areas and typically immediately adjacent to trees, paved areas and buildings	Warmest
Trees	T1CL2	MA	Largest, highly aggregated stretches of urban forest located away from buildings and paved areas	Coldest
	T1CL4	RMA	Well-aggregated patches of trees that could be scattered across large patches of grass or form elongated but relatively wide tree patches at roadsides; also patches of trees located in larger gardens in-between wider-spaced housing	Medium-cold
	T1CL1	RLA	Relatively small but bigger and more aggregated patches typical of terraced housing	Medium-warm
	T1CL3	LA	Very small and fragmented patches typically located near detached or semi-detached housing	Warmest
Water	T1CL3	MA	Large and most aggregated water bodies such as lakes	Coldest
	T1CL1	RMA	Wider rivers, canals or ponds, high aggregation metrics values	Coldest
	T1CL2	RLA	Narrow stream and ditches	Medium-warm
	T1CL4	LA	Narrow stream and ditches, very close proximity to trees	Warmest

3.4 Discussion

3.4.1 LC patch typology

The urban land cover patch typology developed in this study was intended at differentiating sub-divisions of main land cover types relevant for urban thermal studies at micro-scales, i.e. areas 1-10^4 m^2 in size, that are required for studies contributing to climate sustainability of urban design (Georgescu et al., 2015). Whilst micro-scale studies using simulation models of urban thermal environments exist (Perini et al., 2017; Ramyar, Zarghami and Bryant, 2019; Sodoudi et al., 2018), they often utilise unrealistic models of urban form, resulting in crude estimates, (Li et al., 2020) that could be substituted by excerpts from the typology developed here. In fact, urban climatology is known for attempts to stratify urban form into morphological areas contributing to homogenous thermal responses, an example of which is given by the urban climate zones developed by Stewart and Oke (2012) and pertaining to neighbourhood scales. Our typology, which combines patch-level detail with city-scale thermal zoning, can support research aiming at derivation of urban climate zones (Lee and Oh, 2018; Xu et al., 2019) in an automated manner by extracting individual land cover patches with spatial properties related to their LST, especially when additionally attributed with heights of buildings being one of the differentiating factors in the urban climate zone classification. Further practical implications include the opportunity created by this typology to carry out studies of the relationship between LST and urban form at scales relevant to outdoor comfort of pedestrians or in the interiors of buildings, taking into account interactions with neighbouring land cover patches (Zawadzka, Harris and Corstanje, 2020).

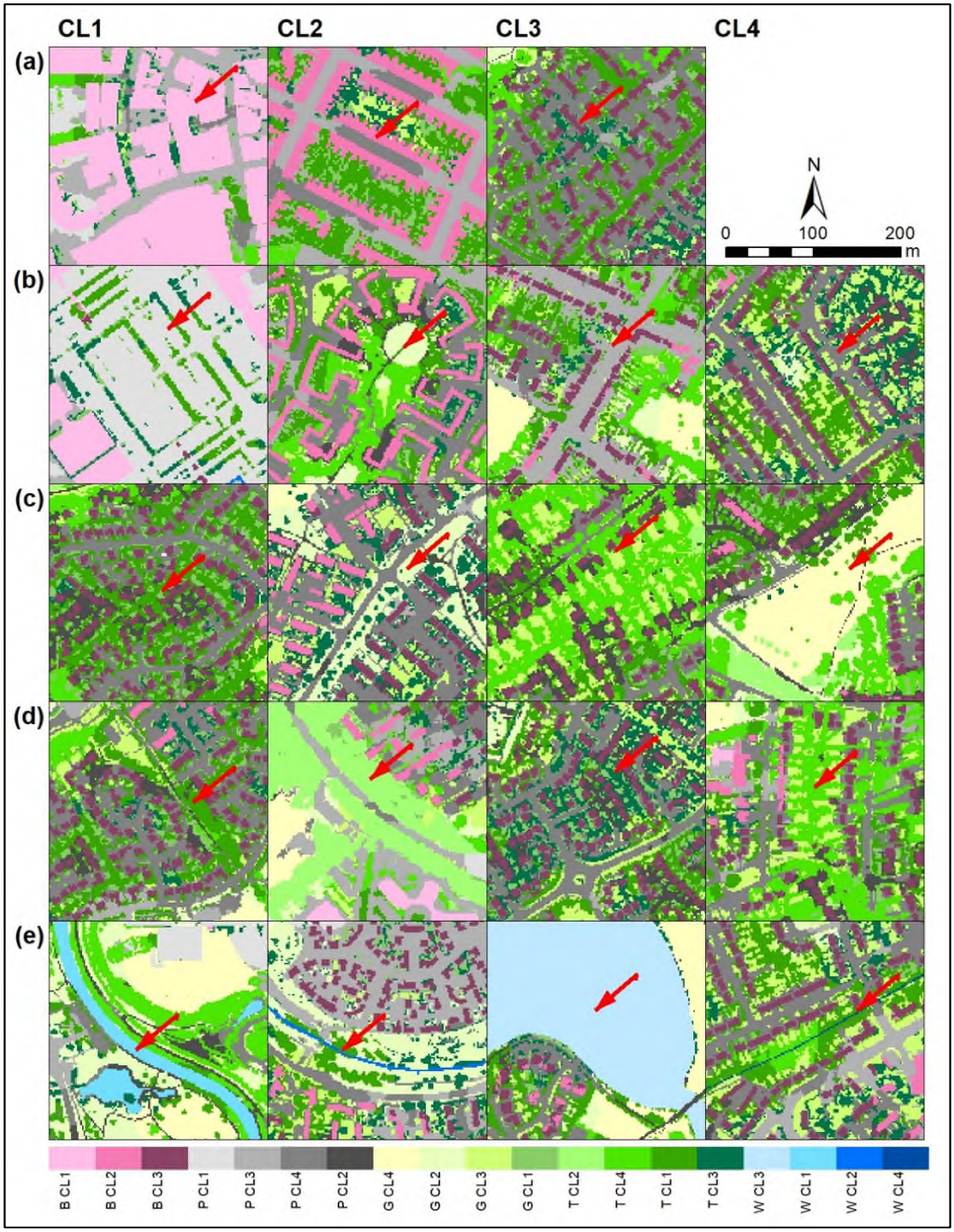

Figure 3-5 Examples of Tier 1 Clusters in (a) Buildings - B, (b) Paved - P, (c) Grass - G, (d) Trees - T, (e) Water - W. Arrows point to the Tier 1 Cluster intended for representation in each image tile. Legend is ordered according to decreasing patch aggregation levels.

3.4.2 Selection of landscape metrics

During development of the urban land cover typology presented here a number of shape and aggregation landscape metrics that had previously been used in studies pertaining to finding relationships between LST and urban form (Chen et al., 2014; Gage and Cooper, 2017; Li et al., 2011; Sodoudi et al., 2018; Wu et al., 2014; Zhou, Huang and Cadenasso, 2011) were tested for strong correlations with LST. Technical considerations of working with a land cover map in the raster format and the intention to automatically determine individual land cover patches of each main land cover type with unique spatial properties enforced the moving window analysis for calculation of the landscape metrics at land cover class-level. The use of moving windows caused the possibility of inclusion of spatial properties of grid cells belonging to adjacent land cover patches into the calculations related to the focal patch, which could lead to erroneous assignment of their spatial properties, exacerbated only in cases when adjacent land cover patches had very contrasting properties and the search window was excessively large. This effect could be regarded as largely negligible given a certain level of spatial homogeneity of urban form due to planning of neighbourhoods (Cortie, 1997).

Nevertheless, the land cover typology was intended at a stratification of urban form for use in studies of urban thermal environment at micro-scales, motivating the selection of both the type of metrics and window size most strongly correlated to LST at 2m resolution. The correlation values pointed to the highest suitability of the moving window 100x100m in size for each land cover class, which assured consistency of any subsequent analyses, however, could potentially be an artefact of the 100m spatial resolution of the thermal infrared sensor mounted on the Landsat 8 satellite. The strength of correlation depended not only on search window size used in Fragstats calculations but also on land cover and metric type. The correlations for aggregation metrics within land cover classes with LST exhibiting a relationship with LST where the strongest at 100m search window size both for green and grey spaces, and at 40 to 80m for selected shape metrics within greenspaces with varied effects for buildings and paved. Weaker correlations with water, especially with LST at 2m resolution, could be attributed

to the downscaling procedure applied to coarse resolution LST data not depicting the thermal response of water bodies correctly, especially for narrow elongated features easily affected by the mixed-pixel effect (Yow, 2007). Effects of search window size on correlations with LST have not previously been investigated citywide and separately for each land cover class within one study, potentially due to a high computational demand of these calculations. Nevertheless, correlations for aggregation metrics with 100m resolution LST still showing an increasing trend for windows 200m in size indicated that larger window sizes are appropriate for coarser resolution LST data. Weakening of the correlations for LST in July when LST was on average 3.7 K higher is in concordance with Li et al. (2011) who observed significant correlations between landscape metrics and LST in spring rather than in summer, and suggests changes in LST regulatory capacity of urban form patterns as the temperatures rise.

The use of three types of class aggregation descriptors in the land cover typology, COHESION, LSI, and PLADJ, allowed for sub-division of each land cover type according to different perspectives, ensuring comprehensiveness of the approach (McGarigal, 2015). COHESION is a measure of physical connectedness of a patch type expressed through the ratio of its perimeter to its area and the size of the landscape (i.e. search window), and as such focuses on the spatial properties of the focal patches, excluding the impact of their neighbours of the same type. PLADJ, on the other hand, analyses the landscape in search of adjacencies between patches of the same type and consequently relates their aggregation to the level of their fragmentation within a specified area. Here, the 4-cell neighbourhood rule used in the calculation of the metrics is pivotal in separating small, closely located patches of land cover that should be treated as separate entities, such as individual trees. LSI complements COHESION and PLADJ by looking at the edge density of a land cover class in the landscape and therefore relating the outcome to the shape of patches forming the class. Class-level landscape metrics used in this study are affected by sensitivities with regards to the size and aggregation of patches in the landscape (Neel, McGarigal and Cushman, 2004). Changes in aggregation level described by PLADJ and COHESION may be difficult to distinguish from the change in patch size due to

strong interactions between patch area and aggregation level within a landscape observed for these metrics, constituting a potential disadvantage depending on the requirements of subsequent studies. LSI has a tendency to display a parabolic relationship between patch size and aggregation level, however, not in natural landscapes, when the relationships are linear, i.e. higher LSI associated with lower patch area and aggregation level. This could also explain good correspondence of LSI of grass and trees to LST and not built and paved classes, which can be roughly characterised with high aggregation and low area or low aggregation and high area, respectively. From the pool of remaining class aggregation metrics considered in this study, AI had similar correlation values to PLADJ, however, its use was discarded due to a tendency to provide misleading estimates when area of the class in the landscape exceeds 50% and having similar meaning to PLADJ (Neel, McGarigal and Cushman, 2004). CLUMPY and IJI had relatively high correlations with LST for land cover classes representing greenspaces, however, CLUMPY is similar to PLADJ by considering grid cell adjacencies and IJI returns valid values only when there are at least three different classes in the considered landscape (McGarigal, 2015).

3.4.3 Clustering techniques

The development of the land cover typology presented in this study involved using pixel-based clustering techniques, which have rarely been used in studies relating landscape metrics to LST, with only Gage and Cooper (2017) having deployed hierarchical clustering to identify land cover typologies within predefined parcels of land – 5ha hexagons – rather than subtypes of a given land cover class as is the case in our study. In fact, this is the first known to the authors study attempting to sub-divide existing maps of land cover into groups of patches with unique spatial configuration properties within a single land cover class. The unsupervised k-means clustering approach was capable of discerning sub-divisions of land cover in a manner convincing to the human eye that could be further subdivided into four thermally distinct subclasses in buildings, paved, grass and trees. Whilst hierarchical object-oriented approaches (e.g. Chen et al. 2009; Grippa et al. 2017) for land cover classification could constitute an

alternative way for generation of similar land cover typologies, K-means clustering has the advantage of an easy implementation with the use of any statistical software. Moreover, our approach combining pixel-based and moving window analyses allowed for consideration of entire patches of a given land cover in the formation of the typology rather than their fragments trimmed by superimposed artificial land parcel boundaries.

3.5 Conclusions

Two-tiered unsupervised k-means clustering approach presented in this study was successful at depicting both spatially and thermally distinct subdivisions of major land cover classes in medium sized towns relevant to studies of the relationship between LST and urban form patterns at a very fine (2m) spatial resolution. Whilst investigation of all effects of spatial configuration of urban form on the LST observed in Tier 2 clusters is still ongoing (Zawadzka et al. In preparation), this study has revealed that the relationships between class-level landscape metrics and 2m resolution LST are the strongest at smaller parcels of land than in the case of coarser resolution LST datasets investigated in other studies, and that these relationships weaken as the summer progresses. This study has also shown that aggregation (LSI, COHESION, PLADJ) and not shape metrics frequently used in other studies investigating relationships between urban form and LST are important for explanation of LST at a fine spatial resolution. Correlations between the class aggregation metrics and LST, investigated as part of the secondary objective, were the strongest when a search window 100x100m in size was used to derive them from raster land cover maps and were stronger in vegetated than non-vegetated land cover classes. This proved that consideration of the interactions between technical aspects of landscape metrics' computation and LST is important for accurate depiction of urban form patterns with applications in urban thermal environment studies.

3.6 References

Bärring, L., Mattsson, J.O. and Lindqvist, S. (1985) 'Canyon geometry, street temperatures and urban heat island in Malmö, Sweden', *Journal of Climatolo*gy,

5(4) John Wiley & Sons, Ltd, pp. 433–444. Available at: 10.1002/joc.3370050410 (Accessed: 3 May 2020).

Basara, J.B., Basara, H.G., Illston, B.G. and Crawford, K.C. (2010) 'The Impact of the Urban Heat Island during an Intense Heat Wave in Oklahoma City', *Advances in Meteorology*, 2010 Hindawi Publishing Corporation, pp. 1–10. Available at: 10.1155/2010/230365.

Chapman, S., Watson, J.E.M., Salazar, A., Thatcher, M. and McAlpine, C.A. (2017) The impact of urbanization and climate change on urban temperatures: a systematic review, *Landscape Ecology*, 32(10) Springer Netherlands, pp. 1921-1935. Available at: 10.1007/s10980-017-0561-4 (Accessed: 3 May 2020).

Chen, A., Yao, L., Sun, R. and Chen, L. (2014) 'How many metrics are required to identify the effects of the landscape pattern on land surface temperature?', *Ecological Indicators*, 45 Elsevier, pp. 424–433. Available at: 10.1016/j.ecolind.2014.05.002 (Accessed: 22 June 2018).

Chen, Y., Su, W., Li, J. and Sun, Z. (2009) 'Hierarchical object oriented classification using very high resolution imagery and LIDAR data over urban areas', *Advances in Space Research*, 43(7) Elsevier Ltd, pp. 1101–1110. Available at: 10.1016/j.asr.2008.11.008 (Accessed: 10 September 2020).

Cortie, C. (1997) 'Planning doctrine and post-industrial urban development: The Amsterdam experience', *GeoJournal*, 43(4) Springer, pp. 351–358. Available at: 10.1023/A:1006817307686 (Accessed: 10 September 2020).

Futcher, J.A., Kershaw, T. and Mills, G. (2013) 'Urban form and function as building performance parameters', *Building and Environment*, 62 Pergamon, pp. 112–123. Available at: 10.1016/j.buildenv.2013.01.021 (Accessed: 30 April 2020).

Gage, E.A. and Cooper, D.J. (2017) 'Relationships between landscape pattern metrics, vertical structure and surface urban Heat Island formation in a Colorado suburb', *Urban Ecosystems*, 20(6) Springer New York LLC, pp. 1229–1238. Available at: 10.1007/s11252-017-0675-0 (Accessed: 8 May 2020).

Garshasbi, S., Haddad, S., Paolini, R., Santamouris, M., Papangelis, G., Dandou, A., Methymaki, G., Portalakis, P. and Tombrou, M. (2020) 'Urban mitigation and building adaptation to minimize the future cooling energy needs', *Solar Energy*, 204 Elsevier Ltd, pp. 708–719. Available at: 10.1016/j.solener.2020.04.089 (Accessed: 7 September 2020).

Georgescu, M., Chow, W.T.L., Wang, Z.H., Brazel, A., Trapido-Lurie, B., Roth, M. and Benson-Lira, V. (2015) 'Prioritizing urban sustainability solutions: Coordinated approaches must incorporate scale-dependent built environment induced effects', *Environmental Research Letters*, 10(6) Institute of Physics Publishing, p. 061001. Available at: 10.1088/1748-9326/10/6/061001 (Accessed: 7 September 2020).

Grafius, D.R., Corstanje, R., Warren, P.H., Evans, K.L., Hancock, S. and Harris, J.A. (2016) 'The impact of land use/land cover scale on modelling urban ecosystem services', *Landscape Ecology*, 31(7) Springer Netherlands, pp. 1509–1522. Available at: 10.1007/s10980-015-0337-7 (Accessed: 3 September 2017).

Grippa, T., Lennert, M., Beaumont, B., Vanhuysse, S., Stephenne, N. and Wolff, E. (2017) 'An Open-Source Semi-Automated Processing Chain for Urban Object-Based Classification', *Remote Sensing*, 9(4) MDPI AG, p. 358. Available at: 10.3390/rs9040358 (Accessed: 10 September 2020).

Heaviside, C., Macintyre, H. and Vardoulakis, S. (2017) 'The Urban Heat Island: Implications for Health in a Changing Environment', *Current Environmental Health Reports*, 4(3) Springer, pp. 296–305. Available at: 10.1007/s40572-017-0150-3 (Accessed: 30 April 2020).

Heaviside, C., Vardoulakis, S. and Cai, X.-M. (2016) 'Attribution of mortality to the urban heat island during heatwaves in the West Midlands, UK', *Environmental Health*, 15(S1) BioMed Central Ltd., p. S27. Available at: 10.1186/s12940-016-0100-9 (Accessed: 30 April 2020).

Jimenez-Munoz, J.C., Sobrino, J.A., Skokovic, D., Mattar, C. and Cristobal, J. (2014) 'Land surface temperature retrieval methods from landsat-8 thermal infrared sensor data', *IEEE Geoscience and Remote Sensing Letters*, 11(10)

IEEE, pp. 1840–1843. Available at: 10.1109/LGRS.2014.2312032 (Accessed: 29 February 2016).

Kong, F., Yin, H., James, P., Hutyra, L.R. and He, H.S. (2014) ‘Effects of spatial pattern of greenspace on urban cooling in a large metropolitan area of eastern China’, *Landscape and Urban Planning*, 128, pp. 35–47. Available at: 10.1016/j.landurbplan.2014.04.018 (Accessed: 27 September 2015).

Lee, D. and Oh, K. (2018) ‘Classifying urban climate zones (UCZs) based on statistical analyses’, *Urban Climate*, 24 Elsevier B.V., pp. 503–516. Available at: 10.1016/j.uclim.2017.06.005 (Accessed: 9 September 2020).

Li, J., Song, C., Cao, L., Zhu, F., Meng, X. and Wu, J. (2011) ‘Impacts of landscape structure on surface urban heat islands: A case study of Shanghai, China’, *Remote Sensing of Environment*, 115(12) Elsevier, pp. 3249–3263. Available at: 10.1016/j.rse.2011.07.008 (Accessed: 15 June 2018).

Li, X., Zhou, W. and Ouyang, Z. (2013) ‘Relationship between land surface temperature and spatial pattern of greenspace: What are the effects of spatial resolution?’, *Landscape and Urban Planning*, 114 Elsevier, pp. 1–8. Available at: 10.1016/j.landurbplan.2013.02.005 (Accessed: 14 June 2018).

Li, Z., Zhang, H., Wen, C.-Y., Yang, A.-S. and Juan, Y.-H. (2020) ‘Effects of frontal area density on outdoor thermal comfort and air quality’, *Building and Environment*, 180 Elsevier Ltd, p. 107028. Available at: 10.1016/j.buildenv.2020.107028 (Accessed: 7 September 2020).

Lin, F.-Y., Huang, K.-T., Lin, T.-P. and Hwang, R.-L. (2019) ‘Generating hourly local weather data with high spatially resolution and the applications in bioclimatic performance’, *Science of The Total Environment*, 653 Elsevier B.V., pp. 1262–1271. Available at: 10.1016/j.scitotenv.2018.10.433 (Accessed: 3 May 2020).

Lin, S., Luo, M., Walker, R.J., Liu, X., Hwang, S.-A. and Chinery, R. (2009) ‘Extreme High Temperatures and Hospital Admissions for Respiratory and Cardiovascular Diseases’, *Epidemiology*, 20(5), pp. 738–746. Available at: 10.1097/EDE.0b013e3181ad5522 (Accessed: 30 April 2020).

Liu, K., Su, H., Li, X., Wang, W., Yang, L. and Liang, H. (2016) 'Quantifying Spatial–Temporal Pattern of Urban Heat Island in Beijing: An Improved Assessment Using Land Surface Temperature (LST) Time Series Observations From LANDSAT, MODIS, and Chinese New Satellite GaoFen-1', *IEEE Journal of Selected Topics in Applied Earth Observations and Remote Sensing*, 9(5) Institute of Electrical and Electronics Engineers, pp. 2028–2042. Available at: 10.1109/JSTARS.2015.2513598 (Accessed: 8 May 2020).

Masoudi, M., Tan, P.Y. and Liew, S.C. (2019) 'Multi-city comparison of the relationships between spatial pattern and cooling effect of urban green spaces in four major Asian cities', *Ecological Indicators*, 98 Elsevier B.V., pp. 200–213. Available at: 10.1016/j.landurbplan.2018.10.023 (Accessed: 8 May 2020).

McGarigal, K. (2015) Fragstats help version 4.2 http://www.umass.edu/landeco/research/fragstats/documents/fragstats.help.4.2.pdf, Available at: 10.1016/S0022-3913(12)00047-9 (Accessed: 10 September 2020).

Milojevic, A., Wilkinson, P., Armstrong, B., Davis, M., Mavrogianni, A., Bohnenstengel, S. and Belcher, S. (2011) 'Impact of London's Urban Heat Island on Heat-related Mortality', *Epidemiology*, 22(1) Ovid Technologies (Wolters Kluwer Health), pp. S182–S183. Available at: 10.1097/01.ede.0000392239.91165.65 (Accessed: 30 April 2020).

Neel, M.C., McGarigal, K. and Cushman, S.A. (2004) 'Behavior of class-level landscape metrics across gradients of class aggregation and area', *Landscape Ecology*, 19(4) Springer, pp. 435–455. Available at: 10.1023/B:LAND.0000030521.19856.cb (Accessed: 4 May 2020).

Office for National Statistics (2013) 2011 census, Key statistics for built up areas in England and Wales (report). United Kingdom Office for National Statistics, London.

Oke, T.R. (1976) 'The distinction between canopy and boundary-layer urban heat islands', *Atmosphere*, 14(4) Taylor & Francis Group, pp. 268–277. Available at: 10.1080/00046973.1976.9648422 (Accessed: 30 April 2020).

Perini, K., Chokhachian, A., Dong, S. and Auer, T. (2017) ‘Modeling and simulating urban outdoor comfort: Coupling ENVI-Met and TRNSYS by grasshopper’, *Energy and Buildings*, 152 Elsevier Ltd, pp. 373–384. Available at: 10.1016/j.enbuild.2017.07.061 (Accessed: 7 September 2020).

Perkins, S.E., Alexander, L. V. and Nairn, J.R. (2012) ‘Increasing frequency, intensity and duration of observed global heatwaves and warm spells’, *Geophysical Research Letters*, 39(20) Blackwell Publishing Ltd, p. 2012GL053361. Available at: 10.1029/2012GL053361 (Accessed: 30 April 2020).

Puth, M.-T., Neuhäuser, M. and Ruxton, G.D. (2015) ‘Effective use of Spearman’s and Kendall’s correlation coefficients for association between two measured traits’, *Animal Behaviour*, 102 Academic Press, pp. 77–84. Available at: 10.1016/j.anbehav.2015.01.010 (Accessed: 13 August 2020).

Ramyar, R., Zarghami, E. and Bryant, M. (2019) ‘Spatio-temporal planning of urban neighborhoods in the context of global climate change: Lessons for urban form design in Tehran, Iran’, *Sustainable Cities and Society*, 51 Elsevier Ltd, p. 101554. Available at: 10.1016/j.scs.2019.101554 (Accessed: 3 May 2020).

Romero Rodríguez, L., Sánchez Ramos, J., Sánchez de la Flor, F.J. and Álvarez Domínguez, S. (2020) ‘Analyzing the urban heat Island: Comprehensive methodology for data gathering and optimal design of mobile transects’, *Sustainable Cities and Society*, 55 Elsevier Ltd, p. 102027. Available at: 10.1016/j.scs.2020.102027 (Accessed: 3 May 2020).

Schwarz, N., Schlink, U., Franck, U. and Großmann, K. (2012) ‘Relationship of land surface and air temperatures and its implications for quantifying urban heat island indicators - An application for the city of Leipzig (Germany)’, *Ecological Indicators*, 18, pp. 693–704. Available at: 10.1016/j.ecolind.2012.01.001 (Accessed: 14 November 2017).

Simwanda, M., Ranagalage, M., Estoque, R.C. and Murayama, Y. (2019) ‘Spatial Analysis of Surface Urban Heat Islands in Four Rapidly Growing African Cities’,

Remote Sensing, 11(14) MDPI AG, p. 1645. Available at: 10.3390/rs11141645 (Accessed: 8 May 2020).

Sodoudi, S., Zhang, H., Chi, X., Müller, F. and Li, H. (2018) 'The influence of spatial configuration of green areas on microclimate and thermal comfort', *Urban Forestry & Urban Greening*, 34 Urban & Fischer, pp. 85–96. Available at: 10.1016/j.ufug.2018.06.002 (Accessed: 12 August 2019).

Spearman, C. (1904) 'The Proof and Measurement of Association between Two Things', *The American Journal of Psychology*, 15(1) JSTOR, p. 72. Available at: 10.2307/1412159 (Accessed: 11 August 2020).

Stewart, I.D. and Oke, T.R. (2012) 'Local climate zones for urban temperature studies', Bulletin of the American Meteorological Society, 93(12) *American Meteorological Society*, pp. 1879–1900. Available at: 10.1175/BAMS-D-11-00019.1 (Accessed: 25 July 2020).

United Nations, Department of Economic and Social Affairs, P.D. (2019) World Urbanization Prospects The 2018 Revision.

Wouters, H., De Ridder, K., Poelmans, L., Willems, P., Brouwers, J., Hosseinzadehtalaei, P., Tabari, H., Vanden Broucke, S., van Lipzig, N.P.M. and Demuzere, M. (2017) 'Heat stress increase under climate change twice as large in cities as in rural areas: A study for a densely populated midlatitude maritime region', *Geophysical Research Letters*, 44(17) Blackwell Publishing Ltd, pp. 8997–9007. Available at: 10.1002/2017GL074889 (Accessed: 30 April 2020).

Wu, H., Ye, L.P., Shi, W.Z. and Clarke, K.C. (2014) 'Assessing the effects of land use spatial structure on urban heat islands using HJ-1B remote sensing imagery in Wuhan, China', *International Journal of Applied Earth Observation and Geoinformation*, 32(1) Elsevier B.V., pp. 67–78. Available at: 10.1016/j.jag.2014.03.019 (Accessed: 8 May 2020).

Wu, Z. and Ren, Y. (2019) 'A bibliometric review of past trends and future prospects in urban heat island research from 1990 to 2017', *Environmental*

Reviews, 27(2) Canadian Science Publishing, pp. 241–251. Available at: 10.1139/er-2018-0029 (Accessed: 3 May 2020).

Xu, G., Zhu, X., Tapper, N. and Bechtel, B. (2019) 'Urban climate zone classification using convolutional neural network and ground-level images', *Progress in Physical Geography*, 43(3) SAGE Publications Ltd, pp. 410–424. Available at: 10.1177/0309133319837711 (Accessed: 9 September 2020).

Yin, C., Yuan, M., Lu, Y., Huang, Y. and Liu, Y. (2018) 'Effects of urban form on the urban heat island effect based on spatial regression model', *Science of The Total Environment*, 634 Elsevier B.V., pp. 696–704. Available at: 10.1016/j.scitotenv.2018.03.350 (Accessed: 22 May 2020).

Yow, D.M. (2007) 'Urban Heat Islands: Observations, Impacts, and Adaptation', *Geography Compass*, 1(6) Wiley, pp. 1227–1251. Available at: 10.1111/j.1749-8198.2007.00063.x (Accessed: 31 August 2020).

Zawadzka, J., Corstanje, R., Harris, J. and Truckell, I. (2020) 'Downscaling Landsat-8 land surface temperature maps in diverse urban landscapes using multivariate adaptive regression splines and very high resolution auxiliary data', *International Journal of Digital Earth*, 13(8) Taylor & Francis, pp. 899–914. Available at: 10.1080/17538947.2019.1593527 (Accessed: 17 April 2019).

Zhou, G., Wang, H., Chen, W., Zhang, G., Luo, Q. and Jia, B. (2020) 'Impacts of Urban land surface temperature on tract landscape pattern, physical and social variables', *International Journal of Remote Sensing*, 41(2) Taylor and Francis Ltd., pp. 683–703. Available at: 10.1080/01431161.2019.1646939 (Accessed: 8 May 2020).

Zhou, W., Huang, G. and Cadenasso, M.L. (2011) 'Does spatial configuration matter? Understanding the effects of land cover pattern on land surface temperature in urban landscapes', *Landscape and Urban Planning*, 102(1), pp. 54–63. Available at: 10.1016/j.landurbplan.2011.03.009 (Accessed: 8 May 2020).

4 CHAPTER FOUR

Unravelling the relationship between land surface temperature of individual land cover patches and spatial configuration of urban form

J.E. Zawadzka[1]*, R. Corstanje[1], J.A. Harris[1]

[1]*Centre for Environmental and Agricultural Informatics, School of Water, Energy and Environment, Cranfield University, Bedfordshire, UK*

*Corresponding author: joanna.zawadzka@cranfield.ac.uk

Intended for submission to Landscape Ecology journal

Abstract

Context

Recommendations regarding excess heat mitigation to urban planners issued from research linking spatial configuration of urban form to coarse resolution land surface temperature (LST) data are relevant to city districts and not micro-scales.

Objectives

To identify spatial configuration descriptors (SCDs) of urban form and the size of zone of influence conducive to the formation of the coldest and hottest land cover patches of different types (buildings, grass, paved and trees) from 2m resolution land cover and 2 and 100m resolution LST maps at two time-steps in the summer.

Methods

Random Forest regression models were deployed to explain the LST of individual land cover patches of different types based on SCDs of core land cover patches and patches in their neighbourhoods. ANOVA was used to determine significantly different means of most important SCDs associated with the coldest and hottest

land cover patches, and analysis of quartiles informed specification of their ranges.

Results

Urban form in the immediate neighbourhood to core land cover patches had a strong influence on their LST, with low elevation, high proximity to water and high aggregation of trees conducive to the formation of the coldest patches of all types. Elevation and proximity to water gained in importance as summer progressed. Spatial configuration of urban form best described the LST of buildings; LST of grass was least accurately represented in our approach. LST of the least aggregated land cover patches was most accurately described across all land cover types considered here. High resolution of LST contributed to higher accuracy of the results, especially for more aggregated land cover patches.

Conclusions

Spatial configuration of urban form in the nearest proximity to individual land cover patches and use of fine resolution LST data are essential for issuing heat mitigation recommendations to urban planners relevant to micro-scales.

Keywords: land surface temperature, spatial configuration of urban form, random forests, micro-scales

4.1 Introduction

The thermal urban environment has been widely studied in the context of the urban heat island (Oke, 1976) effect, occurring when air temperature is consistently higher in urban areas than in their rural surroundings, due to its implications on human health (Heaviside, Macintyre and Vardoulakis, 2017; Heaviside, Vardoulakis and Cai, 2016), ecology (Yow, 2007), and energy use (Santamouris et al. 2015). Air temperature can be approximated by land surface temperature (LST) (Sheng, Lu and Huang, 2015), measurements of which are readily available through remotely sensed satellite imagery, with images at 30 to 120m resolution acquired from Landsat or 90m from ASTER satellites having been most frequently used in studies relating urban LST to 2D or 3D spatial

configuration and composition of urban landscapes, e.g. Connors et al. (2013); Chen et al. (2014); Zhou et al. (2020); Sun et al. (2020). Whilst these studies, due to the coarse spatial resolution of the LST imagery, focus on explanation of the LST within relatively large and variedly defined subdivisions of towns, they may lack in sufficient detail regarding spatial configuration of individual land cover patches contributing to thermal comfort outdoors (Li et al., 2020c; Perini et al., 2017) or within building interiors (Futcher, Kershaw and Mills, 2013; Garshasbi et al., 2020), relevant to microscales rather than neighbourhoods or city districts. The use of fine resolution land cover data in studies relating spatial configuration of urban form and LST has been recommended (Li, Zhou and Ouyang, 2013; Liu et al., 2016) due to their ability to accurately represent fragmented urban landscapes leading to an increased robustness of the analyses, however, the use of equally fine resolution LST imagery has never been investigated in this context.

Therefore, the overarching objective of this work is to address the spatial scale limitations of previous studies by exploring the relationship between spatial configuration descriptors of urban form and LST at a rare fine spatial resolution of 2m, both for LST and land cover data, enabling focus on individual land cover patches rather than larger fragments of towns, and providing a link between coarse- and micro-scale studies, the latter only possible for small areas at a time (Ramyar, Zarghami and Bryant, 2019). We placed a particular interest in the determination of spatial configuration conditions associated with the formation of the coldest and hottest land cover patches, defined through clustering of LST values across the study area. We hypothesise that (1) spatial configuration properties of both the core land cover patches as well as the properties of land cover located in their neighbourhoods are the determining factors of temperature of the core patches, (2) urban form patterns conducive to the formation of the coldest and hottest land cover patches change as the summer progresses, and (3) a set of spatial configuration rules exists that can guide planning and urban design for better thermal regulation of the cities in the summer. Additionally, we determine the optimal neighbourhood size and spatial resolution of LST imagery for patch-orientated studies. The assessment is carried out over a very large representative sample of urban form patterns collected throughout three British

suburban towns and their thermal properties are approximated by land surface temperature captured on two summer days a month apart. Focus on an explanation of LST of individual land cover patches, rather than areas of a city, a very high resolution of LST data, and inclusion of several rarely used spatial configuration descriptors constitute novelty of our approach.

4.2 Materials and Methods

4.2.1 Study Area

The study area comprises three towns located in relatively close proximity in England: Milton Keynes (52°0′N, 0°47′W, appr. 122 km^2), Bedford (52°8′N, 0°27′W, appr. 60 km^2), and Luton/Dunstable (51°52′N, 0°25′W, appr. 86 km^2) (Figure 4-1) with population of 229,941, 106,940, and 258,018 (Office for National Statistics (2013) respectively and a temperate oceanic climate according to the Köppen–Geiger climate classification system. The three towns are characterised with contrasting histories: modern-day garden-city, medieval, and industrial, respectively, collectively representing a wide range of urban form patterns, described in more detail in Grafius et al. (2016) and Zawadzka, Harris and Corstanje (2020).

4.2.2 Data

The data used in this study comprise several datasets derived and described in previous work: very high spatial resolution (2m) LST maps downscaled from Landsat 8 TIR imagery for 6th June and 8th July 2013 using statistical methods Zawadzka et al., 2020), land cover map showing the distribution of five main land cover types at 2m spatial resolution (Grafius et al., 2016), Figure 4-1, and a map of land cover subtypes obtained from two-tiered K-means clustering analysis of selected landscape metrics and LST to yield land cover patches classified according to their spatial configuration and temperature (Zawadzka, Harris and Corstanje, 2020). Additionally, this study makes use of elevation represented by a digital surface model, and feature height data at 2m resolution derived from NERC-ARSF Leica ALS50-II LiDAR survey carried out over the three towns (Grafius et al., 2016), as well as Landsat 8-derived LST image at its original

spatial resolution of 100m, being in fact placed somewhere between 30m and 100m due to resampling carried out by USGS – Landsat data provider.

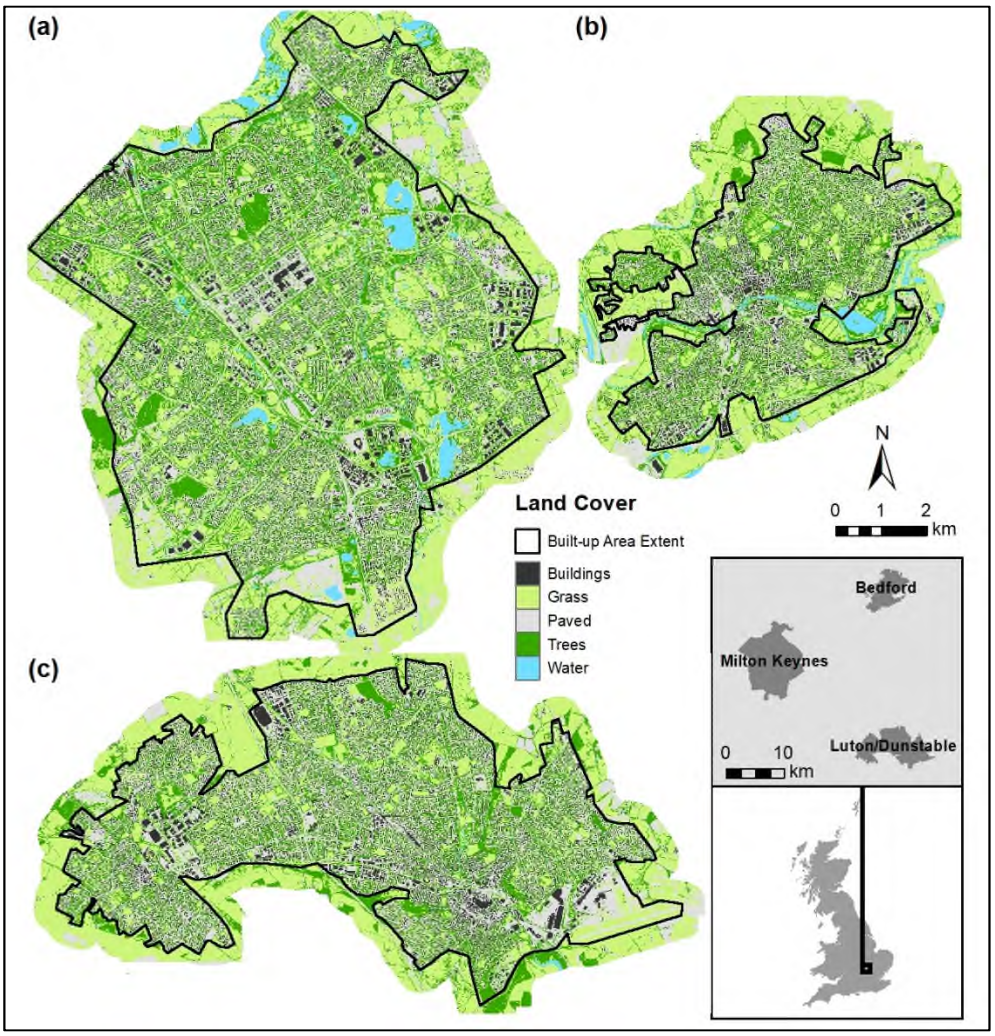

Figure 4-1 Land cover in (a) – Milton Keynes, (b) – Bedford, (c) – Luton/Dunstable. The insert depicts location of the towns within Great Britain. Analyses were carried out for areas within the 'Built-up Area Extent' boundary. Source of image: Zawadzka, Harris and Corstanje (2020).

4.2.3 Methods

The methodology for elucidation of the relationships between the coldest and the hottest land cover subtypes and spatial configuration of urban form can be summarised in three major steps: 1) generation of land cover subtype patches that are characterised with the highest and lowest LST in June and July,

2) identification of the most important spatial configuration descriptors influencing the formation of the hottest and coldest patches of a given land cover sub-type and the distance at which patches located in the neighbourhood can influence the LST of the core patches, and 3) analysis of the most important spatial configuration descriptors of urban form associated with the coldest and hottest land cover subtype patches over the course of a warming summer (Figure 4-2).

Land cover subtype patches were derived separately for each land cover type (buildings, grass, trees, paved and water) by k-means clustering of class-level landscape metrics: COHESION, PLADJ and LSI (McGarigal and Marks 1995) to yield Tier 1 subdivisions of the main land cover types with distinct spatial and thermal properties (Table Apx C-1). Thus formed land cover subtype patches were attributed with means of LST for June and July and further subdivided through Tier 2 k-means clustering to determine these land cover subtype patches that had the highest, intermediary, and lowest LST at both time steps.

Due to a vast number of individual cluster patches across the three towns (circa 2 million subsampling at a rate of 10% of the total number of each Tier 2 clusters was necessary, and was implemented through conditioned Latin hypercube method (cLHS) (Minasny and McBratney, 2006) available in clhs R package (Roudier, 2011). The cLHS method allowed for the creation of a representative sample of all spatial configuration and thermal properties of land cover subtype patches taken into account in this study, which included spatial aggregation metrics, elevation, height, area, and distance to land cover patches of different types (Table 4-1).

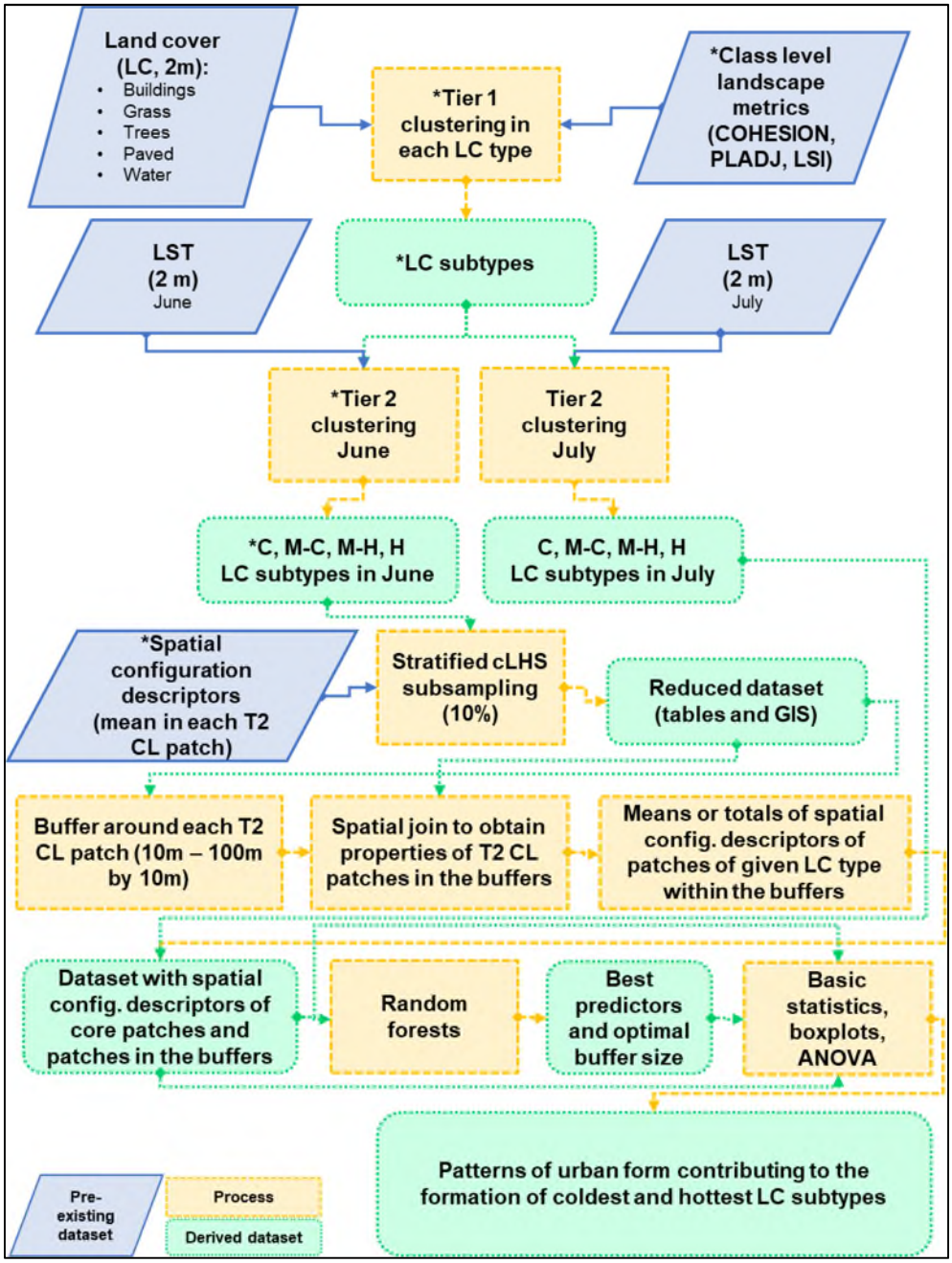

Figure 4-2 Overview of the methodology applied to elucidate the relationship between spatial configuration of urban form and the formation of the coldest and hottest LC sub-type patches. LC – land cover, cLHS – conditioned latin hypercube sampling, T1 – Tier 1, T2 – Tier 2, CL – cluster, C – cold, M-C – medium cold, M-H – medium hot, H – hot, GIS – Geographical Information Systems, COHESION – cohesion index, LSI – landscape shape index, PLADJ – percentage of like adjacencies index; *refers to methodology steps described in detail in Zawadzka, Harris and Corstanje (2020).

Quantification of the impact of spatial configuration of urban form on LST of land cover subtype patches required that spatial configuration properties of land cover patches located in the neighbourhood of the core patches were known. This was achieved by deriving ten buffer zones of varied sizes (starting at 10m and ending at 100m, every 10m) around a subsample of each Tier 2 cluster, except for water (Figure 4-3). Spatial join was carried out between feature classes representing maps of Tier 1 clusters and buffer zones to identify those Tier 1 clusters that intersected with each buffer zone. All GIS operations were implemented in ArcMap 10.6. Since the unique ID number of the core Tier 1 patches was known, it was then possible to link the spatial properties of the core patches to the properties of patches in their neighbourhoods in a one to many relationship. This table was subsequently transformed so that each core land cover cluster patch was attributed with sums or means of properties of land cover type patches in the neighbourhood, depending on the descriptor type (Table 4-1).

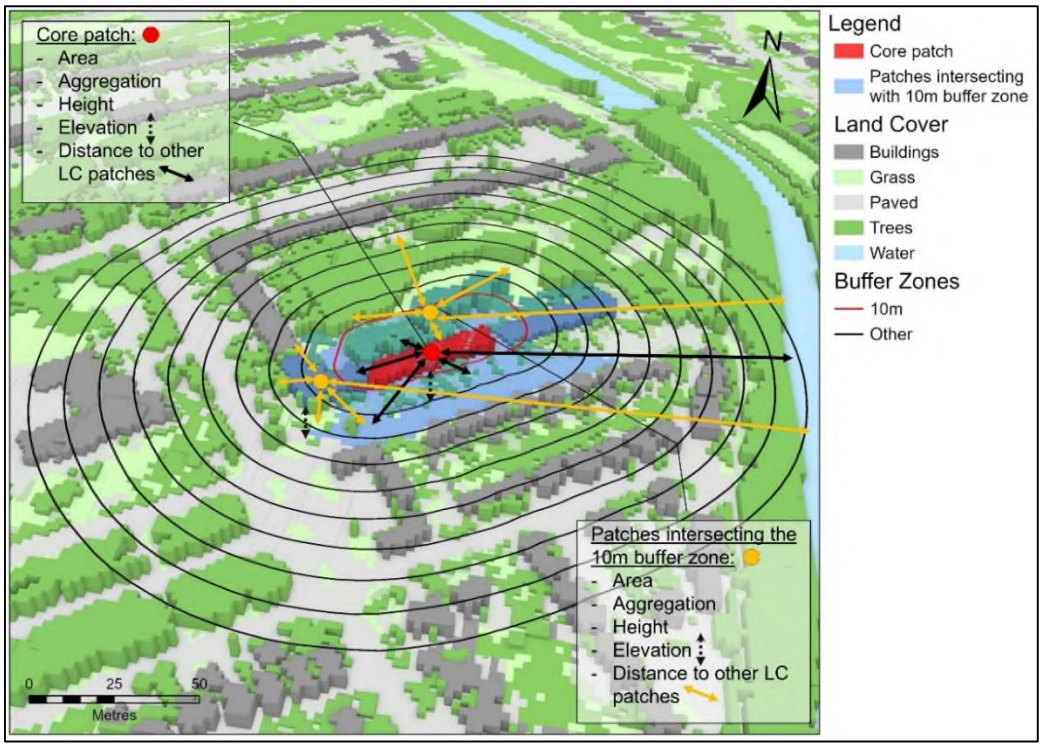

Figure 4-3 Conceptual model of urban form implemented mathematically in this study to elucidate the relationship between LST of core land cover (LC) patches of different types and spatial configuration of urban fabric, represented here by real data for a location in Milton Keynes.

Table 4-1 Type, categories and groups of metrics used to mathematically represent the conceptual model of urban form as well as summarise the outcomes of LST modelling. AGG – aggregation, DIST – distance, ELEV – elevation, FH – feature heights, c – core, bf – buffer, LC – land cover, b – buildings, g – grass, p – paved, t – trees, COH – cohesion index, LSI – landscape shape index, PLADJ – proportion of like adjacencies. n/a refers to instances where further subdivisions added unnecessary complexity to the interpretation of the results.

Type	Category	Group	Data source	Method	Unit
Aggregation	Aggregation of the core patch: c_AGG	n/a	LC map at 2m resolution (raster)	Fragstats class level metrics (COH, LSI PLADJ), 100m x 100m moving window analysis, 4-cell neighbourhood rule, (Zawadzka et al. In Review)	COH [%] LSI [n/a] PLADJ [%]
	Aggregation of non-specific LC types in the buffer zone: bf_AGG	Aggregation of specific LC types in the buffer zone, e.g. buildings: b_bf_AGG			
Area	Area of the core patch: c_AREA	n/a	Tier 1 k-means clusters (LC subtypes) (vector)	Area of polygons (ArcGIS 10.6)	metre squared [m^2]
	Area of non-specific LC types in the buffer zone: bf_AREA	Area of specific LC types in the buffer zone, e.g. grass: g_ bf_AREA			
Distance	Distance of the core patch to any LC type c_DIST	Distance of core patch to a specific LC type, e.g. paved: c_DIST_p	LC map at 2m resolution (raster)	'Euclidean Distance' tool, ArcGIS 10.6, values averaged over Tier 1 cluster patches (LC subtypes)	metre [m]
	Distance of non-specific LC types to any LC type in the buffer zone: bf_DIST	Distance of any LC type in the buffer zone to a specific LC type, e.g. trees: LC_bf_DIST_t			
Elevation	Elevation of the core patch: c_ELEV	n/a	LiDAR survey	Digital elevation model (2m spatial resolution)	metre [m]
	Elevation of non-specific LC types in the buffer zone: bf_ELEV	n/a			
Feature heights	Feature height of the core patch: c_FH	n/a		Feature heights extracted from digital surface model (2m spatial resolution)	
	Feature height of non-specific LC types in the buffer zone: bf_FH	n/a			

The best spatial configuration descriptors of urban form for the explanation of LST of land cover patches in June and separately in July were identified through Random Forests (RF) models (Breiman, 2001) implemented in the 'ranger' R package (Wright and Ziegler 2017). RF models were constructed for all clusters in each land cover type (RF_{ALL}), except for water, and separately for each land cover subtype (LA – least aggregated, RLA – relatively less aggregated, RMA – relatively more aggregated and MA – most aggregated), allowing for the determination of specific conditions for the explanation of LST in

core patches with different spatial properties. Models were constructed with inclusion of the three subsets of spatial configuration descriptors: 1) spatial configuration descriptors of core land cover patches only, 2) core land cover patches and land cover patches intersecting with buffer zones of different sizes, 3) land cover patches in buffer zones only. Out of bag R^2 and root mean square error (RMSE) metrics were used to determine the predictive power of the models, the size of the neighbourhoods with the most significant impact on LST in the core land cover patches, and the spatial resolution of LST imagery (2m vs 100m) yielding more accurate results.

The most important spatial configuration descriptors of urban form influencing LST of land cover patches were identified through the calculation of the percentage of the total variance explained by a given model that could be attributed to each predictor. Given a very large number of descriptors taken into account (up to 66 for models constructed with the properties of the core patches and patches intersecting with the buffer zones), these were grouped together hierarchically, as shown in Table 4-1, to further facilitate the discussion of the results. The groups comprised up to three levels: *predictor type*, i.e. properties related to patch area, aggregation, distance to other patches, elevation, and height, *predictor category*, i.e. distinction between properties of core patches or patches intersecting with a buffer zone, and *group*, specifying the type of land cover patch, where appropriate.

Once the most important predictors of LST were identified, their values were analysed to determine specific spatial configuration conditions for the formation of the coldest (C), medium-cold (M-C), medium-hot (M-H) and the hottest (H) Tier 2 clusters (Table Apx C-1) derived for June and July within each land cover subtype (Tier 1 cluster), with a particular emphasis on the coldest and hottest land cover patches. This was achieved through pairwise Wilcoxon ANOVA analysis of basic statistics (min, max, mean, median, 25^{th} and 75^{th} quantile) as well as a visual comparison through boxplots. These analyses were carried out in R, using ‘stats’, ‘psych’ and ‘ggplot2’ packages respectively (R core team, Revelle (2019), Wickham (2016)).

4.3 Results

4.3.1 Impact of core LC type and subtype on LST

The impact of core patch land cover type and subtype on the ease of prediction of LST using the conceptual model of spatial configuration of urban form implemented in this study was assessed by the R^2 and RMSE model performance metrics for $RF_{c+bf10m}$ models predicting LST at 2m spatial resolution (Figure 4-4) under an assumption that better model performance is indicative of better explanatory capacity of our approach to LST of given LC type and subtype. Whilst average R^2 values for $RF_{LA\text{-}RLA\text{-}RMA\text{-}MA}$ models, excluding ALL to avoid bias resulting from different numbers of land cover subtype patches incorporated in each model, for each land cover type did not differ greatly between different land cover types (0.84-0.86 in June and 0.87-0.90 in July), RMSE had a wider spread of values. LST of buildings was best explained in our analysis, having the lowest overall RMSE of 0.78K in June and 0.76K in July. LST of grass was least accurately explained (RMSE of 1.04K and 1.00K respectively). Random forest models constructed for LST of paved (0.93K and 0.89K) and trees (0.97K and 0.94K) had the intermediate levels of accuracy, indicating that LST of built-up rather than green spaces was better represented in our approach.

The accuracy of predictions of LST within land cover subtypes differed with the overall aggregation level of land cover patches and displayed a common trend such that small and fragmented least aggregated (LA) land cover patches had a lower RMSE and higher R^2 than the largest and most aggregated (MA) ones. An exception to this rule was the LA subtype in paved representing mostly footpaths located near greenspaces, with LST prediction error being higher than that of residential roads (RLA), likely caused by a difficulty of accurately representing these narrow and elongated features at 2m spatial resolution.

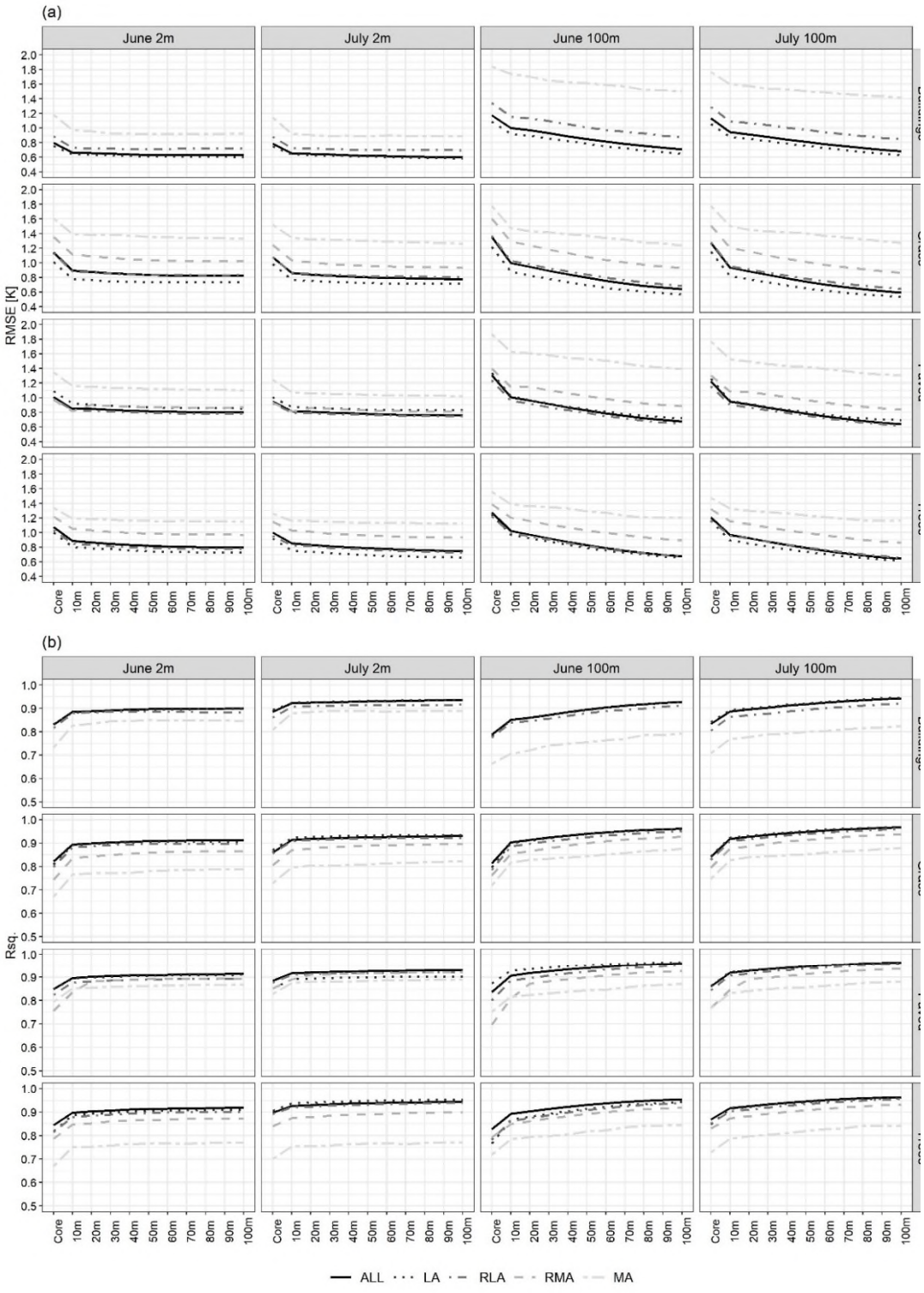

Figure 4-4 Root mean square error (a) and R^2 (b) obtained from RF models relating LST at two dates (June and July 2013) and spatial resolutions (2m and 100m) to spatial configuration descriptors for all patches of a given LC type (ALL) and separately for LC patches contained within Tier 1 clusters (LA – least aggregated, RLA – relatively less aggregated, RMA – relatively more aggregated, MA – most

aggregated). 'Core' refers to models constructed with spatial configuration descriptors for core patches only, whilst 10m, etc., indicate models with the addition of patches intersecting with consecutive zones around the core patches.

4.3.2 LST and scale effects

The relationship between LST of various land cover types and sub-types and spatial configuration of urban form was considered in the context of multiple scale effects: 1) the spatial resolution of LST imagery, 2) the distance over which spatial configuration of land cover impacts the LST of the core patches, and 3) temporal scales.

4.3.2.1 Spatial resolution of LST imagery

The difference between RMSE errors (Figure 4-4) for random forest models predicting LST at 2m and 100m spatial resolution in June varied in magnitude depending on land cover type, subtype and neighbourhood size. In all cases in June, RMSE for LST at 2m resolution in buildings was lower by 0.05 up to 0.77K and tended to decrease with increasing neighbourhood size. For the remaining land cover types (grass, trees and paved), the neighbourhood size influenced the sign of the difference between RMSE at both spatial resolutions – predictions of LST at 2m resolution tended to be more accurate with inclusion of spatial configuration properties of land cover patches intersecting with zones up to 30m to 60m away from core land cover patches, depending on the subtype of the core land cover patches. Here, the predictions at 2m resolution were more accurate by 0.43 to 0.02K at smaller neighbourhood sizes and predictions at 100m resolution were more accurate by 0.07 to 0.18K at larger neighbourhoods. Trends observed for predictions in July were very similar and involved improvement of predictions for LST at 100m over 2m resolution with the increasing neighbourhood size.

4.3.2.2 Neighbourhood size

Model performance metrics (R^2 and RMSE, Figure 4-4) indicated that in all cases inclusion of spatial properties of land cover patches located in the neighbourhood improved the predicting power of the LST of core patches. In fact,

models constructed without spatial properties of the core land cover patches performed comparably to the equivalent models for which spatial properties of core patches were included (Figure Apx C-1), suggesting that the surroundings of the individual land cover patches play a pivotal role in LST regulation. In all cases, the sharpest increase in R^2 and reduction in RMSE occurred at the inclusion of the spatial configuration properties of land cover patches intersecting with the 10m buffer zone, and the incremental improvement due to increases in the neighbourhood size that followed was negligible at 2m resolution, and more pronounced at 100m resolution. This suggests that the most immediate surroundings have the largest impact on the LST of land cover patches and consequently, further discussion of the most important spatial configuration descriptors will be based on data for models constructed for the 10m neighbourhood.

4.3.2.3 Temporal scales

The magnitudes of R^2 returned by the models predicting the LST of core land cover patches using spatial configuration descriptors of core patches and patches in the 10m neighbourhood in June and July showed that models constructed with data for July explained comparable but higher amounts of LST variance, with R^2 ranging between 0.75 to 0.90 in June and 0.75 to 0.94 in July at 2m spatial resolution. Comparable RMSE values were also achieved – 0.64 to 1.40K and 0.64 to 1.34K respectively, suggesting that as far as the overall impact of spatial configuration of urban form on LST of individual land cover patches is concerned, the relationships are maintained at two time steps a month apart during a warm (non-heatwave) summer in an intermediate climate.

4.3.3 Relationship between spatial configuration of urban form and LST of LC patches

4.3.3.1 Spatial configuration predictors determining LST in June and July

Analysis of the percentage of the total variance explained by $RF_{c+bf10m}$ models by spatial configuration descriptors (Figures Apx C-4 to C-6) grouped into the main predictor categories (Figure 4-5) shows that spatial properties of land cover patches intersecting with the 10m buffer zone had a greater LST explanatory

power than the properties of the core patches. Out of these, elevation, aggregation and distances to other land cover types had the best explanatory power, with order alternating somewhat between land cover type, subtype and date, and elevation gaining distinctly in importance as summer progressed. Core patch height and area, on the other hand, had consistently the lowest explanatory power of LST, with the remaining categories of predictors having an intermediary impact, which was still distinctly lower than that of the top three predictor categories.

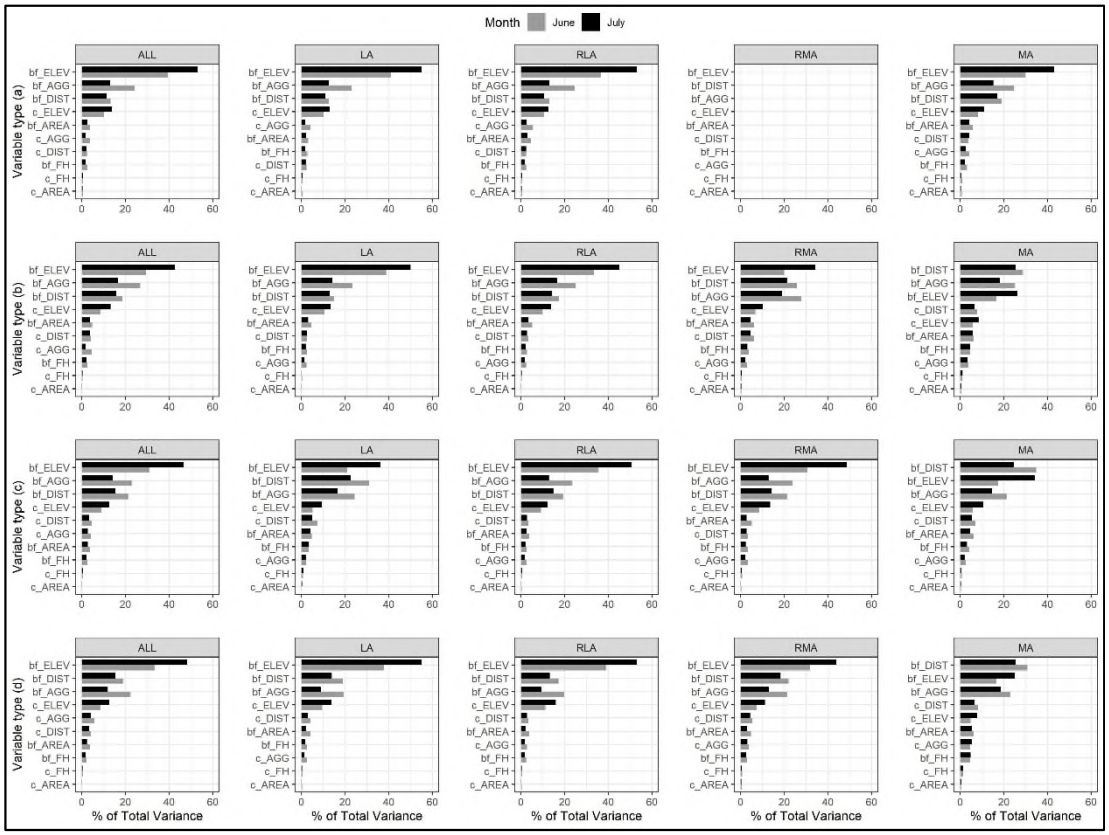

Figure 4-5 **Percentage of the total variance of LST in (a) buildings, (b) grass, (c) paved, (d) trees explained by RF models attributed to the main LST predictor categories (Table 4-1) in June and July at 2m spatial resolution. Predictors are sorted by the decreasing mean percentage of the total variance explained for the two dates.**

Predictor groups indicate specific land cover type for which a given predictor category was derived (Figures Apx C-2a and C-2b). In buildings, spatial aggregation of land cover patches, and especially of neighbouring trees, were the

most important LST predictors after elevation. Distance to water was also important for explanation of LST of the LA and MA buildings, with distance to buildings gaining in importance for the MA buildings as well. Whilst feature heights were generally of lesser importance, in the case of the LA buildings heights of buildings and trees located in the immediate proximity to the core buildings stood out as more important when compared to other buildings subtypes (Figure Apx C-3).

Apart from elevation, aggregation of trees and distance to buildings of neighbouring land cover patches were the most important LST descriptors in grass, with exception of the LA grass patches for which distance to buildings was less important than aggregation of paved patches or distance to water, the latter two being important for explanation of LST in all subtypes of grass patches as well.

In paved land cover patches, besides elevation, distance of neighbouring land cover types to buildings and aggregation of trees were important spatial configuration descriptors, with the former being more important for the LA and MA patches and the latter for the RLA and RMA patches. Here, other important factors included distance to water as well as aggregation of neighbouring grass patches and buildings.

Apart from elevation, distance to water and distance to buildings were important LST predictors for patches of trees, with aggregation of other LC types remaining quite important. Order of importance varied somewhat between tree patches' subtypes, with distance to buildings being more important for the RMA and MA whilst aggregation of grass for the LA and RLA tree patches.

4.3.3.2 Spatial configuration of urban form conducive to the formation of coldest and hottest LC patches

Spatial configuration patterns of urban form conducive to the formation of coldest and hottest land cover patches (Tier 2 clusters) within a given land cover subtype (Tier 1 clusters) in June and July were determined through identification of LST predictors with statistically significant means within each Tier 2 cluster, via the ANOVA analysis, as well as non-overlapping ranges between first and third

quartiles for the coldest and hottest clusters. Whilst selected ranges are shown in Table 4-2, means and standard deviations as well as results of the ANOVA analysis are shown in Table Apx C-2 and Figures Apx C-7 to C-37.

Elevation was an important discerning factor of the hottest clusters, which were typically located above 112-152m a.s.l. depending on land cover type and subtype. The coldest patches of buildings, grass and paved were associated with highly aggregated patches of trees intersecting with the 10m buffer zone, with PLADJ greater than 73 to 85% and COHESION greater than 93 to 97%, and buildings requiring somewhat lower aggregation levels than grass or paved. Thehottest patches of these land cover types were associated with PLADJ smaller than 63-69% and COHESION smaller than 83-87%. Aggregation level of grass patches in the buffer zone was a discerning factor of the coldest patches of LA and RLA and the coldest and hottest RMA and MA patches of trees. The coldest tree patches were located next to highly aggregated grass patches with PLADJ greater than 67-84% and COHESION greater than 84-94%. The hottest RMA and MA tree patches were associated with less aggregated patches of grass, with PLADJ of less than 53-62% and COHESION less than 70-80%. Aggregation level of paved patches, with some exceptions, was associated with the formation of the coldest and hottest patches of buildings, grass, and trees, with coldest patches of these land cover types being associated with PLADJ smaller than 69-79% and hottest patches with PLADJ greater than 77-87%. In all cases, an increasing trend in aggregation of trees, grass or paved associated with the coldest and hottest patches was observed as the aggregation level of core patches increased, and no major differences between months were observed. The hottest and coldest building patches of a given subtype could also be discerned based on the aggregation level of core buildings and buildings located in the buffer zone, with LSI associated with the coldest buildings indicating a higher aggregation level than that of the hottest buildings. Aggregation level of buildings in the 10m buffer zone was a discerning factor for the coldest and hottest clusters of paved patches, with the coldest patches being associated with more aggregated buildings indicated by LSI smaller than 3.2-4.5 and hottest patches – with less aggregated buildings, with LSI greater than

3.8-6.2. Visual examples of spatial patterns of land cover conducive to the formation of the hottest and coldest buildings are shown in Figure 4-6.

When distance to water is concerned, the coldest clusters of all land cover patches types and subtypes were associated with closer proximity to water bodies than the hottest ones, ranging from less than 46-166m and more than 399-676m respectively. More aggregated subtypes of land cover patches were typically associated with a closer proximity to water, both for the coldest and hottest patches, than the less aggregated ones. Distances to buildings were also helpful in discerning the coldest patches of grass, paved and trees, which were formed farther away from buildings, and the distance increased with the increasing aggregation level of these land cover types, ranging from 8 to 86m. Distance to buildings of less than 6-16m could only be used to discern the hottest MA patches of grass, trees and paved.

Table 4-2 Ranges of the selected most important descriptors of spatial configuration of urban form attributed to the coldest and hottest LC patches of different subtypes. (c) – core patch, (bf) – patches intersecting with the 10m buffer zone around (c). DT – descriptor type, SCD – Spatial configuration descriptor. NA indicates instances when ranges of a SCD overlapped making the distinction between cold and hot clusters impossible.

Overall aggregation level of core LC			Least aggregated				Relatively less aggregated				Relatively more aggregated				Most aggregated			
DT	SCD	Core LC	June		July		June		July		June		July		June		July	
			C	H	C	H	C	H	C	H	C	H	C	H	C	H	C	H
Elevation	Elevation (c) [m]	Buildings	NA	NA	NA	>130	NA	NA	NA	>131	-	-	-	-	NA	NA	NA	>130
		Grass	NA	>134	NA	>126	NA	>131	NA	>122	NA	>116	NA	>104	NA	>123	NA	>112
		Paved	NA	NA	NA	>95	NA	>124	NA	>126	<42	NA	NA	>130	NA	>117	NA	>123
		Trees	<74	>146	NA	NA	<75	>152	NA	NA	<73	>128	NA	>136	<75	>152	NA	>112
Aggregation	PLADJ of trees (bf) [%]	Buildings	>73	<63	>74	<64	>75	<63	>73	<61	-	-	-	-	>76	<64	>75	<61
		Grass	>73	<64	>74	<63	>79	<65	>78	<65	>84	<67	>83	<65	>85	<69	>85	<67
		Paved	>82	<67	>81	<65	>76	<63	>74	<64	>78	<64	>76	<64	>84	<66	>81	<63
	COH of trees (bf) [%]	Buildings	>94	<85	>94	<84	>93	<84	>94	<83	-	-	-	-	>91	<81	>91	<79
		Grass	>93	<86	>94	<85	>95	<86	>95	<86	>96	<86	>95	<85	>96	<87	>96	<85
		Paved	>96	<89	>96	<88	>94	<85	>93	<85	>93	<84	>93	<83	>95	<83	>94	<81
	PLADJ of grass (bf) [%]	Trees	>67	NA	>74	NA	>67	<48	>68	NA	>77	<53	>77	<54	>81	<60	>81	<62
	COH of grass (bf) [%]	Trees	>84	NA	>90	NA	>83	NA	>83	NA	>91	<70	>91	<71	>94	<79	>94	<80
	PLADJ of paved (bf) [%]	Buildings	<70	>77	<70	>77	<72	>80	<72	>80	-	-	-	-	<80	>87	<79	>87
		Grass	<70	>78	<70	>79	NA	>80	NA	>79	NA	>82	<71	>83	<69	>83	<69	>85
		Trees	<72	>80	<72	NA	<70	>79	<70	>79	NA	>81	<69	NA	<72	>85	<71	NA
	LSI (c) [-]	Buildings	<5.1	>6.4	<5.1	>6.5	<4.0	>5.5	<4.1	>5.5	-	-	-	-	<2.1	>3.5	<2.2	>3.5
	LSI of buildings (bf) [-]	Buildings	<5.1	>6.4	<5.1	>6.4	<4.1	>5.5	<4.1	>5.6	-	-	-	-	<2.2	>3.6	<2.2	>3.6
		Paved	<4.2	>6	<4.5	NA	<4.5	>6.2	<4.7	>6.1	<3.2	>5.6	<3.1	>5.6	NA	>3.8	NA	>4.1

Table 4-2 Continued

Overall aggregation level of core LC			Least aggregated				Relatively less aggregated				Relatively more aggregated				Most aggregated			
DT	SCD	Core LC	June		July		June		July		June		July		June		July	
			C	H	C	H	C	H	C	H	C	H	C	H	C	H	C	H
Distance	Distance to water (c) [m]	Buildings	<150	NA	<152	>586	<165	NA	<152	>549	-	-	-	-	NA	NA	NA	>570
		Grass	<163	>632	<166	>550	<123	>586	<131	>536	<84	>453	<94	>447	<57	>455	<65	>445
		Paved	<46	>399	<62	>443	<135	>537	<147	>559	<136	>620	<139	>569	<97	>446	<104	>454
		Trees	<145	>672	<141	>616	<139	>676	<142	>689	<95	>508	<103	>547	<87	>447	<77	>428
	Distance to buildings (c) [m]	Grass	>9	NA	>10	NA	>16	NA	>16	NA	>48	NA	>45	NA	>86	<12	>87	<11
		Paved	>42	NA	>32	NA	>9	NA	>7	NA	>18	NA	>14	NA	>60	NA	>45	NA
		Trees	>9	NA	>12	NA	>10	NA	>11	NA	>34	NA	>32	NA	>72	<10	>74	<12
	Distance of trees (bf) to buildings [m]	Grass	>8	NA	>8	NA	>15	NA	>15	NA	>46	<6	>42	NA	>81	<11	>81	<10
		Paved	>39	<5	>28	NA	>9	NA	>8	NA	>18	NA	>15	NA	>59	<6	>39	<5
		Trees	>8	NA	>11	NA	>9	NA	>10	NA	>33	NA	>31	<6	>71	<14	>74	<16
	Distance of grass (bf) to buildings [m]	Grass	>9	NA	>9	NA	>15	NA	>14	<6	>48	<7	>44	<7	>86	<15	>86	<15
		Paved	>42	NA	>34	NA	>10	NA	>9	NA	>20	NA	>16	NA	>64	<7	>48	<6
		Trees	>9	NA	>13	NA	>47	NA	>11	NA	>35	NA	>33	NA	>70	<11	>75	<13

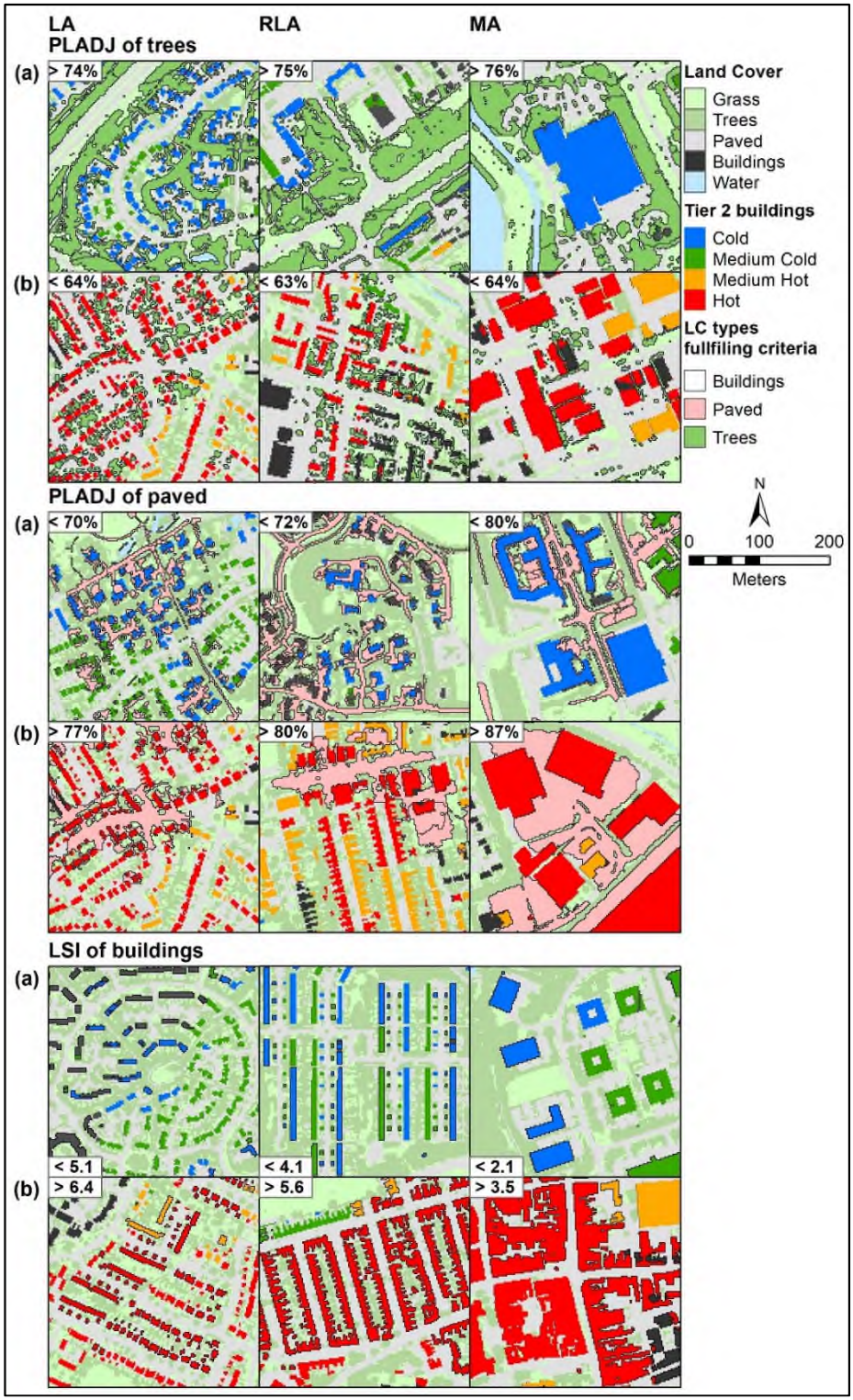

Figure 4-6 Examples of spatial configuration of trees, paved and buildings associated with the formation of the coldest (a) and hottest (b) buildings of different subtypes: LA – least aggregated, RLA – relatively less aggregated, and MA – most aggregated.

4.4 Discussion

4.4.1 Methods in data preparation and analysis

This study represents a unique approach to analysis of the relationship between LST and urban form by attempting to explain LST, through analysis of spatial configuration of urban form, of individual land cover patches rather than the LST of variously defined sub-divisions, often referred to as analytical units, of a town as is the case in similar studies, e.g. Zhou et al. (2011); Kong et al. (2014); Liu et al. (2016); Simwanda et al. (2019); Masoudi et al. (2019). This was made possible through the availability of downscaled LST imagery (Zawadzka et al., 2020) to a resolution better aligned with sharp and complex land cover boundaries typical of urban areas and consequently reducing the mixed pixel effect (Yow, 2007) between contrasting thermal responses of adjacent land cover types.

Whilst the use of analytical units in other studies, e.g. 900m blocks in Berger et al. (2017), was in part necessitated by the need to reduce the computational requirements for the analysis, we used the cLHS method to reduce the sample size without compromising the robustness of the outcomes. cLHS method analyses the feature space of a dataset to include observations at the full range of all variables, and was successfully applied to optimise sampling design in digital soil mapping, including soil modelling with random forests (Wadoux, Brus and Heuvelink, 2019), and LiDAR cloud data processing for accurate DEM generation (Chu et al., 2014).

Our data did not exhibit strong linear relationships between LST of core land cover patches and spatial configuration descriptors and as a result we used random forests models, capable of finding non-linear relationships in large non-normally distributed datasets, to identify best descriptors for LST of core land cover patches, followed by the analysis of means and quartiles to determine values of these spatial configuration descriptors contributing to a particular thermal effect in core land cover patches. This is in contrast to reported methods in other studies, where correlation and linear regression were typically adopted (Masoudi, Tan and Liew, 2019; Wang, Zhan and Ouyang, 2017) with a few

exceptions, such as random forests (Gage and Cooper, 2017; Lemus-Canovas et al., 2020) or spatial regression models (Yin et al., 2018).

The focus of this study was set not only on LST of land cover patches of a given type but also subtype, defined by the aggregation level of patches of a given type, which in most cases could be associated with different functional imprints within the study area, and allowing for bottom-up considerations regarding the relationship between urban form patterns and LST depending on predominant land use. Literature lists several other studies that have attempted to explain LST means within different functional units of cities by coupling with urban form configuration metrics, such as for example Beijing city transects aggregated into specific functional zones (Li et al., 2020b), different types of parks (Li et al., 2020a), and regulatory plan management units (Yin et al., 2018), allowing for a top-down analysis of the relationships. We propose that the bottom-up approach adopted here can provide complementary insights into the spatial arrangement of urban land cover under various uses for effective urban heat island alleviation and microclimate management by exploring urban form detail that can be missed when descriptors of heterogeneous urban form patterns and thermal responses are averaged over larger parcels of land.

4.4.2 Relationships between LST and spatial configuration descriptors

4.4.2.1 Spatial scale effects

Slopes of curves depicting RMSE of random forest models predicting LST of patches vs increasing size of buffer zones displayed the highest enhancement in accuracy at the 10m mark for LST data at both 2m and 100m resolutions, nearly levelling off for the former and continuing to drop for the latter, without a clear levelling-off effect at the maximum buffer zone size of 100m considered here. The effect for 100m resolution LST data is consistent with continuously increasing correlation coefficients between Landsat-8 derived LST and landscape metrics at neighbourhood sizes even beyond 1000m (Masoudi, Tan and Liew, 2019) and in line with the major range of variograms for 100m LST data in the three towns of 900-1100m (Table Apx C-3). Whilst variograms constructed for LST data at 2m

resolution levelled off at 250-450m marks, the highest impact of spatial patterns of urban form on core patches' LST was had at much greater proximity. Since in our analysis properties of entire patches intersecting with a particular buffer zone, even if they expanded beyond its boundary, were taken into account, the actual zone of immediate impact likely approximated the 50m block size recommended for urban design in the context of temperature regulation by Bartesaghi-Koc et al. (2019) or the maximum value of 30 to 50m distance after which the cooling effect of urban parks on air temperature was undetectable (Takebayashi, 2017).

4.4.2.2 Spatial configuration descriptors importance

Out of the available pool of landscape metrics, we utilised only a small subset of class aggregation metrics and only one patch-level metric, i.e. area, excluding a whole range of aggregation and shape metrics widely used in other studies. This was in part due to the unstable correlations between LST and various shape metrics derived at 2m pixel level (Zawadzka, Harris and Corstanje, 2020) for different land cover types across the three towns. From aggregation metrics, PLADJ, COHESION of trees, grass, and paved, and LSI of buildings were more relevant for the explanation of core patches' LST. Should any of these three metrics be used in other studies, they were typically considered as less important due to lower correlations with the LST mean of analytical units.

Contrary to previous studies, e.g. Zhou et al. (2011) and Jenerette et al. (2016), area of core and neighbouring patches was one of the least important LST predictors, which is likely due to the relatively small zone of influence considered here. Area of buildings, trees and paved land cover patches located in the neighbourhood gained somewhat in importance, but not exceeded the importance of patch aggregation metrics, for models constructed for 100m buffer zone (data not shown), which could be consequential from a more detailed focus of our analysis.

Elevation was the strongest exploratory factor of LST that has not been used in other urban LST studies. Whilst the cooling impact of increasing elevation on air temperature is well-known, we detected an opposite outcome whereby higher grounds exhibited higher LST, and the effect was exacerbated over the duration

of the summer. Whilst lower elevations could be related to a higher proximity to water bodies exerting a cooling effect, locations on higher grounds could potentially be exposed to more incoming solar radiation. A decrease in elevation in July associated with hotter land cover patches could possibly be explained by decreased humidity of the ground and air, as compared to June.

Heights of buildings and trees in our study had only complementary impact on LST to other metrics, which is in line with findings of Berger et al. (2017), where these two descriptors were less strongly correlated with LST than 2-dimensional metrics, such as impervious surface area or vegetation fraction, but contradicts the findings of Gage and Cooper (2017) and Sun et al. (2020), where height of trees was one of the most important LST predictors in random forests models constructed for areas with specific land composition patterns within a suburban town. Our study, due to detecting varied importance of tree and building heights to LST of different land cover types and subtypes, provides additional insights to the impacts of vertical structure of urban form on LST. Exclusion of elevation data, which could be conflated with feature heights, from random forest models did not improve the importance of heights in LST prediction in our case study.

In our study, distance to water was the most important distance-related descriptor of LST, with land cover patches located nearer to water being cooler, just as in the case of the distance to sea in Barcelona in the summer or rivers (Lemus-Canovas et al., 2020). It has to be noted that water coming from anthropogenic sources, such as industrial outlets, may act as a heat source rather than sink (Wu et al., 2014), and may have a warming effect in colder seasons of the year, as demonstrated in the Barcelona case study, or have lower cooling capacity in the summer than spring due to warming up of water, amongst other factors (Hathway and Sharples, 2012). Distances to buildings, either of core patches or patches of grass, paved or trees in the neighbourhood were an important explanatory factor of LST, which can be related to the interactions of temperatures of different land cover types located near each other, previously explored in the context of cooling by urban greenspaces (Chen and Wong, 2006;

Lin et al., 2015), that due to our findings could be expanded also onto reduction in the cooling capacity due to presence of built-up areas.

4.4.2.3 Spatial configuration descriptors thresholds and temporal scales

Our results indicated that, generally, higher spatial aggregation of patches of trees and lower aggregation of paved were associated with the coldest core land cover patches of different types and subtypes, with the opposite being true for the hottest patches, with specific thresholds being fairly similar at both dates considered here, set a month apart. Nevertheless, depending on an spatial configuration descriptor, there was a substantial overlap between means for patches of contrasting thermal properties, enforcing the use of quartiles (25^{th} and 75^{th} percentile) as more reliably distinguishing between LST of land cover patches than LST means. The issue of thresholds was raised by Masoudi et al. (2019) who argued that it is impossible to state a definite value for minimum vegetation cover within an analytical unit due to instable results obtained across 14 years in Singapore, attributing the differences to the "artefacts of current situation". Moreover, other multi-temporal studies found that correlations of spatial configuration metrics and LST varied with season and year (Liu et al., 2016). Whilst it is difficult to establish specific thresholds for spatial configuration descriptors yielding a particular thermal effect, our study has demonstrated that a certain threshold exists beyond which increased fragmentation of urban form, and especially tree cover, is unlikely to yield cooling effects towards neighbouring land cover patches. This statement, however, excludes cooling from trees through shading, which could not be explicitly quantified in our experimental setup, but is an important heat mitigation measure at a street level (Aleksandrowicz et al., 2017).

Whilst general consensus exists that greenspaces contribute to cooling effects of urban areas, our study has shown that this is predominantly due to the presence of trees rather than grass, aggregation of the latter being only important for explanation of LST of trees. The use of trees for cooling can also have varied effects depending on climate, as demonstrated in a comparative study (Zhou, Huang and Cadenasso, 2011), where high edge density of trees was more

important for cooling in the city of Sacramento, characterised by hot and dry summer, than Baltimore, with hot and humid summer, where increased fragmentation was detrimental to cooling. Another consideration that is important for greenspace planning is that optimisation of spatial arrangement for day-time heat mitigation may diminish cooling at night, as shown in Zhang et al. (2017).

4.5 Conclusions

Our study set out to determine whether it is possible to accurately explain LST of individual land cover patches with the use of fine resolution LST imagery and spatial configuration descriptors of urban form defined as spatial aggregation level of land cover patches, their area and heights, distances away from land cover patches of different types, and elevation. We found that spatial properties of urban form located in immediate proximity to a land cover patch of any type had a greater influence on the LST of the patch that the spatial properties of the patch itself, confirming that appropriate urban form design can be used for temperature regulation in urban environments. LST of less aggregated land cover patches of each type could be more effectively influenced by appropriate spatial configuration of urban form than LST of more aggregated and therefore larger patches. Elevation followed by aggregation level or distances to water or buildings were the most important descriptors of LST. Coldest land cover patches were situated at relatively low elevations, in closer proximity to water, more aggregated patches of trees and less aggregated patches of paved, with the opposite trends being true for the hottest land cover patches of each type and subtype. As summer progressed, elevation and distance to water gained in importance in LST regulation over other factors. Whilst spatial configuration descriptors used in this study were capable of predicting LST of core patches at a coarser spatial resolution, the accuracy of prediction was lower for buildings as well as more aggregated patches of all types than when high spatial resolution LST was used, suggesting that fine resolution LST data are required for LST studies at micro-scales. Future work should focus on elucidating the relationships between LST and spatial configuration of urban form after controlling for the effects of elevation and distance to water as well as include descriptors related

to urban fabric, such as albedo determining heat storage capacity of surface materials, which could improve the accuracy of the assessment, and provide further insights to urban planners.

4.6 References

Aleksandrowicz, O., Vuckovic, M., Kiesel, K. and Mahdavi, A. (2017) 'Current trends in urban heat island mitigation research: Observations based on a comprehensive research repository', *Urban Climate*, 21 Elsevier B.V., pp. 1–26. Available at: 10.1016/j.uclim.2017.04.002 (Accessed: 3 May 2020).

Bartesaghi-Koc, C., Osmond, P. and Peters, A. (2019) 'Spatio-temporal patterns in green infrastructure as driver of land surface temperature variability: The case of Sydney', *International Journal of Applied Earth Observation and Geoinformation*, 83 Elsevier B.V., p. 101903.

Berger, C., Rosentreter, J., Voltersen, M., Baumgart, C., Schmullius, C. and Hese, S. (2017) 'Spatio-temporal analysis of the relationship between 2D/3D urban site characteristics and land surface temperature', *Remote Sensing of Environment*, 193 Elsevier Inc., pp. 225–243.

Breiman, L. (2001) 'Random forests', *Machine Learning*, 45(1), SpringerLink, pp. 5–32. Available at: 10.1023/A:1010933404324 (Accessed: 16 July 2020).

Chen, A., Yao, L., Sun, R. and Chen, L. (2014) 'How many metrics are required to identify the effects of the landscape pattern on land surface temperature?', *Ecological Indicators*, 45 Elsevier, pp. 424–433. Available at: 10.1016/j.ecolind.2014.05.002 (Accessed: 22 June 2018).

Chen, Y. and Wong, N.H. (2006) 'Thermal benefits of city parks', *Energy and Buildings*, 38(2) Elsevier, pp. 105–120. Available at: 10.1016/j.enbuild.2005.04.003 (Accessed: 3 July 2018).

Chu, H.J., Chen, R.A., Tseng, Y.H. and Wang, C.K. (2014) 'Identifying LiDAR sample uncertainty on terrain features from DEM simulation', *Geomorphology*, 204, Elsevier, pp. 325–333. Available at: 10.1016/j.geomorph.2013.08.016 (Accessed: 16 July 2020).

Connors, J.P., Galletti, C.S. and Chow, W.T.L. (2013) ‘Landscape configuration and urban heat island effects: Assessing the relationship between landscape characteristics and land surface temperature in Phoenix, Arizona’, *Landscape Ecology*, 28(2), Springer, pp. 271–283. Available at: 10.1007/s10980-012-9833-1 (Accessed: 8 May 2020)

Futcher, J.A., Kershaw, T. and Mills, G. (2013) ‘Urban form and function as building performance parameters’, *Building and Environment*, 62 Pergamon, pp. 112–123. Available at: 10.1016/j.buildenv.2013.01.021 (Accessed: 30 April 2020).

Gage, E.A. and Cooper, D.J. (2017) ‘Relationships between landscape pattern metrics, vertical structure and surface urban Heat Island formation in a Colorado suburb’, *Urban Ecosystems*, 20(6) Springer New York LLC, pp. 1229–1238. Available at: 10.1007/s11252-017-0675-0 (Accessed: 8 May 2020).

Garshasbi, S., Haddad, S., Paolini, R., Santamouris, M., Papangelis, G., Dandou, A., Methymaki, G., Portalakis, P. and Tombrou, M. (2020) ‘Urban mitigation and building adaptation to minimize the future cooling energy needs’, *Solar Energy*, 204 Elsevier Ltd, pp. 708–719. Available at: 10.1016/j.solener.2020.04.089 (Accessed: 7 September 2020).

Grafius, D.R., Corstanje, R., Warren, P.H., Evans, K.L., Hancock, S. and Harris, J.A. (2016) ‘The impact of land use/land cover scale on modelling urban ecosystem services’, *Landscape Ecology*, 31(7) Springer Netherlands, pp. 1509–1522. Available at: 10.1007/s10980-015-0337-7 (Accessed: 3 September 2017).

Hathway, E.A. and Sharples, S. (2012) ‘The interaction of rivers and urban form in mitigating the Urban Heat Island effect: A UK case study’, *Building and Environment*, 58 Pergamon, pp. 14–22. Available at: 10.1016/j.buildenv.2012.06.013 (Accessed: 3 May 2020).

Heaviside, C., Macintyre, H. and Vardoulakis, S. (2017) ‘The Urban Heat Island: Implications for Health in a Changing Environment’, *Current Environmental Health Reports*, 4(3) Springer, pp. 296–305. Available at: 10.1007/s40572-017-0150-3 (Accessed: 30 April 2020).

Heaviside, C., Vardoulakis, S. and Cai, X.-M. (2016) ‘Attribution of mortality to the urban heat island during heatwaves in the West Midlands, UK’, *Environmental Health*, 15(S1) BioMed Central Ltd., p. S27. Available at: 10.1186/s12940-016-0100-9 (Accessed: 30 April 2020).

Jenerette, G.D., Harlan, S.L., Buyantuev, A., Stefanov, W.L., Declet-Barreto, J., Ruddell, B.L., Myint, S.W., Kaplan, S. and Li, X. (2016) ‘Micro-scale urban surface temperatures are related to land-cover features and residential heat related health impacts in Phoenix, AZ USA’, *Landscape Ecology*, 31(4) Kluwer Academic Publishers, pp. 745–760. Available at: 10.1007/s10980-015-0284-3 (Accessed: 1 November 2015).

Kong, F., Yin, H., James, P., Hutyra, L.R. and He, H.S. (2014) ‘Effects of spatial pattern of greenspace on urban cooling in a large metropolitan area of eastern China’, *Landscape and Urban Planning*, 128, pp. 35–47. Available at: 10.1016/j.landurbplan.2014.04.018 (Accessed: 27 September 2015).

Lemus-Canovas, M., Martin-Vide, J., Moreno-Garcia, M.C. and Lopez-Bustins, J.A. (2020) ‘Estimating Barcelona’s metropolitan daytime hot and cold poles using Landsat-8 Land Surface Temperature’, *Science of the Total Environment*, 699 Elsevier B.V., p. 134307. Available at: 10.1016/j.buildenv.2012.06.013 (Accessed: 3 May 2020).

Li, H., Wang, G., Tian, G. and Jombach, S. (2020a) ‘Mapping and analyzing the park cooling effect on Urban Heat Island in an expanding city: A case study in Zhengzhou City, China’, *Land*, 9(2) MDPI AG. Available at: 10.3390/land9020057 (Accessed: 8 May 2020).

Li, T., Cao, J., Xu, M., Wu, Q. and Yao, L. (2020b) ‘The influence of urban spatial pattern on land surface temperature for different functional zones’, *Landscape and Ecological Engineering*, 16(3) Springer, pp. 249–262. Available at: 10.1007/s11355-020-00417-8 (Accessed: 8 May 2020).

Li, X., Zhou, W. and Ouyang, Z. (2013) ‘Relationship between land surface temperature and spatial pattern of greenspace: What are the effects of spatial

resolution?', *Landscape and Urban Planning*, 114, Elsevier, pp. 1–8. Available at: 10.1016/j.landurbplan.2013.02.005 (Accessed: 15 March 2016).

Li, Z., Zhang, H., Wen, C.-Y., Yang, A.-S. and Juan, Y.-H. (2020c) 'Effects of frontal area density on outdoor thermal comfort and air quality', *Building and Environment*, 180 Elsevier Ltd, p. 107028. Available at: 10.1016/j.buildenv.2020.107028 (Accessed: 7 September 2020).

Lin, W., Yu, T., Chang, X., Wu, W. and Zhang, Y. (2015) 'Calculating cooling extents of green parks using remote sensing: Method and test', *Landscape and Urban Planning*, 134, pp. 66–75. Available at: 10.1016/j.landurbplan.2014.10.012 (Accessed: 6 June 2016).

Liu, K., Su, H., Li, X., Wang, W., Yang, L. and Liang, H. (2016) 'Quantifying Spatial–Temporal Pattern of Urban Heat Island in Beijing: An Improved Assessment Using Land Surface Temperature (LST) Time Series Observations From LANDSAT, MODIS, and Chinese New Satellite GaoFen-1', *IEEE Journal of Selected Topics in Applied Earth Observations and Remote Sensing*, 9(5) Institute of Electrical and Electronics Engineers, pp. 2028–2042. Available at: 10.1109/JSTARS.2015.2513598 (Accessed: 8 May 2020).

Masoudi, M., Tan, P.Y. and Liew, S.C. (2019) 'Multi-city comparison of the relationships between spatial pattern and cooling effect of urban green spaces in four major Asian cities', *Ecological Indicators*, 98 Elsevier B.V., pp. 200–213. Available at: 10.1016/j.landurbplan.2018.10.023 (Accessed: 8 May 2020).

McGarigal, K. and Marks, B.J. (1995) FRAGSTATS: spatial pattern analysis program for quantifying landscape structure. Available at: 10.2737/PNW-GTR-351 (Accessed: 4 May 2020).

Minasny, B. and McBratney, A.B. (2006) 'A conditioned Latin hypercube method for sampling in the presence of ancillary information', *Computers & Geosciences*, 32(9), pp. 1378–1388. Available at: 10.1016/j.cageo.2005.12.009 (Accessed: 11 May 2016).

Oke, T.R. (1976) ‘The distinction between canopy and boundary-layer urban heat islands’, *Atmosphere*, 14(4) Taylor & Francis Group, pp. 268–277. Available at: 10.1080/00046973.1976.9648422 (Accessed: 30 April 2020).

Perini, K., Chokhachian, A., Dong, S. and Auer, T. (2017) ‘Modeling and simulating urban outdoor comfort: Coupling ENVI-Met and TRNSYS by grasshopper’, *Energy and Buildings*, 152 Elsevier Ltd, pp. 373–384. Available at: 10.1016/j.enbuild.2017.07.061 (Accessed: 7 September 2020).

Ramyar, R., Zarghami, E. and Bryant, M. (2019) ‘Spatio-temporal planning of urban neighborhoods in the context of global climate change: Lessons for urban form design in Tehran, Iran’, *Sustainable Cities and Society*, 51 Elsevier Ltd, p. 101554. Available at: 10.1016/j.scs.2019.101554 (Accessed: 3 May 2020).

Revelle W (2019). ‘psych: Procedures for Psychological, Psychometric, and Personality Research’. Northwestern University, Evanston, Illinois. R package version 1.9.12. Available at: https://CRAN.R-project.org/package=psych.

Roudier P (2011). ‘clhs: a R package for conditioned Latin hypercube sampling’. Available at: https://github.com/pierreroudier/clhs/.

Santamouris, M., Cartalis, C., Synnefa, A. and Kolokotsa, D. (2015) ‘On the impact of urban heat island and global warming on the power demand and electricity consumption of buildings—A review’, *Energy and Buildings*, 98 Elsevier Ltd, pp. 119–124. Available at: 10.1016/j.enbuild.2014.09.052 (Accessed: 29 August 2020).

Sheng, L., Lu, D. and Huang, J. (2015) ‘Impacts of land-cover types on an urban heat island in Hangzhou, China’, *International Journal of Remote Sensing*, 36(6) Taylor and Francis Ltd., pp. 1584–1603. Available at: 10.1080/01431161.2015.1019016 (Accessed: 22 July 2020).

Simwanda, M., Ranagalage, M., Estoque, R.C. and Murayama, Y. (2019) ‘Spatial Analysis of Surface Urban Heat Islands in Four Rapidly Growing African Cities’, *Remote Sensing*, 11(14) MDPI AG, p. 1645. Available at: 10.3390/rs11141645 (Accessed: 8 May 2020).

Sun, F., Liu, M., Wang, Y., Wang, H. and Che, Y. (2020) ‘The effects of 3D architectural patterns on the urban surface temperature at a neighborhood scale: Relative contributions and marginal effects’, *Journal of Cleaner Production*, 258 Elsevier Ltd, p. 120706. Available at: 10.1016/j.jclepro.2020.120706 (Accessed: 3 May 2020).

Takebayashi, H. (2017) ‘Influence of Urban Green Area on Air Temperature of Surrounding Built-Up Area’, *Climate*, 5(3) Multidisciplinary Digital Publishing Institute, p. 60. Available at: 10.3390/cli5030060 (Accessed: 14 November 2017).

Wadoux, A.M.J.C., Brus, D.J. and Heuvelink, G.B.M. (2019) ‘Sampling design optimization for soil mapping with random forest’, *Geoderma*, 355 Elsevier B.V., p. 113913. Available at: 10.1016/j.geoderma.2019.113913 (Accessed: 16 July 2020).

Wang, Y., Zhan, Q. and Ouyang, W. (2017) ‘Impact of Urban climate landscape patterns on land surface temperature in Wuhan, China’, *Sustainability (Switzerland)*, 9(10) MDPI AG. Available at: 10.3390/su9101700 (Accessed: 8 May 2020).

Wickham H (2016). ‘ggplot2: Elegant Graphics for Data Analysis’. Springer-Verlag New York. ISBN 978-3-319-24277-4. Available at: https://ggplot2.tidyverse.org.

Wright, M.N. and Ziegler, A. (2017) ‘ranger : A Fast Implementation of Random Forests for High Dimensional Data in C++ and R’, *Journal of Statistical Software*, 77(1) American Statistical Association Available at: 10.18637/jss.v077.i01 (Accessed: 24 January 2021).

Wu, H., Ye, L.-P., Shi, W.-Z. and Clarke, K.C. (2014) ‘Assessing the effects of land use spatial structure on urban heat islands using HJ-1B remote sensing imagery in Wuhan, China’, *International Journal of Applied Earth Observation and Geoinformation*, 32(1) Elsevier B.V., pp. 67–78. Available at: 10.1016/j.jag.2014.03.019 (Accessed: 8 May 2020).

Yin, C., Yuan, M., Lu, Y., Huang, Y. and Liu, Y. (2018) ‘Effects of urban form on the urban heat island effect based on spatial regression model’, *Science of The Total Environment*, 634 Elsevier B.V., pp. 696–704. Available at: 10.1016/j.scitotenv.2018.03.350 (Accessed: 22 May 2020).

Yow, D.M. (2007) ‘Urban Heat Islands: Observations, Impacts, and Adaptation’, *Geography Compass*, 1(6) Wiley, pp. 1227–1251. Available at: 10.1111/j.1749-8198.2007.00063.x (Accessed: 31 August 2020).

Zawadzka, J., Corstanje, R., Harris, J. and Truckell, I. (2020) ‘Downscaling Landsat-8 land surface temperature maps in diverse urban landscapes using multivariate adaptive regression splines and very high resolution auxiliary data’, *International Journal of Digital Earth*, 13(8) Taylor & Francis, pp. 899–914. Available at: 10.1080/17538947.2019.1593527 (Accessed: 17 April 2019).

Zawadzka, J.E., Harris, J.A. and Corstanje, R. (2020) ‘A simple method for determination of fine resolution urban form patterns with distinct thermal properties using class-level landscape metrics’, *Landscape Ecology*, Springer Science and Business Media B.V., pp. 1–14. Available at: 10.1007/s10980-020-01156-9 (Accessed: 17 January 2021).

Zhang, Y., Murray, A.T. and Turner, B.L. (2017) ‘Optimizing green space locations to reduce daytime and nighttime urban heat island effects in Phoenix, Arizona’, *Landscape and Urban Planning*, 165(April), pp. 162–171. Available at: 10.1016/j.landurbplan.2017.04.009 (Accessed: 6 July 2017).

Zhou, G., Wang, H., Chen, W., Zhang, G., Luo, Q. and Jia, B. (2020) ‘Impacts of Urban land surface temperature on tract landscape pattern, physical and social variables’, *International Journal of Remote Sensing*, 41(2) Taylor and Francis Ltd., pp. 683–703. Available at: 10.1080/01431161.2019.1646939 (Accessed: 8 May 2020).

Zhou, W., Huang, G. and Cadenasso, M.L. (2011) ‘Does spatial configuration matter? Understanding the effects of land cover pattern on land surface temperature in urban landscapes’, *Landscape and Urban Planning*, 102(1), pp. 54–63. Available at: 10.1016/j.landurbplan.2011.03.009 (Accessed: 8 May 2020).

5 CHAPTER FIVE

Assessment of heat mitigation capacity of urban greenspaces with the use of InVEST Urban Cooling model, verified with day-time land surface temperature data

J.E. Zawadzka[1]*, R. Corstanje[1], J.A. Harris[1]

[1]*Centre for Environmental and Agricultural Informatics, School of Water, Energy and Environment, Cranfield University, Bedfordshire, UK*

*Corresponding author: joanna.zawadzka@cranfield.ac.uk

Intended for submission to Landscape and Urban Planning journal

Highlights

- InVEST Urban Cooling model was validated with day-time land surface temperature data
- Heat mitigation index adequately approximates LST at 30m resolution
- The index is sensitive to cooling distance and spatial resolution of the analysis
- InVEST Urban Cooling model can support decisions at masterplan level

Abstract

Accurate quantification of the heat mitigation (HM) capacity of urban greenspaces is essential in planning decisions due to increased thermal pressures on existing and new urban environments associated with climate change. However, this often requires data analytical skillsets that may not be available to planning community. The recently developed InVEST 3.8.7 Urban Cooling model addresses this limitation by using several easily accessible parameters, assigned to a land cover map, to produce the HM index intended at estimating the cooling

capacity of vegetation in a spatial context. In this study, we validated the HM index derived for three towns with differing morphologies by comparison to land surface temperature (LST) data using linear regression analysis. We found that the HM index can be used to explain a variable proportion of the variation in LST, with R^2 ranging from 0.48 to 0.64 depending on town, with stronger associations obtained for towns with a higher range of LST values. Higher resemblance to LST data was achieved after resampling of the 2m resolution model outputs to 30m resolution, inclusion of water bodies as cooling features, and using cooling distance away from large greenspaces of 100m. On average, change in HM index of 0.1 was associated with 0.76°C change in LST. We conclude that the model is suitable for assessment of HM interventions through incorporation of vegetation and water bodies into city plans at scales relevant to masterplans rather than fine-tuning of urban design.

Keywords: InVEST Urban Cooling model, urban heat island, temperature regulation, land surface temperature

5.1 Introduction

Urban areas are affected by the urban heat island effect, whereby ambient temperatures of towns and cities are generally warmer than in the surrounding rural environments (Oke, 1976). The urban heat island is associated with detrimental effects on human health (e.g. Heaviside, Macintyre, & Vardoulakis, 2017; Heaviside, Vardoulakis, & Cai, 2016), increased energy consumption for air conditioning (Santamouris et al., 2015), increased occupational heat stress (Casanueva et al., 2020; Kjellstrom et al., 2018), and changes to ecological cycles (Yow, 2007). The incidence of heatwaves is expected to rise in frequency and intensity this century (Perkins, Alexander and Nairn, 2012; Wouters et al., 2017), highlighting the need for rapid implementation of heat mitigation measures across cities in order to avoid or reduce their negative impacts.

The urban thermal environment is often described in the context of the formation of the urban heat islands or surface urban heat islands. The urban heat island is a phenomenon originally conceived as occurring at night, moderated through radiative fluxes of sensible and latent heat, the former characteristic of the urban built environment and associated with increased air temperatures and the latter – of vegetated surfaces, associated with cooling properties (Lin et al., 2017; Oke, 1988). The formation and intensity of the urban heat island effect is governed by complex interactions between multiple factors that include decreased long-wave radiation loss from and multiple reflections of short-wave radiation between buildings, increased storage of sensible heat in the urban fabric, decreased evapotranspiration due to low vegetation coverage as compared to rural areas, anthropogenic heat sources, and air pollution (Oke et al., 1991). The surface urban heat island relates to the temperature of the urban land surface and is associated with urban heat island through modulation of air temperature at the lowest layers of the atmosphere (Voogt and Oke, 2003), however, with differences induced through air advection (Wang, Yao and Shu, 2020), and being more prominent during the day (Roth, Oke and Emery, 1989).

In urban planning, urban heat island mitigation is primarily concerned with regulation of microclimates at pedestrian or building scales (Erell, 2008) that

could be related to the street or site (micro-scale) levels (Norton et al., 2015). Whilst pedestrian scales mostly relate to the creation of outdoor spaces providing thermal comfort to humans, building scales focus on measures leading to energy conservation in buildings. Multiple typologies of the surface and urban heat island mitigation methods exist (Aleksandrowicz et al., 2017; Kleerekoper, van Esch and Salcedo, 2012; Meng, 2017; Sung, 2013), and include introduction of strategically distributed vegetation and water bodies across the landscape, which reduce surface and ambient temperatures through shading, evapotranspiration, and evaporation, both on-site and at a distance away.

Incorporation of green infrastructure as a surface and urban heat island mitigation measure into urban plans requires assessment of benefits derived from them, both in biophysical and economic terms (Cortinovis and Geneletti, 2019). Biophysical assessments of heat mitigation capacity of vegetation can be carried out through air temperature measurements (Bowler et al., 2010), analysis of remotely sensed land surface temperature (LST) imagery (Zhou et al., 2018), or simulations of urban thermal environment (Tsoka et al., 2020) – approaches that require substantial academic expertise that is rarely available in many planning departments (Bherwani, Singh and Kumar, 2020; Norton et al., 2015). An example of a recently developed model dedicated to a simplified assessment of the UHI mitigation capacity of vegetation, which has a potential to bridge this gap, is the InVEST 3.8.7 Urban Cooling model (Sharp et al. 2020). The model calculates heat mitigation index, based on evapotranspiration from vegetation, cooling distance of large urban parks, and albedo assigned to a land cover (LC) map, which is then used to estimate monetary value of vegetative cooling, and as such is the key model output determining the accuracy of subsequent evaluations. Consequently, the goal of this study was to verify the representativeness of the HM index returned by the InVEST 3.8.7 Urban Cooling model of urban thermal environment as depicted by LST imagery captured on a warm summer day, at spatial resolutions relevant to micro- and broad-scale assessments: 2 and 30m. We therefore hypothesised that the HM index generated by the InVEST 3.8.7 Urban Cooling model can be used as a substitute for LST mapping in assessment of the cooling capacity of urban greenspaces

under an assumption that low HM values should correspond to highest temperatures in the LST image with the opposite being true for the high values of HM. We next estimated the amount of change in LST due to gradual change in the HM index for model outputs with the highest resemblance to the LST data as indicated by the highest value of R^2. Our analysis was carried out using an example of three sub-urban towns collectively characterised with a high variety of urban form, and is the first study known to the authors aiming at validation of the InVEST 3.8.7 Urban Cooling model.

5.2 Materials and Methods

5.2.1 Study Area

The study area comprises three towns located in a relatively close proximity in England: Milton Keynes (52°0′N, 0°47′W, appr. 122 km^2), Bedford (52°8′N, 0°27′W, appr. 60 km^2), and Luton/Dunstable (51°52′N, 0°25′W, appr. 86 km^2) (Figure 5-1) with population of 229,941, 106,940, and 258,018 (Office for National Statistics (2013) respectively and a temperate oceanic climate according to the Köppen–Geiger climate classification system. The three towns are characterised with contrasting histories: modern-day garden-city, medieval, and industrial, respectively, collectively representing a wide range of urban form patterns, described in more detail in Grafius et al. (2016) and Zawadzka et al. (2020) and reflecting on their land cover properties (Table 5-1). Major differences in land cover composition of the towns comprise lowest abundance of greenspaces and highest of impervious areas in Luton, and the largest extent of greenspaces and water bodies in Milton Keynes.

Table 5-1 Land cover composition and patch size (mean and standard deviation) of main land cover types within Bedford (BD), Luton (LT) and Milton Keynes (MK) summarised for the built-up area extents of the towns from the land cover maps available in this study.

LC		LC area [% of total town area]			Patch size [m^2]					
		BD	LT	MK	BD		LT		MK	
					Mean	Std.	Mean	Std.	Mean	Std.
Buildings	B	18.8	16.1	12.1	160	529	154	918	178	896
Grass - Short <0.5m	G	28.4	21.3	28.5	49	823	48	1108	68	1327
Shrub/Tall Grass/Hedge (0.5 - 2m)	SGH	9.9	7.7	7.7	13	24	13	26	14	37
Broadleaf Trees >2m tall	Tb	24.7	18.0	22.7	49	462	52	935	69	1174
Coniferous Trees >2m tall	Tc	0.3	N/A	4.0	84	255	N/A	N/A	55	267
Paved	P	35.6	36.8	34.1	122	7648	156	45672	124	44987
Water	W	1.2	0.1	3.0	283	2115	96	432	640	9899

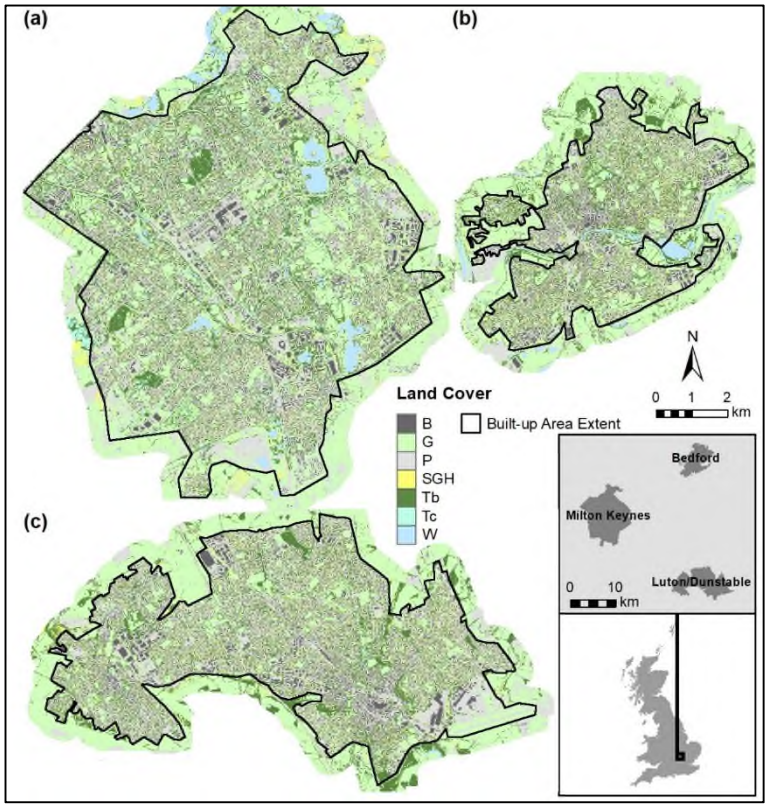

Figure 5-1 Land cover in (a) – Milton Keynes, (b) – Bedford, (c) – Luton/Dunstable. The insert depicts location of the towns within Great Britain. B – buildings, G – grass, P – paved, SGH – short trees/tall grass/hedge, Tb – broadleaf trees, Tc – coniferous trees, W – water.

5.2.2 Materials and Methods

The following sections explain the main assumptions of the InVEST 3.8.7 Urban Cooling model leading to the generation of the heat mitigation index as well as steps undertaken to assess the strength of the relationship between the heat mitigation index and land surface temperature data available for the three towns.

5.2.2.1 InVEST Urban Cooling model

InVEST 3.8.7 Urban Cooling model generates maps of the HM index estimating the cooling capacity of urban greenspaces on all land cover classes present in the study area taking into account the cooling capacity of larger urban parks extending beyond their boundaries (InVEST 3.8.7 User Guide). The functionality of the model is based on and expands upon the methodology for the estimation of cooling capacity of urban green infrastructure, encompassing land cover features such as grass, trees, green walls/roofs and water, in the planning context proposed by Zardo et al. (2017).

In the Urban Cooling model, cooling capacity is calculated as a weighted function of shading (S), evapotranspiration index (ETI) and albedo (A) (Equation 5-1), the latter constituting an extension to the method presented by Zardo et al. (2017). Albedo expresses the proportion of solar radiation reflected by land surface, and is therefore representative of the amount of solar heat than can be absorbed by surface materials, with lower absorption, i.e. higher albedo, associated with lower land surface temperature (Phelan et al., 2015).

Equation 5-1

$$CC = 0.6 \cdot S + 0.2 \cdot ETI + 0.2 \cdot A,$$

Where: CC – cooling capacity index, ranging from 0 to 1, with 0 as no cooling capacity, and 1 maximum cooling capacity within the study area, S – capacity of trees to provide shading, set to 1 for trees taller than 2 metres or 0 for trees below the 2 metre cut-off, ETI – evapotranspiration index, calculated from Equation 5-2, A – albedo, ranging from 0 to 1, with 1 indicating maximum reflectance of solar radiation, and 0 – maximum absorption.

ETI is the normalised value of evapotranspiration across the study area calculated as actual evapotranspiration (ET_a) divided by the maximum value of ET_0 within the study area (ET_{max}) (Equation 5-3). ET_a is calculated as potential evapotranspiration ET_0 modified by the value of crop coefficient K_c determining the fraction of ET_0 evaporated by specific type of land cover (Equation 5-3).

Equation 5-2

$$ETI = \frac{ET_a}{ET_{max}}$$

Equation 5-3

$$ET_a = ET_0 \cdot K_c$$

Potential evapotranspiration ET_0 was calculated from the modified Hargreaves equation (Equation 5-4) (Droogers and Allen, 2002).

Equation 5-4

$$ET_0 = 0.0013 \cdot 0.408 \cdot RA \cdot (T_{avg} + 17) \cdot (TD - 0.0123 \cdot P)^{0.76},$$

where: ET_0 – reference evapotranspiration, [mm d^{-1}], RA – extra-terrestrial radiation, estimated as 41.6 MJ $m^{-2}d^{-1}$, equivalent to RA of the 15th day of June at 52°N in Allen et al.(1998), P – Precipitation [mm], T_{avg} – the average of the daily minimum and daily maximum temperatures [°C], TD – the difference between daily maximum and mean daily minimum temperatures [°C].

The HM index is equivalent to cooling capacity derived for each grid cell of a land cover map submitted to the model based on several conditions. These conditions distinguish between grid cell location within a large greenspace (over 2ha in size), location within a cooling distance away from large greenspaces, and location outside of the cooling zone of influence of large greenspaces on temperature, indicated by the cooling distance (Equation 5-5).

Equation 5-5

$$HM_i = \begin{cases} CC_i \; if \; CC_i \geq CC_{Park_i} \; or \; GA_i < 2ha \\ CC_{Park_i} \qquad\qquad\qquad otherwise \end{cases},$$

where: HM_i – heat mitigation value at grid cell *i*, CC_i – cooling capacity of grid cell *i*, calculated from Equation 5-1, $CC_{Park\ i}$ – cooling capacity calculated as distance weighted average of the CC values from green spaces (Equation 5-7), GA_i – the amount of green areas within a search distance d_{cool} around each pixel (Equation 5-6).

Equation 5-6

$$GA_i = cell_{area} \cdot \sum_{\substack{j \in d\ radius \\ from\ i}} g_j,$$

where: GA_i – the amount of greenspaces around grid cell *i* within a radius defined by cooling distance d_{cool}, $cell_{area}$ – area of grid cells $_j$ within the input raster land cover map, expressed in hectares, g_j – a switch assuming the value of 1 if a grid cell located within the cooling distance radius represents greenspaces, otherwise set to 0.

Equation 5-7

$$CC_{Park_i} = \sum_{\substack{j \in d\ radius \\ from\ i}} g_j \cdot CC_i \cdot e^{\left(\frac{-d(i,j)}{d_{cool}}\right)},$$

where: $CC_{Park\ i}$ – cooling capacity assigned to areas located within the cooling distance radius d_{cool} from large greenspaces (>2h in size), calculated as a weighted average of the distance between cells *i* and *j*, $d_{(i,j)}$ – distance between cells *i* and *j* located within the cooling distance radius.

The Urban Cooling model can also be used to estimate night-time heat mitigation for buildings, air temperature anomalies as well as economic value of heat mitigation by urban greenspaces, however, these functions are derivative from the HM index and are not covered in this study.

5.2.2.2 Model parameterisation and data sources

The primary input required by the InVEST 3.8.7 Urban Cooling model is a land use/land cover map, classes of which are attributed with parameters required for the calculation of the HM index. In this study, a 2m spatial resolution land cover map in a raster format was used. The map was collated for the purpose

of previous studies from three datasets: NDVI-derived locations of grass and trees, footprints of buildings and paved areas captured by a large-scale topographic map (Ordnance Survey MasterMap), and feature heights acquired from a LiDAR data survey of the three towns (Grafius et al., 2016). The parameters assigned to each LC class include potential evapotranspiration ET_0, evapotranspiration coefficient (K_c), albedo, cooling distance away from large greenspaces, as well as greenspace and shading switches (Table 5-2).

Table 5-2 Key parameters assigned to each land cover class within the study area submitted to the model as the biophysical table.*Separate runs of the model were carried out where water was treated as the greenspace to include its evaporative cooling capacity in the calculation of the HM index for each town.

LC	Description	Shade	K_c	Albedo	Greenspace
B	Buildings	0	0.001	0.25	0
G	Grass - Short <0.5m	0	0.95	0.16	1
SGH	Shrub/Tall Grass/Hedge (0.5 - 2m)	0	0.95	0.18	1
Tb	Broadleaf Trees >2m tall	1	0.95	0.2	1
Tc	Coniferous Trees >2m tall	1	1	0.15	1
P	Paved	0	0.001	0.14	0
W	Water	0	0.6525	0.09	0 or 1*

Precipitation and temperature data needed for the ET_0 estimation were obtained from the HadUK-Grid Gridded Climate Observations on a 1km grid over the UK (MetOffice, 2019) for 8 June 2013 and calculated as a mean value for each town. Evapotranspiration coefficients, due to the lack of data for other types of vegetation, were approximated from an existing guidance, whose use is advised by the InVEST User Guide, on crop evapotranspiration calculation (Allen et al., 1998) as the mid-season values for apple orchards without ground cover for broadleaf trees, coniferous trees for coniferous trees, turf grass for grass, and temperate climate water bodies for water. Buildings and paved areas were assigned a very small value of K_c (0.001) to avoid creation of empty grid cells in the intermediary outputs of the model. Albedo values for each LC class were estimated from the list of typical values in Taha et al. (1988), assuming highest absorption of solar radiation by water followed by paved areas due to dark colour of asphalt roads, and lowest for buildings, with vegetated areas taking intermediary values. Following the methodology for cooling capacity estimation

presented by Zardo et al. (2017) that included evaporative cooling of water bodies as well as vegetation, the greenspace switch was assigned not only to grassed and treed LC classes but also water, resulting with model runs capturing cooling capacity of vegetation only (V) or water and vegetation (W&V) (Figure 5-5-2). Three cooling distances away from large greenspaces were considered: 100m, 200m, and 300m, which approximated distances reported in literature regarding the cooling capacity of urban parks, ranging between 20 and 440m (Aram et al., 2019; Vaz Monteiro et al., 2016).

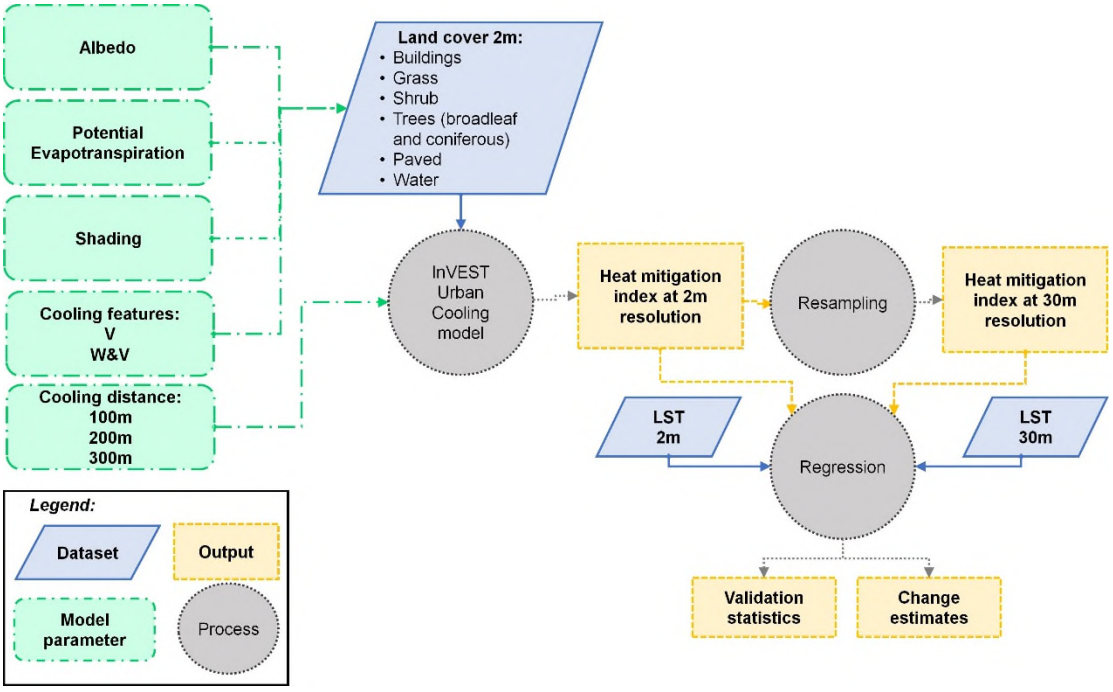

Figure 5-5-2 Schematic of the methodology undertaken to assess the representativeness of the heat mitigation index derived from land cover maps with different cooling distance and cooling features settings in relation to land surface temperature (LST). V – vegetation, W – water.

Additional settings required by the model included the air temperature reference value and the UHI magnitude, which were set to the minimum air temperature observed within a 10km radius away from each town and the difference between maximum air temperature value within each town and the reference value, all captured from the HadUK-Grid Gridded Climate Observations

on a 1km grid over the UK (MetOffice, 2019) dataset. Air mixing distance was kept as the default value of 2000m. Whilst these settings were required for the model to run, they did not affect the HM index values returned by the model that are subject of this study.

5.2.2.3 Verification of model outputs

The heat mitigation maps obtained from InVEST 3.8.7 Urban Cooling model were compared to LST data available for 8 June 2013 for the three towns. LST maps were available at two spatial resolutions: 2(4)m and 30(100)m, for simplicity referred to as 2 and 30m throughout the manuscript. The coarser resolution LST image was obtained from Landsat 8 thermal infra-red bands using split-window algorithm (Jimenez-Munoz et al., 2014). Its mixed spatial resolution stems from the fact that the Landsat 8 thermal infra-red data are captured at 100m resolution and are subsequently resampled to 30m resolution by the data provider (USGS). The finer resolution image was generated from the Landsat 8 LST map through a downscaling procedure (Zawadzka et al., 2020) whereby coarse resolution LST was related through a multivariate adaptive regression splines algorithm to spectral indices at 2 and 4m resolution to produce the fine resolution images across the three towns.

The comparison between the HM index and LST data was carried out with the use of ordinary least squares (OLS) linear regression. Whilst the HM index maps that were generated at 2m resolution by the model could directly be compared to the 2(4)m resolution LST images, the comparison to 30(100)m LST data required that the HM datasets were resampled to match the mixed spatial resolution. This was done through imitation of the post-processing procedure for the Landsat 8 TIR bands by first upscaling of the 2m HM index to 100m using a mean function within a 100m x100m focal moving window and subsequent resampling, using the cubic convolution method, to 30m with GIS procedures implemented in ESRI ArcGIS 10.6. Ultimately, twelve HM index maps were generated for each town, accommodating for three different cooling distances away from large vegetated patches: 100, 200, and 300m; two sets of cooling features: V or W&V; and two spatial resolutions of the outputs: 2 and 30m.

5.3 Results

5.3.1 Validation with LST data

5.3.1.1 City-wide assessment

Ordinary least squares regression analysis between spatially distributed values of the HM index and LST revealed that the Urban Cooling model managed to reflect some portion of variation in thermal response of the land surface, however, the strength of the association depended on various factors considered in this study (Table 5-3 and Figure 5-3). The largest differences in the coefficient of determination R^2 were observed for regressions at different spatial resolutions, with associations between datasets at 30m being at least twice as strong as at 2m in Bedford and Luton, however, very similar in Milton Keynes. Whilst the generally higher R^2 values at 30m resolution could be attributed to the introduction of a greater variance of values into the HM index maps during resampling from 2m to 30m resolution, the different behaviour in Milton Keynes could potentially be caused by the distinct morphology of this town, being designed as a Garden City and consequently containing distinctly larger patches of grass, trees and water than the remaining towns.

In all towns, the cooling distance of 100m resulted in higher R^2 values, however, inclusion of water bodies as cooling features had a varied effect on the strength of associations between the HM index and LST. The highest increase in R^2 values was observed in Milton Keynes, followed by Bedford, and no increase was observed in Luton, which can be explained by the decreasing proportion of water in land cover of these cities, respectively. Whilst the changes in R^2 are only marginal at 2m resolution, they are distinct for data at 30m resolution, which could attributed to the increased variance of the HM index values resulting from the resampling.

It has to be noted, however, that HM index values obtained with the 100m cooling distance were distinctly lower than in the case of the remaining distances (Tables Apx D-1 and D- 2). This could be attributed to the fact that at the smaller distance no greenspaces were considered as large by the model (Figure D-3)

and therefore their cooling capacity was constrained only to their footprints. Conversely, resampling of the 2m model outputs to 30m helped mitigate this limitation.

The differences in HM index due to the various model parameterisations explored in this study are easily discernible visually (Figure 5-4 and Figures Apx D-1 and D-2). Maps created for the 100m cooling distance away from large greenspaces depict lower HM values in buildings and paved areas than maps generated with larger cooling distances displaying greater variability of the HM index values within those land cover classes. The sharp delineations of the HM index at 100m distance are likely resultant from the lack of recognition of any greenspaces as large (over 2ha in size) by the model, not allowing for consideration of cooling capacity of vegetation beyond its footprint (Figure D-3). Whilst maps at 2m resolution generated with 100m cooling distance showed very little variation in HM values within areas covered by grey infrastructure as compared to the LST map, resampling to 30m resulted in a greater variability of HM values and overall greater resemblance to the LST map at this resolution. HM index maps generated with 200m and 300m cooling distances appeared similar regardless of spatial resolution, however, depicting a lower contrast in HM values between green, blue and grey land cover as the cooling distance increased. This increasing dilution of the HM index resulted from depiction of only selected greenspaces at the 200m distance and all greenspaces as large at the 300m distance, and therefore having a cooling effect on neighbouring land cover. Finally, inclusion of the cooling capacity of water bodies in the calculation of the HM index significantly increased their resemblance to LST maps at all cooling distances and spatial resolutions by increasing its values in areas corresponding to low LST of water bodies.

Table 5-3 The outcomes of linear regression between the HM index and LST data for three towns (Bedford – BD, Luton – LT and Milton Keynes – MK) between HM index and LST obtained at various spatial resolutions, cooling distances and cooling features (V – Vegetation, W&V – water and vegetation) settings.

Town	*Cooling distance*	*Cooling features*	*Rsq*		*adj Rsq*		*Std Error*		*Intercept a*		*Coefficient b*		*Std Error a*		*Std Error b*	
			2m	*30m*	*2m*	*30m*	*2m*	*30m*	*2m*	*30m*	*2m*	*30m*	*2m*	*30m*	*2m*	*30m*
BD	100m	V	0.24	0.48	0.24	0.48	1.75	2.29	31.45	32.28	-2.87	-7.29	0.00	0.02	0.00	0.03
		W&V	0.28	0.63	0.28	0.63	1.71	1.94	31.56	32.97	-3.08	-8.05	0.00	0.02	0.00	0.03
	200m	V	0.16	0.44	0.16	0.44	1.84	2.37	33.81	38.61	-5.48	-14.86	0.00	0.05	0.00	0.07
		W&V	0.18	0.59	0.18	0.59	1.81	2.03	34.21	40.59	-5.99	-17.11	0.00	0.04	0.00	0.06
	300m	V	0.12	0.46	0.12	0.46	1.88	2.34	33.88	41.54	-5.47	-19.11	0.00	0.06	0.01	0.09
		W&V	0.14	0.58	0.14	0.58	1.86	2.05	34.39	43.86	-6.13	-21.71	0.00	0.06	0.01	0.08
LT	100m	V	0.24	0.64	0.24	0.64	1.59	1.84	31.70	32.19	-2.81	-7.86	0.00	0.01	0.00	0.02
		W&V	0.25	0.64	0.25	0.64	1.58	1.83	31.70	32.20	-2.83	-7.85	0.00	0.01	0.00	0.02
	200m	V	0.19	0.63	0.19	0.63	1.64	1.87	33.42	37.87	-4.60	-14.66	0.00	0.03	0.00	0.04
		W&V	0.19	0.63	0.19	0.63	1.64	1.87	33.44	37.87	-4.63	-14.63	0.00	0.03	0.00	0.04
	300m	V	0.14	0.63	0.14	0.63	1.70	1.85	33.47	40.67	-4.54	-19.06	0.00	0.03	0.00	0.05
		W&V	0.14	0.63	0.14	0.63	1.70	1.85	33.50	40.69	-4.58	-19.06	0.00	0.03	0.00	0.05
MK	100m	V	0.31	0.30	0.31	0.30	1.57	2.33	29.05	29.25	-3.04	-5.65	0.00	0.01	0.00	0.02
		W&V	0.33	0.48	0.33	0.48	1.54	2.01	29.12	30.02	-3.09	-6.80	0.00	0.01	0.00	0.02
	200m	V	0.22	0.22	0.22	0.22	1.67	2.44	31.60	34.09	-6.06	-11.53	0.00	0.04	0.00	0.06
		W&V	0.24	0.44	0.24	0.44	1.64	2.07	31.93	37.18	-6.42	-15.69	0.00	0.03	0.00	0.05
	300m	V	0.18	0.26	0.18	0.26	1.71	2.39	31.79	37.56	-6.28	-16.83	0.00	0.05	0.00	0.08
		W&V	0.20	0.45	0.20	0.45	1.69	2.06	32.21	40.68	-6.76	-20.85	0.00	0.04	0.00	0.06

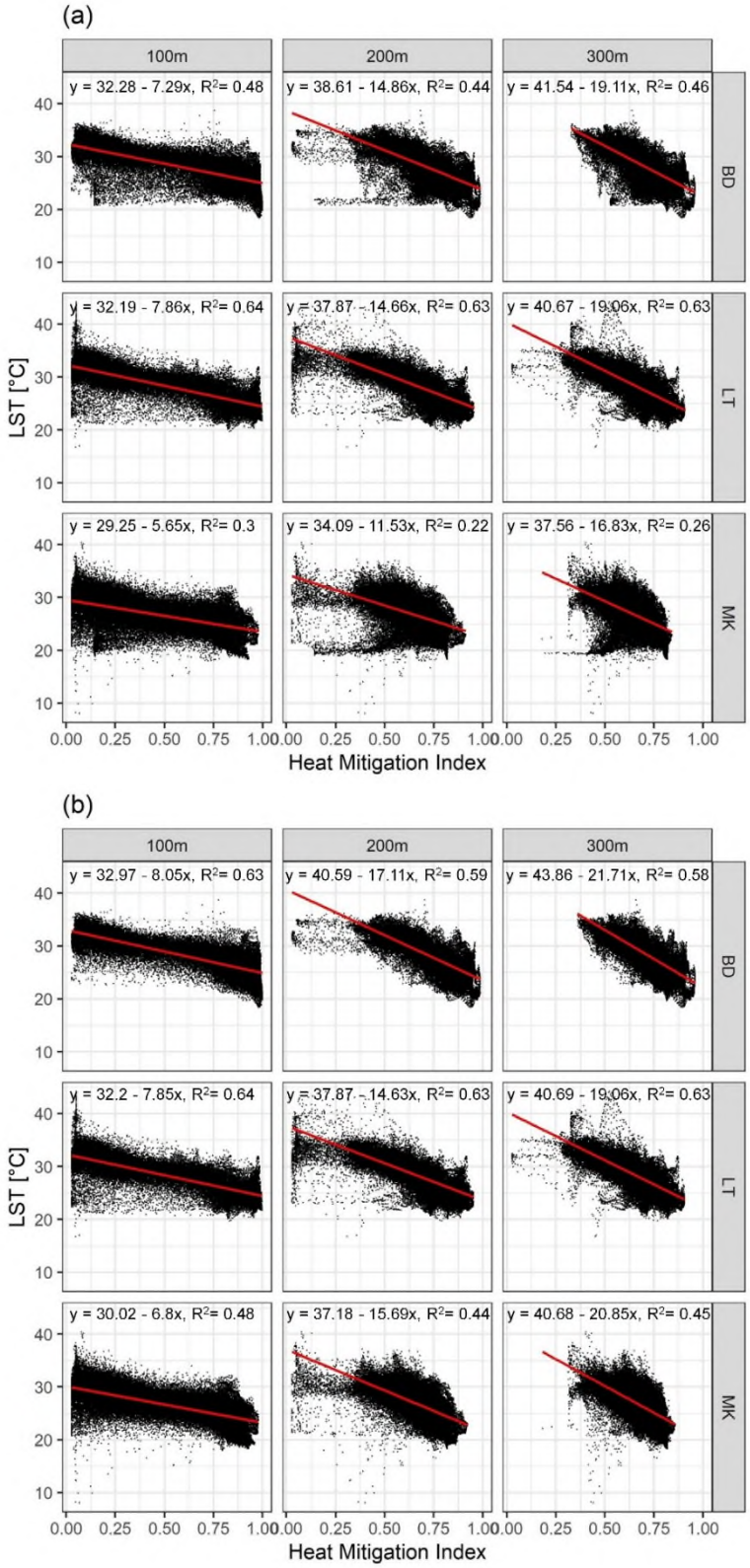

Figure 5-3 Results of OLS regression between the HM index and LST at 30m resolution for models (a) excluding and (b) including cooling capacity of water.

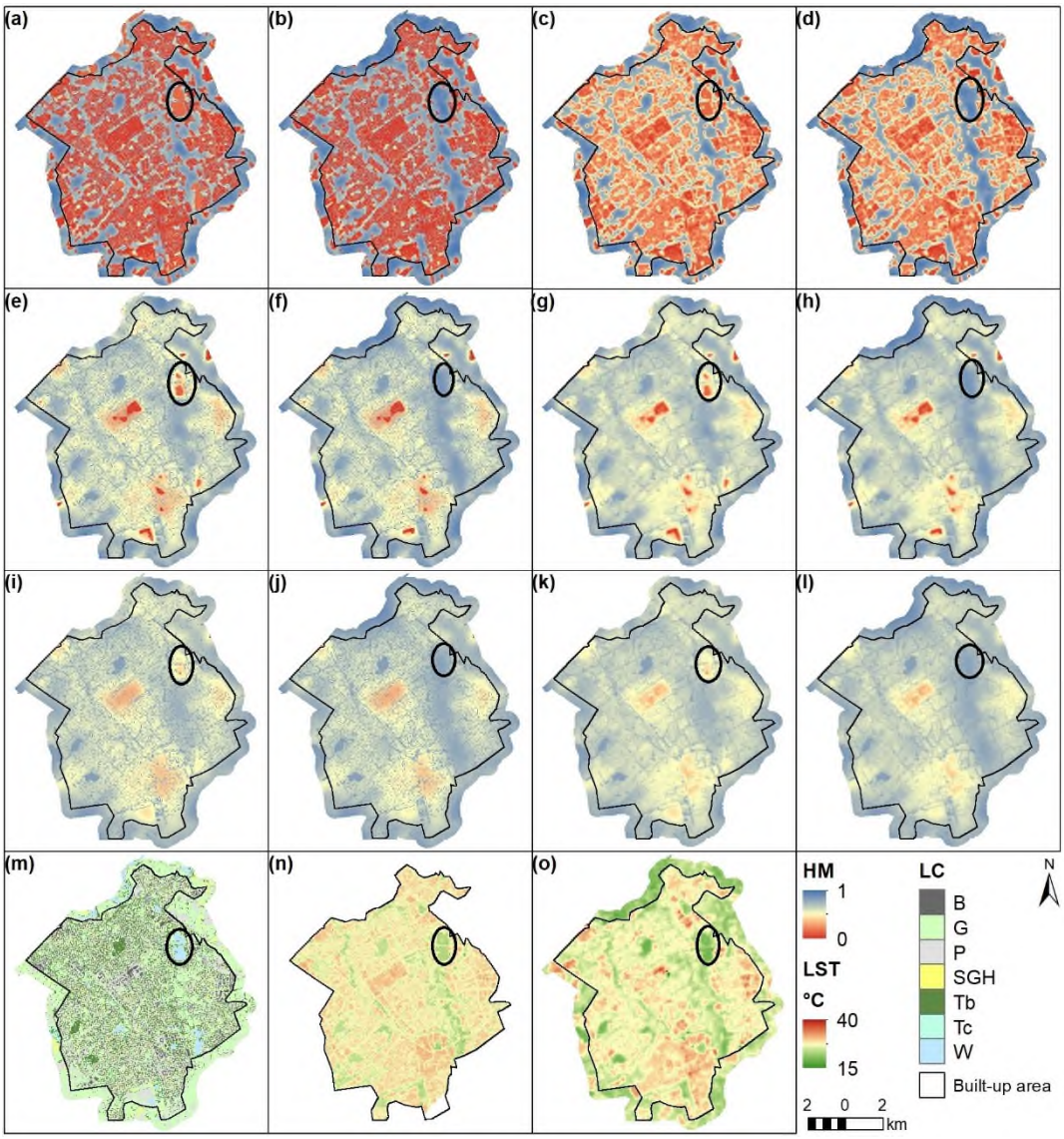

Figure 5-4 Heat mitigation index maps at 2m and 30m resolution for Milton Keynes at various vegetation cooling distance and cooling feature settings. (a) 100m, V, 2m; (b) 100m W&V, 2m; (c)100m, V, 30m; (d) 100m, W&V, 30m; (d) 200m, V, 2m; (e) 200m W&V, 2m; (f)200m, V, 30m; (g) 200m, W&V, 30m; (h) 300m, V, 2m; (i) 300m W&V, 2m; (j)300m, V, 30m; (k) 300m, W&V, 30m. Land cover map is shown in image (m) and land surface temperature in image (n) for 2m and (o) 30m resolution. V – vegetation, W&V – water & vegetation. Equivalent images for Bedford and Luton are available in Appendix D Figures Apx D-1 – D-2. Black ovals indicate the difference in how the HM index depicts Willen Lake with different cooling features settings.

5.3.1.2 Assessment within individual LC types

Analysis of R^2 values obtained from the comparison between spatially distributed HM index and LST values, summarised by land cover type (Figure 5-5 and Tables Apx D-3 to D-5) revealed more complex trends of associations than in the city-wide assessments. First of all, the strength of associations varied simultaneously with land cover type and spatial resolution as comparisons at 2m resolution yielded higher R^2 values for buildings, paved and grass than for trees and water whilst the opposite was true for the 30m resolution, where the HM index for trees appeared to have a stronger association with LST than that for buildings, paved and grass. Moreover, R^2 differed also with the cooling distance of large greenspaces with the highest R^2 for buildings and paved classes observed for distance of 200m at 2m spatial resolution as well as at 30m resolution for buildings in Luton, with the HM index for the remaining land cover classes having the strongest relationship to LST at 100m cooling distance. Inclusion of the cooling capacity of water into the assessment increased the strength of the relationship between the HM index and LST in all land cover classes at 30m resolution in Bedford and Milton Keynes and had no effect in Luton. At 2m resolution, small improvements in R^2 were observed in all land cover classes apart from water in Bedford and Milton Keynes.

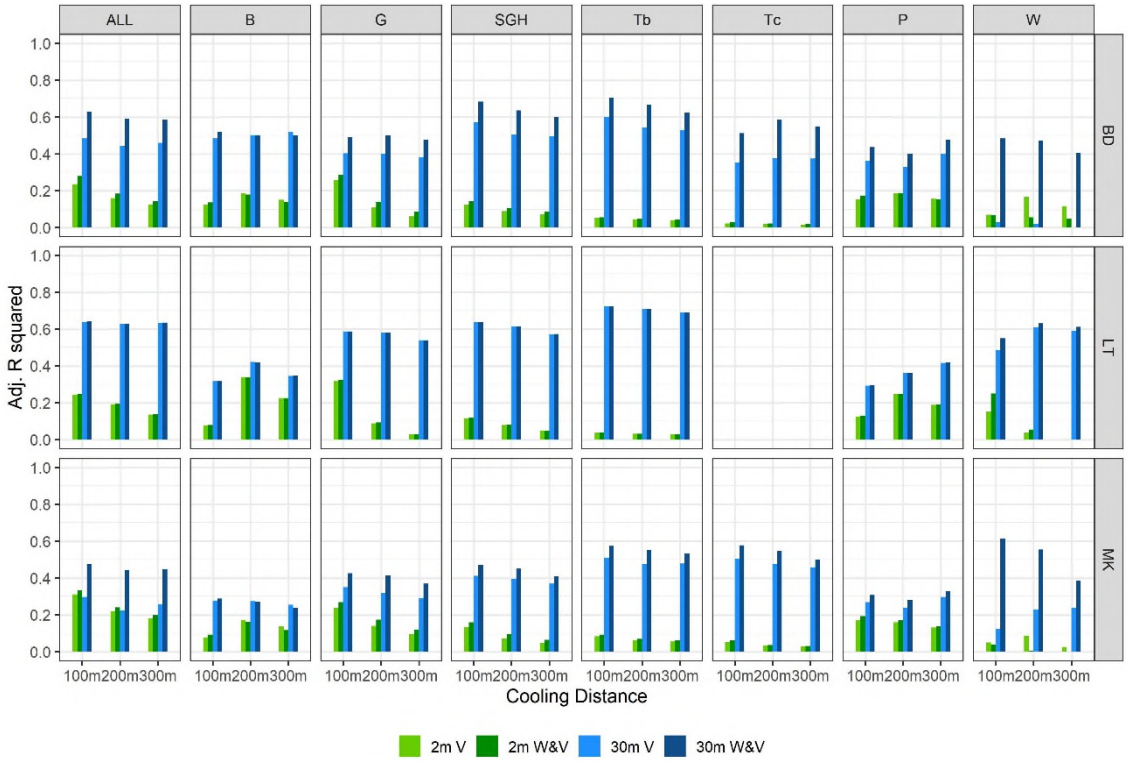

Figure 5-5 Adjusted R squared values obtained from ordinary least squares regression between the HM index and LST values at 2m (green) and 30m (blue) resolutions with cooling features set as vegetation (V) or vegetation and water (W&V) and three different cooling distances of large greenspaces for ALL as well as individual land cover classes. B – buildings, G – grass, P – paved, SGH – short trees/tall grass/hedge, Tb – broadleaf trees, Tc – coniferous trees, W – water

5.3.2 Changes of LST due to changes in the HM index

Validation of the HM index revealed that it most accurately represented LST after resampling to 30m resolution with model parameterisation including water as a cooling feature and when the 100m cooling distance away from large vegetated patches was considered. Consequently, linear regression equations obtained from the comparison for these parameters were used to calculate the amount of change in LST due to the gradual change in the HM index for all three towns and LC types (Table 5-4). On average, across all towns, the change in LST due to 0.1 change in the HM index was 0.76 °C, with the largest change of 0.96°C attributed to water, followed by trees (app.0.9 °C), and lowest amount of change occurring within paved (0.65°C). Differences in observed changes in LST could be attributed to the range of LST values observed within the land cover types in

each town, with lower ranges of LST (Figure Apx D-4) yielding a smaller degree of change.

Table 5-4 The amount of change in LST due to 0.1 change in the HM index for ALL and separate LC types in each town derived with inclusion of the cooling capacity of water and cooling distance away from large greenspaces of 100m, resampled to 30m resolution. B – buildings, G – grass, P – paved, SGH – short trees/tall grass/hedge, Tb – broadleaf trees, Tc – coniferous trees, W – water

Town	LC	Change in LST [°C]	Average change [°C]	Std. [°C]
BD		0.81		
LT	ALL	0.78		
MK		0.68	0.76	0.07
BD		0.76		
LT	B	1.05		
MK		0.82	0.88	0.15
BD		0.81		
LT	G	0.75		
MK		0.61	0.72	0.10
BD		0.64		
LT	P	0.72		
MK		0.58	0.65	0.07
BD		0.82		
LT	SGH	0.79		
MK		0.66	0.76	0.08
BD		0.99		
LT	Tb	0.93		
MK		0.82	0.91	0.08
BD		0.99		
LT	Tc	-		
MK		0.81	0.90	0.12
BD		0.88		
LT	W	0.84		
MK		1.17	0.96	0.18

5.4 Discussion

5.4.1 Factors determining the accuracy of the HM index

The InVEST 3.8.7 Urban Cooling model is aimed at describing the cooling capacity of greenspaces at their location as well as at a distance away and opens possibilities for testing thermal effects of various urban form designs and urban heat island mitigation measures without carrying out on-site measurements or complex analyses of remotely sensed thermal data. The model incorporates information on key properties of land surface that have been shown to determine

air and surface temperatures, and these include evaporative cooling of vegetation, shading by tall trees, and albedo. Whilst consideration of these factors by the model yielded the HM index values that represented some trends in LST, as demonstrated by the inverse relationship in linear regression, there was a large proportion of variation in LST that remained unexplained.

The magnitudes of the HM index and the outcomes of the comparison to LST data were impacted by the spatial resolution of datasets used in the assessment. Whilst associations between the HM index and LST at 2m resolution, corresponding to the spatial resolution of the input land cover map, were modest to low, they gained in strength after resampling of the HM index to match the mixed 30m resolution of Landsat-8 derived LST map – an effect that was observed in both the city-wide and individual land cover class assessments. This varied behaviour could be an indicator of an under-representation of the natural variation of LST by the HM index within each land cover class in 2m resolution outputs, which was mitigated through the resampling procedure to 30m that captured responses from different land cover classes into each coarser resolution grid cell through introduction of mixed pixels (Yow, 2007).

Cooling distance of large greenspaces was another factor that impacted the HM index magnitudes and the strength of the relationships with LST data. Whilst some of the observed differences in HM driven from different cooling extents of large vegetated patches were expected, it is important to note that the model uses the cooling distance set by the user as the radius of the circular moving window within which the total area of greenspaces is calculated and assigned to each grid cell of the land cover map submitted to the model. Consequently the amount of greenspace considered as large will increase with the increasing cooling distance. This instability of the model could be easily resolved in future releases by separating the cooling distance setting from the size of the search window within which to calculate the amount of greenspaces, however, at this stage makes the results difficult to interpret.

Inclusion of water as a cooling feature provided a small improvement in the strength of the relationship between the HM index and LST data, especially in

towns with a higher abundance of water bodies. The role of blue infrastructure in the reduction of the urban heat island effect is well recognised (Hathway and Sharples, 2012; Peng et al., 2020; Yu et al., 2020) and consequently it is recommended that its cooling capacity is included in the Urban Cooling model.

5.4.2 Opportunities for improvement of the accuracy of the HM index

Whilst at 30m resolution surface temperature of greenspaces was generally well represented by the HM index, some improvement is necessary for buildings and paved areas. This is especially important in the context of the Urban Cooling model's capacity to assess economic value of vegetative cooling by considering the energy savings due to a decreased use of air conditioning requiring accurate heat mitigation estimates for buildings. The Urban Cooling model attempts at representation temperature of grey infrastructure through the interplay of albedo and cooling capacity of large greenspaces at a distance away. Albedo, which corresponds to the amount of solar radiation reflected and therefore not absorbed by the land surface, manifests in the visible light spectrum as the brightness of colour, which can be captured through analysis of multispectral aerial or satellite remotely sensed data, allowing for diversification of its values within paved areas and buildings (Ejiagha et al., 2020; Hofierka et al., 2020). Moreover, LST of urban land cover is affected not only by albedo, but also the spatial properties of individual land cover patches, as demonstrated by Zhou, Huang, & Cadenasso (2011), which is further confirmed by the variable HM index magnitudes obtained in this study for towns with different morphologies. Adaptation of the input land cover map for differences in albedo as well as spatial properties of land cover classes could offer a possibility for improvement in representation of their temperature by the HM index, however, these would involve a more sophisticated approach to data preparation, requiring extensive expertise in spatial data analysis that may not be available for all model users (Norton et al., 2015).

5.4.3 Applicability of the model

It is important to note that the applicability of the results obtained from the Urban Cooling model will depend on climatic properties of the study area as evaporative cooling of vegetation in regions experiencing large precipitation, such

as for example South East Asia, is of lesser importance and UHI mitigation strategies should focus on maximising shading and ventilation (Manoli et al., 2019). Furthermore, as demonstrated by higher comparability of coarse resolution HM and LST datasets, the model outputs are more suitable for broader assessments that are equivalent to neighbourhood or city scales as suggested by Parsaee et al. (2019) and can therefore support decisions aimed at mitigation of the surface urban heat island at the master plan level.

5.5 Conclusions

In this study, the heat mitigation index generated by the InVEST 3.8.7 Urban Cooling model was validated by comparison to land surface temperature images captured on a warm summer day at two spatial resolutions: 2 and 30m in three sub-urban towns. The results suggested that the index is capable of depicting a portion of the thermal response of land surface, especially for towns with a denser built-up structure and at a coarser spatial resolution, with LST of greenspaces being better represented than of built-up land cover. Future work should focus on testing of the model under different heat scenarios that may affect the evaporative capacity of the vegetation as well as the possibility of diversification of not only the weights for shading, evapotranspiration and albedo but also the input land cover maps according to internal variability of these factors within each land cover type. This study has also demonstrated that inclusion of evaporation from water bodies in cooling capacity calculations can improve the accuracy of the heat mitigation index computed by the model, especially in cities with higher abundance of water bodies, indicating that cooling capacity of water can be successfully represented by the model. We found one important limitation of the model affecting the definition of large greenspaces and their cooling capacity estimates beyond their footprints, rendering the results difficult to interpret. Nevertheless, despite this issue, the heat mitigation index generated by the InVEST 3.8.7 Urban Cooling model had a fair resemblance to day-time land surface temperature data especially at a coarser spatial resolution. Consequently, the model can be used for high-level assessments of the cooling capacity of urban blue- and greenspaces that are adequate for masterplan

applications rather than fine-tuning of urban design, requiring only basic spatial data processing and analysis skills from its users.

5.6 References

Aleksandrowicz, O., Vuckovic, M., Kiesel, K. and Mahdavi, A. (2017) ‘Current trends in urban heat island mitigation research: Observations based on a comprehensive research repository’, *Urban Climate*, 21 Elsevier B.V., pp. 1–26. Available at: 10.1016/j.uclim.2017.04.002 (Accessed: 3 May 2020).

Allen, R.G., Pereira, L.S., Raes, D. and Smith, M. (1998) Crop evapotranspiration-Guidelines for computing crop water requirements-FAO Irrigation and drainage paper 56. Rome. Available at: https://www.researchgate.net/publication/235704197 (Accessed: 22 August 2020).

Aram, F., Higueras García, E., Solgi, E. and Mansournia, S. (2019) ‘Urban green space cooling effect in cities’, *Heliyon*, 5(4) Elsevier Ltd, p. e01339. Available at: 10.1016/j.heliyon.2019.e01339 (Accessed: 6 August 2020).

Bherwani, H., Singh, A. and Kumar, R. (2020) ‘Assessment methods of urban microclimate and its parameters: A critical review to take the research from lab to land’, *Urban Climate*, 34 Elsevier B.V., p. 100690. Available at: 10.1016/j.uclim.2020.100690 (Accessed: 14 September 2020).

Bowler, D.E., Buyung-Ali, L., Knight, T.M. and Pullin, A.S. (2010) ‘Urban greening to cool towns and cities: A systematic review of the empirical evidence’, *Landscape and Urban Planning*, 97(3) Elsevier, pp. 147–155. Available at: 10.1016/j.landurbplan.2010.05.006 (Accessed: 28 July 2020).

Casanueva, A., Kotlarski, S., Fischer, A.M., Flouris, A.D., Kjellstrom, T., Lemke, B., Nybo, L., Schwierz, C. and Liniger, M.A. (2020) ‘Escalating environmental summer heat exposure—a future threat for the European workforce’, *Regional Environmental Change*, 20(2) Springer, pp. 1–14. Available at: 10.1007/s10113-020-01625-6 (Accessed: 29 August 2020).

Cortinovis, C. and Geneletti, D. (2019) ‘A framework to explore the effects of urban planning decisions on regulating ecosystem services in cities’, *Ecosystem Services*, 38 Elsevier B.V., p. 100946. Available at: 10.1016/j.ecoser.2019.100946 (Accessed: 4 September 2020).

Droogers, P. and Allen, R.G. (2002) ‘Estimating reference evapotranspiration under inaccurate data conditions’, *Irrigation and Drainage Systems*, 16(1), pp. 33–45. Available at: 10.1023/A:1015508322413 (Accessed: 22 August 2020).

Ejiagha, I.R., Ahmed, M.R., Hassan, Q.K., Dewan, A., Gupta, A. and Rangelova, E. (2020) ‘Use of Remote Sensing in Comprehending the Influence of Urban Landscape’s Composition and Configuration on Land Surface Temperature at Neighbourhood Scale’, *Remote Sensing*, 12(15) MDPI AG, p. 2508. Available at: 10.3390/rs12152508 (Accessed: 30 August 2020).

Erell, E. (2008) ‘The Application of Urban Climate Research in the Design of Cities’, *Advances in Building Energy Research*, 2(1), pp. 95–121. Available at: 10.3763/aber.2008.0204 (Accessed: 31 August 2020).

Grafius, D.R., Corstanje, R., Warren, P.H., Evans, K.L., Hancock, S. and Harris, J.A. (2016) ‘The impact of land use/land cover scale on modelling urban ecosystem services’, *Landscape Ecology*, 31(7) Springer Netherlands, pp. 1509–1522. Available at: 10.1007/s10980-015-0337-7 (Accessed: 3 September 2017).

Hathway, E.A. and Sharples, S. (2012) ‘The interaction of rivers and urban form in mitigating the Urban Heat Island effect: A UK case study’, *Building and Environment*, 58 Pergamon, pp. 14–22. Available at: 10.1016/j.buildenv.2012.06.013 (Accessed: 3 May 2020).

Heaviside, C., Macintyre, H. and Vardoulakis, S. (2017) ‘The Urban Heat Island: Implications for Health in a Changing Environment’, *Current Environmental Health Reports*, 4(3) Springer, pp. 296–305. Available at: 10.1007/s40572-017-0150-3 (Accessed: 30 April 2020).

Heaviside, C., Vardoulakis, S. and Cai, X.-M. (2016) ‘Attribution of mortality to the urban heat island during heatwaves in the West Midlands, UK’, *Environmental*

Health, 15(S1) BioMed Central Ltd., p. S27. Available at: 10.1186/s12940-016-0100-9 (Accessed: 30 April 2020).

Hofierka, J., Gallay, M., Onačillová, K. and Hofierka, J. (2020) 'Physically-based land surface temperature modeling in urban areas using a 3-D city model and multispectral satellite data', *Urban Climate*, 31 Elsevier B.V., p. 100566. Available at: 10.1016/j.uclim.2019.100566 (Accessed: 30 August 2020).

Jimenez-Munoz, J.C., Sobrino, J.A., Skokovic, D., Mattar, C. and Cristobal, J. (2014) 'Land surface temperature retrieval methods from landsat-8 thermal infrared sensor data', *IEEE Geoscience and Remote Sensing Letters*, 11(10), pp. 1840–1843. Available at: 10.1109/LGRS.2014.2312032 (Accessed: 15 February 2018).

Kjellstrom, T., Freyberg, C., Lemke, B., Otto, M. and Briggs, D. (2018) 'Estimating population heat exposure and impacts on working people in conjunction with climate change', *International Journal of Biometeorology*, 62(3) Springer New York LLC, pp. 291–306. Available at: 10.1007/s00484-017-1407-0 (Accessed: 29 August 2020).

Kleerekoper, L., van Esch, M. and Salcedo, T.B. (2012) 'How to make a city climate-proof, addressing the urban heat island effect', *Resources, Conservation and Recycling*, 64 Elsevier B.V., pp. 30–38. Available at: 10.1016/j.resconrec.2011.06.004 (Accessed: 4 September 2020).

Lin, P., Gou, Z., Lau, S. and Qin, H. (2017) 'The Impact of Urban Design Descriptors on Outdoor Thermal Environment: A Literature Review', *Energies*, 10(12) MDPI AG, p. 2151. Available at: 10.3390/en10122151 (Accessed: 2 September 2020).

Manoli, G., Fatichi, S., Schläpfer, M., Yu, K., Crowther, T.W., Meili, N., Burlando, P., Katul, G.G. and Bou-Zeid, E. (2019) 'Magnitude of urban heat islands largely explained by climate and population', *Nature*, 573(7772) Nature Publishing Group, pp. 55–60. Available at: 10.1038/s41586-019-1512-9 (Accessed: 2 September 2020).

Meng, C. (2017) ‘Mitigating the surface urban heat island: Mechanism study and sensitivity analysis’, *Asia-Pacific Journal of Atmospheric Sciences*, 53(3) Korean Meteorological Society, pp. 327–338. Available at: 10.1007/s13143-017-0036-1 (Accessed: 3 September 2020).

Met Office; Hollis, D.; McCarthy, M.; Kendon, M.; Legg, T.; Simpson, I. (2019) ‘HadUK-Grid Gridded Climate Observations on a 1km grid over the UK, v1.0.1.0 (1862-2018)’. Centre for Environmental Data Analysis, 14 November 2019. Available at: 10.5285/d134335808894b2bb249e9f222e2eca8.

Norton, B.A., Coutts, A.M., Livesley, S.J., Harris, R.J., Hunter, A.M. and Williams, N.S.G. (2015) ‘Planning for cooler cities: A framework to prioritise green infrastructure to mitigate high temperatures in urban landscapes’, *Landscape and Urban Planning*, 134 Elsevier, pp. 127–138. Available at: 10.1016/j.landurbplan.2014.10.018 (Accessed: 29 August 2020).

Oke, T.R. (1976) ‘The distinction between canopy and boundary-layer urban heat islands’, *Atmosphere*, 14(4) Taylor & Francis Group, pp. 268–277. Available at: 10.1080/00046973.1976.9648422 (Accessed: 30 April 2020).

Oke, T.R. (1988) ‘The urban energy balance’, *Progress in Physical Geography*, 12(4) Sage Publications Sage CA: Thousand Oaks, CA, pp. 471–508. Available at: 10.1177/030913338801200401 (Accessed: 31 August 2020).

Oke, T.R., Johnson, G.T., Steyn, D.G. and Watson, I.D. (1991) ‘Simulation of surface urban heat islands under “ideal” conditions at night part 2: Diagnosis of causation’, *Boundary-Layer Meteorology*, 56(4) Kluwer Academic Publishers, pp. 339–358. Available at: 10.1007/BF00119211 (Accessed: 29 August 2020).

Office for National Statistics (2013) 2011 census, Key statistics for built up areas in England and Wales (report). United Kingdom Office for National Statistics, London.

Parsaee, M., Joybari, M.M., Mirzaei, P.A. and Haghighat, F. (2019) Urban heat island, urban climate maps and urban development policies and action plans.

Environmental Technology and Innovation. Elsevier B.V.,pp. 100341. Available at: 10.1016/j.eti.2019.100341 (Accessed: 31 August 2020).

Peng, J., Liu, Q., Xu, Z., Lyu, D., Du, Y., Qiao, R. and Wu, J. (2020) 'How to effectively mitigate urban heat island effect? A perspective of waterbody patch size threshold', *Landscape and Urban Planning*, 202 Elsevier B.V., p. 103873. Available at: 10.1016/j.landurbplan.2020.103873 (Accessed: 4 September 2020).

Perkins, S.E., Alexander, L. V. and Nairn, J.R. (2012) 'Increasing frequency, intensity and duration of observed global heatwaves and warm spells', *Geophysical Research Letters*, 39(20) Blackwell Publishing Ltd, p. 2012GL053361. Available at: 10.1029/2012GL053361 (Accessed: 30 April 2020).

Phelan, P.E., Kaloush, K., Miner, M., Golden, J., Phelan, B., Silva, H. and Taylor, R.A. (2015) 'Urban Heat Island: Mechanisms, Implications, and Possible Remedies', *Annual Review of Environment and Resources*, 40(1) Annual Reviews Inc., pp. 285–307. Available at: 10.1146/annurev-environ-102014-021155 (Accessed: 22 August 2020).

Roth, M., Oke, T.R. and Emery, W.J. (1989) 'Satellite-derived urban heat islands from three coastal cities and the utilization of such data in urban climatology', *International Journal of Remote Sensing*, 10(11) Taylor & Francis Group , pp. 1699–1720. Available at: 10.1080/01431168908904002 (Accessed: 3 September 2020).

Santamouris, M., Cartalis, C., Synnefa, A. and Kolokotsa, D. (2015) 'On the impact of urban heat island and global warming on the power demand and electricity consumption of buildings—A review', *Energy and Buildings*, 98 Elsevier Ltd, pp. 119–124. Available at: 10.1016/j.enbuild.2014.09.052 (Accessed: 29 August 2020).

Sharp, R., Douglass, J., Wolny, S., Arkema, K., Bernhardt, J., Bierbower, W., Chaumont, N., Denu, D., Fisher, D., Glowinski, K., Griffin, R., Guannel, G., Guerry, A., Johnson, J., Hamel, P., Kennedy, C., Kim, C.K., Lacayo, M., Lonsdorf, E., Mandle, L., Rogers, L., Silver, J., Toft, J., Verutes, G., Vogl, A. L., Wood, S,

and Wyatt, K. 2020, InVEST 3.8.7.post12+ug.gbcad34f User's Guide. The Natural Capital Project, Stanford University, University of Minnesota, The Nature Conservancy, and World Wildlife Fund.

Sung, C.Y. (2013) 'Mitigating surface urban heat island by a tree protection policy: A case study of The Woodland, Texas, USA', *Urban Forestry & Urban Greening*, 12(4) Urban & Fischer, pp. 474–480. Available at: 10.1016/j.ufug.2013.05.009 (Accessed: 3 September 2020).

Taha, H., Akbari, H., Rosenfeld, A. and Huang, J. (1988) 'Residential cooling loads and the urban heat island—the effects of albedo', *Building and Environment*, 23(4) Pergamon, pp. 271–283. Available at: 10.1016/0360-1323(88)90033-9 (Accessed: 26 July 2020).

Tsoka, S., Tsikaloudaki, K., Theodosiou, T. and Bikas, D. (2020) 'Urban warming and cities' microclimates: Investigation methods and mitigation strategies—A review', *Energies*, 13(6) MDPI AG, p. 1414. Available at: 10.3390/en13061414 (Accessed: 14 September 2020).

Vaz Monteiro, M., Doick, K.J., Handley, P. and Peace, A. (2016) 'The impact of greenspace size on the extent of local nocturnal air temperature cooling in London', *Urban Forestry and Urban Greening*, 16 Elsevier GmbH, pp. 160–169. Available at: 10.1016/j.ufug.2016.02.008 (Accessed: 28 July 2020).

Voogt, J. and Oke, T. (2003) 'Thermal remote sensing of urban climates', *Remote Sensing of Environment,* 86(3) Elsevier, pp. 370–384. Available at: 10.1016/S0034-4257(03)00079-8 (Accessed: 3 July 2018).

Wang, W., Yao, X. and Shu, J. (2020) 'Air advection induced differences between canopy and surface heat islands', *Science of The Total Environment*, 725, p. 138120. Available at: 10.1016/j.scitotenv.2020.138120.

Wouters, H., De Ridder, K., Poelmans, L., Willems, P., Brouwers, J., Hosseinzadehtalaei, P., Tabari, H., Vanden Broucke, S., van Lipzig, N.P.M. and Demuzere, M. (2017) 'Heat stress increase under climate change twice as large in cities as in rural areas: A study for a densely populated midlatitude maritime

region', *Geophysical Research Letters*, 44(17) Blackwell Publishing Ltd, pp. 8997–9007. Available at: 10.1002/2017GL074889 (Accessed: 30 April 2020).

Yow, D.M. (2007) 'Urban Heat Islands: Observations, Impacts, and Adaptation', *Geography Compass*, 1(6) Wiley, pp. 1227–1251. Available at: 10.1111/j.1749-8198.2007.00063.x (Accessed: 31 August 2020).

Yu, Z., Yang, G., Zuo, S., Jørgensen, G., Koga, M. and Vejre, H. (2020) 'Critical review on the cooling effect of urban blue-green space: A threshold-size perspective', *Urban Forestry & Urban Greening*, 49 Elsevier GmbH, p. 126630. Available at: 10.1016/j.ufug.2020.126630 (Accessed: 31 August 2020).

Zardo, L., Geneletti, D., Pérez-Soba, M. and Van Eupen, M. (2017) 'Estimating the cooling capacity of green infrastructures to support urban planning', *Ecosystem Services*, 26 Elsevier B.V., pp. 225–235. Available at: 10.1016/j.ecoser.2017.06.016 (Accessed: 24 July 2020).

Zawadzka, J., Corstanje, R., Harris, J. and Truckell, I. (2020) 'Downscaling Landsat-8 land surface temperature maps in diverse urban landscapes using multivariate adaptive regression splines and very high resolution auxiliary data', *International Journal of Digital Earth*, 13(8) Taylor & Francis, pp. 899–914. Available at: 10.1080/17538947.2019.1593527 (Accessed: 17 April 2019).

Zhou, D., Xiao, J., Bonafoni, S., Berger, C., Deilami, K., Zhou, Y., Frolking, S., Yao, R., Qiao, Z. and Sobrino, J. (2018) 'Satellite Remote Sensing of Surface Urban Heat Islands: Progress, Challenges, and Perspectives', *Remote Sensing*, 11(1) MDPI AG, p. 48. Available at: 10.3390/rs11010048 (Accessed: 14 September 2020).

Zhou, W., Huang, G. and Cadenasso, M.L. (2011) 'Does spatial configuration matter? Understanding the effects of land cover pattern on land surface temperature in urban landscapes', *Landscape and Urban Planning*, 102(1), pp. 54–63. Available at: 10.1016/j.landurbplan.2011.03.009 (Accessed: 8 May 2020).

6 CHAPTER SIX

Discussion of wider implications of the research presented in this thesis

6.1 Overview of findings

6.1.1 Findings addressing hypotheses

This thesis set out to verify three hypotheses:

HS1: Urban form, through the existence of specific spatial configuration conditions contributing to the formation of cool- and hot spots within urban areas, has the capacity to regulate land surface temperature of individual land cover patches and that capacity is dependent on properties of target and neighbouring land cover patches.

HS2: Urban form's capacity to regulate land surface temperature of individual land cover patches is resilient throughout a warming summer.

HS3: Simplified urban cooling models can substitute sophisticated spatial analyses in assessment of the land surface temperature regulation capacity of urban form at microscales.

The first hypothesis was confirmed. Specific spatial configuration conditions of urban form associated with the formation of the coldest and hottest patches of buildings, paved, grass and trees were determined within the study area. Spatial configuration properties of land cover patches in the nearest neighbourhood were of higher importance than these of the target land cover patches, however, the type and aggregation level of the target patches influenced the ease of LST regulation and modified the magnitude of spatial configuration descriptors needed to achieve a given thermal effect. In particular, the role of spatial configuration of urban form in LST regulation was the strongest for buildings as well as less aggregated patches of all land cover types. The coldest patches of buildings, grass and paved were formed in the neighbourhood of more-aggregated patches of trees, less-aggregated patches of paved and at a higher proximity to water than the hottest patches of these land cover types. The coldest

patches of trees were associated with well-aggregated patches of grass and high proximity to water. Relatively higher distance from buildings was also helpful in discerning the coldest patches of grass, paved and trees. Further details on these findings are described in Chapter 4.

The second hypothesis was partially confirmed. Whilst spatial aggregation of trees, grass or paved located in the neighbourhood of the core land cover patches yielding a particular thermal effect did not change distinctly between the two dates investigated here set a month apart over summer, the importance of various spatial configuration descriptors shifted over time. In particular, the distance to water and elevation gained in importance as well as changed in magnitudes as summer progressed, with the effect of spatial aggregation of neighbouring land cover patches declining over time. Further details on these findings are described in Chapter 4.

The third hypothesis was rejected. The heat mitigation index generated by the InVEST Urban Cooling model based on information on evapotranspiration, albedo and cooling distance away from large vegetated patches was unable to accurately represent LST at 2m resolution, relevant to micro-scales. The model represented LST at 30m with at least doubled accuracy, as measured by R^2 returned by linear regression models between LST and HM index, indicating that it is more suitable for overview studies, with results applicable to urban planning at the masterplan level. The applicability of the model at smaller scales was recently confirmed by a study of cooling capacity of city districts in Milan, utilising an earlier version of the model (Ronchi, Salata and Arcidiacono, 2020). Further details on these findings are described in Chapter 5.

6.1.2 Additional findings

Additional findings derived as part of this thesis comprise elucidation of an improved downscaling method for coarse resolution LST imagery (Chapter 2), generation of a new typology of urban land cover (Chapter 3), and assessment of the accuracy of a new model for estimation of cooling capacity of urban greenspaces (Chapter 5).

The improved methodology for LST downscaling described in Chapter 2 was the first-time application of the multivariate adaptive regression splines and scaling factors that included rarely or never before used spectral indices (NDBI, CMR, FMR, IOR) to downscale Landsat 8 thermal images at 30(100)m to a 2(4)m resolution, with RMSE showing an improvement over previously developed methods. Additional contribution of this work comprised the development of a method for adjustment of spectral indices for temporal mismatches between acquisition dates of the satellite and ancillary aerial imagery that was successful for both winter- and summer-time imagery. Very fine resolution LST maps generated with this method helped mitigate the risk of introduction of mixed pixels (Yow, 2007) into the analyses of the associations between spatial configuration of urban form and LST of individual land cover patches, increasing the precision of the findings.

The new urban land cover typology, described in Chapter 3, stratifying all main urban land cover types, i.e. buildings, grass, paved, trees, and water, into sub-types with different spatial aggregation and thermal properties, allowed for accurate depiction of individual land cover patches with unique properties, which would otherwise be impossible from high resolution land cover maps in a raster format, prone to over-representing land cover class connectivity. The typology was of high significance for addressing the first hypothesis of the project, as it allowed for an accurate representation of land cover patches with unique spatial properties within the study area.

Deployment of the InVEST Urban Cooling model described in Chapter 5 was the first known attempt to validate the main model output – the HM index. Low accuracy of the index at micro-scales confirmed that more sophisticated studies of the urban thermal environment, e.g. methods applied as part of this thesis, are still necessary to inform urban design for excess heat mitigation at scales relevant to human outdoor and indoor thermal comfort.

6.2 Discussion

Temperature regulation capacity of urban form elucidated in this study at micro-scales, relevant to human thermal comfort at street- or building level, can

be viewed as a refinement of existing studies linking spatial configuration of urban form to LST at coarser spatial scales. Focussing on individual land cover patches rather than neighbourhoods or districts allowed for determination of specific spatial configuration conditions leading to particular thermal effects, providing additional insights into appropriate arrangement of urban space in the context of excess heat mitigation. Moreover, the development of a new typology for urban land cover based on morphometric and thermal properties of individual land cover patches is both in line with and a refinement of the existing classification of local climate zones (Stewart and Oke, 2012) that distinguishes urban morphologies for applications in urban temperature studies at neighbourhood scales. As such, methodology for automated extraction of the land cover typology developed here can contribute to other studies aiming at stratification of cities into local climate zones.

This study has also provided insights into the distance over which LST of individual land cover patches is influenced by neighbouring land cover patches, which can be related to studies of the cooling distance of urban parks. Although this study focussed on individual land cover patches rather than parks, which are typically composites of land cover patches of different types, the size of the zone of influence elucidated here was comparable to the lower distance values established in other studies.

There are, however, several limitations of this study that still need to be addressed. Firstly, the results were derived from LST images that were downscaled, using statistical methods, to a finer resolution. Whilst this was essential for reduction of the mixed pixel effect affecting coarser resolution data as well as for improvement of overall accuracy of assessment, the downscaling procedure was still affected by a degree of error, and could lead to a misrepresentation of LST extremes. Consequently, similar studies using very high resolution directly captured thermal imagery are recommended to verify findings presented here. Further limitation related to the LST data is that available images represented LST captured at 11 a.m. on two regular summer dates, and therefore further studies investigating the link between urban form and LST of

individual land cover patches should be carried out for data representing overall warmer and therefore more challenging conditions such as heatwaves and afternoons, when LST is expected to be higher. Antecedent weather conditions and duration of heatwaves and overall climate characteristics should be accounted for as well.

Another limitation of this study, preventing upscaling of the results to all urban areas, is that the spatial configuration conditions conducive to the formation of the coldest and hottest land cover patches of a given type were derived for sub-urban towns, which excluded certain types of urban morphologies from the assessment, such as, for example, high-rise buildings typical of commercial city centres or high-density residential blocks of flats. Consequently, land cover typology derived here should be expanded to accommodate for morphologies missed in this study, and the relationships between urban form and LST re-tested on the expanded dataset.

There was also a certain limitation related to development of the InVEST Urban Cooling model, explored in Chapter 5, which affected the way large greenspaces were identified within the study area. This limitation lead to an underestimation of the abundance of large parks at the lowest cooling distance of vegetation, which could have affected the accuracy of the assessment carried out for this model setting. Despite this limitation, that could be easily fixed by model developers in future releases, the overall conclusion that the model is better suited for heat mitigation studies at the masterplan level has not changed, given better performance of the results at a coarser rather than finer spatial resolution for model runs quantifying the cooling effect of large greenspaces.

6.3 Implications

The outcomes of this thesis have strong implications for urban planning both at urban design and masterplan level. At masterplan level, the contribution of this thesis is substantiated in the assessment of the InVEST Urban Cooling model, which can be deployed at early stages of urban design to assess the need and the optimal location of greenspaces in the context of excess heat mitigation at city-scale. Once these locations are identified, fine-scale recommendations

regarding the spatial arrangement of urban form can be utilised to design urban spaces conducive to indoor and outdoor thermal comfort. Whilst urban greenspaces, and trees in particular, were identified as important features of urban structure for heat mitigation, findings of this thesis highlighted the role of spatial properties and the distribution of water, paved areas and buildings in formation of cooler urban spaces. Whilst the cooling impact of water bodies has already been extensively investigated in other studies (Hathway and Sharples, 2012; Yu et al., 2020), quantification of the effect of spatial configuration of grey land cover classes presented in this thesis is consistent with and provides further evidence for the observation that the spatial configuration of all and not just vegetated land cover classes is important for urban heat mitigation (Zhou, Huang and Cadenasso, 2011)

Development the new urban land cover typology presented in Chapter 3 that combines spatial and thermal properties of individual land cover patches may serve as a link between site-level model simulations (Tsoka et al., 2020) and broad-scale LST-urban form studies by providing opportunities for upscaling of the modelling results, that are only computationally feasible for small fragments of cities. Further developments to the land cover typology might be required to account for feature heights or shape of urban canyons to enable upscaling of the simulation results that rely on these factors.

The land cover typology presented in Chapter 3 can also be applied in studies of the cooling effects of urban parks extending beyond their footprints. So far, a high variability of cooling distances of parks has been identified (Aram et al., 2019), with the effect attributed to spatial properties of the parks. A recent study of water bodies, however, indicated that local levels of socio-economic development had an impact on their cooling intensity (Peng et al., 2020). Consequently, analysis of urban structure surrounding urban parks facilitated by the land cover typology can offer additional insights to the observed variation in their cooling capacity, and contribute further recommendations to urban design.

Another implication of this research concerns the creation of multifunctional urban spaces in the context of provision of multiple ecosystem services by urban

greenspaces (Lovell and Taylor, 2013). Ecosystem services can be loosely defined as the benefits people derive from nature (Millennium Ecosystem Assessment, 2005), with urban areas benefitting from the capacity of urban greenspaces to reduce noise, purify air, retain excess run-off, cool down temperatures and provide space for recreation as well as sequester carbon for global climate regulation (Derkzen, van Teeffelen and Verburg, 2015), provide opportunities for pollination (Hamblin, Youngsteadt and Frank, 2018), food production (Edmondson et al., 2020), and maintenance of ecological networks for biodiversity (Vergnes, Viol and Clergeau, 2012). It is therefore necessary to undertake studies aiming at reconciliation of all these functions in the context of an appropriate space allocation to ensure their maximised supply. These studies should involve assessments of the public perception of proposed planning solutions to ensure provision of urban spaces that are multifunctional, liveable and accepted by the general public.

6.4 References

Aram, F., Higueras García, E., Solgi, E. and Mansournia, S. (2019) 'Urban green space cooling effect in cities', *Heliyon*, 5(4) Elsevier Ltd, p. e01339. Available at: 10.1016/j.heliyon.2019.e01339 (Accessed: 6 August 2020).

Derkzen, M.L., van Teeffelen, A.J.A. and Verburg, P.H. (2015) 'Quantifying urban ecosystem services based on high-resolution data of urban green space: An assessment for Rotterdam, the Netherlands', *Journal of Applied Ecology*, 52(4), pp. 1020–1032. Available at: 10.1111/1365-2664.12469 (Accessed: 18 June 2015).

Edmondson, J.L., Childs, D.Z., Dobson, M.C., Gaston, K.J., Warren, P.H. and Leake, J.R. (2020) 'Feeding a city – Leicester as a case study of the importance of allotments for horticultural production in the UK', *Science of The Total Environment*, 705 Elsevier B.V., p. 135930. Available at: 10.1016/j.scitotenv.2019.135930 (Accessed: 28 September 2020).

Hamblin, A.L., Youngsteadt, E. and Frank, S.D. (2018) 'Wild bee abundance declines with urban warming, regardless of floral density', *Urban Ecosystems*,

21(3) Springer New York LLC, pp. 419–428. Available at: 10.1007/s11252-018-0731-4 (Accessed: 28 September 2020).

Hathway, E.A. and Sharples, S. (2012) ‘The interaction of rivers and urban form in mitigating the Urban Heat Island effect: A UK case study’, *Building and Environment*, 58 Pergamon, pp. 14–22. Available at: 10.1016/j.buildenv.2012.06.013 (Accessed: 3 May 2020).

Lovell, S.T. and Taylor, J.R. (2013) ‘Supplying urban ecosystem services through multifunctional green infrastructure in the United States’, *Landscape Ecology*, 28(8), pp. 1447–1463. Available at: 10.1007/s10980-013-9912-y (Accessed: 26 March 2015).

Millennium Ecosystem Assessment (2005) Ecosystems and Human Well-being: Synthesis. Island Press, Washington, DC.

Peng, J., Liu, Q., Xu, Z., Lyu, D., Du, Y., Qiao, R. and Wu, J. (2020) ‘How to effectively mitigate urban heat island effect? A perspective of waterbody patch size threshold’, *Landscape and Urban Planning*, 202 Elsevier B.V., p. 103873. Available at: 10.1016/j.landurbplan.2020.103873 (Accessed: 4 September 2020).

Ronchi, S., Salata, S. and Arcidiacono, A. (2020) ‘Which urban design parameters provide climate-proof cities? An application of the Urban Cooling InVEST Model in the city of Milan comparing historical planning morphologies’, *Sustainable Cities and Society*, 63, p. 102459. Available at: 10.1016/j.scs.2020.102459.

Stewart, I.D. and Oke, T.R. (2012) ‘Local climate zones for urban temperature studies’, Bulletin of the American Meteorological Society, 93(12) *American Meteorological Society*, pp. 1879–1900. Available at: 10.1175/BAMS-D-11-00019.1 (Accessed: 5 September 2020).

Tsoka, S., Tsikaloudaki, K., Theodosiou, T. and Bikas, D. (2020) ‘Urban warming and cities’ microclimates: Investigation methods and mitigation strategies—A review’, *Energies*, 13(6) MDPI AG, p. 1414. Available at: 10.3390/en13061414 (Accessed: 14 September 2020).

Vergnes, A., Viol, I. Le and Clergeau, P. (2012) ‘Green corridors in urban landscapes affect the arthropod communities of domestic gardens’, *Biological Conservation*, 145(1) Elsevier, pp. 171–178. Available at: 10.1016/j.biocon.2011.11.002 (Accessed: 28 September 2020).

Yow, D.M. (2007) ‘Urban Heat Islands: Observations, Impacts, and Adaptation’, *Geography Compass*, 1(6) Wiley, pp. 1227–1251. Available at: 10.1111/j.1749-8198.2007.00063.x (Accessed: 31 August 2020).

Yu, Z., Yang, G., Zuo, S., Jørgensen, G., Koga, M. and Vejre, H. (2020) ‘Critical review on the cooling effect of urban blue-green space: A threshold-size perspective’, *Urban Forestry & Urban Greening*, 49 Elsevier GmbH, p. 126630. Available at: 10.1016/j.ufug.2020.126630 (Accessed: 31 August 2020).

Zhou, W., Huang, G. and Cadenasso, M.L. (2011) ‘Does spatial configuration matter? Understanding the effects of land cover pattern on land surface temperature in urban landscapes’, *Landscape and Urban Planning*, 102(1), pp. 54–63. Available at: 10.1016/j.landurbplan.2011.03.009 (Accessed: 8 May 2020).

7 CHAPTER SEVEN

Conclusions and future work

7.1 CONCLUSIONS

The overall findings of this thesis demonstrate that micro-scale studies of the relationship between spatial configuration of urban form and LST can support fine-tuning of urban design for improved temperature regulation in the context of urban heat island mitigation, with less sophisticated assessment methods suppling useful information for decision making at a master plan level. Specific conclusions to the objectives of this thesis are as follows:

O1-1: Evaluate the performance of multiple adaptive regression spline method and ancillary data in downscaling of coarse resolution land surface temperature imagery to a very fine spatial resolution suitable for microscale temperature studies

- LST downscaling procedure from 30(100) to 2(4)m resolution employing the MARS algorithm and high resolution ancillary data was suitable for depiction of fine-scale variation in LST across three British towns in the summer, with adjusted R^2 ranging from 0.64 to 0.84 and RMSE from 1.83 to 1.40K depending on town and date, and an improved performance as compared to equivalent multiple regression models. (Chapter 2)
- LST downscaling with the use of the MARS algorithm, spectral indices and fractional vegetation cover was not successful under low vegetation cover conditions, as demonstrated by poor performance of the downscaling models constructed for winter-time LST images, achieving adjusted R^2 values of 0.06 to 0.21 depending on town and date. (Chapter 2)
- Adjustment of spectral indices used as scaling factors in LST downscaling for values of equivalent coarse-resolution indices allowed for correction of the temporal mismatch between acquisition dates of the high resolution ancillary data and LST imagery, demonstrated by a substantial improvement in accuracy, measured by RMSE, of the multiple regression

models constructed with adjusted and unadjusted datasets, ranging from 0.62 to 1.27K depending on town and date. (Chapter 2)

O1-2: Develop a fine-resolution urban land cover typology and evaluate its relevance to urban temperature studies at microscales.

- Correlation analysis between class-level metrics related to shape and aggregation of land cover patches derived from a raster format land cover map with the use of moving window analysis of different sizes revealed that aggregation and not shape metrics are consistently correlated to LST, the strength of correlation depends on land cover type, and the strongest correlations with fine resolution LST data are obtained for metrics derived with a 100x100m moving window. (Chapter 3)
- The use of selected class aggregation landscape metrics (LSI, COHESION, PLADJ) and fine resolution LST data coupled with a two-tiered unsupervised k-means clustering procedure was capable to identify sub-types of land cover patches of each type (buildings, grass, paved, trees and water) with distinct spatial and thermal properties as demonstrated by significantly different means of various spatial configuration descriptors for a great majority of derived land cover sub-types. (Chapter 3)

O1-3: Determine and evaluate the zone of influence of urban form on land surface temperature of individual land cover patches

- The impact of spatial configuration of urban form on LST of individual land cover patches was the strongest at the immediate neighbourhood defined through a 10m buffer plotted around each land cover patch, as demonstrated by the largest drop in RMSE and increase in R^2 for Random Forest models relating LST of core land cover patches to spatial configuration descriptors of urban form. (Chapter 4)
- The actual size of the zone of influence may extend beyond the nearest 10m buffer due to the experimental set-up of the study whereby properties of entire land cover patches intersecting with the buffer zone were taken into account in the analysis. (Chapter 4)

O1-4: Evaluate the impact of spatial configuration properties of urban form on the formation of the coldest and hottest land cover patches of different types.

- Well aggregated patches of trees and grass, fragmented patches of paved or buildings, close proximity to water and location away from buildings were the discerning factors for the coldest patches of various land cover types, as quantified by the 1st or 3rd quartiles of spatial configuration descriptors with significantly different means for the coldest, medium-cold, medium-hot and hottest patches. (Chapter 4)
- The opposite trends as described for the coldest land cover patches with the addition of location at higher elevations contributed to the formation of the hottest land cover patches of various types. (Chapter 4)
- Spatial configuration descriptors of urban form neighbouring core land cover patches had a greater influence on their LST than the spatial properties of the land cover patches themselves, as demonstrated by performance statistics of Random Forest models linking LST of core patches to the respective spatial configuration properties, indicating that appropriate urban design is essential for excess heat mitigation in urban areas. (Chapter 4)
- Nevertheless, increasing spatial aggregation levels of core land cover patches demanded a higher aggregation level of vegetated patches to exhibit a cooling effect. (Chapter 4)
- The aggregation level of land cover patches of each type influenced the ease of prediction of their LST demonstrated by consistently lower and higher RMSE associated with Random Forest models for less and more aggregated land cover patches, respectively, suggesting that LST of more fragmented patches can be better controlled by spatial configuration of urban form in their neighbourhood. (Chapter 4)

O1-5: Evaluate the impact of spatial resolution of land surface temperature imagery on the outcome of temperature regulation studies at microscales.

- The size of the zone of the strongest influence of spatial configuration of urban form on LST of core land cover patches was in agreement between

analyses carried out at both fine and coarse spatial resolutions, however, the accuracy of the prediction was consistently lower in models constructed with the coarser resolution data, especially for buildings and the most aggregated patches of all types. Consequently, coarse resolution data are of indicative value and fine resolution LST datasets are needed to accurately represent temperature regulation capacity of spatial configuration of urban form at micro-scales. (Chapter 4)

O2-1: Evaluate the capacity of spatial configuration of urban form to continuously deliver a regulatory function for land surface temperature of individual land cover patches.

- Whilst the aggregation level of trees neighbouring land cover patches of various types required for the formation of the coldest or hottest patches did not substantially vary across two dates considered here, proximity to water and elevation associated with contrasting thermal responses of land cover patches changed as the summer progressed, suggesting that temperature regulation capacity of spatial configuration of urban form is dependent on the overall thermal conditions of a town. Further work is required to establish behaviours depending on various weather conditions, including heatwaves. (Chapter 4)

O3-1: Validate the performance of the heat mitigation index generated by the InVEST 3.8.7 Urban Cooling model in estimation of land surface temperature at microscales

- The magnitude of the R^2 statistic, ranging from 0.48 to 0.64 depending on town, returned by linear regression models relating the heat mitigation index to LST at both 2m and 30m resolution indicated a higher performance of the Urban Cooling model at the coarser resolution making the outputs applicable to planning decisions at a masterplan level rather than fine-tuning of urban design. (Chapter 5)

O3-2: Evaluate the capacity of the heat mitigation index, generated by the InVEST 3.8.7 Urban Cooling model, to accurately represent land surface temperature of different land cover types at microscales.

- At masterplan level, the heat mitigation index returned by the model was capable of representing a varied proportion of variation in LST, with the highest magnitude of the R^2 metric obtained for treed land cover types (0.47-0.73) and the lowest for paved (0.29-0.44) and buildings (0.29-0.52), making the model in its current form particularly suitable for the assessment of cooling capacity of greenspaces without off-site effects. This finding may change in future releases of the model after a fault affecting the estimation of the spatial distribution of large greenspaces assumed to have off-site cooling effects is corrected. (Chapter 5)

7.2 FUTURE WORK

Future work identified through discussion of the findings of the research presented in this thesis can be classified into several fields of interest: LST downscaling, development of urban form typologies, elucidation of relationships between urban form and thermal environment, and links to other fields of research with collaboration opportunities.

LST downscaling (Chapter 2):

- Explore the use of landscape metrics, which have been shown in this thesis to be useful in prediction of LST of individual land cover patches, in LST downscaling, with the caveat that both the LST downscaling and subsequent analyses should be carefully designed to avoid bias.

Urban form typologies (Chapter 3):

- Include a wider range of urban morphologies from cities and towns located worldwide as well as urban form and fabric descriptors not tested as part of this thesis in the development of urban form typologies relevant to excess heat mitigation studies at both micro- and masterplan scales,

potentially contributing to an automated identification or refinement of local climate zones.

- Apply alternative algorithms to k-means clustering analysis, such as hierarchical object-oriented classification methods, in the development of an improved urban form typology.

Elucidation of relationships between urban form and thermal environment (Chapters 4 and 5):

- Carry out studies of the relationships between LST and urban form using directly captured, either through aerial or unmanned aerial vehicle (UAV) surveys, very high resolution LST imagery to confirm temperature extremes within the study area as well as the size of zone of influence of spatial configuration of urban form on LST of individual land cover patches.
- Test the impact of spatial configuration of urban form, using a carefully selected land cover typology, on heat mitigation in towns and cities and verify recommendations to urban form design developed as part of this study for different weather conditions and times of day with a particular focus on heatwaves that pose the greatest threat to human health and well-being.
- Carry out a full sensitivity analysis of the InVEST Urban Cooling model and validate model outputs for heatwave weather conditions. Investigate the possibility of diversifying of the land cover map, serving as the main model input, to make account of the variation in albedo values of land cover types related to grey infrastructure, with the overall goal of improving the accuracy of representation of their LST by the heat mitigation index returned by the model.

Links to other fields of research with collaboration opportunities:

- Liaise with the urban planning community with regards to the development of urban form typologies as well as recommendations for urban design aimed at excess heat mitigation that are practicable and easy to use by the community at both the urban design and masterplan level.

- Explore possibilities for utilising the land cover typology developed in this study in upscaling of the results from micro-scale simulations of urban thermal environments, which incorporate the effects of air flow and street orientation on the thermal response of typically small sections of a city, to city-wide scales, in liaison with appropriate experts.
- Investigate the impact of recommendations for urban from design developed as part of this thesis or follow-up work on the supply of other urban ecosystem services, that include but are not limited to water and sediment retention, pollination, carbon sequestration, air quality modulation, habitat creation for biodiversity, and mental health and well-being of city dwellers, and develop recommendations ensuring maximised delivery of all ecosystem services.
- Investigate, in cooperation with social scientists, the public perception of urban forms identified as conducive to the improved temperature regulation and provision of other ecosystem services in towns and cities, with the overarching goal of creation of urban spaces that are liveable as well as ecologically sound.
- Explore applicability of micro-scale urban form typologies, either in the current or an improved form, in studies that use air temperature measurements to determine the cooling distance of urban parks that has been shown to be dependent of the spatial configuration of the parks, with the impact of properties of neighbouring urban form types remaining to be yet explicitly quantified.

APPENDICES

Appendix A Supplementary Materials to Chapter 2

A.1 Methodology for land surface temperature mapping at medium spatial resolution from Landsat 8 thermal data.

Emissivity for bands 10 and 11 of the Landsat 8 sensor was estimated using the NDVI thresholds method that involves the assignment of emissivity values for different types of land cover based on NDVI values obtained from red and near-infrared bands of satellite images of the study area. Typically, NDVI is used to determine the locations of bare ground and fully vegetated areas, to which respective emissivity values are assigned. The intermediary emissivity values are calculated from predefined equations, taking into account the vegetation fraction within a given pixel. In this study we used the simplified NDVI thresholds method, as presented in Sobrino et al. (2008), with a modification to allow for the assignment of emissivity values for pixels occupied by water as well as built-up areas rather than soil (Equation_Apx A-1). Based on visual inspection of the available imagery, NDVI threshold for water-occupied pixels was set to ≤-0.0001, built-up pixels to the range between -0.0001 and 0.05, and purely vegetated pixels to >0.5. Emissivity values for the pure land cover pixels were calculated as averages of data supplied by the MODIS UCSB Emissivity Library (https://icess.eri.ucsb.edu/modis/EMIS/html/em.html) for wavelengths equivalent to the thermal bands of Landsat 8. The emissivity for built-up areas was calculated as a mean of corresponding emissivity measurements for asphalt and apache interlocking pavement (0.973 and 0.965 respectively for bands 10 and 11), the emissivity for vegetation as a mean for oak and pine trees (0.976 and 0.975), and for water as a mean of values provided for water (0.987 and 0.992). Emissivity layers were derived from NDVI calculated at a 30 m resolution from Landsat 8 imagery acquired for each date considered in this study. Subsequently, the mean and difference between emissivity for band 10 and 11 were calculated. The resulting layers at 30m resolution were sharper than the thermal bands of the Landsat 8, which were captured at 100m resolution and subsequently resampled to 30m by the data provider, and therefore mismatching the thermal information available from Landsat 8. In order to mitigate this

mismatch we have upscaled the 30m resolution emissivity mean and difference layers by first resampling them to 10m with the nearest neighbour method retaining the 30m pixel values, then aggregating to 100m resolution with a mean function, and finally resampling back to 30m resolution with the bilinear convolution method to match the processing method of Landsat 8 TIR bands.

Equation_Apx A-1

$$\varepsilon_{i,j} = \begin{cases} \varepsilon_w, NDVI \leq NDVI_w \\ \varepsilon_{b\,i,j}, NDVI_w \leq NDVI \leq NDVI_b \\ \varepsilon_{b\,i,j} + (\varepsilon_{v\,i,j} - \varepsilon_{b\,i,j}) P_v, NDVI_b \leq NDVI \leq NDVI_v \\ \varepsilon_{v\,i,j}, NDVI > NDVI_v \end{cases}$$

Where:

$\varepsilon_{i,j}$ – emissivity for bands *i* and *j*;

$\varepsilon_{w\,i,j}$ – emissivity value for water for bands *i* and *j*, obtained from spectral libraries;

$\varepsilon_{b\,i,j}$ – emissivity value for built-up areas for bands *i* and *j*, obtained from spectral libraries;

$\varepsilon_{v\,i,j}$ – emissivity value for vegetation for bands *i* and *j*, obtained from spectral libraries;

NDVI – NDVI pixel value at a given location;

$NDVI_b$ – NDVI threshold value for built-up areas;

$NDVI_v$ – NDVI threshold value for vegetation;

P_v – vegetation fraction, calculated based on NDVI values (Equation_Apx A-2)

Equation_Apx A-2

$$P_v = \left[\frac{NDVI - NDVI_{min}}{NDVI_{max} - NDVI_{min}}\right]^2$$

Where:

P_v – vegetation fraction in a pixel at a given location, after Yu et al. (2014);

NDVI – NDVI pixel value at a given location;

$NDVI_{min}$ – NDVI threshold value equivalent to pure built-up pixels (0.05);

$NDVI_{max}$ – NDVI threshold value equivalent to pure vegetated pixels (0.5).

Water vapour values derived from the Near Infrared Total Precipitable Water Vapour Test Result (MOD05_L2) dataset derived from Terra MODIS used for atmospheric correction of Landsat 8 images are listed in Table_Apx A-1 below.

Table_Apx A-1 Mean and standard deviation of water vapour values of Milton Keynes (MK), Bedford (BD) and Luton (LT) for the four dates of interest [g cm^{-2}]

Date	MK	BD	LT
06-Jun-13	1.741 ± 0.0062	1.625 ± 0.0071	1.808 ± 0.0033
08-Jul-13	3.392 ± 0.0056	3.494 ± 0.0088	3.436 ± 0.0039
01-Feb-14	0.838 ± 0.0049	0.746 ± 0.0018	0.721 ± 0.0020
19-Jan-15	0.696 ± 0.0023	0.722 ± 0.0019	0.669 ± 0.0018

A.2 Spectral indices used in LST downscaling

Table_Apx A-2 List of LST predictors used in LST downscaling for Milton Keynes, Bedford and Luton.

Spectral Index	Formula*	References
Normalised Difference Vegetation Index	$\mathrm{NDVI} = \frac{(\mathrm{NIR} - \mathrm{Red})}{(\mathrm{NIR} + \mathrm{Red})}$	(Purevdorj et al., 1998)
Normalised Difference Built-Up Index (NDBI)	$\mathrm{NDBI} = \frac{(\mathrm{SWIR\ 1} - \mathrm{NIR})}{(\mathrm{SWIR\ 1} + \mathrm{NIR})}$	Zha et al. (2003)
Clay minerals ratio	$\mathrm{CMR} = \frac{\mathrm{SWIR\ 1}}{\mathrm{SWIR\ 2}}$	Drury (1987)
Ferrous minerals ratio	$\mathrm{FMR} = \frac{\mathrm{SWIR\ 1}}{\mathrm{NIR}}$	
Iron Oxide Ratio	$\mathrm{IOR} = \frac{\mathrm{Red}}{\mathrm{Blue}}$	
Built-Up Area Extraction Index (BAEI)	$\mathrm{BUAEI} = \frac{(\mathrm{Red} + \mathrm{L})}{(\mathrm{Green} + \mathrm{SWIR\ 1})}$	Bouzekri et al. (2015)
Percent Manmade (MNMD) Percent Water (WTR)	Percentage of either water or impervious land cover features within 2m resolution pixels derived from OS MasterMap	Chun and Guldmann (2014)

*Blue – band 2 equivalent of Landsat 8, 0.45–0.51 µm; Green – band 3 equivalent of Landsat 8, 0.53–0.59 µm; Red – band 4 equivalent of Landsat 8, 0.63–0.67 µm; NIR – band 5 equivalent of Landsat 8, 0.85–0.88 µm; SWIR 1 – band 6 equivalent of Landsat 8, 1.57–1.65 µm; SWIR 2 – band 7 equivalent of Landsat 8, 2.11–2.29 µm; L – an arithmetic constant equal to 0.3.

A.3 Results of the adjustment of the very high resolution spectral indices for the temporal mismatch caused by different dates of aerial and satellite data acquisition

Table_Apx A-3 Correlation coefficients calculated between pairs of spectral indices derived from the Landsat 8 imagery and (1) aggregated original spectral indices derived from hyperspectral imagery (Orig.), (2) aggregated adjusted spectral indices derived from very high resolution hyperspectral imagery (Adj.), and (3) differences in the magnitude of the correlation coefficients calculated between adjusted and original spectral indices (Diff.). Negative values of the differences indicate cases were the adjustment procedure decreased the resemblance of the original very high resolution spectral indices to the equivalent indices derived from satellite data.

Date	Town	Bedford			Luton			Milton Keynes		
	Spectral index	Orig.	Adj.	Diff.	Orig.	Adj.	Diff.	Orig.	Adj.	Diff.
02-Feb-14	BUAEI	*0.10*	0.36	0.26	*0.13*	0.51	0.38	*0.15*	0.49	0.34
	CMR	*0.36*	0.40	0.04	*0.35*	0.34	**-0.01**	*0.37*	0.27	**-0.10**
	FMR	*0.10*	0.96	0.86	*0.21*	0.89	0.69	*0.37*	0.91	0.53
	IOR	*0.27*	0.68	0.41	*0.47*	0.67	0.19	*0.31*	0.58	0.27
	NDBI	*0.07*	0.90	0.83	*0.17*	0.75	0.58	*0.33*	0.63	0.30
	NDVI	*0.30*	0.74	0.44	*0.31*	0.56	0.25	*0.47*	0.61	0.14
19-Jan-15	BUAEI	*0.15*	0.29	0.14	*0.18*	0.44	0.25	*0.24*	0.47	0.23
	CMR	*0.40*	0.35	**-0.05**	*0.33*	0.28	**-0.05**	*0.38*	0.20	**-0.18**
	FMR	*0.19*	0.95	0.76	*0.20*	0.91	0.71	*0.40*	0.43	0.03
	IOR	*0.31*	0.33	0.01	*0.45*	0.69	0.24	*0.35*	0.49	0.15
	NDBI	*0.17*	0.86	0.70	*0.18*	0.81	0.63	*0.36*	0.57	0.21
	NDVI	*0.39*	0.70	0.31	*0.32*	0.50	0.18	*0.49*	0.48	**-0.01**
08-Jul-13	BUAEI	*0.36*	0.67	0.31	*0.52*	0.81	0.30	*0.47*	0.81	0.35
	CMR	*0.71*	0.72	0.02	*0.72*	0.73	0.01	*0.64*	0.59	**-0.06**
	FMR	*0.25*	0.76	0.51	*0.11*	0.98	0.86	*0.52*	0.97	0.44
	IOR	*0.23*	0.91	0.68	***-0.05***	0.91	0.96	*0.23*	0.86	0.63
	NDBI	*0.19*	0.99	0.80	*0.05*	0.96	0.91	*0.46*	0.87	0.40
	NDVI	*0.53*	0.86	0.33	*0.37*	0.83	0.46	*0.65*	0.76	0.11
06-Jun-13	BUAEI	*0.33*	0.70	0.37	*0.44*	0.83	0.39	*0.49*	0.80	0.31
	CMR	*0.67*	0.76	0.09	*0.71*	0.43	**-0.28**	*0.64*	0.58	**-0.05**
	FMR	*0.36*	0.98	0.62	*0.29*	0.96	0.67	*0.55*	0.95	0.41
	IOR	*0.35*	0.96	0.61	*0.23*	0.84	0.61	*0.38*	0.86	0.48
	NDBI	*0.32*	0.97	0.65	*0.23*	0.96	0.73	*0.51*	0.87	0.37
	NDVI	*0.59*	0.88	0.29	*0.49*	0.84	0.35	*0.69*	0.81	0.13

Figures A-1 – A-4

Scatterplots and Pearson correlation coefficients calculated between pairs of spectral indices derived from the Landsat 8 imagery and (1) aggregated original spectral indices derived from hyperspectral imagery (dark grey, dashed regression line and cursive r values), (2) aggregated adjusted spectral indices derived from very high resolution hyperspectral imagery (light grey, solid regression line and bold r values). BD, LT, MK denote Bedford, Luton and Milton Keynes, respectively. X axis refers to the values of indices derived from hyperspectral aerial imagery, both original and adjusted for values of Landsat 8 indices at a given date, and Y axis shows the values of Landsat 8 derived spectral indices. Aggregation of spectral indices derived from aerial imagery refers to averaging of the fine resolution pixel values over 30m resolution grid cells aligned with Landsat 8 pixels carried out with the purpose of matching the spatial scales of these indices.

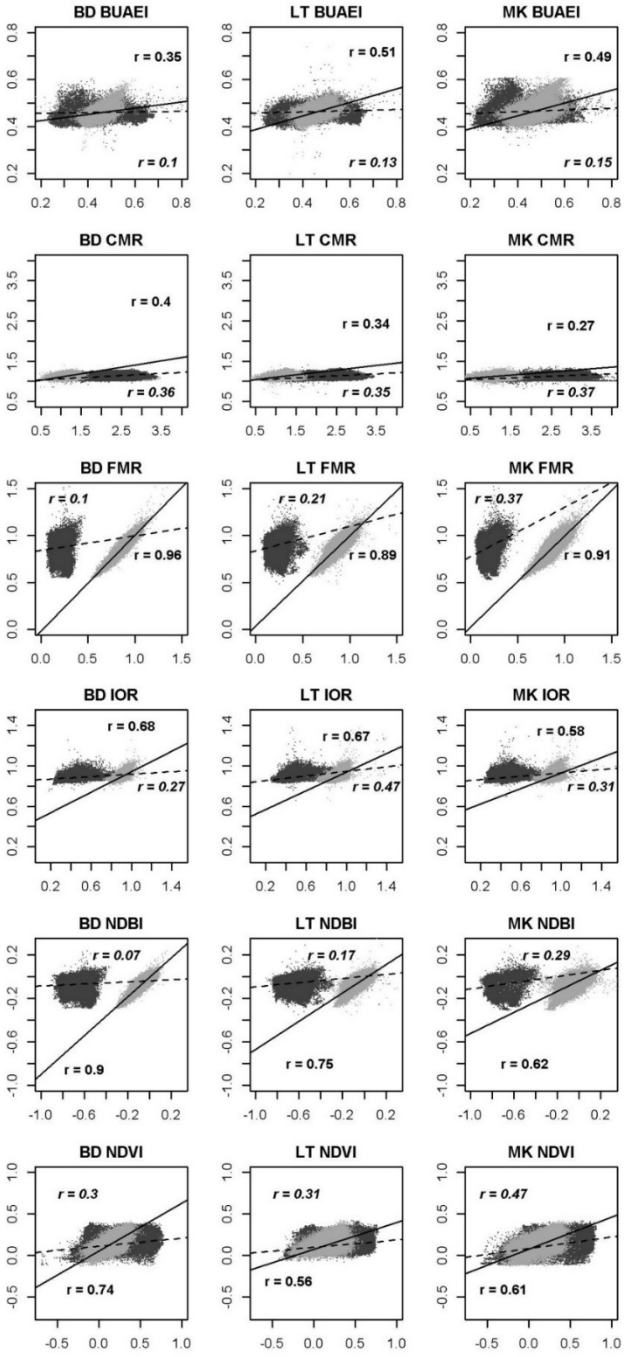

Figure_Apx A-1 Comparison of Landsat 8 spectral indices (y axis) with equivalent aggregated spectral indices derived from aerial imagery (x axis) before (dark grey, dashed regression line) and after (light grey, solid regression line) adjustment for the values of Landsat 8 indices for satellite data captured on 02 Feb 2014. Full explanation of the figure given in the first paragraph of Appendix A3.

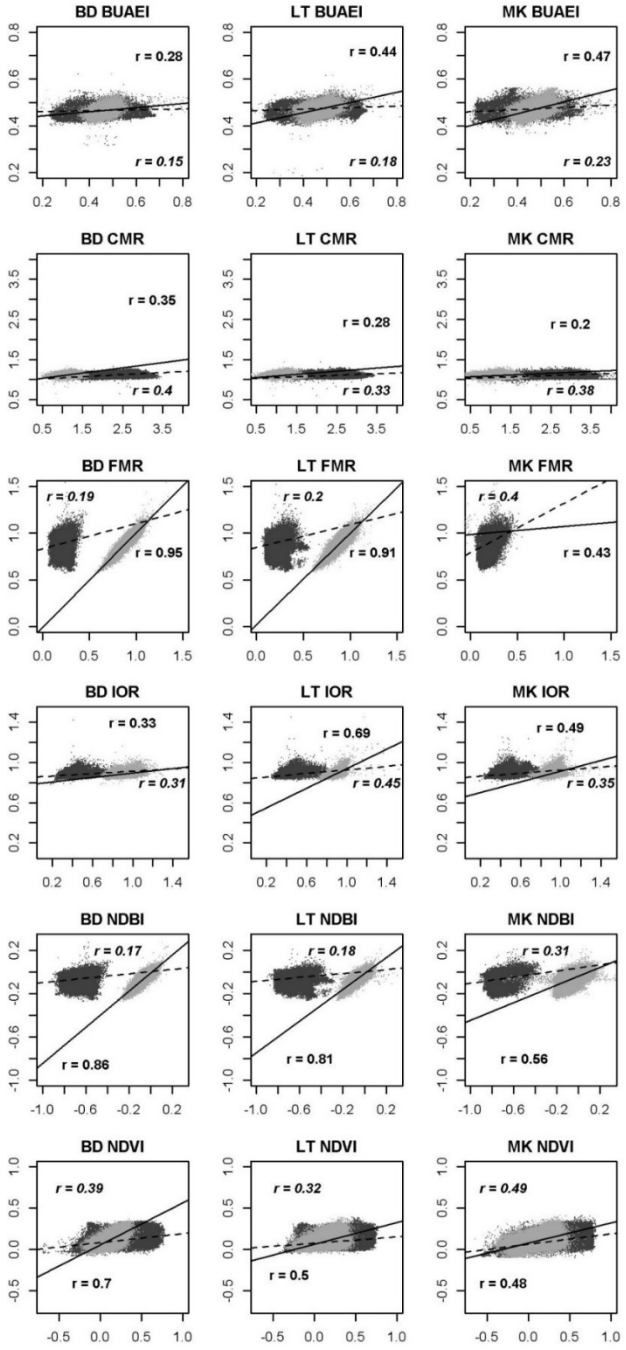

Figure_Apx A-2 Comparison of Landsat 8 spectral indices (y axis) with equivalent aggregated spectral indices derived from aerial imagery (x axis) before (dark grey, dashed regression line) and after (light grey, solid regression line) adjustment for the values of Landsat 8 indices for satellite data captured on 19 Jan 2015. Full explanation of the figure given in the first paragraph of Appendix A3.

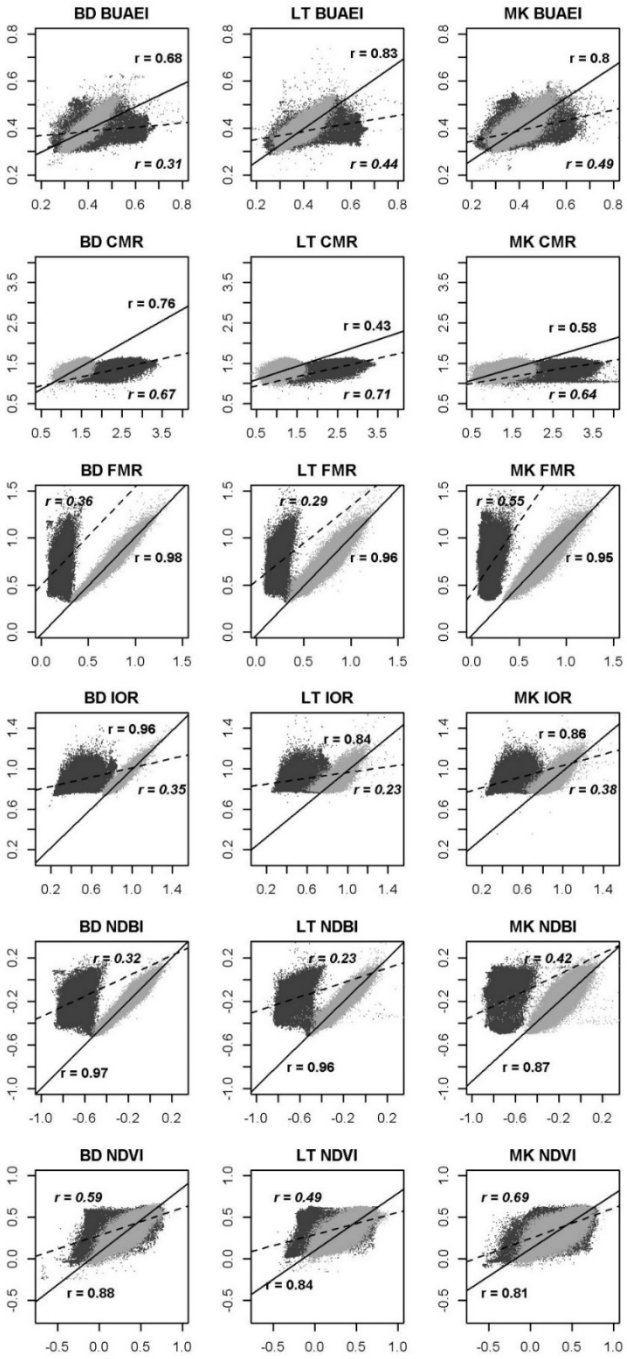

Figure_Apx A-3 Comparison of Landsat 8 spectral indices (y axis) with equivalent aggregated spectral indices derived from aerial imagery (x axis) before (dark grey, dashed regression line) and after (light grey, solid regression line) adjustment for the values of Landsat 8 indices for satellite data captured on 06 Jun 2013. Full explanation of the figure given in the first paragraph of Appendix A3.

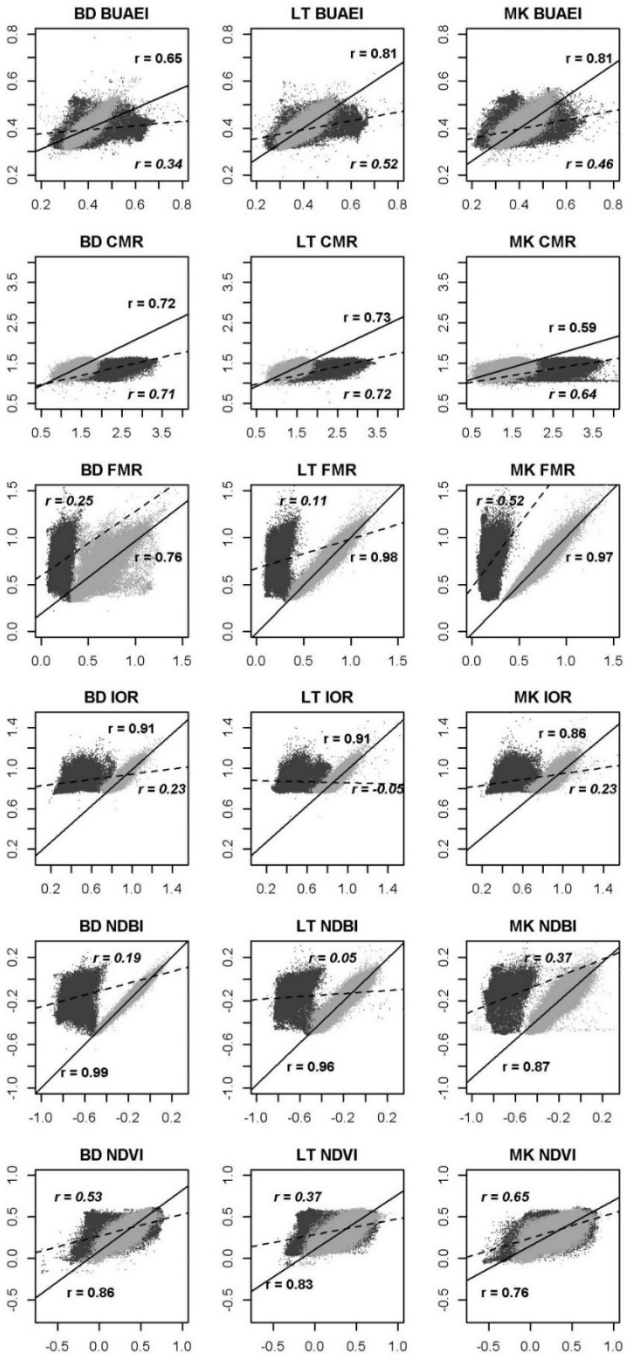

Figure_Apx A-4 Comparison of Landsat 8 spectral indices (y axis) with equivalent aggregated spectral indices derived from aerial imagery (x axis) before (dark grey, dashed regression line) and after (light grey, solid regression line) adjustment for the values of Landsat 8 indices for satellite data captured on 08 Jul 2013. Full explanation of the figure given in the first paragraph of Appendix A3.

A.4 Predictor importance in MARS models used in LST downscaling

Table_Apx A-4 MARS equations, generated with the Statistica software, used for LST downscaling in Bedford.

Bedford, 02 Feb 2014

LST_FEB_BD = 9.35352629553633e+000 + 8.95683970005979e-004*max(0, mnmd_BD-2.25480804443359e+001) - 5.24097858788039e-003*max(0, 2.25480804443359e+001-mnmd_BD) - 6.39257449247337e-002*max(0, CMR_FEB_BD-1.14625322818756e+000) - 1.97833755719236e-001*max(0, 1.14625322818756e+000-CMR_FEB_BD) + 5.13936482567572e-001*max(0, BUAEI_FEB_BD-4.63528275489807e-001) + 1.28112609091631e-001*max(0, 4.63528275489807e-001-BUAEI_FEB_BD) - 1.53055292433981e+002*max(0, wtr_BD-9.99995269775391e+001) + 7.18288508889315e-004*max(0, 9.99995269775391e+001-wtr_BD) + 5.75716901596961e-002*max(0, IOR_FEB_BD-9.55171287059784e-001) - 6.07758245703217e-001*max(0, 9.55171287059784e-001-IOR_FEB_BD) + 8.35419390247879e-001*max(0, NDVI_FEB_BD-2.74427950382233e-001) - 1.53167276534035e-001*max(0, 2.74427950382233e-001-NDVI_FEB_BD) - 2.83158217979280e-001*max(0, NDBI_FEB_BD+1.75494760274887e-001) - 1.18777247787260e+000*max(0, -1.75494760274887e-001-NDBI_FEB_BD) - 5.29308626464895e-001*max(0, NDVI_FEB_BD+9.92088541388512e-002) - 1.08476597446567e+000*max(0, BUAEI_FEB_BD-5.37508726119995e-002)

Bedford, 19 Jan 2015

LST_JAN_BD = 7.67710168366022e+000 - 5.15358008203914e-002*max(0, wtr_BD-4.99985694885254e+001) - 2.32889703826208e-002*max(0, 4.99985694885254e+001-wtr_BD) + 1.22429063438004e-003*max(0, mnmd_BD-2.25636844635010e+001) - 4.62090199942209e-003*max(0, 2.25636844635010e+001-mnmd_BD) + 3.20428497508927e-002*max(0, IOR_JAN_BD-1.08994817733765e+000) - 1.33310358542313e+000*max(0, 1.08994817733765e+000-IOR_JAN_BD) - 1.47578273637958e+000*max(0, BUAEI_JAN_BD-1.37384325265884e-001) + 5.16325893811117e-002*max(0, 1.37384325265884e-001-BUAEI_JAN_BD) - 3.06548876037324e-001*max(0, NDBI_JAB_BD-1.28105878829956e-002) - 1.48713379538319e+000*max(0, 1.28105878829956e-002-NDBI_JAB_BD) + 1.39500578663435e+000*max(0, NDVI_JAN_BD-2.54180788993835e-001) - 8.34433388312855e-001*max(0, 2.54180788993835e-001-NDVI_JAN_BD) + 9.44891659946003e-002*max(0, wtr_BD-7.66757125854492e+001) - 5.00234878377148e-002*max(0, CMR_JAN_BD-9.53488469123840e-001) - 3.46980646092921e-001*max(0, 9.53488469123840e-001-CMR_JAN_BD) - 1.55869193420676e+000*max(0, NDVI_JAN_BD+9.30313616991043e-002) + 1.17235457230060e+000*max(0, NDVI_JAN_BD-9.47636365890503e-002)

Bedford, 06 Jun 2013

LST_JUN_BD = 2.74564456032957e+001 + 1.37938421732014e+001*max(0, NDBI_JUN_BD+1.87999784946442e-001) - 2.52902501544114e+001*max(0, -1.87999784946442e-001-NDBI_JUN_BD) + 1.66761967051721e-001*max(0, wtr_BD-5.00000000000000e+001) + 8.60664731142638e-002*max(0, 5.00000000000000e+001-wtr_BD) + 1.77456437982270e+001*max(0, NDVI_JUN_BD-4.48368877172470e-001) - 6.36015439521035e+000*max(0, 4.48368877172470e-001-NDVI_JUN_BD) + 2.76197213946934e-003*max(0, mnmd_BD-2.27888813018799e+001) - 6.02990743682226e-002*max(0, 2.27888813018799e+001-mnmd_BD) - 1.55125110166977e+000*max(0, IOR_JUN_BD-9.44522440433502e-001) - 6.74228152875435e+000*max(0, 9.44522440433502e-001-IOR_JUN_BD) - 1.18416114227356e+001*max(0, NDBI_JUN_BD-3.24028730392456e-003) - 4.06784516593544e-001*max(0, CMR_JUN_BD-9.62374210357666e-001) - 2.82586472120663e+000*max(0, 9.62374210357666e-001-CMR_JUN_BD) - 2.91665710400558e-001*max(0, wtr_BD-7.68483734130859e+001) + 9.63784567429320e+000*max(0, BUAEI_JUN_BD-5.04963397979736e-001) + 1.31102542804218e+000*max(0, 5.04963397979736e-001-BUAEI_JUN_BD) - 4.90719999627658e+000*max(0, NDVI_JUN_BD-4.32529188692570e-002)

Bedford, 08 Jul 2013

LST_JUL_BD = 3.85861563882998e+001 + 1.39898352692557e+001*max(0, NDBI_JUL_BD+7.42961764335632e-002) - 2.35034260145147e+001*max(0, -7.42961764335632e-002-NDBI_JUL_BD) - 8.95147565943523e+000*max(0, mnmd_BD-4.90942627191544e-001) + 1.86981556674656e+001*max(0, 4.90942627191544e-001-mnmd_BD) + 7.03244444064443e+000*max(0, NDVI_JUL_BD-4.72034811973572e-001) - 9.81329721276825e-001*max(0, 4.72034811973572e-001-NDVI_JUL_BD) + 4.63012299453887e+000*max(0, IOR_JUL_BD-8.82818639278412e-001) - 1.13724079701179e+001*max(0, 8.82818639278412e-001-IOR_JUL_BD) - 9.98256939558051e+000*max(0, BUAEI_JUL_BD-2.89033681154251e-001) - 6.21249132903780e-001*max(0, 2.89033681154251e-001-BUAEI_JUL_BD) - 1.53884775181943e+000*max(0, CMR_JUL_BD-9.28904712200165e-001) - 2.01226835550789e+000*max(0, 9.28904712200165e-001-CMR_JUL_BD) + 1.75638761919558e+000*max(0, CMR_JUL_BD-1.45547020435333e+000) + 2.68184447275441e-002*max(0, wtr_BD-4.99985694885254e+001) + 1.97807334813855e-002*max(0, 4.99985694885254e+001-wtr_BD) + 1.00287328497026e+001*max(0, BUAEI_JUL_BD-5.13547539710999e-001) - 6.13881362926549e+000*max(0, NDBI_JUL_BD-2.72986888885498e-002)

Table_Apx A-5 MARS equations, generated with the Statistica software, used for LST downscaling in Luton.

Luton, 02 Feb 2014
LST_FEB_LT = 8.34809276475131e+000 + 1.02581217547888e-003*max(0, mnmd_LT-2.31616477966309e+001) - 5.51419655353715e-003*max(0, 2.31616477966309e+001-mnmd_LT) + 2.49324779018106e+000*max(0, NDVI_FEB_LT-1.72812387347221e-001) - 5.40698522222858e-001*max(0, 1.72812387347221e-001-NDVI_FEB_LT) + 1.02125303764020e-001*max(0, IOR_FEB_LT-1.02638590335846e+000) - 1.53974705131776e+000*max(0, 1.02638590335846e+000-IOR_FEB_LT) + 1.18860654420629e-001*max(0, BUAEI_FEB_LT-6.24055981636047e-001) + 2.13298337235517e+000*max(0, 6.24055981636047e-001-BUAEI_FEB_LT) + 9.08053605220683e+001*max(0, wtr_LT-9.99968032836914e+001) - 5.14688564319000e-003*max(0, 9.99968032836914e+001-wtr_LT) - 1.32392267340292e+000*max(0, NDVI_FEB_LT+8.89369174838066e-002) - 1.12737566112435e+000*max(0, NDVI_FEB_LT-2.70264536142349e-001)
Luton, 19 Jan 2015
LST_JAN_LT = 7.46164436708598e+000 + 1.65015094993469e-003*max(0, mnmd_LT-2.31478881835938e+001) - 1.20419028152070e-002*max(0, 2.31478881835938e+001-mnmd_LT) + 4.69883651685027e+000*max(0, NDVI_JAN_LT-8.35649073123932e-002) - 6.20133054732581e-001*max(0, 8.35649073123932e-002-NDVI_JAN_LT) - 1.47720681162434e+000*max(0, IOR_JAN_LT-1.06564664840698e+000) - 2.19941068365437e+000*max(0, 1.06564664840698e+000-IOR_JAN_LT) - 5.04318278286875e+000*max(0, BUAEI_JAN_LT-1.55521482229233e-001) - 2.90154353413655e+000*max(0, NDVI_JAN_LT+1.12471915781498e-001) - 2.47828563076748e+000*max(0, NDVI_JAN_LT-1.84967577457428e-001) + 2.39679452114741e-002*max(0, NDBI_JAN_LT+5.29110431671143e-002) + 1.60564047911816e+000*max(0, -5.29110431671143e-002-NDBI_JAN_LT) + 4.38758507450180e+000*max(0, BUAEI_JAN_LT-6.16560935974121e-001) + 1.05650096412307e+003*max(0, wtr_LT-9.99994277954102e+001) - 2.27350264254038e-003*max(0, 9.99994277954102e+001-wtr_LT) + 1.51042304013478e+000*max(0, IOR_JAN_LT-8.42680156230927e-001)
Luton, 06 Jun 2013
LST_JUN_LT = 3.15118816168130e+001 - 2.66849656853215e+000*max(0, NDBI_JUN_LT+1.36008799076080e-001) - 1.89203636225006e+001*max(0, -1.36008799076080e-001-NDBI_JUN_LT) + 2.02723778051538e+001*max(0, NDVI_JUN_LT-4.00124460458755e-001) - 6.90869459134091e+000*max(0, 4.00124460458755e-001-NDVI_JUN_LT) + 4.12257220151343e-003*max(0, mnmd_LT-2.34507999420166e+001) - 4.87447756108710e-002*max(0, 2.34507999420166e+001-mnmd_LT) - 4.83483670143644e+000*max(0, IOR_JUN_LT-8.77538561820984e-001) - 1.14113348493845e+001*max(0, 8.77538561820984e-001-IOR_JUN_LT) + 8.24853441604587e-001*max(0, CMR_JUN_LT-8.12690436840057e-001) - 3.56584609147563e+000*max(0, 8.12690436840057e-001-CMR_JUN_LT) + 1.30491266486665e+001*max(0, BUAEI_JUN_LT-4.44665998220444e-001) - 3.10165929121667e+000*max(0, 4.44665998220444e-001-BUAEI_JUN_LT) - 8.05475957955484e+000*max(0, NDVI_JUN_LT-4.63897250592709e-002) + 5.21677602196392e+000*max(0, IOR_JUN_LT-2.10069060325623e+000) + 6.90218689217178e+000*max(0, NDBI_JUN_LT+3.55976730585098e-001) - 3.86450973421080e+003*max(0, wtr_LT-9.99994277954102e+001) + 1.12636397403023e-003*max(0, 9.99994277954102e+001-wtr_LT)
Luton, 08 Jul 2013
LST_JUL_LT = 3.55455187680548e+001 - 3.42501085857586e+000*max(0, NDBI_JUL_LT+1.13112390041351e-001) - 2.09447624434404e+001*max(0, -1.13112390041351e-001-NDBI_JUL_LT) + 1.57288064405600e+001*max(0, NDVI_JUL_LT-3.95924627780914e-001) - 7.77385514361228e+000*max(0, 3.95924627780914e-001-NDVI_JUL_LT) + 4.77176445514039e-003*max(0, mnmd_LT-2.34982872009277e+001) - 3.74958552988311e-002*max(0, 2.34982872009277e+001-mnmd_LT) - 6.60341121052901e-001*max(0, IOR_JUL_LT-9.12221014499664e-001) - 5.84401133108461e+000*max(0, 9.12221014499664e-001-IOR_JUL_LT) + 4.46164062434845e+000*max(0, BUAEI_JUL_LT-3.02418857812881e-001) - 2.34529642674120e+001*max(0, 3.02418857812881e-001-BUAEI_JUL_LT) - 1.28323311268470e+000*max(0, CMR_JUL_LT-9.96365666389465e-001) - 2.51543254281204e+000*max(0, 9.96365666389465e-001-CMR_JUL_LT) - 7.73575511829594e+000*max(0, NDVI_JUL_LT-1.32234841585159e-002) + 6.66253062169172e+000*max(0, NDVI_JUL_LT-2.62203723192215e-001) + 8.00703372489208e+000*max(0, NDBI_JUL_LT+3.75013709068298e-001) + 1.71606243673268e+000*max(0, CMR_JUL_LT-1.56669938564301e+000)

Table_Apx A-6 MARS equations, generated with the Statistica software, used for LST downscaling in Milton Keynes.

Milton Keynes, 02 Feb 2014
LST_FEB_MK = 8.10769015412983e+000 - 3.10619831631067e-001*max(0, NDBI_FEB_MK+7.63151645660400e-002) + 2.68881493866209e-001*max(0, -7.63151645660400e-002-NDBI_FEB_MK) - 2.30835969238999e-001*max(0, IOR_FEB_MK-9.51169371604919e-001) - 5.06186521075420e-001*max(0, 9.51169371604919e-001-IOR_FEB_MK) + 5.40803610739142e-003*max(0, wtr_MK-4.99951629638672e+001) + 1.77065628779337e-003*max(0, 4.99951629638672e+001-wtr_MK)
Milton Keynes, 19 Jan 2015
LST_JAN_MK = 4.56567800366657e+000 + 2.11362122871733e+003*max(0, wtr_MK-9.99997100830078e+001) - 1.75524039760114e-003*max(0, 9.99997100830078e+001-wtr_MK) + 2.78749399458494e-001*max(0, CMR_JAN_MK-7.59739875793457e-001) - 1.72219794525527e-001*max(0, 7.59739875793457e-001-CMR_JAN_MK) + 7.35295374086938e-001*max(0, NDVI_JAN_MK-2.80027031898499e-001) - 7.79000956326649e-001*max(0, 2.80027031898499e-001-NDVI_JAN_MK) - 1.57652057582078e+000*max(0, NDBI_JAN_MK-1.74736976623535e-003) - 1.279873423417 99e-001*max(0, 1.74736976623535e-003-NDBI_JAN_MK) - 2.05618175195483e+000*max(0, IOR_JAN_MK-9.30608332157135e-001) + 4.36876949393381e-001*max(0, 9.30608332157135e-001-IOR_JAN_MK) - 1.47855556818390e+000*max(0, NDVI_JAN_MK+1.31542295217514e-001) + 1.87147530046317e+000*max(0, NDVI_JAN_MK-1.65037542581558e-001) - 4.86585617907494e-001*max(0, CMR_JAN_MK-1.14544093608856e+000) + 1.72612328004810e+000*max(0, IOR_JAN_MK-7.94646203517914e-001) + 1.26552717616670e+000*max(0, NDBI_JAN_MK+1.32827818393707e-001)
Milton Keynes, 06 Jun 2013
LST_JUN_MK = 3.16145325502259e+001 + 5.00512031560374e+000*max(0, NDBI_JUN_MK+3.51608991622925e-002) - 1.56567633163297e+001*max(0, -3.51608991622925e-002-NDBI_JUN_MK) + 1.39179842479948e+001*max(0, NDVI_JUN_MK-4.75337445735931e-001) - 1.28662705555742e+000*max(0, 4.75337445735931e-001-NDVI_JUN_MK) - 2.09373196914596e+004*max(0, wtr_MK-9.99999008178711e+001) + 1.60000211454816e-002*max(0, 9.99999008178711e+001-wtr_MK) + 7.13789186921252e-001*max(0, CMR_JUN_MK-8.48855078220367e-001) - 2.95003930425920e+000*max(0, 8.48855078220367e-001-CMR_JUN_MK) + 3.16899856950515e-003*max(0, mnmd_MK-2.17027015686035e+001) - 4.22726522010481e-002*max(0, 2.17027015686035e+001-mnmd_MK) + 3.78557088036876e+000*max(0, IOR_JUN_MK-9.14385676383972e-001) - 1.01888761248971e+001*max(0, 9.14385676383972e-001-IOR_JUN_MK) + 1.21102374635811e+001*max(0, BUAEI_JUN_MK-5.13219833374023e-001) + 3.93010792397706e+000*max(0, 5.13219833374023e-001-BUAEI_JUN_MK) - 7.81921419847556e+000*max(0, NDVI_JUN_MK-4.63529378175735e-002) - 8.08360037250700e+000*max(0, NDBI_JUN_MK+2.04050838947296e-001) - 1.38445015709328e+001*max(0, BUAEI_JUN_MK-3.06692719459534e-001)
Luton, 08 Jul 2013
LST_JUL_MK = 3.49290373013733e+001 - 8.06396552008399e-001*max(0, NDBI_JUL_MK+1.08186483383179e-001) - 1.36793330751633e+001*max(0, -1.08186483383179e-001-NDBI_JUL_MK) + 1.14468832876355e+001*max(0, NDVI_JUL_MK-4.61925178766251e-001) - 2.16461509622334e+000*max(0, 4.61925178766251e-001-NDVI_JUL_MK) - 1.62318894331971e+004*max(0, wtr_MK-9.99999008178711e+001) + 9.93154087138701e-003*max(0, 9.99999008178711e+001-wtr_MK) - 3.16819938303890e-001*max(0, CMR_JUL_MK-8.74632298946381e-001) - 2.50435355816165e+000*max(0, 8.74632298946381e-001-CMR_JUL_MK) + 3.90368373521225e-003*max(0, mnmd_MK-2.17354965209961e+001) - 3.14110162149845e-002*max(0, 2.17354965209961e+001-mnmd_MK) + 2.96382485671142e+000*max(0, IOR_JUL_MK-8.93855333328247e-001) - 7.60542475665607e+000*max(0, 8.93855333328247e-001-IOR_JUL_MK) + 1.25305929620202e+001*max(0, BUAEI_JUL_MK-5.53946435451508e-001) - 2.10180249916012e+000*max(0, 5.53946435451508e-001-BUAEI_JUL_MK) - 5.65831990899602e+000*max(0, NDVI_JUL_MK-1.50935538113117e-002) - 1.31512797869724e+001*max(0, BUAEI_JUL_MK-2.92499601840973e-001) + 1.20225518173797e+000*max(0, CMR_JUL_MK-1.44332516193390e+000)

Table_Apx A-7 Frequency of use of scaling factors in the LST downscaling MARS models developed at 2(4)m resolution.

Date	06-Jun-13			08-Jul-13			19-Jan-15			02-Feb-14		
Scaling factor (2 to 4 m)	**MK**	**LT**	**BD**	**MK**	**LT**	**BD**	**MK**	**LT**	**BD**	**MK**	**LT**	**BD**
BUAEI	2	2	2	2	2	2	2	3	3	1	2	2
CMR	2	2	0	2	2	2	0	0	0	0	2	0
FMR	3	3	3	3	3	3	5	2	2	5	3	3
IOR	2	3	2	2	3	2	3	3	3	2	2	2
MNMD	2	2	2	2	2	2	2	2	2	0	2	2
NDBI	2	2	2	2	2	3	2	2	3	2	3	3
NDVI	3	2	3	3	2	2	0	3	2	2	2	2
WTR	2	2	3	2	2	2	2	0	2	3	0	3
Total number of references	18	18	17	18	18	18	16	15	17	15	16	17

A.5 Performance of LST downscaling models

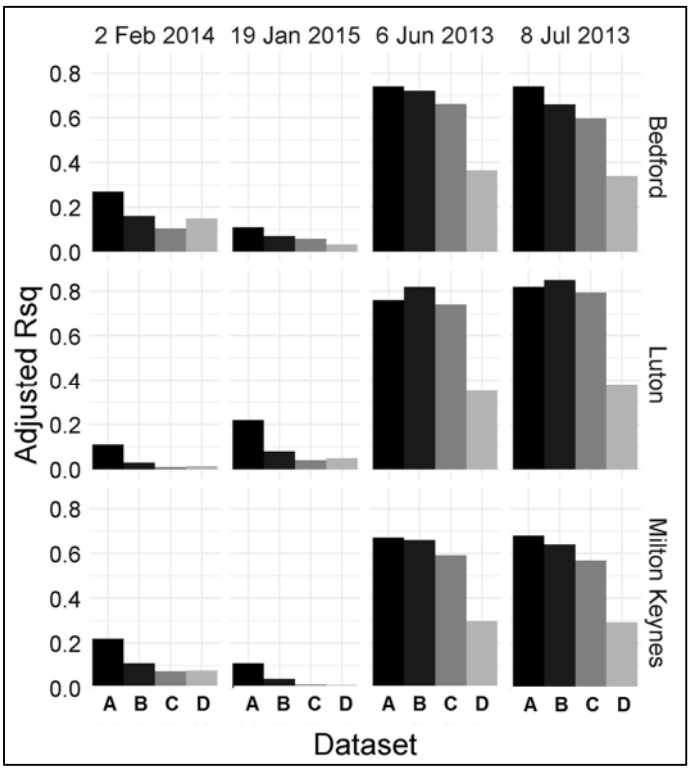

Figure_Apx A-5 Adjusted R squared for different models tested in the study for all towns and dates: A – MARS 30m, B – MARS 2/4m adjusted, C – multiple regression (MR) 2/4m adjusted, D – MR 2/4m unadjusted.

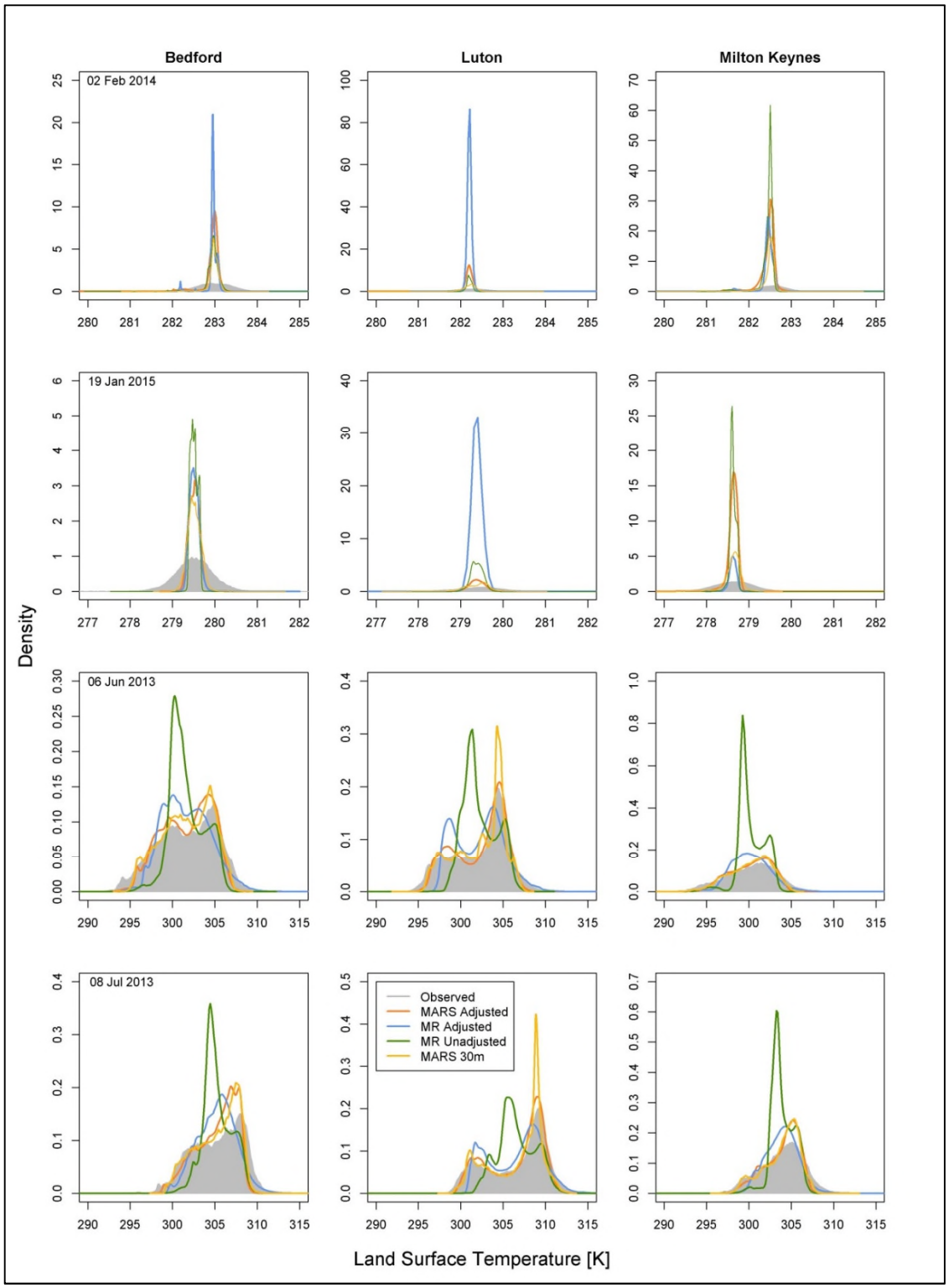

Figure_Apx A-6 Distribution of LST values in the Landsat-derived (Observed) and downscaled maps without adjustment for residuals.

A.6 Land surface temperature maps

Table_Apx A-8 Basic statistics for LST derived from Landsat 8 TIR bands [K].

Date/Town	*02 Feb 2014*			*19-Jan-15*			*06-Jun-13*			*08-Jul-13*		
Statistic	***BD***	***LT***	***MK***	***BD***	***LT***	***MK***	***BD***	***LT***	***MK***	***BD***	***LT***	***MK***
Min	277.7	268.7	264.1	275.2	268.2	255.9	291.4	290.2	282.6	297.2	294.8	291.6
Max	284.5	284.1	285.2	283	282.8	283.7	313.2	319.2	312.4	315.7	322.7	317.3
Range	6.8	15.4	21.1	7.8	14.6	27.8	21.8	29.0	29.8	18.5	27.9	25.7
Mean	282.9	282.2	282.5	279.5	279.4	278.6	301.6	302.2	300.2	305.2	306.5	303.9
Std	0.5	0.5	0.6	0.5	0.6	0.6	3.5	3.4	3	2.9	3.6	2.6

Table_Apx A-9 Basic statistics for downscaled LST maps with the $MARS_{2/4ma}$ models [K].

Date/Town	*02 Feb 2014*			*19-Jan-15*			*06-Jun-13*			*08-Jul-13*		
Statistic	***BD***	***LT***	***MK***	***BD***	***LT***	***MK***	***BD***	***LT***	***MK***	***BD***	***LT***	***MK***
Min	278.6	278.4	275.2	278.7	277.3	273.9	289.4	292.4	288.1	290.9	297.4	294.0
Max	285.9	285.3	300.9	280.5	282.2	287.3	317.6	331.0	313.7	313.8	329.6	316.4
Range	7.2	6.9	25.7	1.8	4.8	13.4	28.2	38.5	25.5	22.9	32.2	22.4
Mean	282.9	282.2	282.5	279.5	279.4	278.6	301.6	302.2	300.2	305.2	306.5	303.9
Std	0.2	0.1	0.2	0.1	0.2	0.1	2.9	3.0	2.5	2.4	3.3	2.1

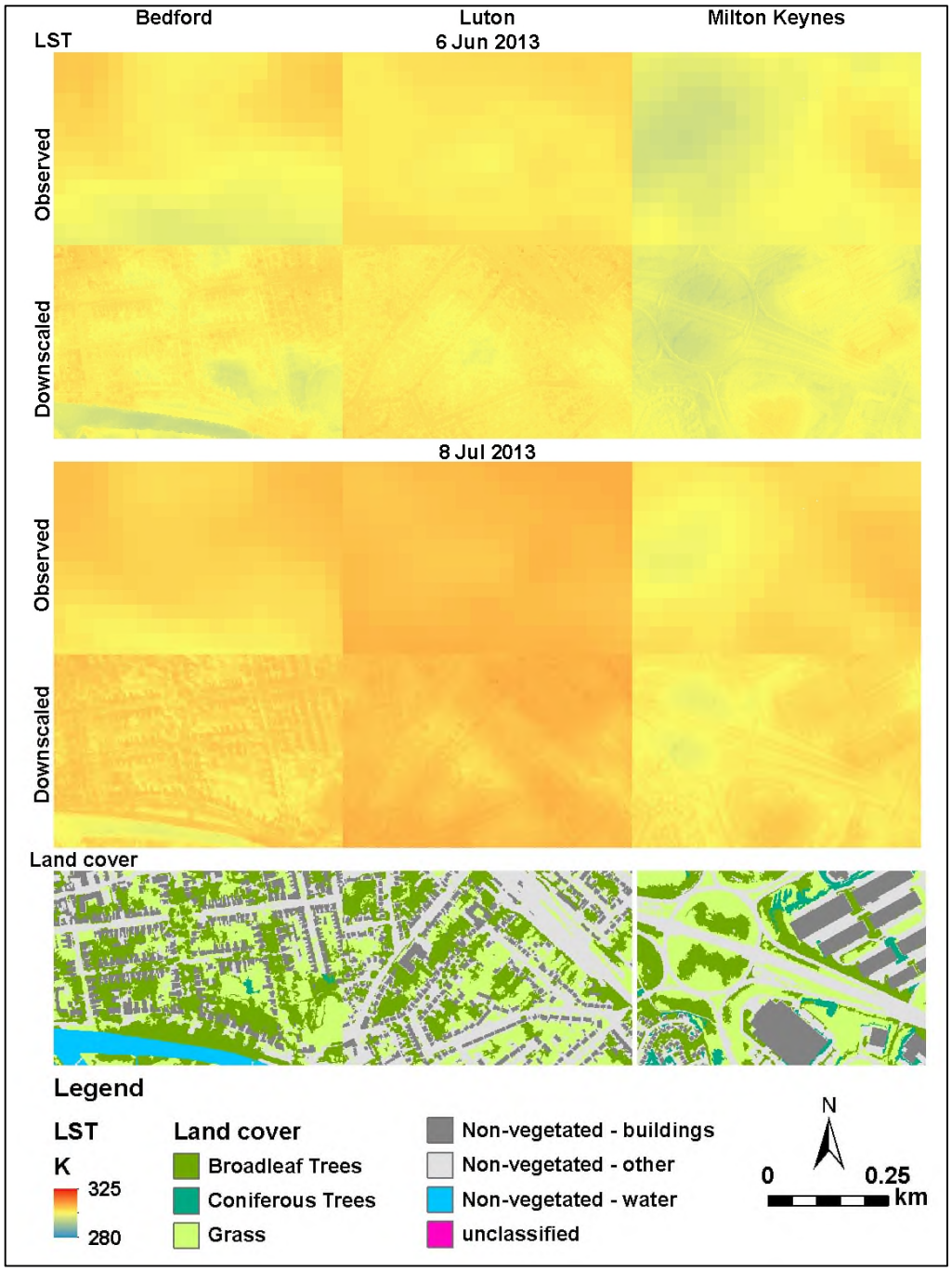

Figure_Apx A-7 Large-scale comparison of the LST downscaled maps with the MARS method at target 2 to 4m spatial resolution for summer dates.

A.7 References

Bouzekri, S., Lasbet, A.A. and Lachehab, A. (2015) ‘A New Spectral Index for Extraction of Built-Up Area Using Landsat-8 Data’, Journal of the Indian Society of *Remote Sensing*, 43(4), pp. 867–873. Available at: 10.1007/s12524-015-0460-6 (Accessed: 13 September 2016).

Chun, B. and Guldmann, J.-M. (2014) ‘Spatial statistical analysis and simulation of the urban heat island in high-density central cities’, *Landscape and Urban Planning*, 125, pp. 76–88. Available at: 10.1016/j.landurbplan.2014.01.016 (Accessed: 15 December 2015).

Drury, S.A. (1987) ‘Image interpretation in geology’, *Geocarto International*, 2(2) Allen & Unwin, p. 48. Available at: 10.1080/10106048709354098 (Accessed: 21 August 2017).

Purevdorj, T., Tateishi, R., Ishiyama, T. and Honda, Y. (1998) ‘Relationships between percent vegetation cover and vegetation indices’, *International Journal of Remote Sensing*, 19(18) Taylor & Francis Group, pp. 3519–3535. Available at: 10.1080/014311698213795 (Accessed: 27 January 2018).

Sobrino, J.A., Jimenez-Munoz, J.C., Soria, G., Romaguera, M., Guanter, L., Moreno, J., Plaza, A. and Martinez, P. (2008) ‘Land Surface Emissivity Retrieval From Different VNIR and TIR Sensors’, *IEEE Transactions on Geoscience and Remote Sensing*, 46(2), pp. 316–327. Available at: 10.1109/TGRS.2007.904834 (Accessed: 9 September 2016).

Yu, X., Guo, X. and Wu, Z. (2014) ‘Land Surface Temperature Retrieval from Landsat 8 TIRS—Comparison between Radiative Transfer Equation-Based Method, Split Window Algorithm and Single Channel Method’, *Remote Sensing*, 6(10) Multidisciplinary Digital Publishing Institute, pp. 9829–9852. Available at: 10.3390/rs6109829 (Accessed: 29 August 2017).

Zha, Y., Gao, J. and Ni, S. (2003) ‘Use of normalized difference built-up index in automatically mapping urban areas from TM imagery’, *International Journal of Remote Sensing*, 24(3) Taylor & Francis Group, pp. 583–594. Available at: 10.1080/01431160304987 (Accessed: 31 August 2017).

Appendix B Supplementary materials to Chapter 3

Table_Apx B-1 Class level patch metrics derived from a 2m resolution land cover map showing the distribution of buildings, paved, grass, trees and water in Bedford. Descriptions are based on the Fragstats help file. Metrics marked with * were used in subsequent analyses. Source: Fragstats documentation: https://www.umass.edu/landeco/research/fragstats/documents/fragstats_documents.html

Metric Type	***Metrics***	***Description***
Shape	Mean of perimeter to area ratio - PARA_MN	PARA equals the ratio of the patch perimeter (m) to area (m^2)
	Shape index - SHAPE_MN	SHAPE equals patch perimeter (m) divided by the square root of patch area (m^2), adjusted by a constant to adjust for a square standard; values less than 1 indicate irregular shape of patches deviating from a square, indicated by the value of 1
	Fractal dimension index - FRAC_MN	FRAC equals 2 times the logarithm of patch perimeter (m) divided by the logarithm of patch area (m^2); the perimeter is adjusted to correct for the raster bias in perimeter. Assumes values between 1 and 2, with 1 indicating shapes with simples perimeters, such as squares, and 2 – shapes with highly convoluted perimeters
	Contiguity index - CONTIG_MN	CONTIG equals the average contiguity value for the cells in a patch (i.e., sum of the cell values divided by the total number of pixels in the patch) minus 1, divided by the sum of the template values minus 1. Assumes values between 0 and 1, with 0 indicating a patch 1 pixel in size, and 1 – a patch with a high level of connectedness between pixels belonging to that patch.
Aggregation	Interspersion and juxtaposition index - IJI	IJI depicts the observed interspersion over the maximum possible interspersion for the given number of patch types. Assumes values between 0 and 100 where 0 indicates a patch adjacent to only one other patch type and 100 – a patch equally adjacent to all other patch types
	Clumpiness - CLUMPY	CLUMPY equals the proportional deviation of the proportion of like adjacencies involving the corresponding class from that expected under a spatially random distribution. CLUMPY equals -1 when the focal patch type is maximally disaggregated; CLUMPY equals 0 when the focal patch type is distributed randomly, and approaches 1 when the patch type is maximally aggregated.
	Landscape shape index – LSI*	LSI provides a standardized measure of total edge or edge density that adjusts for the size of the landscape. It is equal to 1 for a landscape that consists of a single patch and increases without limit as landscape shape becomes more irregular and/or as the length of edge within the landscape of the corresponding patch type increases.
	Normalised landscape shape index - NLSI	It is a normalised version of LSI. Ranges between 0 and 1, where 0 depicts landscapes composed of a single maximally compact patch and 1 – when the patch type is maximally disaggregated.
	Patch cohesion index – COHESION*	Patch cohesion index measures the physical connectedness of the corresponding patch type by relating the perimeter of a patch to its area and the total size of the landscape. Approaches 0 for landscapes in which the focal class type becomes increasingly subdivided and less physically connected, and 1 for landscapes with increasing proportion of the focal class type.
	Percentage of like adjacencies – PLADJ*	PLADJ equals the number of like adjacencies involving the focal class, divided by the total number of cell adjacencies involving the focal class. PLADJ equals 0 when the corresponding patch type is maximally disaggregated and there is no like adjacencies and increases up to 100 when the corresponding patch type becomes increasingly aggregated such that the proportion of like adjacencies increases.

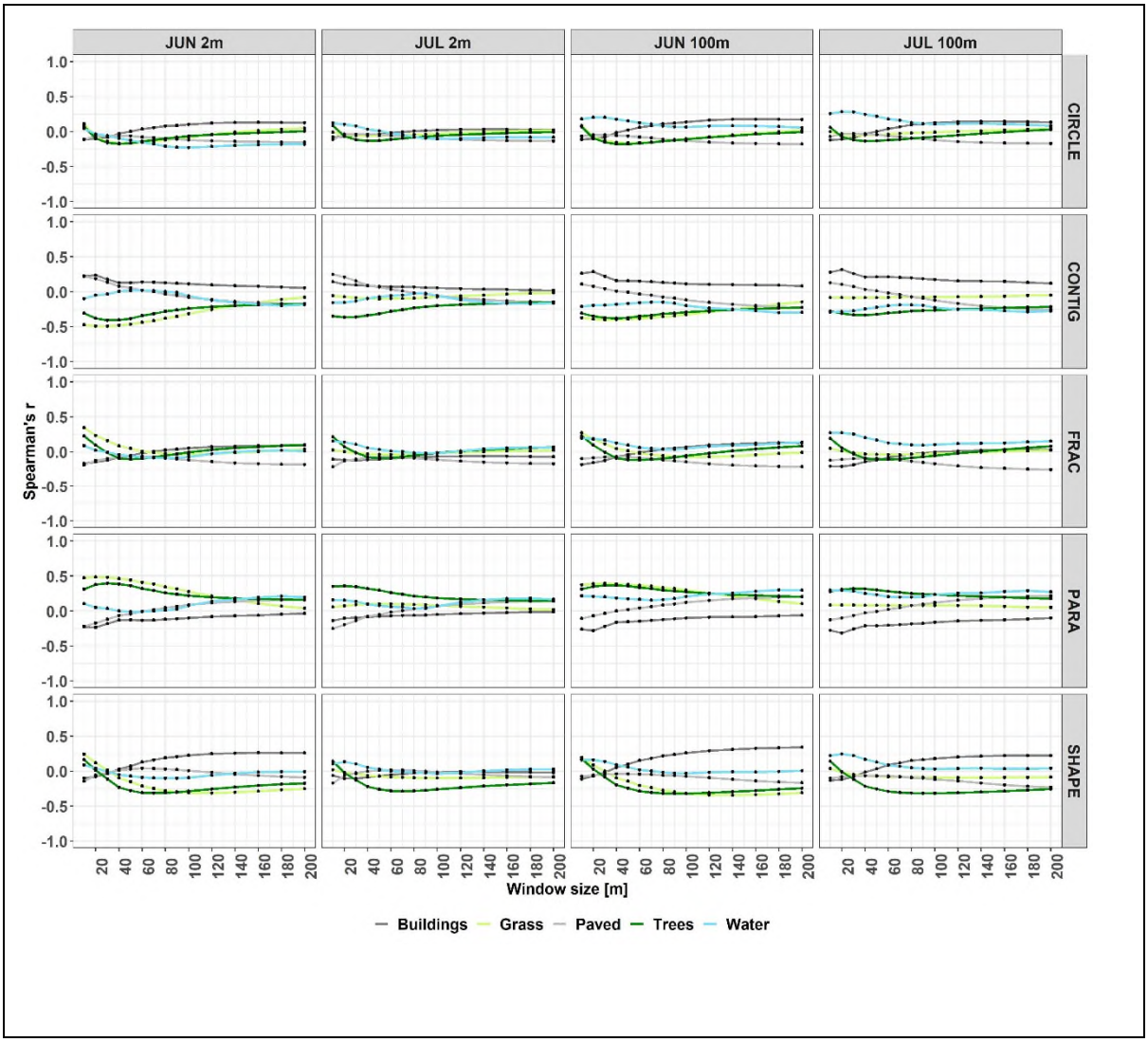

Figure_Apx B-1 Spearman correlations between selected class shape metrics and LST for 8th June and 6th July at 2m and 100m spatial resolutions in various land cover types for Bedford.

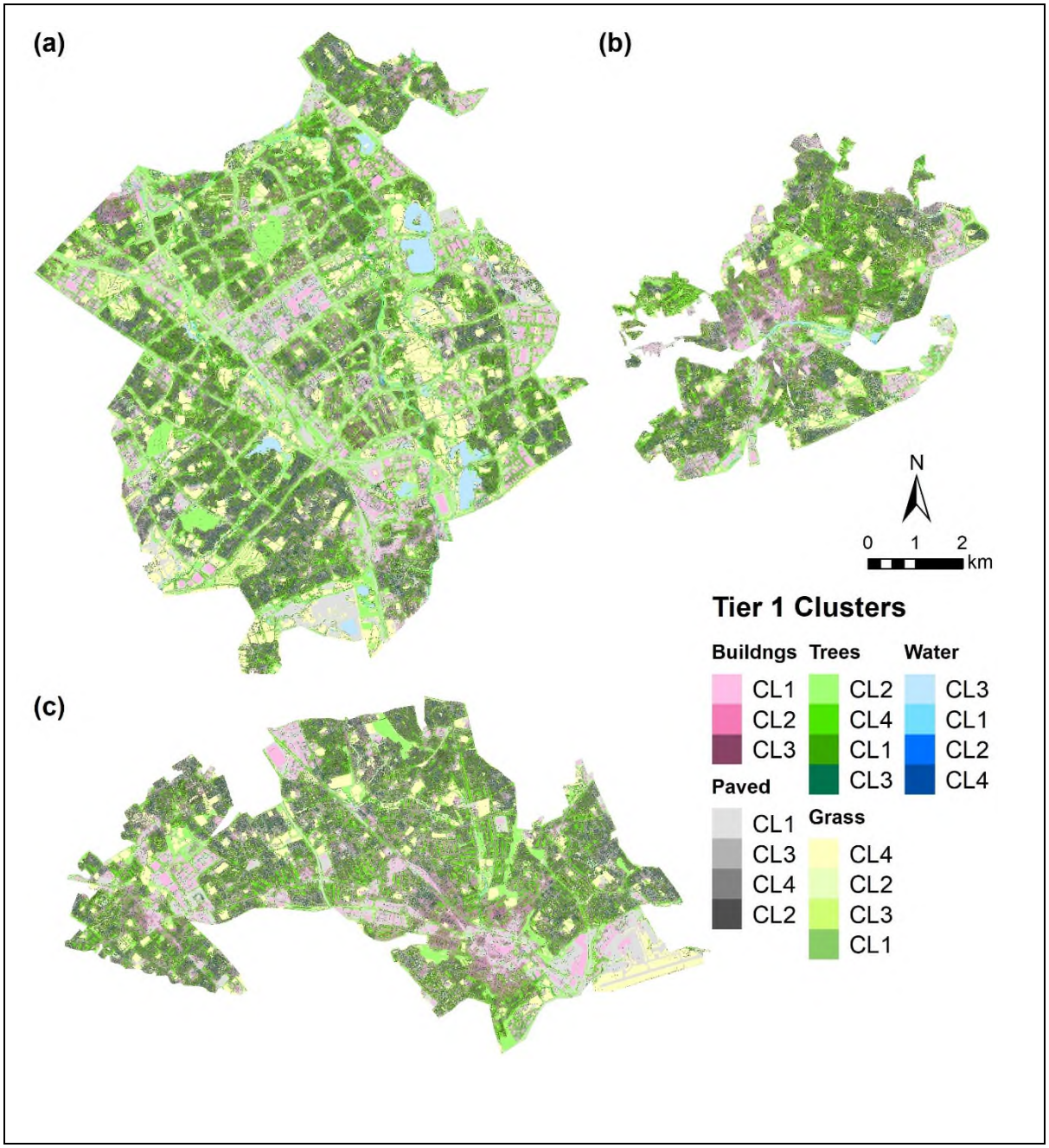

Figure_Apx B-2 Tier 1 Clusters in A – Milton Keynes, B – Bedford, C – Luton. Legend ordered by decreasing spatial aggregation levels of clusters (decreasing values of COH and PLADJ, increasing values of LSI).

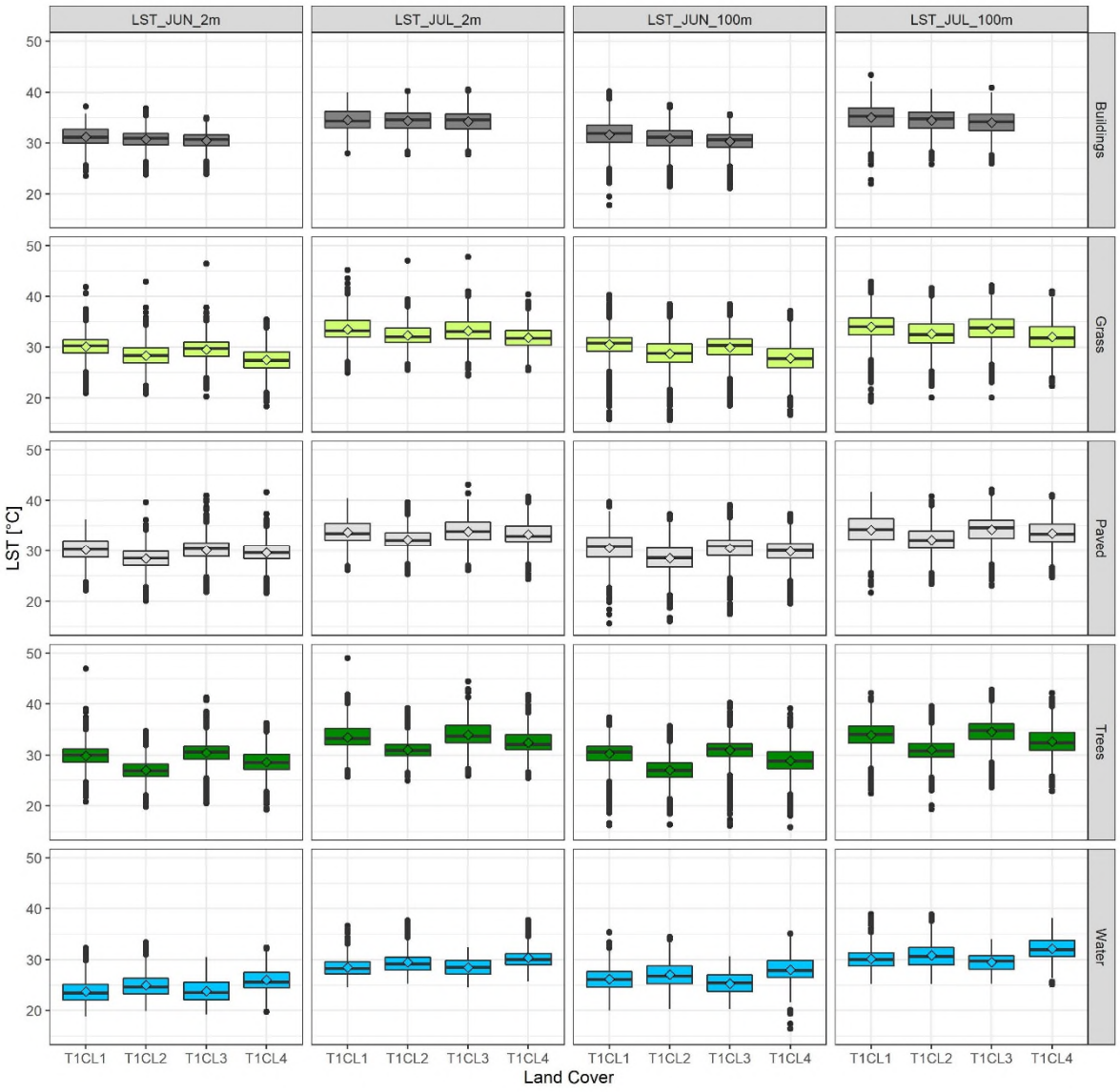

Figure_Apx B-3 Land surface temperature (LST) in Tier 1 Clusters derived for each land cover type in June and July 2013 at 2m and 100m spatial resolution.

Table_Apx B-2 Statistics for Tier 1 Clusters – spatial aggregation metrics. MN – Mean, SD – standard deviation, MD – median.

Land Cover	Tier 1 Cluster	AREA			COHESION			LSI			PLADJ		
		MN	SD	MD	MN	SD	MD	MN	SD	MD	MN	SD	MD
Buildings	T1CL1	1212	3766	116	95.0	1.8	94.8	2.8	0.8	2.8	89.0	2.9	88.3
	T1CL2	155	265	52	88.3	2.8	87.8	4.8	1.0	4.8	77.9	3.4	77.1
	T1CL3	78	66	72	81.1	3.5	81.1	5.7	0.9	5.7	70.9	3.2	71.1
Grass	T1CL4	620	5374	8	95.7	1.7	95.7	4.2	0.8	4.2	87.9	2.4	87.3
	T1CL2	72	379	8	90.2	3.3	90.2	6.3	1.2	6.3	76.6	4.9	76.1
	T1CL3	28	70	8	79.1	4.6	78.8	8.3	1.3	8.3	61.5	4.8	61.0
	T1CL1	16	25	8	63.4	8.0	65.1	9.0	1.4	9.1	47.4	6.5	48.7
Paved	T1CL1	771	13599	8	97.4	1.3	97.6	4.1	0.8	4.2	88.1	1.9	87.4
	T1CL3	141	1652	8	95.9	1.8	96.2	6.2	1.2	6.3	80.3	2.8	79.5
	T1CL4	74	964	8	93.6	2.4	93.8	7.8	1.2	7.9	73.1	2.9	73.3
	T1CL2	31	97	8	83.8	10.9	87.3	7.9	1.6	8.1	62.7	9.3	65.8
Trees	T1CL2	439	4678	8	96.2	1.5	96.3	4.5	1.0	4.5	86.9	2.2	86.3
	T1CL4	113	661	8	93.7	2.3	93.9	6.5	1.3	6.6	78.5	3.2	78.0
	T1CL1	50	206	8	89.3	3.0	89.4	8.2	1.4	8.3	69.3	3.4	69.3
	T1CL3	27	64	8	79.0	8.2	81.1	8.7	1.8	9.1	58.9	6.7	60.5
Water	T1CL3	11698	45341	218	97.8	0.9	97.6	1.8	0.4	1.7	94.0	1.5	93.5
	T1CL1	680	1553	86	93.1	3.6	93.7	2.5	0.7	2.5	85.2	5.3	85.3
	T1CL2	92	215	16	79.6	7.5	79.9	3.8	1.0	3.9	59.9	10.8	60.5
	T1CL4	9	10	4	35.7	19.4	35.9	4.6	0.8	4.6	24.4	12.5	25.0

Table 4 Statistics for Tier 1 Clusters – land surface temperature [K]. MN – Mean, SD – standard deviation, MD – median.

Land Cover	Tier 1 Cluster	LST JUN 2m			LST JUL 2m			LST JUN 100m			LST JUL 100m		
		MN	SD	MD	MN	SD	MD	MN	SD	MD	MN	SD	MD
Buildings	T1CL1	304.4	1.7	304.4	307.7	1.9	307.5	304.9	2.4	305.1	308.3	2.4	308.5
	T1CL2	303.9	1.5	304.1	307.6	1.7	307.7	304.1	2.1	304.3	307.7	2.1	307.9
	T1CL3	303.7	1.4	303.9	307.4	1.7	307.7	303.5	1.7	303.8	307.2	1.9	307.3
Grass	T1CL4	300.7	2.2	300.6	305.1	2.2	304.9	301.0	2.6	301.0	305.3	2.6	305.0
	T1CL2	301.6	2.0	301.5	305.5	2.1	305.2	301.9	2.5	301.9	305.8	2.5	305.7
	T1CL3	302.7	1.9	302.9	306.4	2.1	306.2	303.2	2.2	303.5	306.9	2.3	307.0
	T1CL1	303.3	1.7	303.4	306.7	2.0	306.4	303.7	2.0	304.0	307.2	2.1	307.2
Paved	T1CL1	303.4	2.2	303.5	306.9	2.3	306.6	303.8	2.8	304.0	307.4	2.8	307.5
	T1CL3	303.3	1.9	303.6	307.1	2.1	307.1	303.7	2.3	304.1	307.4	2.4	307.8
	T1CL4	302.8	1.7	302.8	306.5	1.9	306.1	303.1	2.1	303.3	306.7	2.1	306.5
	T1CL2	301.6	2.0	301.7	305.4	1.9	305.3	301.7	2.7	301.8	305.3	2.5	305.3
Trees	T1CL2	300.3	1.9	300.1	304.2	1.8	304.1	300.3	2.3	300.1	304.2	2.2	304.0
	T1CL4	301.8	2.0	301.7	305.6	2.0	305.3	302.1	2.3	302.0	305.8	2.3	305.6
	T1CL1	303.0	1.7	303.2	306.7	1.9	306.5	303.5	2.0	303.7	307.1	2.1	307.2
	T1CL3	303.6	1.7	303.8	307.2	2.0	306.9	304.1	2.0	304.3	307.7	2.1	308.0
Water	T1CL3	297.0	2.3	296.7	301.6	1.7	301.6	298.5	2.3	298.6	302.6	1.8	302.9
	T1CL1	296.9	2.4	296.6	301.7	1.8	301.4	299.4	2.4	299.3	303.3	2.3	303.2
	T1CL2	298.2	2.4	297.8	302.7	2.1	302.3	300.2	2.5	300.0	304.0	2.5	303.8
	T1CL4	299.2	2.3	298.8	303.6	2.1	303.2	301.2	2.4	301.1	305.3	2.4	305.1

Table_Apx B-3 Statistics for Tier 1 Clusters – distances to other land cover types and feature heights [m]. MN – Mean, SD – standard deviation, MD – median

Land Cover	Tier 1 Cluster	Distance to Buildings			Distance to Grass			Distance to Paved			Distance to Trees			Distance to Water			Feature Heights		
		MN	SD	MD	MN	SD	MN	MN	MN	MD	MN	SD	MD	MN	SD	MD	MN	SD	MD
Buildings	T1CL1	0.0	0.0	0.0	13.3	10.4	10.8	5.1	4.0	4.1	10.1	8.5	7.9	366	269	308	5.7	3.6	5.3
	T1CL2	0.0	0.0	0.0	7.1	5.4	5.9	3.5	4.0	2.9	5.1	4.6	4.0	410	284	357	4.8	2.4	5.1
	T1CL3	0.0	0.0	0.0	6.0	4.2	5.4	3.2	4.6	2.6	4.4	3.9	3.8	410	312	330	4.5	1.8	5.1
Grass	T1CL4	60.1	68.4	38.3	0.0	0.0	0.0	8.6	12.7	2.8	4.4	7.8	2.0	273	281	178			
	T1CL2	34.1	50.8	16.1	0.0	0.0	0.0	5.5	8.7	2.4	3.1	5.1	2.0	305	280	229			
	T1CL3	14.7	25.3	7.5	0.0	0.0	0.0	3.9	4.2	2.3	2.6	2.4	2.0	381	302	313			
	T1CL1	9.2	14.7	6.0	0.0	0.0	0.0	3.4	3.6	2.2	2.4	1.7	2.0	408	290	338			
Paved	T1CL1	36.1	69.7	9.5	6.9	9.1	3.0	0.0	0.0	0.0	6.9	12.2	2.8	321	261	252			
	T1CL3	15.0	37.2	2.9	4.5	4.6	3.0	0.0	0.0	0.0	3.7	4.7	2.2	398	306	325			
	T1CL4	9.5	23.6	2.6	3.9	3.3	2.9	0.0	0.0	0.0	3.0	3.5	2.0	385	295	316			
	T1CL2	28.4	50.3	6.0	3.9	4.0	2.8	0.0	0.0	0.0	3.6	5.4	2.1	282	247	229			
Trees	T1CL2	53.3	53.2	40.5	3.5	4.3	2.0	8.3	11.7	3.1	0.0	0.0	0.0	267	264	191	3.6	3.3	2.5
	T1CL4	23.9	39.0	8.0	3.4	3.4	2.0	5.1	7.2	2.4	0.0	0.0	0.0	329	290	257	2.9	2.5	2.2
	T1CL1	11.3	24.5	4.9	3.2	3.0	2.1	3.7	5.4	2.2	0.0	0.0	0.0	397	307	324	2.5	1.9	2.0
	T1CL3	13.3	38.6	4.5	3.2	3.5	2.0	3.7	6.0	2.0	0.0	0.0	0.0	387	287	315	2.5	1.9	1.9
Water	T1CL3	82.4	67.1	57.3	13.4	12.4	10.5	18.1	15.3	15.5	10.8	14.4	6.3						
	T1CL1	76.6	79.1	48.8	8.2	6.5	6.5	14.3	12.6	10.6	4.9	6.3	3.3						
	T1CL2	74.2	78.7	47.9	6.3	5.0	5.0	11.9	10.4	9.0	3.5	6.1	2.0						
	T1CL4	54.3	77.7	24.2	6.3	4.7	5.6	11.9	10.0	8.6	2.4	2.6	2.0						

Table_Apx B-4 Wilcox pairwise comparison test of Tier 1 Cluster means – COHESION class aggregation metric at p <0.001 (***), p<0.01 (**) or p<0.05(*). Non-significant group differences are marked by ns.

COHESION	Land Cover	Buildings			Grass				Paved				Trees				Water		
Land Cover	Tier 1 Cluster	T1CL1	T1CL2	T1CL3	T1CL1	T1CL2	T1CL3	T1CL4	T1CL1	T1CL2	T1CL3	T1CL4	T1CL1	T1CL2	T1CL3	T1CL4	T1CL1	T1CL2	T1CL3
Buildings	T1CL2	***																	
	T1CL3	***	***																
Grass	T1CL1	***	***	***															
	T1CL2	***	***	***	***														
	T1CL3	***	***	***	***	***													
	T1CL4	***	***	***	***	***	***												
Paved	T1CL1	***	***	***	***	***	***	***											
	T1CL2	***	***	***	***	***	***	***	***										
	T1CL3	***	***	***	***	***	***	***	***	***									
	T1CL4	***	***	***	***	***	***	***	***	***	***								
Trees	T1CL1	***	***	***	***	***	***	***	***	***	***	***							
	T1CL2	***	***	***	***	***	***	***	***	***	***	***	***						
	T1CL3	***	***	***	***	***	***	***	***	***	***	***	***	***					
	T1CL4	***	***	***	***	***	***	***	***	***	***	***	***	***	***				
Water	T1CL1	***	***	***	***	***	***	***	***	***	***	ns	***	***	***	ns			
	T1CL2	***	***	***	***	***	***	***	***	***	***	***	***	***	ns	***	***		
	T1CL3	***	***	***	***	***	***	***	*	***	***	***	***	***	***	***	***	***	
	T1CL4	***	***	***	***	***	***	***	***	***	***	***	***	***	***	***	***	***	***

Table_Apx B-5 Wilcox pairwise comparison test of Tier 1 Cluster means – LSI class aggregation metric at p <0.001 (***), p<0.01 (**) or p<0.05(*). Non-significant group differences are marked by ns.

LSI	Land Cover	Buildings			Grass				Paved				Trees				Water		
Land Cover	Tier 1 Cluster	T1CL 1	T1CL 2	T1CL 3	T1CL 1	T1CL 2	T1CL 3	T1CL 4	T1CL 1	T1CL 2	T1CL 3	T1CL 4	T1CL 1	T1CL 2	T1CL 3	T1CL 4	T1CL 1	T1CL 2	T1CL 3
Buildings	T1CL2	***																	
	T1CL3	***	***																
Grass	T1CL1	***	***	***															
	T1CL2	***	***	***	***														
	T1CL3	***	***	***	***	***													
	T1CL4	***	***	***	***	***	***												
Paved	T1CL1	***	***	***	***	***	***	ns											
	T1CL2	***	***	***	***	***	***	***	***										
	T1CL3	***	***	***	***	***	***	***	***	***									
	T1CL4	***	***	***	***	***	***	***	***	***	***								
Trees	T1CL1	***	***	***	***	***	***	***	***	***	***	***							
	T1CL2	***	***	***	***	***	***	***	***	***	***	***	***						
	T1CL3	***	***	***	***	***	***	***	***	***	***	***	***	***					
	T1CL4	***	***	***	***	***	***	***	***	***	***	***	***	***	***				
Water	T1CL1	***	***	***	***	***	***	***	***	***	***	***	***	***	***	***			
	T1CL2	***	***	***	***	***	***	***	***	***	***	***	***	***	***	***	***		
	T1CL3	***	***	***	***	***	***	***	***	***	***	***	***	***	***	***	***	***	
	T1CL4	***	***	***	***	***	***	***	***	***	***	***	***	***	***	***	***	***	***

Table_Apx B-6 Wilcox pairwise comparison test of Tier 1 Cluster means – PLADJ class aggregation metric at p <0.001 (***), p<0.01 (**) or p<0.05(*). Non-significant group differences are marked by ns.

PLADJ	Land Cover	Buildings			Grass				Paved				Trees				Water		
Land Cover	Tier 1 Cluster	T1CL1	T1CL2	T1CL3	T1CL1	T1CL2	T1CL3	T1CL4	T1CL1	T1CL2	T1CL3	T1CL4	T1CL1	T1CL2	T1CL3	T1CL4	T1CL1	T1CL2	T1CL3
Buildings	T1CL2	***																	
	T1CL3	***	***																
Grass	T1CL1	***	***	***															
	T1CL2	***	***	***	***														
	T1CL3	***	***	***	***	***													
	T1CL4	***	***	***	***	***	***												
Paved	T1CL1	***	***	***	***	***	***	***											
	T1CL2	***	***	***	***	***	***	***	***										
	T1CL3	***	***	***	***	***	***	***	***	***									
	T1CL4	***	***	***	***	***	***	***	***	***	***								
Trees	T1CL1	***	***	***	***	***	***	***	***	***	***	***							
	T1CL2	***	***	***	***	***	***	***	***	***	***	***	***						
	T1CL3	***	***	***	***	***	***	***	***	***	***	***	***	***					
	T1CL4	***	***	***	***	***	***	***	***	***	***	***	***	***	***				
Water	T1CL1	***	***	***	***	***	***	***	***	***	***	***	***	***	***	***			
	T1CL2	***	***	***	***	***	***	***	***	***	***	***	***	***	***	***	***		
	T1CL3	***	***	***	***	***	***	***	***	***	***	***	***	***	***	***	***	***	
	T1CL4	***	***	***	***	***	***	***	***	***	***	***	***	***	***	***	***	***	***

Table_Apx B-7 Wilcox pairwise comparison test of Tier 1 Cluster means – LST June 2m at p <0.001 (***), p<0.01 (**) or p<0.05(*). Non-significant group differences are marked by ns.

JUN 2m	Land Cover	Buildings			Grass				Paved				Trees				Water		
Land Cover	Tier 1 Cluster	T1CL1	T1CL2	T1CL3	T1CL1	T1CL2	T1CL3	T1CL4	T1CL1	T1CL2	T1CL3	T1CL4	T1CL1	T1CL2	T1CL3	T1CL4	T1CL1	T1CL2	T1CL3
Buildings	T1CL2	***																	
	T1CL3	***	***																
Grass	T1CL1	***	***	***															
	T1CL2	***	***	***	***														
	T1CL3	***	***	***	***	***													
	T1CL4	***	***	***	***	***	***												
Paved	T1CL1	***	***	***	***	***	***	***											
	T1CL2	***	***	***	***	***	***	***	***										
	T1CL3	***	***	***	***	***	***	***	***	***									
	T1CL4	***	***	***	***	***	***	***	***	***	***								
Trees	T1CL1	***	***	***	***	***	***	***	***	***	***	***							
	T1CL2	***	***	***	***	***	***	***	***	***	***	***	***						
	T1CL3	***	***	***	***	***	***	***	***	***	***	***	***	***					
	T1CL4	***	***	***	***	***	***	***	***	***	***	***	***	***	***				
Water	T1CL1	***	***	***	***	***	***	***	***	***	***	***	***	***	***	***			
	T1CL2	***	***	***	***	***	***	***	***	***	***	***	***	***	***	***	***		
	T1CL3	***	***	***	***	***	***	***	***	***	***	***	***	***	***	***	ns	***	
	T1CL4	***	***	***	***	***	***	***	***	***	***	***	***	***	***	***	***	***	***

Table_Apx B-8 Wilcox pairwise comparison test of Tier 1 Cluster means – LST July 2m at p <0.001 (***), p<0.01 (**) or p<0.05(*). Non-significant group differences are marked by ns.

JUL 2m	Land Cover	Buildings			Grass				Paved				Trees				Water		
Land Cover	Tier 1 Cluster	T1CL 1	T1CL 2	T1CL 3	T1CL 1	T1CL 2	T1CL 3	T1CL 4	T1CL 1	T1CL 2	T1CL 3	T1CL 4	T1CL 1	T1CL 2	T1CL 3	T1CL 4	T1CL 1	T1CL 2	T1CL 3
Buildings	T1CL2	***																	
	T1CL3	***	***																
Grass	T1CL1	***	***	***															
	T1CL2	***	***	***	***														
	T1CL3	***	***	***	***	***													
	T1CL4	***	***	***	***	***	***												
Paved	T1CL1	***	***	***	***	***	***	***											
	T1CL2	***	***	***	***	ns	***	***	***										
	T1CL3	***	***	***	***	***	***	***	***	***									
	T1CL4	***	***	***	***	***	***	***	***	***	***								
Trees	T1CL1	***	***	***	***	***	***	***	***	***	***	***							
	T1CL2	***	***	***	***	***	***	***	***	***	***	***	***						
	T1CL3	***	***	***	***	***	***	***	***	***	***	***	***	***					
	T1CL4	***	***	***	***	***	***	***	***	***	***	***	***	***	***				
Water	T1CL1	***	***	***	***	***	***	***	***	***	***	***	***	***	***	***			
	T1CL2	***	***	***	***	***	***	***	***	***	***	***	***	***	***	***	***		
	T1CL3	***	***	***	***	***	***	***	***	***	***	***	***	***	***	***	ns	***	
	T1CL4	***	***	***	***	***	***	***	***	***	***	***	***	***	***	***	***	***	***

Table_Apx B-9 Wilcox pairwise comparison test of Tier 1 Cluster means – LST June 100m at p <0.001 (***), p<0.01 (**) or p<0.05(*). Non-significant group differences are marked by ns.

JUN 100m	Land Cover	Buildings			Grass				Paved				Trees				Water		
Land Cover	Tier 1 Cluster	T1CL1	T1CL2	T1CL3	T1CL1	T1CL2	T1CL3	T1CL4	T1CL1	T1CL2	T1CL3	T1CL4	T1CL1	T1CL2	T1CL3	T1CL4	T1CL1	T1CL2	T1CL3
Buildings	T1CL2	***																	
	T1CL3	***	***																
Grass	T1CL1	***	***	***															
	T1CL2	***	***	***	***														
	T1CL3	***	***	***	***	***													
	T1CL4	***	***	***	***	***	***												
Paved	T1CL1	***	***	***	***	***	***	***											
	T1CL2	***	***	***	***	***	***	***	***										
	T1CL3	***	***	***	***	***	***	***	***	***									
	T1CL4	***	***	***	***	***	***	***	***	***	***								
Trees	T1CL1	***	***	***	***	***	***	***	***	***	***	***							
	T1CL2	***	***	***	***	***	***	***	***	***	***	***	***						
	T1CL3	***	ns	***	***	***	***	***	***	***	***	***	***	***					
	T1CL4	***	***	***	***	***	***	***	***	***	***	***	***	***	***				
Water	T1CL1	***	***	***	***	***	***	***	***	***	***	***	***	***	***	***			
	T1CL2	***	***	***	***	***	***	***	***	***	***	***	***	ns	***	***	***		
	T1CL3	***	***	***	***	***	***	***	***	***	***	***	***	***	***	***	***	***	
	T1CL4	***	***	***	***	***	***	***	***	***	***	***	***	***	***	***	***	***	***

Table_Apx B-10 Wilcox pairwise comparison test of Tier 1 Cluster means – LST July 100m at p <0.001 (***), p<0.01 (**) or p<0.05(*). Non-significant group differences are marked by ns.

JUL 100m	Land Cover	Buildings			Grass				Paved				Trees				Water		
Land Cover	Tier 1 Cluster	T1CL 1	T1CL 2	T1CL 3	T1CL 1	T1CL 2	T1CL 3	T1CL 4	T1CL 1	T1CL 2	T1CL 3	T1CL 4	T1CL 1	T1CL 2	T1CL 3	T1CL 4	T1CL 1	T1CL 2	T1CL 3
Buildings	T1CL2	***																	
	T1CL3	***	***																
Grass	T1CL1	***	***	*															
	T1CL2	***	***	***	***														
	T1CL3	***	***	***	***	***													
	T1CL4	***	***	***	***	***	***												
Paved	T1CL1	***	***	***	***	***	***	***											
	T1CL2	***	***	***	***	***	***	***	***										
	T1CL3	***	***	***	***	***	***	***	*	***									
	T1CL4	***	***	***	***	***	***	***	***	***	***								
Trees	T1CL1	***	***	***	***	***	***	***	***	***	***	***							
	T1CL2	***	***	***	***	***	***	***	***	***	***	***	***						
	T1CL3	***	***	***	***	***	***	***	***	***	***	***	***	***					
	T1CL4	***	***	***	***	**	***	***	***	***	***	***	***	***	***				
Water	T1CL1	***	***	***	***	***	***	***	***	***	***	***	***	***	***	***			
	T1CL2	***	***	***	***	***	***	***	***	***	***	***	***	***	***	***	***		
	T1CL3	***	***	***	***	***	***	***	***	***	***	***	***	***	***	***	***	***	
	T1CL4	***	***	***	***	***	***	**	***	ns	***	***	***	***	***	***	***	***	***

Table_Apx B-11 Wilcox pairwise comparison test of Tier 1 Cluster means – distance to grass at p <0.001 (***), p<0.01 (**) or p<0.05(*). Non-significant group differences are marked by ns.

d to g	Land Cover	Buildings			Grass				Paved				Trees				Water		
Land Cover	Tier 1 Cluster	T1CL1	T1CL2	T1CL3	T1CL1	T1CL2	T1CL3	T1CL4	T1CL1	T1CL2	T1CL3	T1CL4	T1CL1	T1CL2	T1CL3	T1CL4	T1CL1	T1CL2	T1CL3
Buildings	T1CL2	***																	
	T1CL3	***	***																
Grass	T1CL1	***	***	***															
	T1CL2	***	***	***															
	T1CL3	***	***	***															
	T1CL4	***	***	***															
Paved	T1CL1	***	***	***	***	***	***	***											
	T1CL2	***	***	***	***	***	***	***	***										
	T1CL3	***	***	***	***	***	***	***	***	***									
	T1CL4	***	***	***	***	***	***	***	***	***	***								
Trees	T1CL1	***	***	***	***	***	***	***	***	***	***	***							
	T1CL2	***	***	***	***	***	***	***	***	***	***	***	***						
	T1CL3	***	***	***	***	***	***	***	***	***	***	***	***	***					
	T1CL4	***	***	***	***	***	***	***	***	***	***	***	ns	***	***				
Water	T1CL1	***	***	***	***	***	***	***	***	***	***	***	***	***	***	***			
	T1CL2	***	***	***	***	***	***	***	***	***	***	***	***	***	***	***	***		
	T1CL3	ns	***	***	***	***	***	***	***	***	***	***	***	***	***	***	***	***	
	T1CL4	***	***	***	***	***	***	***	***	***	***	***	***	***	***	***	***	ns	***

Table_Apx B-12 Wilcox pairwise comparison test of Tier 1 Cluster means – distance to trees at p <0.001 (***), p<0.01 (**) or p<0.05(*). Non-significant group differences are marked by ns.

d to t	Land Cover	Buildings			Grass				Paved				Trees				Water		
Land Cover	Tier 1 Cluster	T1CL1	T1CL2	T1CL3	T1CL1	T1CL2	T1CL3	T1CL4	T1CL1	T1CL2	T1CL3	T1CL4	T1CL1	T1CL2	T1CL3	T1CL4	T1CL1	T1CL2	T1CL3
Buildings	T1CL2	***																	
	T1CL3	***	***																
Grass	T1CL1	***	***	***															
	T1CL2	***	***	***	***														
	T1CL3	***	***	***	***	***													
	T1CL4	***	***	***	***	***	***												
Paved	T1CL1	***	***	***	***	***	***	***											
	T1CL2	***	***	***	***	***	***	***	***										
	T1CL3	***	***	***	***	***	***	***	***	***									
	T1CL4	***	***	***	***	***	***	***	***	***	***								
Trees	T1CL1	***	***	***	***	***	***	***	***	***	***	***							
	T1CL2	***	***	***	***	***	***	***	***	***	***	***							
	T1CL3	***	***	***	***	***	***	***	***	***	***	***							
	T1CL4	***	***	***	***	***	***	***	***	***	***	***							
Water	T1CL1	***	***	***	***	***	***	***	ns	***	***	***	***	***	***	***			
	T1CL2	***	***	***	***	***	***	ns	***	***	***	**	***	***	***	***	***		
	T1CL3	**	***	***	***	***	***	***	***	***	***	***	***	***	***	***	***	***	
	T1CL4	***	***	***	***	***	***	***	***	***	***	***	***	***	***	***	***	***	***

Table_Apx B-13 Wilcox pairwise comparison test of Tier 1 Cluster means – distance to buildings at p <0.001 (***), p<0.01 (**) or p<0.05(*). Non-significant group differences are marked by ns.

d to b	Land Cover	Buildings			Grass				Paved				Trees				Water		
Land Cover	Tier 1 Cluster	T1CL1	T1CL2	T1CL3	T1CL1	T1CL2	T1CL3	T1CL4	T1CL1	T1CL2	T1CL3	T1CL4	T1CL1	T1CL2	T1CL3	T1CL4	T1CL1	T1CL2	T1CL3
Buildings	T1CL2																		
	T1CL3																		
Grass	T1CL1	***	***	***															
	T1CL2	***	***	***	***														
	T1CL3	***	***	***	***	***													
	T1CL4	***	***	***	***	***	***												
Paved	T1CL1	***	***	***	***	***	ns	***											
	T1CL2	***	***	***	ns	***	***	***	***										
	T1CL3	***	***	***	***	***	***	***	***	***									
	T1CL4	***	***	***	***	***	***	***	***	***	***								
Trees	T1CL1	***	***	***	***	***	***	***	***	***	***	***							
	T1CL2	***	***	***	***	***	***	***	***	***	***	***	***						
	T1CL3	***	***	***	***	***	***	***	***	***	***	***	***	***					
	T1CL4	***	***	***	***	***	***	***	***	***	***	***	***	***	***				
Water	T1CL1	***	***	***	***	***	***	***	***	***	***	***	***	***	***	***			
	T1CL2	***	***	***	***	***	***	***	***	***	***	***	***	***	***	***	ns		
	T1CL3	***	***	***	***	***	***	***	***	***	***	***	***	***	***	***	*	**	
	T1CL4	***	***	***	***	***	***	***	***	***	***	***	***	***	***	***	***	***	***

Table_Apx B-14 Wilcox pairwise comparison test of Tier 1 Cluster means – distance to paved at p <0.001 (***), p<0.01 (**) or p<0.05(*). Non-significant group differences are marked by ns.

d to p	Land Cover	Buildings			Grass				Paved				Trees				Water		
Land Cover	Tier 1 Cluster	T1CL1	T1CL2	T1CL3	T1CL1	T1CL2	T1CL3	T1CL4	T1CL1	T1CL2	T1CL3	T1CL4	T1CL1	T1CL2	T1CL3	T1CL4	T1CL1	T1CL2	T1CL3
Buildings	T1CL2	***																	
	T1CL3	***	***																
Grass	T1CL1	***	***	***															
	T1CL2	***	***	***	***														
	T1CL3	***	***	***	***	***													
	T1CL4	***	***	***	***	***	***												
Paved	T1CL1	***	***	***	***	***	***	***											
	T1CL2	***	***	***	***	***	***	***											
	T1CL3	***	***	***	***	***	***	***											
	T1CL4	***	***	***	***	***	***	***											
Trees	T1CL1	***	***	***	**	***	***	***	***	***	***	***							
	T1CL2	***	***	***	***	***	***	***	***	***	***	***	***						
	T1CL3	***	***	***	***	***	***	***	***	***	***	***	***	***					
	T1CL4	***	***	***	***	***	***	***	***	***	***	***	***	***	***				
Water	T1CL1	***	***	***	***	***	***	***	***	***	***	***	***	***	***	***			
	T1CL2	***	***	***	***	***	***	***	***	***	***	***	***	***	***	***	***		
	T1CL3	***	***	***	***	***	***	***	***	***	***	***	***	***	***	***	**	***	
	T1CL4	***	***	***	***	***	***	***	***	***	***	***	***	***	***	***	***	ns	***

Table_Apx B-15 Wilcox pairwise comparison test of Tier 1 Cluster means – distance to water at p <0.001 (***), p<0.01 (**) or p<0.05(*). Non-significant group differences are marked by ns.

d to w	Land Cover	Buildings			Grass				Paved				Trees				Water		
Land Cover	Tier 1 Cluster	T1CL1	T1CL2	T1CL3	T1CL1	T1CL2	T1CL3	T1CL4	T1CL1	T1CL2	T1CL3	T1CL4	T1CL1	T1CL2	T1CL3	T1CL4	T1CL1	T1CL2	T1CL3
Buildings	T1CL2	***																	
	T1CL3	***	***																
Grass	T1CL1	***	***	***															
	T1CL2	***	***	***	***														
	T1CL3	ns	***	***	***	***													
	T1CL4	***	***	***	***	***	***												
Paved	T1CL1	***	***	***	***	***	***	***											
	T1CL2	***	***	***	***	***	***	***	***										
	T1CL3	***	***	***	***	***	***	***	***	***									
	T1CL4	***	***	***	***	***	***	***	***	***	***								
Trees	T1CL1	***	***	***	***	***	***	***	***	***	ns	***							
	T1CL2	***	***	***	***	***	***	*	***	***	***	***	***						
	T1CL3	***	***	***	***	***	***	***	***	***	***	***	***	***					
	T1CL4	***	***	***	***	***	***	***	*	***	***	***	***	***	***				
Water	T1CL1	***	***	***	***	***	***	***	***	***	***	***	***	***	***	***			
	T1CL2	***	***	***	***	***	***	***	***	***	***	***	***	***	***	***			
	T1CL3	***	***	***	***	***	***	***	***	***	***	***	***	***	***	***			
	T1CL4	***	***	***	***	***	***	***	***	***	***	***	***	***	***	***			

Table_Apx B-16 Wilcox pairwise comparison test of Tier 1 Cluster means – cluster patch area at p <0.001 (***), p<0.01 (**) or p<0.05(*). Non-significant group differences are marked by ns.

Area	Land Cover	Buildings			Grass				Paved				Trees				Water		
Land Cover	Tier 1 Cluster	T1CL 1	T1CL 2	T1CL 3	T1CL 1	T1CL 2	T1CL 3	T1CL 4	T1CL 1	T1CL 2	T1CL 3	T1CL 4	T1CL 1	T1CL 2	T1CL 3	T1CL 4	T1CL 1	T1CL 2	T1CL 3
Buildings	T1CL2	***																	
	T1CL3	***	*																
Grass	T1CL1	***	***	***															
	T1CL2	***	***	***	***														
	T1CL3	***	***	***	***	ns													
	T1CL4	***	***	***	***	***	***												
Paved	T1CL1	***	***	***	***	***	***	ns											
	T1CL2	***	***	***	***	***	***	***	***										
	T1CL3	***	***	***	***	***	***	**	*	*									
	T1CL4	***	***	***	***	***	***	**	*	***	***								
Trees	T1CL1	***	***	***	***	***	***	***	***	***	***	***							
	T1CL2	***	***	***	***	**	*	*	ns	ns	ns	***	***						
	T1CL3	***	***	***	***	**	*	***	***	ns	***	***	***	ns					
	T1CL4	***	***	***	***	***	***	***	***	***	***	***	ns	***	***				
Water	T1CL1	***	***	***	***	***	***	***	***	***	***	***	***	***	***	***			
	T1CL2	***	***	***	***	***	***	***	***	***	***	***	***	***	***	***	***		
	T1CL3	*	***	***	***	***	***	***	***	***	***	***	***	***	***	***	***	***	
	T1CL4	***	***	***	***	***	***	***	***	***	***	***	***	***	***	***	***	***	***

Table_Apx B-17 Wilcox pairwise comparison test of Tier 2 Cluster means of the COHESION index at p <0.001 (***), p<0.01 (**) or p<0.05 (*) for core patches of buildings. Non-significant group differences are marked by ns.

		LA				RLA				MA		
		C	M-C	M-H	H	C	M-C	M-H	H	C	M-C	M-H
LA	M-C	ns										
	M-H	ns	*									
	H	ns	**	ns								
RLA	C	***	***	***	***							
	M-C	***	***	***	***	**						
	M-H	***	***	***	***	ns	***					
	H	***	***	***	***	***	***	***				
MA	C	***	***	***	***	***	***	***	***			
	M-C	***	***	***	***	***	***	***	***	ns		
	M-H	***	***	***	***	***	***	***	***	ns	ns	
	H	***	***	***	***	***	***	***	***	ns	ns	ns

Table_Apx B-18 Wilcox pairwise comparison test of Tier 2 Cluster means of the LSI index at p <0.001 (***), p<0.01 (**) or p<0.05 (*) for core patches of buildings. Non-significant group differences are marked by ns.

		LA				RLA				MA		
		C	M-C	M-H	H	C	M-C	M-H	H	C	M-C	M-H
LA	M-C	***										
	M-H	***	***									
	H	***	***	***								
RLA	C	***	***	***	***							
	M-C	***	***	***	***	***						
	M-H	ns	***	***	***	***	***					
	H	***	***	***	***	***	***	***				
MA	C	***	***	***	***	***	***	***	***			
	M-C	***	***	***	***	***	***	***	***	**		
	M-H	***	***	***	***	***	***	***	***	***	***	
	H	***	***	***	***	***	***	***	***	***	***	**

Table_Apx B-19 Wilcox pairwise comparison test of Tier 2 Cluster means of the PLADJ index at p <0.001 (***), p<0.01 (**) or p<0.05 (*) for core patches of buildings. Non-significant group differences are marked by ns.

		LA				RLA				MA		
		C	M-C	M-H	H	C	M-C	M-H	H	C	M-C	M-H
LA	M-C	*										
	M-H	*	***									
	H	***	***	ns								
RLA	C	***	***	***	***							
	M-C	***	***	***	***	ns						
	M-H	***	***	***	***	***	**					
	H	***	***	***	***	**	***	***				
MA	C	***	***	***	***	***	***	***	***			
	M-C	***	***	***	***	***	***	***	***	ns		
	M-H	***	***	***	***	***	***	***	***	ns	*	
	H	***	***	***	***	***	***	***	***	ns	*	ns

Table_Apx B-20 Wilcox pairwise comparison test of Tier 2 Cluster means of the distance to water at p <0.001 (***), p<0.01 (**) or p<0.05 (*) for core patches of buildings. Non-significant group differences are marked by ns.

		LA				RLA				MA		
		C	M-C	M-H	H	C	M-C	M-H	H	C	M-C	M-H
LA	M-C	***										
	M-H	***	***									
	H	***	***	ns								
RLA	C	ns	***	***	***							
	M-C	***	***	***	***	***						
	M-H	***	***	ns	ns	***	***					
	H	***	***	ns	ns	***	***	ns				
MA	C	ns	ns	***	***	ns	*	***	***			
	M-C	*	ns	***	***	ns	**	***	***	ns		
	M-H	***	***	*	*	***	*	ns	ns	***	***	
	H	***	***	ns	ns	***	***	ns	ns	***	***	ns

Table_Apx B-21 Wilcox pairwise comparison test of Tier 2 Cluster means of the distance to grass at p <0.001 (***), p<0.01 (**) or p<0.05 (*) for core patches of buildings. Non-significant group differences are marked by ns.

		LA				RLA				MA		
		C	M-C	M-H	H	C	M-C	M-H	H	C	M-C	M-H
LA	M-C	ns										
	M-H	**	***									
	H	**	***	ns								
RLA	C	***	***	***	***							
	M-C	***	***	***	***	ns						
	M-H	*	**	***	***	**	**					
	H	***	***	***	***	***	***	***				
MA	C	***	***	***	***	***	***	***	***			
	M-C	***	***	***	***	***	***	***	***	ns		
	M-H	***	***	***	***	***	***	***	***	ns	ns	
	H	***	***	***	***	***	***	***	***	***	***	***

Table_Apx B-22 Wilcox pairwise comparison test of Tier 2 Cluster means of the distance to paved at p <0.001 (***), p<0.01 (**) or p<0.05 (*) for core patches of buildings. Non-significant group differences are marked by ns.

		LA				RLA				MA		
		C	M-C	M-H	H	C	M-C	M-H	H	C	M-C	M-H
LA	M-C	***										
	M-H	***	*									
	H	***	**	ns								
RLA	C	***	***	***	***							
	M-C	***	***	***	***	ns						
	M-H	***	***	***	***	ns	ns					
	H	***	***	***	***	ns	ns	ns				
MA	C	***	***	***	***	***	***	***	***			
	M-C	***	***	***	***	***	***	***	***	ns		
	M-H	***	***	***	***	***	***	***	***	ns	ns	
	H	***	***	***	***	***	***	***	***	ns	ns	ns

Table_Apx B-23 Wilcox pairwise comparison test of Tier 2 Cluster means of the distance to trees at p <0.001 (***), p<0.01 (**) or p<0.05 (*) for core patches of buildings. Non-significant group differences are marked by ns.

		LA				RLA				MA		
		C	M-C	M-H	H	C	M-C	M-H	H	C	M-C	M-H
LA	M-C	***										
	M-H	***	**									
	H	***	*	ns								
RLA	C	***	***	*	*							
	M-C	***	***	***	***	ns						
	M-H	***	***	**	**	ns	ns					
	H	***	***	***	***	***	***	***				
MA	C	***	***	***	***	***	***	***	**			
	M-C	***	***	***	***	***	***	***	***	ns		
	M-H	***	***	***	***	***	***	***	***	*	ns	
	H	***	***	***	***	***	***	***	***	***	***	***

Table_Apx B-24 Wilcox pairwise comparison test of Tier 2 Cluster means of area at p <0.001 (***), p<0.01 (**) or p<0.05 (*) for core patches of buildings. Non-significant group differences are marked by ns.

		LA				RLA				MA		
		C	M-C	M-H	H	C	M-C	M-H	H	C	M-C	M-H
LA	M-C	ns										
	M-H	ns	ns									
	H	***	***	*								
RLA	C	***	***	***	***							
	M-C	**	**	***	***	ns						
	M-H	ns	ns	**	***	*	*					
	H	***	***	***	***	*	**	***				
MA	C	***	***	***	***	***	***	***	**			
	M-C	***	***	***	***	***	***	***	***	ns		
	M-H	***	***	***	***	***	***	***	***	ns	ns	
	H	***	***	***	***	***	***	***	***	ns	ns	ns

Table_Apx B-25 Wilcox pairwise comparison test of Tier 2 Cluster means of LST in June at 2m resolution at p <0.001 (***), p<0.01 (**) or p<0.05 (*) for core patches of buildings. Non-significant group differences are marked by ns.

		LA				RLA				MA		
		C	M-C	M-H	H	C	M-C	M-H	H	C	M-C	M-H
LA	M-C	***										
	M-H	***	***									
	H	***	***	***								
RLA	C	ns	***	***	***							
	M-C	***	***	***	***	***						
	M-H	***	***	***	***	***	***					
	H	***	***	***	***	***	***	***				
MA	C	***	***	***	***	***	***	***	***			
	M-C	***	***	***	***	***	***	***	***	***		
	M-H	***	***	***	***	***	***	***	***	***	***	
	H	***	***	***	***	***	***	***	***	***	***	***

Table_Apx B-26 Wilcox pairwise comparison test of Tier 2 Cluster means of LST in June at 100m resolution at p <0.001 (***), p<0.01 (**) or p<0.05 (*) for core patches of buildings. Non-significant group differences are marked by ns.

		LA				RLA				MA		
		C	M-C	M-H	H	C	M-C	M-H	H	C	M-C	M-H
LA	M-C	***										
	M-H	***	***									
	H	***	***	***								
RLA	C	ns	***	***	***							
	M-C	***	***	***	***	***						
	M-H	***	***	***	***	***	***					
	H	***	***	***	***	***	***	***				
MA	C	***	*	***	***	***	***	***	***			
	M-C	***	***	ns	***	***	***	***	***	***		
	M-H	***	***	***	***	***	***	***	***	***	***	
	H	***	***	***	***	***	***	***	***	***	***	***

Table_Apx B-27 Wilcox pairwise comparison test of Tier 2 Cluster means of LST in July at 2m resolution at p <0.001 (***), p<0.01 (**) or p<0.05 (*) for core patches of buildings. Non-significant group differences are marked by ns.

		LA				RLA				MA		
		C	M-C	M-H	H	C	M-C	M-H	H	C	M-C	M-H
LA	M-C	***										
	M-H	***	***									
	H	***	***	***								
RLA	C	ns	***	***	***							
	M-C	***	***	***	***	***						
	M-H	***	***	**	***	***	***					
	H	***	***	***	***	***	***	***				
MA	C	*	***	***	***	ns	***	***	***			
	M-C	***	***	***	***	***	***	***	***	***		
	M-H	***	***	***	***	***	***	*	***	***	***	
	H	***	***	***	***	***	***	***	***	***	***	***

Table_Apx B-28 Wilcox pairwise comparison test of Tier 2 Cluster means of LST in July at 100m resolution at p <0.001 (***), p<0.01 (**) or p<0.05 (*) for core patches of buildings. Non-significant group differences are marked by ns.

		LA				RLA				MA		
		C	M-C	M-H	H	C	M-C	M-H	H	C	M-C	M-H
LA	M-C	***										
	M-H	***	***									
	H	***	***	***								
RLA	C	ns	***	***	***							
	M-C	***	***	***	***	***						
	M-H	***	***	***	***	***	***					
	H	***	***	***	***	***	***	***				
MA	C	***	*	***	***	***	***	***	***			
	M-C	***	***	***	***	***	***	***	***	***		
	M-H	***	***	***	***	***	***	***	ns	***	***	
	H	***	***	***	***	***	***	***	***	***	***	***

Table_Apx B-29 Wilcox pairwise comparison test of Tier 2 Cluster means of the COHESION index at p <0.001 (***), p<0.01 (**) or p<0.05 (*) for core patches of grass. Non-significant group differences are marked by ns.

		LA				RLA				RMA				MA		
		C	M-C	M-H	H	C	M-C	M-H	H	C	M-C	M-H	H	C	M-C	M-H
LA	M-C	***														
	M-H	ns	***													
	H	***	***	***												
RLA	C	***	***	***	***											
	M-C	***	***	***	***	***										
	M-H	***	***	***	***	***	***									
	H	***	***	***	***	***	***	***								
RMA	C	***	***	***	***	***	***	***	***							
	M-C	***	***	***	***	***	***	***	***	***						
	M-H	***	***	***	***	***	***	***	***	***	ns					
	H	***	***	***	***	***	***	***	***	***	***	***				
MA	C	***	***	***	***	***	***	***	***	***	***	***	***			
	M-C	***	***	***	***	***	***	***	***	***	***	***	***	***		
	M-H	***	***	***	***	***	***	***	***	***	***	***	***	***	ns	
	H	***	***	***	***	***	***	***	***	***	***	***	***	***	ns	ns

Table_Apx B-30 Wilcox pairwise comparison test of Tier 2 Cluster means of the LSI index at p <0.001 (***), p<0.01 (**) or p<0.05 (*) for core patches of grass. Non-significant group differences are marked by ns.

		LA				RLA				RMA				MA		
		C	M-C	M-H	H	C	M-C	M-H	H	C	M-C	M-H	H	C	M-C	M-H
LA	M-C	***														
	M-H	***	***													
	H	***	***	***												
RLA	C	***	***	***	***											
	M-C	***	***	***	***	***										
	M-H	ns	***	***	***	***	***									
	H	*	***	***	***	***	***	*								
RMA	C	***	***	***	***	***	***	***	***							
	M-C	***	***	***	***	***	***	***	***	***						
	M-H	***	***	***	***	***	***	***	***	***	***					
	H	***	***	***	***	***	***	***	***	***	***	ns				
MA	C	***	***	***	***	***	***	***	***	***	***	***	***			
	M-C	***	***	***	***	***	***	***	***	***	***	***	***	**		
	M-H	***	***	***	***	***	***	***	***	***	***	***	***	***	ns	
	H	***	***	***	***	***	***	***	***	***	***	***	***	ns	*	***

Table_Apx B-31 Wilcox pairwise comparison test of Tier 2 Cluster means of the PLADJ index at p <0.001 (***), p<0.01 (**) or p<0.05 (*) for core patches of grass. Non-significant group differences are marked by ns.

		LA				RLA				RMA				MA		
		C	M-C	M-H	H	C	M-C	M-H	H	C	M-C	M-H	H	C	M-C	M-H
LA	M-C	***														
	M-H	ns	***													
	H	***	ns	***												
RLA	C	***	***	***	***											
	M-C	***	***	***	***	***										
	M-H	***	***	***	***	***	***									
	H	***	***	***	***	***	***	***								
RMA	C	***	***	***	***	***	***	***	***							
	M-C	***	***	***	***	***	***	***	***	***						
	M-H	***	***	***	***	***	***	***	***	***	***					
	H	***	***	***	***	***	***	***	***	***	***	***				
MA	C	***	***	***	***	***	***	***	***	***	***	***	***			
	M-C	***	***	***	***	***	***	***	***	***	***	***	***	ns		
	M-H	***	***	***	***	***	***	***	***	***	***	***	***	***	ns	
	H	***	***	***	***	***	***	***	***	***	***	***	***	*	ns	ns

Table_Apx B-32 Wilcox pairwise comparison test of Tier 2 Cluster means of distance to water at p <0.001 (***), p<0.01 (**) or p<0.05 (*) for core patches of grass. Non-significant group differences are marked by ns.

		LA				RLA				RMA				MA		
		C	M-C	M-H	H	C	M-C	M-H	H	C	M-C	M-H	H	C	M-C	M-H
LA	M-C	***														
	M-H	***	***													
	H	***	***	***												
RLA	C	***	***	***	***											
	M-C	***	***	***	***	***										
	M-H	***	***	***	***	***	***									
	H	***	***	**	***	***	***	***								
RMA	C	***	***	***	***	***	***	***	***							
	M-C	***	***	***	***	*	***	***	***	***						
	M-H	***	***	***	***	***	**	***	***	***	***					
	H	***	***	***	***	***	***	*	***	***	***	***				
MA	C	***	***	***	***	***	***	***	***	***	***	***	***			
	M-C	***	***	***	***	***	***	***	***	***	***	***	***	***		
	M-H	ns	***	***	***	***	ns	***	***	***	***	*	***	***	***	
	H	***	*	***	***	***	***	***	***	***	***	***	**	***	***	***

Table_Apx B-33 Wilcox pairwise comparison test of Tier 2 Cluster means of distance to buildings at p <0.001 (***), p<0.01 (**) or p<0.05 (*) for core patches of grass. Non-significant group differences are marked by ns.

		LA				RLA				RMA				MA		
		C	M-C	M-H	H	C	M-C	M-H	H	C	M-C	M-H	H	C	M-C	M-H
LA	M-C	***														
	M-H	***	ns													
	H	***	*	*												
RLA	C	***	***	***	***											
	M-C	***	***	***	***	***										
	M-H	**	***	***	***	***	***									
	H	***	***	***	***	***	***	**								
RMA	C	***	***	***	***	***	***	***	***							
	M-C	***	***	***	***	***	***	***	***	***						
	M-H	***	***	***	***	***	***	***	***	***	***					
	H	***	***	***	***	***	***	***	***	***	***	***				
MA	C	***	***	***	***	***	***	***	***	***	***	***	***			
	M-C	***	***	***	***	***	***	***	***	*	***	***	***	***		
	M-H	***	***	***	***	***	***	***	***	***	***	***	***	***	***	
	H	***	***	***	***	ns	***	***	***	***	*	***	***	***	***	***

Table_Apx B-34 Wilcox pairwise comparison test of Tier 2 Cluster means of distance to paved at p <0.001 (***), p<0.01 (**) or p<0.05 (*) for core patches of grass. Non-significant group differences are marked by ns.

		LA				RLA				RMA				MA		
		C	M-C	M-H	H	C	M-C	M-H	H	C	M-C	M-H	H	C	M-C	M-H
LA	M-C	***														
	M-H	***	***													
	H	***	ns	*												
RLA	C	***	***	***	***											
	M-C	ns	***	***	***	***										
	M-H	*	***	***	***	***	***									
	H	*	***	**	***	***	ns	***								
RMA	C	***	***	***	***	***	***	***	***							
	M-C	***	***	***	***	ns	***	***	***	***						
	M-H	***	***	***	***	***	***	**	***	***	**					
	H	ns	***	***	***	***	ns	**	ns	***	***	***				
MA	C	***	***	***	***	***	***	***	***	***	***	***	***			
	M-C	***	***	***	***	***	***	***	***	***	***	***	***	*		
	M-H	***	***	***	***	***	***	***	***	ns	***	***	***	***	***	
	H	***	***	***	***	ns	***	***	***	**	*	***	***	***	***	ns

Table_Apx B-35 Wilcox pairwise comparison test of Tier 2 Cluster means of distance to trees at p <0.001 (***), p<0.01 (**) or p<0.05 (*) for core patches of grass. Non-significant group differences are marked by ns.

		LA				RLA				RMA				MA		
		C	M-C	M-H	H	C	M-C	M-H	H	C	M-C	M-H	H	C	M-C	M-H
LA	M-C	***														
	M-H	***	ns													
	H	***	**	*												
RLA	C	***	ns	ns	ns											
	M-C	***	***	***	***	***										
	M-H	***	***	***	***	***	ns									
	H	***	***	***	***	***	**	***								
RMA	C	***	***	***	*	*	ns	ns	**							
	M-C	***	***	***	***	***	***	***	***	***						
	M-H	***	***	***	***	***	***	***	*	***	ns					
	H	***	***	***	***	***	***	***	***	***	ns	**				
MA	C	***	***	***	***	***	***	***	**	***	ns	ns	ns			
	M-C	***	***	***	***	***	***	***	***	***	**	**	ns	ns		
	M-H	***	***	***	***	***	***	***	***	***	***	***	*	ns	ns	
	H	***	***	***	***	***	***	***	***	***	***	***	***	*	*	ns

Table_Apx B-36 Wilcox pairwise comparison test of Tier 2 Cluster means of area at p <0.001 (***), p<0.01 (**) or p<0.05 (*) for core patches of grass. Non-significant group differences are marked by ns.

		LA				RLA				RMA				MA		
		C	M-C	M-H	H	C	M-C	M-H	H	C	M-C	M-H	H	C	M-C	M-H
LA	M-C	***														
	M-H	***	ns													
	H	***	ns	ns												
RLA	C	***	***	***	***											
	M-C	***	***	***	***	ns										
	M-H	***	***	***	***	ns	ns									
	H	***	***	***	***	ns	ns	ns								
RMA	C	***	***	***	***	ns	ns	ns	ns							
	M-C	***	***	***	***	***	***	***	***	*						
	M-H	***	***	***	***	ns	ns	ns	ns	ns	*					
	H	***	***	***	***	*	**	*	ns	ns	ns	ns				
MA	C	***	***	**	**	ns	ns	ns	ns	ns	ns	ns	ns			
	M-C	***	***	***	***	***	***	***	***	**	ns	**	*	ns		
	M-H	***	***	***	***	ns	ns	ns	ns	ns	ns	ns	ns	ns	ns	
	H	***	***	***	***	ns	ns	ns	ns	ns	ns	ns	ns	ns	ns	ns

Table_Apx B-37 Wilcox pairwise comparison test of Tier 2 Cluster means of LST in June at 2m resolution at p <0.001 (***), p<0.01 (**) or p<0.05 (*) for core patches of grass. Non-significant group differences are marked by ns.

		LA				RLA				RMA				MA		
		C	M-C	M-H	H	C	M-C	M-H	H	C	M-C	M-H	H	C	M-C	M-H
LA	M-C	***														
	M-H	***	***													
	H	***	***	***												
RLA	C	***	***	***	***											
	M-C	***	***	***	***	***										
	M-H	***	***	***	***	***	***									
	H	***	***	***	***	***	***	***								
RMA	C	***	***	***	***	***	***	***	***							
	M-C	***	***	***	***	***	***	***	***	***						
	M-H	***	***	***	***	***	***	***	***	***	***					
	H	***	***	***	***	***	***	***	***	***	***	***				
MA	C	***	***	***	***	***	***	***	***	***	***	***	***			
	M-C	***	***	***	***	***	***	***	***	***	***	***	***	***		
	M-H	***	***	***	***	***	***	***	***	***	***	***	***	***	***	
	H	***	***	***	***	***	***	***	***	***	***	***	***	***	***	***

Table_Apx B-38 Wilcox pairwise comparison test of Tier 2 Cluster means of LST in June at 100m resolution at p <0.001 (***), p<0.01 (**) or p<0.05 (*) for core patches of grass. Non-significant group differences are marked by ns.

		LA				RLA				RMA				MA		
		C	M-C	M-H	H	C	M-C	M-H	H	C	M-C	M-H	H	C	M-C	M-H
LA	M-C	***														
	M-H	***	***													
	H	***	***	***												
RLA	C	***	***	***	***											
	M-C	***	***	***	***	***										
	M-H	***	***	***	***	***	***									
	H	***	***	***	***	***	***	***								
RMA	C	***	***	***	***	***	***	***	***							
	M-C	***	***	***	***	***	***	***	***	***						
	M-H	***	***	***	***	***	***	***	***	***	***					
	H	***	***	***	***	***	***	***	***	***	***	***				
MA	C	***	***	***	***	***	***	***	***	***	***	***	***			
	M-C	***	***	***	***	ns	***	***	***	***	***	***	***	***		
	M-H	***	***	***	***	***	ns	***	***	***	***	***	***	***	***	
	H	***	***	***	***	***	***	ns	***	***	***	***	***	***	***	***

Table_Apx B-39 Wilcox pairwise comparison test of Tier 2 Cluster means of LST in July at 2m resolution at p <0.001 (***), p<0.01 (**) or p<0.05 (*) for core patches of grass. Non-significant group differences are marked by ns.

		LA				RLA				RMA				MA		
		C	M-C	M-H	H	C	M-C	M-H	H	C	M-C	M-H	H	C	M-C	M-H
LA	M-C	***														
	M-H	***	***													
	H	***	***	***												
RLA	C	***	***	***	***											
	M-C	***	***	***	***	***										
	M-H	***	***	***	***	***	***									
	H	***	***	***	***	***	***	***								
RMA	C	***	***	***	***	***	***	***	***							
	M-C	***	***	***	***	***	***	***	***	***						
	M-H	***	***	***	***	***	***	***	***	***	***					
	H	***	***	***	***	***	***	***	***	***	***	***				
MA	C	***	***	***	***	***	***	***	***	***	***	***	***			
	M-C	***	***	***	***	***	***	***	***	***	***	***	***	***		
	M-H	***	***	***	***	***	***	***	***	***	***	***	***	***	***	
	H	***	***	***	***	***	***	***	***	***	***	***	**	***	***	***

Table_Apx B-40 Wilcox pairwise comparison test of Tier 2 Cluster means of LST in July at 100m resolution at p <0.001 (***), p<0.01 (**) or p<0.05 (*) for core patches of grass. Non-significant group differences are marked by ns.

		LA				RLA				RMA				MA		
		C	M-C	M-H	H	C	M-C	M-H	H	C	M-C	M-H	H	C	M-C	M-H
LA	M-C	***														
	M-H	***	***													
	H	***	***	***												
RLA	C	***	***	***	***											
	M-C	***	***	***	***	***										
	M-H	***	***	***	***	***	***									
	H	***	***	***	***	***	***	***								
RMA	C	***	***	***	***	***	***	***	***							
	M-C	**	***	***	***	***	***	***	***	***						
	M-H	***	***	***	***	***	***	***	***	***	***					
	H	***	***	***	***	***	***	***	***	***	***	***				
MA	C	***	***	***	***	***	***	***	***	***	***	***	***			
	M-C	***	***	***	***	***	***	***	***	***	***	***	***	***		
	M-H	***	***	***	***	***	***	***	***	***	***	***	***	***	***	
	H	***	***	***	***	***	***	***	***	***	***	***	**	***	***	***

Table_Apx B-41 Wilcox pairwise comparison test of Tier 2 Cluster means of the COHESION index at p <0.001 (***), p<0.01 (**) or p<0.05 (*) for core patches of paved. Non-significant group differences are marked by ns.

		LA				RLA				RMA				MA		
		C	M-C	M-H	H	C	M-C	M-H	H	C	M-C	M-H	H	C	M-C	M-H
LA	M-C	***														
	M-H	***	***													
	H	***	***	**												
RLA	C	***	***	***	***											
	M-C	***	***	***	***	***										
	M-H	***	***	***	***	***	**									
	H	***	***	***	***	***	***	ns								
RMA	C	***	***	***	***	***	***	**	**							
	M-C	***	***	***	***	***	***	***	***	***						
	M-H	***	***	***	***	***	***	***	***	***	ns					
	H	***	***	***	***	***	***	***	***	***	**	***				
MA	C	***	***	***	***	***	***	***	***	***	***	***	***			
	M-C	***	***	***	***	***	***	***	***	***	***	***	***	***		
	M-H	***	***	***	***	***	***	***	***	***	***	***	***	***	***	
	H	***	***	***	***	***	***	***	***	***	***	***	***	***	***	*

Table_Apx B-42 Wilcox pairwise comparison test of Tier 2 Cluster means of the LSI index at p <0.001 (***), p<0.01 (**) or p<0.05 (*) for core patches of paved. Non-significant group differences are marked by ns.

		LA				RLA				RMA				MA		
		C	M-C	M-H	H	C	M-C	M-H	H	C	M-C	M-H	H	C	M-C	M-H
LA	M-C	***														
	M-H	***	***													
	H	***	***	***												
RLA	C	***	***	***	***											
	M-C	***	***	***	***	***										
	M-H	***	***	***	***	***	***									
	H	***	ns	***	***	***	***	***								
RMA	C	***	***	***	***	***	***	***	***							
	M-C	***	***	***	***	***	***	***	***	***						
	M-H	*	***	***	***	***	***	***	***	***	***					
	H	ns	***	***	***	***	***	***	***	***	***	***				
MA	C	***	***	***	***	***	***	***	***	***	***	***	***			
	M-C	***	***	***	***	***	***	***	***	***	***	***	***	***		
	M-H	***	***	***	***	***	***	***	***	*	***	***	***	***	***	
	H	***	***	***	***	***	***	***	***	ns	***	***	***	***	***	*

Table_Apx B-43 Wilcox pairwise comparison test of Tier 2 Cluster means of the PLADJ index at p <0.001 (***), p<0.01 (**) or p<0.05 (*) for core patches of paved. Non-significant group differences are marked by ns.

		LA				RLA				RMA				MA		
		C	M-C	M-H	H	C	M-C	M-H	H	C	M-C	M-H	H	C	M-C	M-H
LA	M-C	***														
	M-H	***	***													
	H	***	***	***												
RLA	C	***	***	***	***											
	M-C	***	***	***	***	***										
	M-H	***	***	***	***	ns	***									
	H	***	***	***	***	***	***	***								
RMA	C	***	***	***	***	***	***	***	***							
	M-C	***	***	***	***	***	***	***	***	***						
	M-H	***	***	***	***	***	***	***	***	***	**					
	H	***	***	***	***	***	***	***	***	**	***	***				
MA	C	***	***	***	***	***	***	***	***	***	***	***	***			
	M-C	***	***	***	***	***	***	***	***	***	***	***	***	**		
	M-H	***	***	***	***	***	***	***	***	***	***	***	***	***	ns	
	H	***	***	***	***	***	***	***	***	***	***	***	***	**	ns	ns

Table_Apx B-44 Wilcox pairwise comparison test of Tier 2 Cluster means of the distance to water at p <0.001 (***), p<0.01 (**) or p<0.05 (*) for core patches of paved. Non-significant group differences are marked by ns.

		LA				RLA				RMA				MA		
		C	M-C	M-H	H	C	M-C	M-H	H	C	M-C	M-H	H	C	M-C	M-H
LA	M-C	***														
	M-H	***	***													
	H	***	***	***												
RLA	C	***	***	***	***											
	M-C	***	***	ns	***	***										
	M-H	***	***	***	***	***	***									
	H	***	***	***	***	***	***	***								
RMA	C	***	***	ns	***	ns	ns	***	***							
	M-C	***	***	ns	***	***	ns	***	***	ns						
	M-H	***	***	***	*	***	***	***	***	***	***					
	H	***	***	***	***	***	***	***	ns	***	***	***				
MA	C	***	ns	***	***	***	***	***	***	***	***	***	***			
	M-C	***	***	***	***	ns	***	***	***	ns	***	***	***	***		
	M-H	***	***	ns	***	***	ns	***	***	ns	ns	***	***	***	***	
	H	***	***	***	ns	***	***	***	***	***	***	ns	***	***	***	***

Table_Apx B-45 Wilcox pairwise comparison test of Tier 2 Cluster means of the distance to buildings at p <0.001 (***), p<0.01 (**) or p<0.05 (*) for core patches of paved. Non-significant group differences are marked by ns.

		LA				RLA				RMA				MA		
		C	M-C	M-H	H	C	M-C	M-H	H	C	M-C	M-H	H	C	M-C	M-H
LA	M-C	***														
	M-H	***	***													
	H	***	***	***												
RLA	C	***	ns	***	***											
	M-C	***	***	***	***	***										
	M-H	***	***	***	***	***	***									
	H	***	***	***	***	***	***	***								
RMA	C	***	*	***	***	*	***	***	***							
	M-C	***	***	***	***	***	***	***	***	***						
	M-H	***	***	***	ns	***	***	***	***	***	***					
	H	***	***	***	***	***	***	***	ns	***	***	***				
MA	C	ns	***	***	***	***	***	***	***	***	***	***	***			
	M-C	***	***	***	***	***	***	***	***	ns	***	***	***	***		
	M-H	***	***	***	***	***	***	***	***	***	***	***	***	***	***	
	H	***	***	***	ns	***	***	ns	***	***	***	ns	***	***	***	***

Table_Apx B-46 Wilcox pairwise comparison test of Tier 2 Cluster means of the distance to grass at p <0.001 (***), p<0.01 (**) or p<0.05 (*) for core patches of paved. Non-significant group differences are marked by ns.

		LA				RLA				RMA				MA		
		C	M-C	M-H	H	C	M-C	M-H	H	C	M-C	M-H	H	C	M-C	M-H
LA	M-C	ns														
	M-H	***	***													
	H	***	*	ns												
RLA	C	***	***	ns	ns											
	M-C	***	***	**	***	*										
	M-H	***	**	ns	ns	ns	***									
	H	***	***	ns	*	ns	ns	**								
RMA	C	*	***	***	***	***	***	***	***							
	M-C	***	***	*	**	*	ns	***	ns	***						
	M-H	***	***	**	***	**	ns	***	*	***	ns					
	H	***	***	***	***	***	***	***	***	***	***	***				
MA	C	*	ns	ns	ns	ns	ns	ns	ns	***	ns	ns	*			
	M-C	***	***	**	***	**	*	***	**	***	*	ns	ns	ns		
	M-H	***	***	***	***	***	***	***	***	***	***	***	ns	*	ns	
	H	***	***	***	***	***	***	***	***	***	***	***	***	***	***	***

Table_Apx B-47 Wilcox pairwise comparison test of Tier 2 Cluster means of the distance to trees at p <0.001 (***), p<0.01 (**) or p<0.05 (*) for core patches of paved. Non-significant group differences are marked by ns.

		LA				RLA				RMA				MA		
		C	M-C	M-H	H	C	M-C	M-H	H	C	M-C	M-H	H	C	M-C	M-H
LA	M-C	ns														
	M-H	ns	ns													
	H	***	***	***												
RLA	C	*	**	ns	***											
	M-C	***	***	***	***	**										
	M-H	ns	*	ns	***	ns	***									
	H	ns	*	***	***	***	***	***								
RMA	C	***	***	***	**	***	***	***	***							
	M-C	**	***	***	ns	***	***	***	**	**						
	M-H	***	***	***	ns	***	***	***	***	**	ns					
	H	***	***	***	*	***	***	***	***	*	**	ns				
MA	C	***	***	***	***	***	***	***	***	ns	***	***	***			
	M-C	***	***	***	***	***	***	***	***	ns	***	***	***	ns		
	M-H	***	***	***	***	***	***	***	***	ns	***	***	***	ns	ns	
	H	***	***	***	***	***	***	***	***	*	***	***	***	ns	*	ns

Table_Apx B-48 Wilcox pairwise comparison test of Tier 2 Cluster means of area at p <0.001 (***), p<0.01 (**) or p<0.05 (*) for core patches of paved. Non-significant group differences are marked by ns.

		LA				RLA				RMA				MA		
		C	M-C	M-H	H	C	M-C	M-H	H	C	M-C	M-H	H	C	M-C	M-H
LA	M-C	ns														
	M-H	ns	ns													
	H	ns	ns	ns												
RLA	C	ns	ns	ns	ns											
	M-C	ns	***	*	**	**										
	M-H	***	***	***	***	***	***									
	H	***	***	***	***	***	***	*								
RMA	C	ns	ns	ns	ns	ns	ns	**	*							
	M-C	ns	ns	ns	ns	ns	***	***	***	ns						
	M-H	ns	ns	ns	ns	ns	***	***	***	ns	ns					
	H	ns	***	ns	**	*	ns	***	**	ns	**	**				
MA	C	**	*	**	*	**	***	***	***	ns	*	*	***			
	M-C	**	*	**	**	**	***	***	***	ns	**	**	***	ns		
	M-H	*	ns	*	ns	ns	**	***	***	ns	ns	ns	**	ns	ns	
	H	ns	ns	ns	ns	ns	ns	***	**	ns	ns	ns	ns	*	*	ns

Table_Apx B-49 Wilcox pairwise comparison test of Tier 2 Cluster means of LST in June at 2m resolution at p <0.001 (***), p<0.01 (**) or p<0.05 (*) for core patches of paved. Non-significant group differences are marked by ns.

		LA				RLA				RMA				MA		
		C	M-C	M-H	H	C	M-C	M-H	H	C	M-C	M-H	H	C	M-C	M-H
LA	M-C	***														
	M-H	***	***													
	H	***	***	***												
RLA	C	***	***	***	***											
	M-C	***	***	***	***	***										
	M-H	***	***	***	***	***	***									
	H	***	***	***	***	***	***	***								
RMA	C	***	***	***	***	***	***	***	***							
	M-C	***	***	**	***	***	***	***	***	***						
	M-H	***	***	***	***	***	***	***	***	***	***					
	H	***	***	***	***	***	***	***	***	***	***	***				
MA	C	***	***	***	***	***	***	***	***	***	***	***	***			
	M-C	***	***	***	***	***	***	***	***	***	***	***	***	***		
	M-H	***	***	***	***	***	***	***	***	***	***	***	***	***	***	
	H	***	***	***	***	***	***	***	***	***	***	***	***	***	***	***

Table_Apx B-50 Wilcox pairwise comparison test of Tier 2 Cluster means of LST in June at 100m resolution at p <0.001 (***), p<0.01 (**) or p<0.05 (*) for core patches of paved. Non-significant group differences are marked by ns.

		LA				RLA				RMA				MA		
		C	M-C	M-H	H	C	M-C	M-H	H	C	M-C	M-H	H	C	M-C	M-H
LA	M-C	***														
	M-H	***	***													
	H	***	***	***												
RLA	C	***	***	***	***											
	M-C	***	***	***	***	***										
	M-H	***	***	***	***	***	***									
	H	***	***	***	***	***	***	***								
RMA	C	***	***	***	***	***	***	***	***							
	M-C	***	***	***	***	***	***	***	***	***						
	M-H	***	***	***	***	***	***	***	***	***	***					
	H	***	***	***	***	***	***	***	***	***	***	***				
MA	C	***	***	***	***	***	***	***	***	***	***	***	***			
	M-C	***	***	ns	***	***	**	***	***	***	***	***	***	***		
	M-H	***	***	***	***	***	***	***	***	***	***	***	***	***	***	
	H	***	***	***	***	***	***	***	***	***	***	***	***	***	***	***

Table_Apx B-51 Wilcox pairwise comparison test of Tier 2 Cluster means of LST in July at 2m resolution at p <0.001 (***), p<0.01 (**) or p<0.05 (*) for core patches of paved. Non-significant group differences are marked by ns.

		LA				RLA				RMA				MA		
		C	M-C	M-H	H	C	M-C	M-H	H	C	M-C	M-H	H	C	M-C	M-H
LA	M-C	***														
	M-H	***	***													
	H	***	***	***												
RLA	C	***	***	***	***											
	M-C	***	***	***	***	***										
	M-H	***	***	***	***	***	***									
	H	***	***	***	***	***	***	***								
RMA	C	***	***	***	***	***	ns	***	***							
	M-C	***	***	ns	***	***	***	***	***	***						
	M-H	***	***	***	***	***	***	***	***	***	***					
	H	***	***	***	***	***	***	***	***	***	***	***				
MA	C	***	***	***	***	*	***	***	***	***	***	***	***			
	M-C	***	***	***	***	***	***	***	***	ns	***	***	***	***		
	M-H	***	***	***	***	***	***	***	***	***	***	***	***	***	***	
	H	***	***	***	***	***	***	***	***	***	***	***	***	***	***	***

Table_Apx B-52 Wilcox pairwise comparison test of Tier 2 Cluster means of LST in July at 100m resolution at p <0.001 (***), p<0.01 (**) or p<0.05 (*) for core patches of paved. Non-significant group differences are marked by ns.

		LA				RLA				RMA				MA		
		C	M-C	M-H	H	C	M-C	M-H	H	C	M-C	M-H	H	C	M-C	M-H
LA	M-C	***														
	M-H	***	***													
	H	***	***	***												
RLA	C	***	***	***	***											
	M-C	***	***	***	***	***										
	M-H	***	***	***	***	***	***									
	H	***	***	***	***	***	***	***								
RMA	C	***	***	**	***	***	***	***	***							
	M-C	***	***	***	***	***	***	***	***	ns						
	M-H	***	***	***	***	***	***	***	***	***	***					
	H	***	***	***	***	***	***	***	***	***	***	***				
MA	C	***	***	***	***	***	***	***	***	***	***	***	***			
	M-C	***	***	**	***	***	***	***	***	ns	***	***	***	***		
	M-H	***	***	***	***	***	***	***	***	***	***	***	***	***	***	
	H	***	***	***	***	***	***	***	***	***	***	***	***	***	***	***

Table_Apx B-53 Wilcox pairwise comparison test of Tier 2 Cluster means of the COHESION index at p <0.001 (***), p<0.01 (**) or p<0.05 (*) for core patches of trees. Non-significant group differences are marked by ns.

		LA				RLA				RMA				MA		
		C	M-C	M-H	H	C	M-C	M-H	H	C	M-C	M-H	H	C	M-C	M-H
LA	M-C	***														
	M-H	ns	***													
	H	*	***	***												
RLA	C	***	***	***	***											
	M-C	***	***	***	***	***										
	M-H	***	***	***	***	***	*									
	H	***	***	***	***	ns	***	***								
RMA	C	***	***	***	***	***	***	***	***							
	M-C	***	***	***	***	***	***	***	***	ns						
	M-H	***	***	***	***	***	***	***	***	ns	ns					
	H	***	***	***	***	***	***	***	***	ns	**	ns				
MA	C	***	***	***	***	***	***	***	***	***	***	***	***			
	M-C	***	***	***	***	***	***	***	***	***	***	***	***	**		
	M-H	***	***	***	***	***	***	***	***	***	***	***	***	**	ns	
	H	***	***	***	***	***	***	***	***	***	***	***	***	**	ns	ns

Table_Apx B-54 Wilcox pairwise comparison test of Tier 2 Cluster means of the LSI index at p <0.001 (***), p<0.01 (**) or p<0.05 (*) for core patches of trees. Non-significant group differences are marked by ns.

		LA				RLA				RMA				MA		
		C	M-C	M-H	H	C	M-C	M-H	H	C	M-C	M-H	H	C	M-C	M-H
LA	M-C	***														
	M-H	***	***													
	H	***	***	***												
RLA	C	***	***	***	***											
	M-C	***	***	***	***	***										
	M-H	*	***	***	***	***	***									
	H	ns	***	***	***	***	***	***								
RMA	C	***	***	***	***	***	***	***	***							
	M-C	***	***	***	***	***	***	***	***	***						
	M-H	***	***	***	***	***	***	***	***	***	ns					
	H	***	***	***	***	***	***	***	***	***	**	ns				
MA	C	***	***	***	***	***	***	***	***	***	***	***	***			
	M-C	***	***	***	***	***	***	***	***	***	***	***	***	***		
	M-H	***	***	***	***	***	***	***	***	***	***	***	***	**	ns	
	H	***	***	***	***	***	***	***	***	***	***	***	***	ns	**	**

Table_Apx B-55 Wilcox pairwise comparison test of Tier 2 Cluster means of the PLADJ index at p <0.001 (***), p<0.01 (**) or p<0.05 (*) for core patches of trees. Non-significant group differences are marked by ns.

		LA				RLA				RMA				MA		
		C	M-C	M-H	H	C	M-C	M-H	H	C	M-C	M-H	H	C	M-C	M-H
LA	M-C	***														
	M-H	***	ns													
	H	***	***	***												
RLA	C	***	***	***	***											
	M-C	***	***	***	***	***										
	M-H	***	***	***	***	***	ns									
	H	***	***	***	***	***	***	***								
RMA	C	***	***	***	***	***	***	***	***							
	M-C	***	***	***	***	***	***	***	***	***						
	M-H	***	***	***	***	***	***	***	***	***	***					
	H	***	***	***	***	***	***	***	***	***	***	***				
MA	C	***	***	***	***	***	***	***	***	***	***	***	***			
	M-C	***	***	***	***	***	***	***	***	***	***	***	***	***		
	M-H	***	***	***	***	***	***	***	***	***	***	***	***	***	**	
	H	***	***	***	***	***	***	***	***	***	***	***	***	***	***	*

Table_Apx B-56 Wilcox pairwise comparison test of Tier 2 Cluster means of distance to water at p <0.001 (***), p<0.01 (**) or p<0.05 (*) for core patches of trees. Non-significant group differences are marked by ns.

		LA				RLA				RMA				MA		
		C	M-C	M-H	H	C	M-C	M-H	H	C	M-C	M-H	H	C	M-C	M-H
LA	M-C	***														
	M-H	***	***													
	H	***	***	***												
RLA	C	ns	***	***	***											
	M-C	***	ns	***	***	***										
	M-H	***	***	ns	***	***	***									
	H	***	***	***	ns	***	***	***								
RMA	C	***	***	***	***	***	***	***	***							
	M-C	***	***	***	***	***	***	***	***	***						
	M-H	***	***	***	***	***	***	***	***	***	***					
	H	***	***	***	***	***	***	***	***	***	***	***				
MA	C	***	***	***	***	***	***	***	***	*	***	***	***			
	M-C	ns	***	***	***	**	***	***	***	***	ns	***	***	***		
	M-H	***	ns	***	***	***	ns	***	***	***	***	***	***	***	***	
	H	***	***	ns	***	***	***	ns	***	***	***	***	*	***	***	***

Table_Apx B-57 Wilcox pairwise comparison test of Tier 2 Cluster means of distance to buildings at p <0.001 (***), p<0.01 (**) or p<0.05 (*) for core patches of trees. Non-significant group differences are marked by ns.

		LA				RLA				RMA				MA		
		C	M-C	M-H	H	C	M-C	M-H	H	C	M-C	M-H	H	C	M-C	M-H
LA	M-C	***														
	M-H	***	**													
	H	***	***	*												
RLA	C	ns	***	***	***											
	M-C	***	ns	**	***	***										
	M-H	***	***	ns	*	***	***									
	H	***	***	ns	ns	***	***	ns								
RMA	C	***	***	***	***	***	***	***	***							
	M-C	***	***	***	***	***	***	***	***	***						
	M-H	***	***	***	***	***	***	***	***	***	***					
	H	***	***	***	***	***	***	***	***	***	***	***				
MA	C	***	***	***	***	***	***	***	***	***	***	***	***			
	M-C	***	***	***	***	***	***	***	***	ns	***	***	***	***		
	M-H	***	***	***	***	***	***	***	***	***	***	***	***	***	***	
	H	ns	***	***	***	ns	***	***	***	***	ns	***	***	***	***	***

Table_Apx B-58 Wilcox pairwise comparison test of Tier 2 Cluster means of distance to grass at p <0.001 (***), p<0.01 (**) or p<0.05 (*) for core patches of trees. Non-significant group differences are marked by ns.

		LA				RLA				RMA				MA		
		C	M-C	M-H	H	C	M-C	M-H	H	C	M-C	M-H	H	C	M-C	M-H
LA	M-C	***														
	M-H	ns	***													
	H	***	*	***												
RLA	C	***	**	***	ns											
	M-C	***	**	***	***	***										
	M-H	***	***	**	**	ns	***									
	H	***	**	***	ns	ns	***	**								
RMA	C	***	**	***	ns	ns	***	ns	ns							
	M-C	***	**	***	ns	ns	***	*	ns	ns						
	M-H	***	ns	***	ns	ns	***	**	ns	ns	ns					
	H	***	*	***	***	***	ns	***	***	***	***	**				
MA	C	ns	***	ns	**	*	***	ns	**	*	*	**	***			
	M-C	ns	***	ns	*	ns	***	ns	*	ns	ns	**	***	ns		
	M-H	*	*	ns	ns	ns	***	ns	ns	ns	ns	ns	***	ns	ns	
	H	***	*	***	**	**	ns	***	**	**	**	*	ns	***	***	**

Table_Apx B-59 Wilcox pairwise comparison test of Tier 2 Cluster means of distance to paved at p <0.001 (***), p<0.01 (**) or p<0.05 (*) for core patches of trees. Non-significant group differences are marked by ns.

		LA				RLA				RMA				MA		
		C	M-C	M-H	H	C	M-C	M-H	H	C	M-C	M-H	H	C	M-C	M-H
LA	M-C	***														
	M-H	***	ns													
	H	***	*	ns												
RLA	C	ns	***	***	***											
	M-C	***	**	ns	ns	***										
	M-H	***	ns	ns	ns	***	ns									
	H	***	***	***	***	***	***	***								
RMA	C	***	***	***	***	***	***	***	***							
	M-C	ns	***	***	***	*	***	***	***	***						
	M-H	**	***	***	***	***	***	***	***	***	***					
	H	*	***	***	***	***	***	***	***	***	*	ns				
MA	C	***	***	***	***	***	***	***	***	***	***	***	***			
	M-C	***	***	***	***	***	***	***	***	**	***	***	***	***		
	M-H	**	***	***	***	**	***	***	***	***	***	***	***	***	*	
	H	*	***	***	***	*	***	***	***	***	**	***	***	***	*	ns

Table_Apx B-60 Wilcox pairwise comparison test of Tier 2 Cluster means of area at p <0.001 (***), p<0.01 (**) or p<0.05 (*) for core patches of trees. Non-significant group differences are marked by ns.

		LA				RLA				RMA				MA		
		C	M-C	M-H	H	C	M-C	M-H	H	C	M-C	M-H	H	C	M-C	M-H
LA	M-C	*														
	M-H	ns	***													
	H	*	ns	***												
RLA	C	***	*	***	ns											
	M-C	***	*	***	ns	ns										
	M-H	ns	***	ns	***	***	***									
	H	**	ns	***	ns	ns	ns	***								
RMA	C	***	***	***	***	***	***	***	***							
	M-C	***	ns	***	ns	ns	ns	***	ns	***						
	M-H	ns	ns	*	ns	**	**	**	*	***	*					
	H	*	ns	***	ns	ns	ns	***	ns	***	ns	ns				
MA	C	**	*	***	*	ns	ns	***	ns	ns	ns	**	ns			
	M-C	*	ns	**	ns	ns	ns	**	ns	**	ns	ns	ns	ns		
	M-H	ns	ns	*	ns	ns	ns	*	ns	***	ns	ns	ns	ns	ns	
	H	ns	ns	*	ns	ns	ns	*	ns	ns	ns	ns	ns	ns	ns	ns

Table_Apx B-61 Wilcox pairwise comparison test of Tier 2 Cluster means of LST in June at 2m resolution at p <0.001 (***), p<0.01 (**) or p<0.05 (*) for core patches of trees. Non-significant group differences are marked by ns.

		LA				RLA				RMA				MA		
		C	M-C	M-H	H	C	M-C	M-H	H	C	M-C	M-H	H	C	M-C	M-H
LA	M-C	***														
	M-H	***	***													
	H	***	***	***												
RLA	C	***	***	***	***											
	M-C	***	***	***	***	***										
	M-H	***	***	***	***	***	***									
	H	***	***	***	***	***	***	***								
RMA	C	***	***	***	***	***	***	***	***							
	M-C	***	***	***	***	***	***	***	***	***						
	M-H	***	***	***	***	***	***	***	***	***	***					
	H	***	***	***	***	***	***	***	***	***	***	***				
MA	C	***	***	***	***	***	***	***	***	***	***	***	***			
	M-C	***	***	***	***	***	***	***	***	***	***	***	***	***		
	M-H	***	***	***	***	***	***	***	***	***	***	***	***	***	***	
	H	***	***	***	***	***	***	***	***	***	***	***	***	***	***	***

Table_Apx B-62 Wilcox pairwise comparison test of Tier 2 Cluster means of LST in June at 100m resolution at p <0.001 (***), p<0.01 (**) or p<0.05 (*) for core patches of trees. Non-significant group differences are marked by ns.

		LA				RLA				RMA				MA		
		C	M-C	M-H	H	C	M-C	M-H	H	C	M-C	M-H	H	C	M-C	M-H
LA	M-C	***														
	M-H	***	***													
	H	***	***	***												
RLA	C	***	***	***	***											
	M-C	***	***	***	***	***										
	M-H	***	***	***	***	***	***									
	H	***	***	***	***	***	***	***								
RMA	C	***	***	***	***	***	***	***	***							
	M-C	***	***	***	***	***	***	***	***	***						
	M-H	***	***	***	***	***	***	***	***	***	***					
	H	***	***	**	***	***	***	***	***	***	***	***				
MA	C	***	***	***	***	***	***	***	***	***	***	***	***			
	M-C	***	***	***	***	***	***	***	***	***	***	***	***	***		
	M-H	*	***	***	***	***	***	***	***	***	ns	***	***	***	***	
	H	***	ns	***	***	***	***	***	***	***	***	***	***	***	***	***

Table_Apx B-63 Wilcox pairwise comparison test of Tier 2 Cluster means of LST in July at 2m resolution at p <0.001 (***), p<0.01 (**) or p<0.05 (*) for core patches of trees. Non-significant group differences are marked by ns.

		LA				RLA				RMA				MA		
		C	M-C	M-H	H	C	M-C	M-H	H	C	M-C	M-H	H	C	M-C	M-H
LA	M-C	***														
	M-H	***	***													
	H	***	***	***												
RLA	C	***	***	***	***											
	M-C	***	***	***	***	***										
	M-H	***	***	***	***	***	***									
	H	***	***	***	***	***	***	***								
RMA	C	***	***	***	***	***	***	***	***							
	M-C	ns	***	***	***	***	***	***	***	***						
	M-H	***	***	***	***	***	***	***	***	***	***					
	H	***	***	***	***	***	***	***	***	***	***	***				
MA	C	***	***	***	***	***	***	***	***	***	***	***	***			
	M-C	***	***	***	***	***	***	***	***	***	***	***	***	***		
	M-H	***	***	***	***	***	***	***	***	***	***	***	***	***	***	
	H	***	***	***	***	***	***	***	***	***	***	***	***	***	***	***

Table_Apx B-64 Wilcox pairwise comparison test of Tier 2 Cluster means of LST in July at 100m resolution at p <0.001 (***), p<0.01 (**) or p<0.05 (*) for core patches of trees. Non-significant group differences are marked by ns.

		LA				RLA				RMA				MA		
		C	M-C	M-H	H	C	M-C	M-H	H	C	M-C	M-H	H	C	M-C	M-H
LA	M-C	***														
	M-H	***	***													
	H	***	***	***												
RLA	C	***	***	***	***											
	M-C	***	***	***	***	***										
	M-H	***	***	***	***	***	***									
	H	***	***	***	***	***	***	***								
RMA	C	***	***	***	***	***	***	***	***							
	M-C	***	***	***	***	ns	***	***	***	***						
	M-H	***	ns	***	***	***	***	***	***	***	***					
	H	***	***	**	***	***	***	***	***	***	***	***				
MA	C	***	***	***	***	***	***	***	***	***	***	***	***			
	M-C	***	***	***	***	***	***	***	***	***	***	***	***	***		
	M-H	ns	***	***	***	***	***	***	***	***	***	***	***	***	***	
	H	***	***	***	***	***	***	***	***	***	***	***	***	***	***	***

Appendix C Supplementary Materials to Chapter 4

C.1 Thermal properties of Tier 2 cluster patches

Differences in LST of various Tier 2 clusters between June and July ranged from 3.2 to 4.8K and were typically the lowest in buildings, followed by the least/less aggregated grass, paved, trees and the more/most aggregated grass. However, LST differences for the coldest and hottest Tier 2 clusters within each LC subtype ranged between 3.9 and 6.6K and depended on LC type and its aggregation level, and were somewhat higher in July than June (Table_Apx C-1). These findings indicate that despite a rise in LST over the course of one month, there were certain factors other than the shape of LC patches of a given type influencing their surface temperature, and that their influence on LST remained fairly unchanged within the time step considered here.

Table_Apx C-1 LST [ºC] Mean and standard deviation (in brackets) of Tier 2 subdivisions of LC sybtypes (Tier 1 clusters) in June and July acquired from 2m resolution images, including the LST difference between the hottest and the coldest LC patches.

Tier 1	Tier 2	Buildings		Grass		Paved		Trees	
		June	July	June	July	June	July	June	July
Least aggregated	C	28.1 (0.7)	31.8 (0.5)	27.1 (1)	30.5 (0.9)	25.1 (0.8)	29.3 (0.8)	27.1 (1.1)	31.1 (0.8)
	M-C	29.6 (0.4)	33 (0.4)	29 (0.5)	32.3 (0.5)	27.3 (0.6)	31.4 (0.5)	29.1 (0.5)	32.5 (0.4)
	M-H	31 (0.3)	34.9 (0.4)	30.7 (0.5)	34.1 (0.6)	28.9 (0.5)	33 (0.6)	31 (0.5)	34.4 (0.6)
	H	32 (0.4)	36.2 (0.4)	32.2 (0.6)	36.1 (0.7)	31 (0.7)	35.2 (0.8)	32.5 (0.6)	36.4 (0.7)
	H min C	3.9	4.4	5.1	5.6	5.9	5.9	5.4	5.3
Relatively less aggregated	C	28.2 (0.7)	31.8 (0.6)	26.3 (0.9)	30.1 (0.8)	26.4 (0.8)	30.5 (0.8)	26.7 (0.9)	30.6 (0.8)
	M-C	29.8 (0.4)	33.1 (0.4)	28.4 (0.5)	32 (0.5)	28.4 (0.5)	32.3 (0.5)	28.6 (0.5)	32.2 (0.4)
	M-H	31.3 (0.4)	34.9 (0.4)	30.2 (0.5)	33.9 (0.6)	29.9 (0.5)	34.1 (0.5)	30.4 (0.5)	34.2 (0.6)
	H	32.6 (0.5)	36.5 (0.6)	31.7 (0.6)	35.9 (0.7)	31.5 (0.6)	35.9 (0.6)	31.9 (0.6)	35.9 (0.6)
	H min C	4.4	4.7	5.4	5.8	5.1	5.4	5.2	5.3
Relatively more aggregated	C	n/a	n/a	25.4 (0.8)	29.5 (0.8)	26.9 (0.8)	31.1 (0.4)	25.5 (0.8)	29.6 (0.8)
	M-C	n/a	n/a	27.4 (0.5)	31.5 (0.5)	28.9 (0.6)	32.5 (0.5)	27.5 (0.5)	31.4 (0.5)
	M-H	n/a	n/a	29.2 (0.5)	33.3 (0.6)	30.7 (0.5)	34.5 (0.6)	29.2 (0.5)	33.2 (0.6)
	H	n/a	n/a	31.1 (0.8)	35.6 (0.8)	32.2 (0.6)	36.3 (0.6)	31.2 (0.7)	35.4 (0.7)
	H min C	n/a	n/a	5.7	6.1	5.3	5.2	5.7	5.8
Most aggregated	C	28.5 (0.8)	32 (0.7)	24.6 (0.7)	29 (0.8)	26 (1)	30.4 (1)	24.7 (0.7)	28.8 (0.7)
	M-C	30.2 (0.4)	33.4 (0.4)	26.6 (0.6)	31.2 (0.6)	28.6 (0.6)	32.6 (0.6)	26.5 (0.5)	30.5 (0.5)
	M-H	31.8 (0.4)	35.3 (0.5)	28.5 (0.6)	33 (0.6)	30.5 (0.6)	34.7 (0.6)	28.2 (0.6)	32 (0.5)
	H	33.2 (0.5)	37.2 (0.6)	30.7 (0.9)	35.5 (0.9)	32.6 (0.7)	36.8 (0.7)	30.3 (0.9)	34.4 (1)
	H min C	4.7	5.2	6.1	6.5	6.6	6.4	5.6	5.6

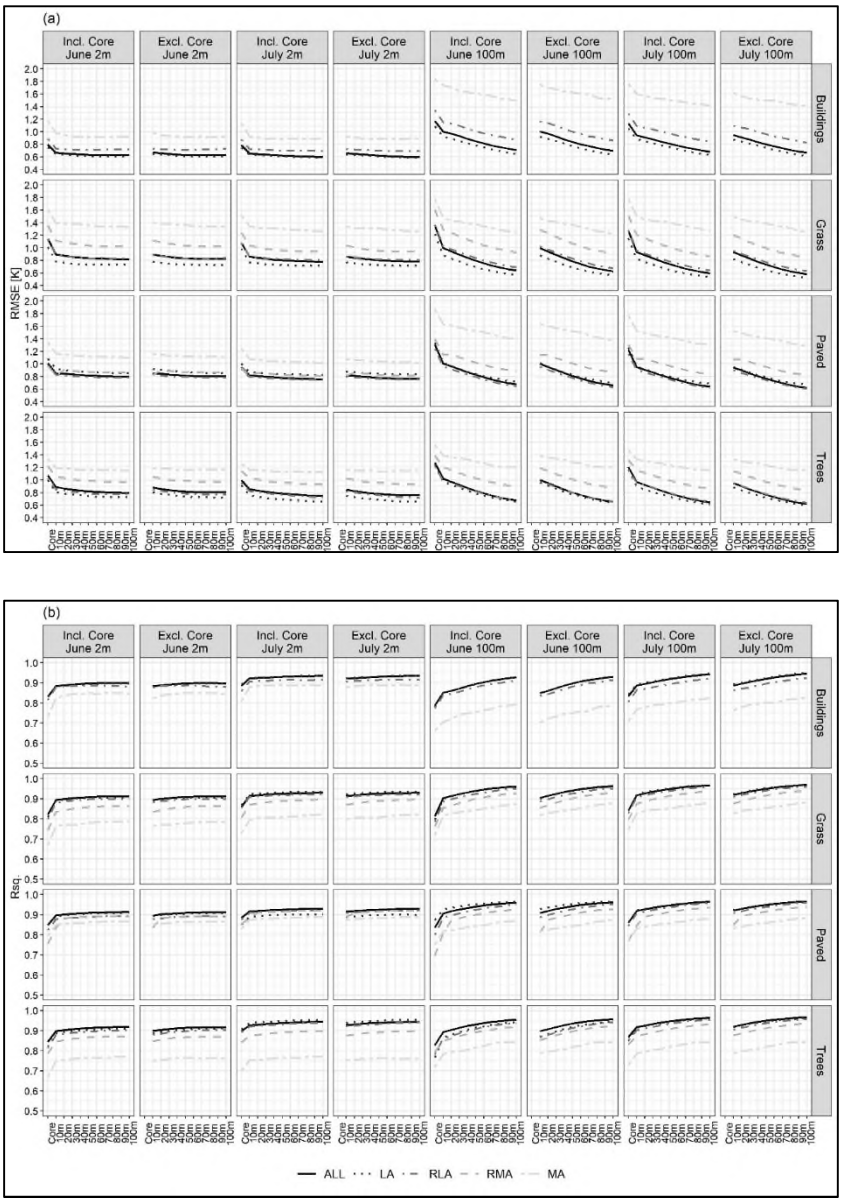

Figure_Apx C-1 Root mean square error (a) and R^2 (b) obtained from RF models relating LST at two dates (6th June and 8th July 2013) and spatial resolutions (2m and 100m) to spatial configuration descriptors for all patches of a given LC type (ALL) and separately for LC patches contained within Tier 1 clusters (LA – least aggregated, RLA – relatively less aggregated, RMA – relatively more aggregated, MA – most aggregated). 'Core' refers to models constructed with spatial configuration descriptors for core patches only, whilst 10m, etc., indicate models with addition of patches intersecting with consecutive zones around the core patches. Metrics for models that included or excluded spatial configuration descriptors for core patches are shown.

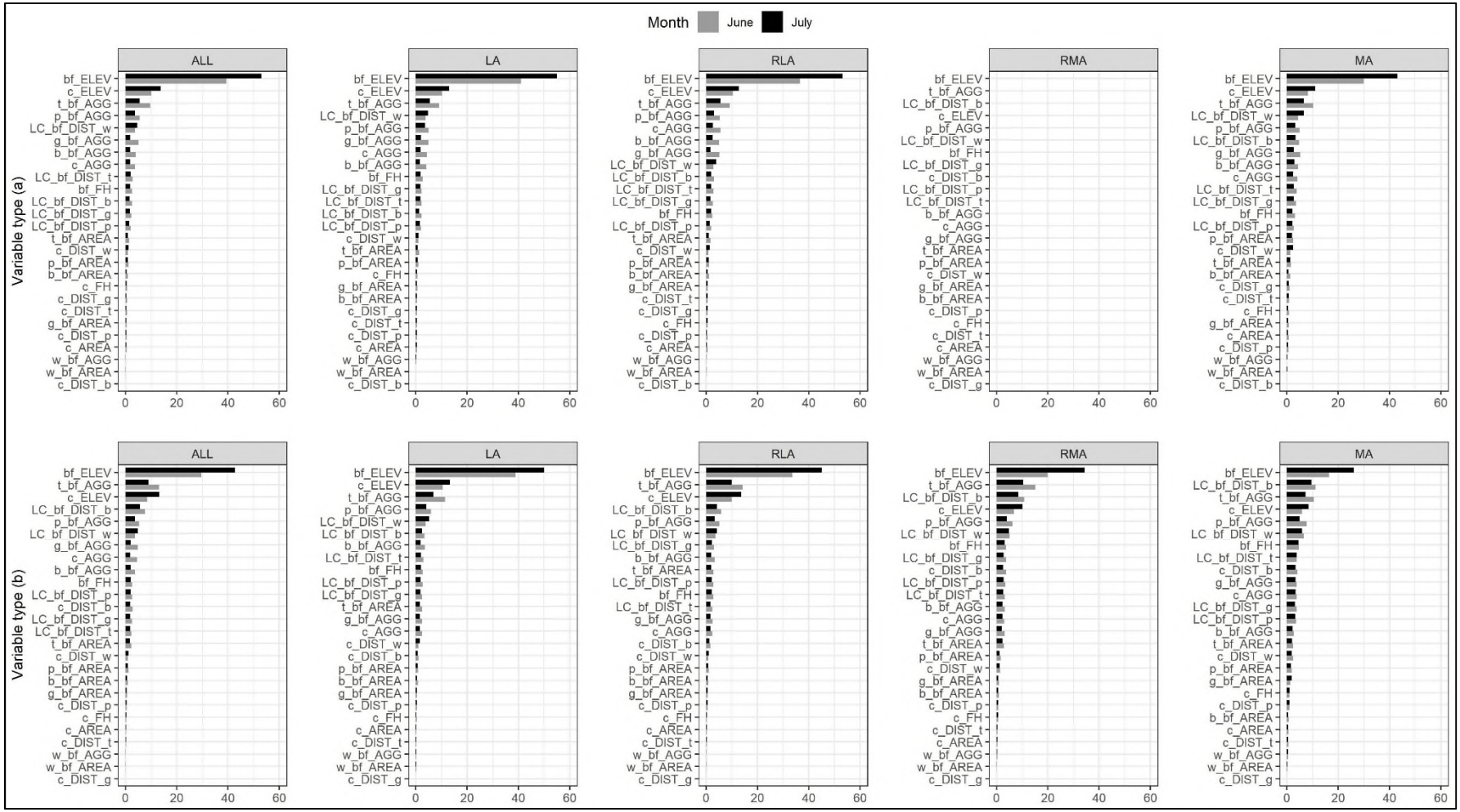

Figure_Apx C-2a Percentage of the total variance of LST in (a) buildings and (b) grass explained by RF models attributed to the main LST predictor groups, Table 4-1, main text) in June and July at 2m spatial resolution. Predictors are sorted by the decreasing mean percentage of the total variance explained for the two dates.

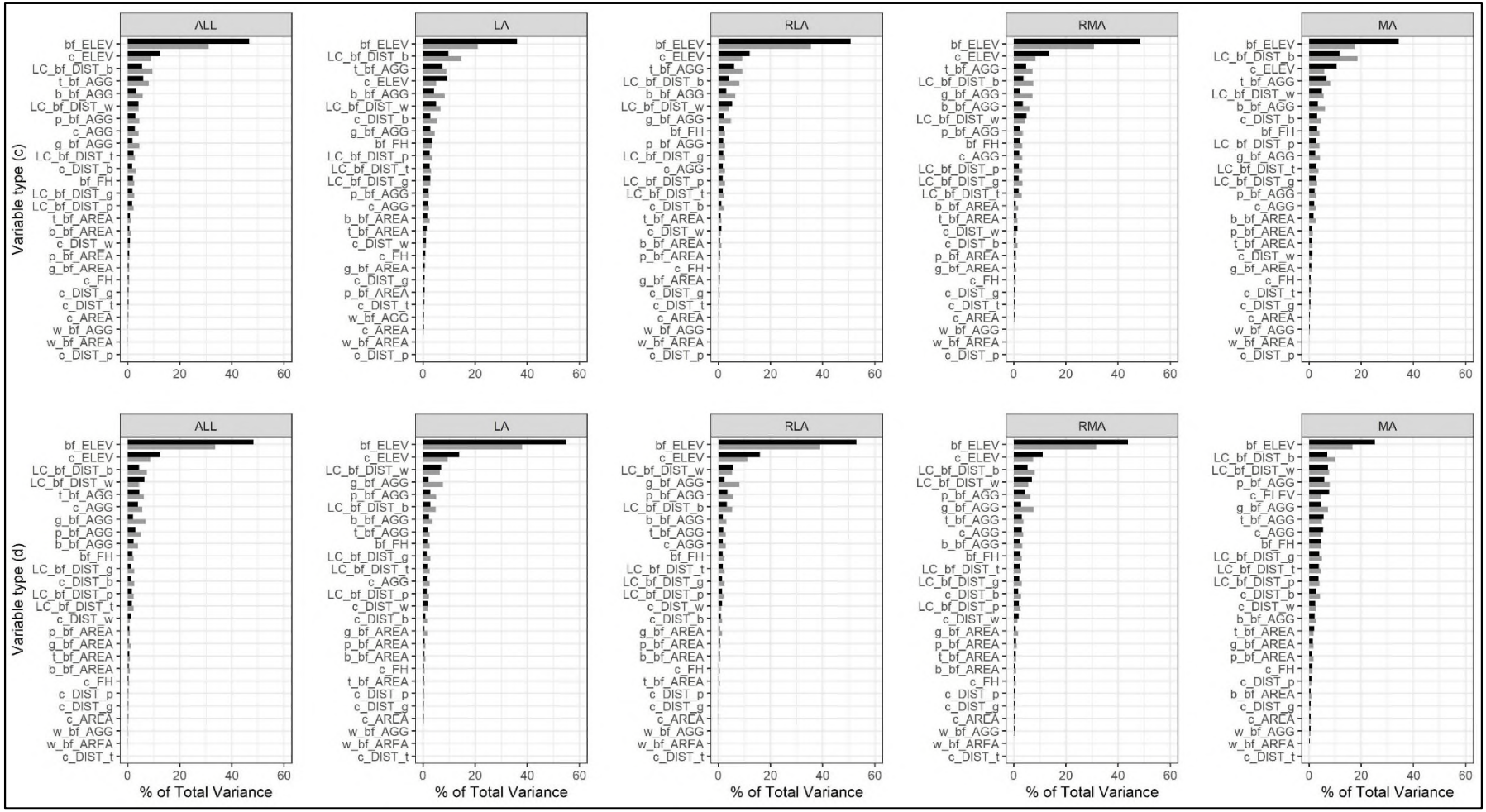

Figure_Apx C-2b Percentage of the total variance of LST in (c) paved and (d) trees explained by RF models attributed to the main LST predictor groups (Table 4-1, main text) in June and July at 2m spatial resolution. Predictors are sorted by the decreasing mean percentage of the total variance explained for the two dates.

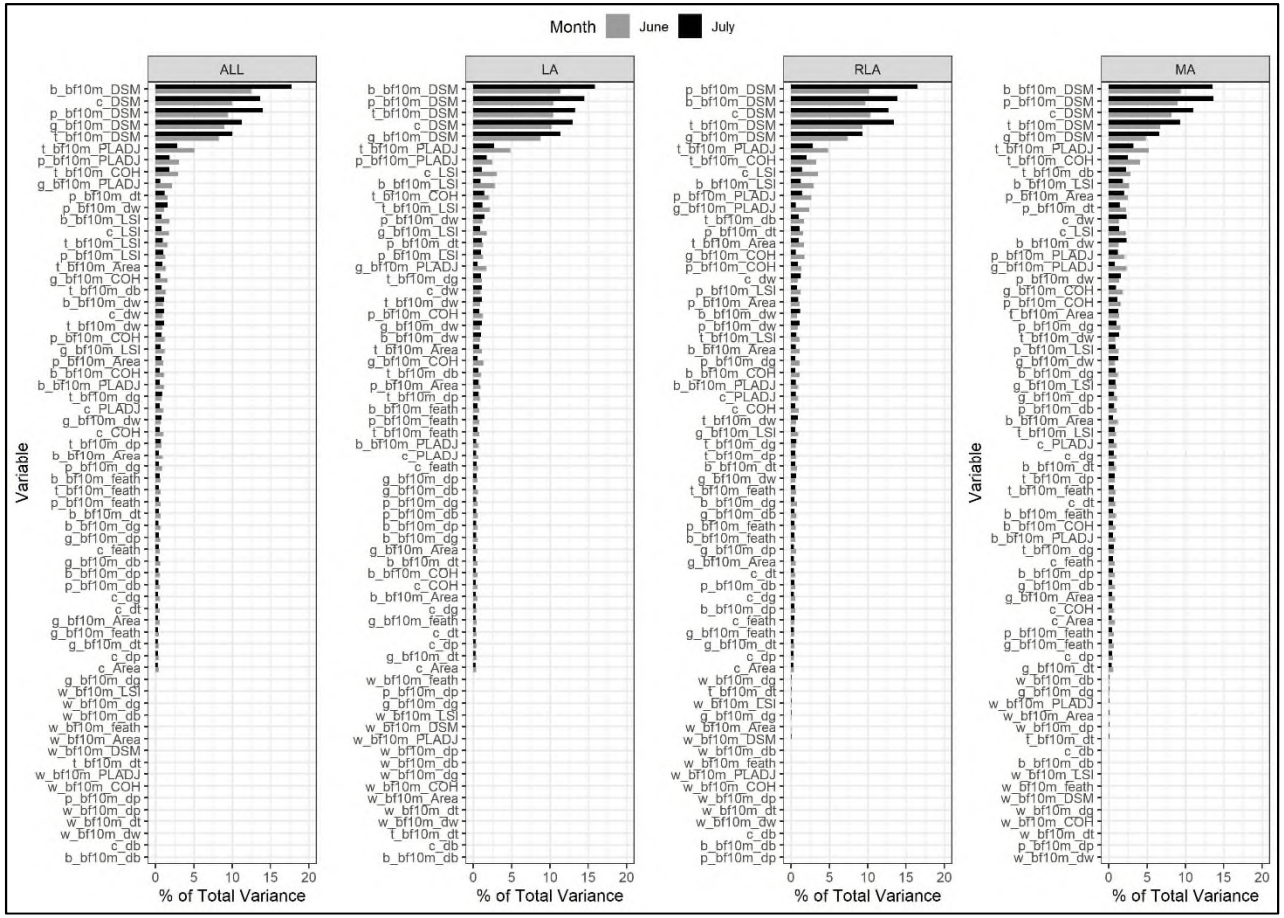

Figure_Apx C-3 Importance of spatial configuration descriptors of LST of three subtypes of buildings in June and July ordered by the decreasing variable importance in June expressed as the amount of variance in LST explained by the RF models. 'bf10m' indicates properties of LC types in the 10m buffer zone around the core ('c') patches, 'b' – buildings, 'g' – grass, 'p' – paved, 't' – trees, 'db, dg, dp, dt, dw' - distance to buildings, grass, paved, trees, water, DSM – elevation, COH – cohesion index, LSI – landscape shape index, PLADJ – percentage of like adjacencies index.

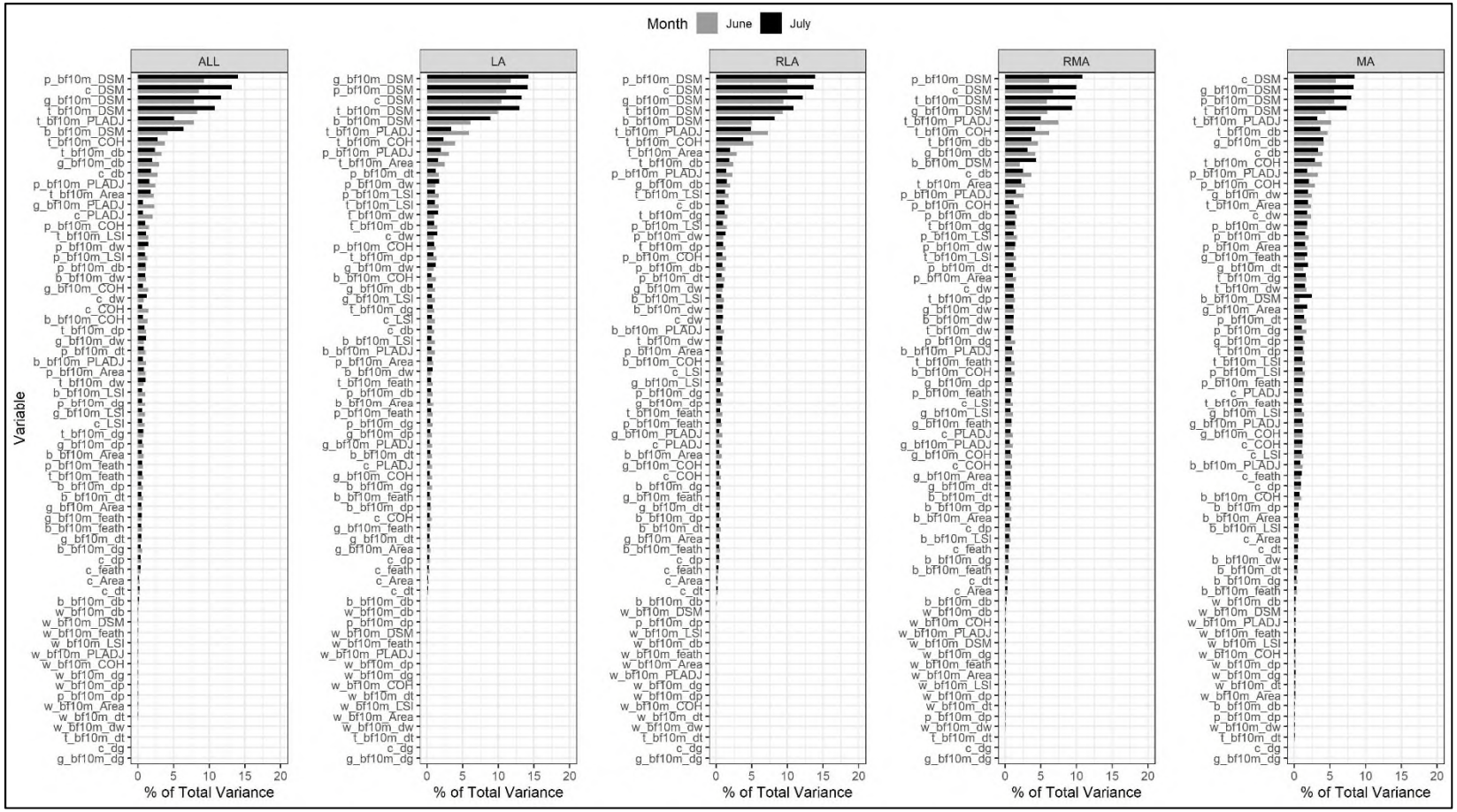

Figure_Apx C-4 Importance of spatial configuration descriptors of LST of four subtypes of grass in June and July ordered by the decreasing variable importance in June expressed as the amount of variance in LST explained by the RF models. 'bf10m' indicates properties of LC types in the 10m buffer zone around the core ('c') patches, 'b' – buildings, 'g' – grass, 'p' – paved, 't' – trees, 'db, dg, dp, dt, dw' - distance to buildings, grass, paved, trees, water, DSM – elevation, COH – cohesion index, LSI – landscape shape index, PLADJ – percentage of like adjacencies index.

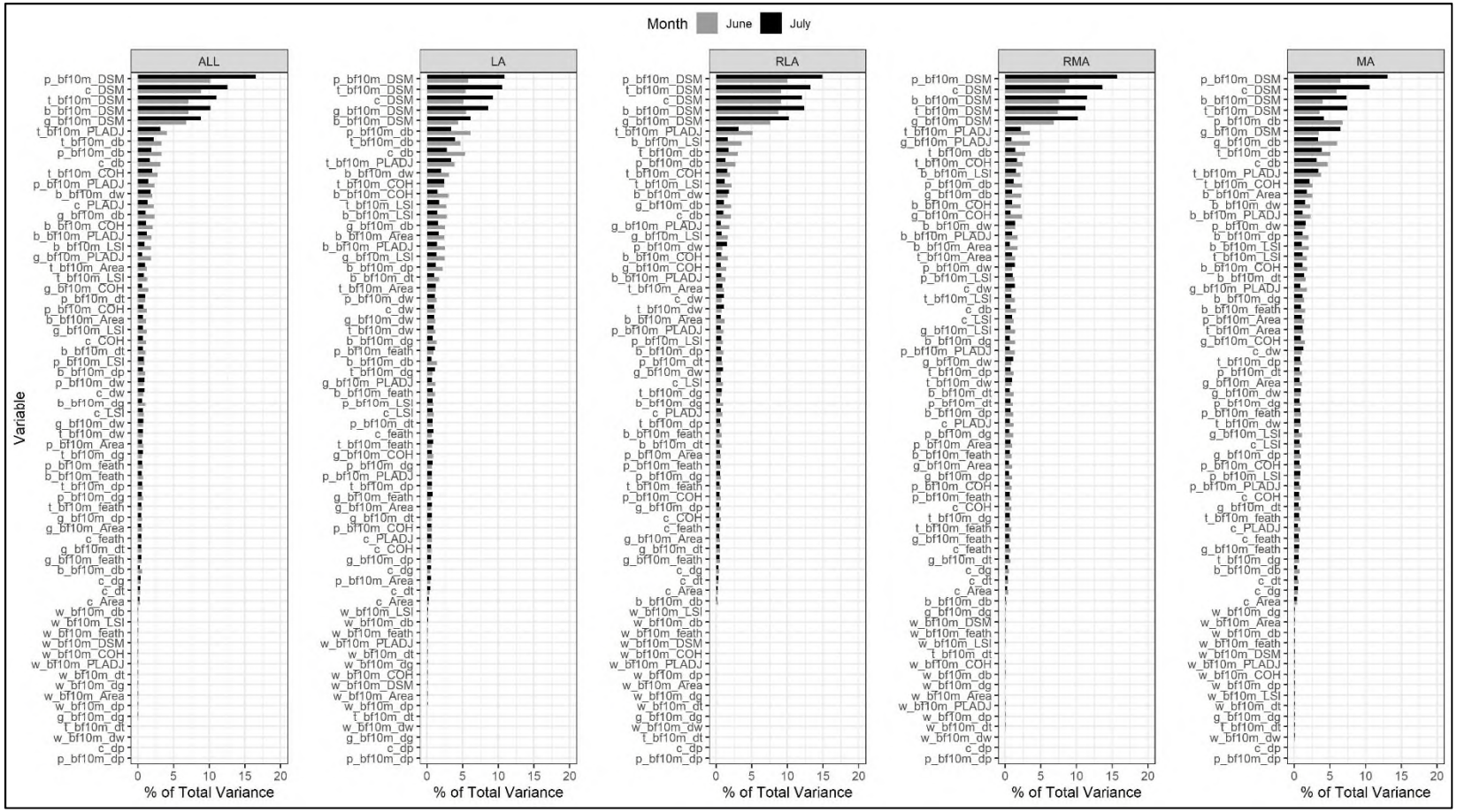

Figure_Apx C-5 Importance of spatial configuration descriptors of LST of four subtypes of paved in June and July ordered by the decreasing variable importance in June expressed as the amount of variance in LST explained by the RF models. 'bf10m' indicates properties of LC types in the 10m buffer zone around the core ('c') patches, 'b' – buildings, 'g' – grass, 'p' – paved, 't' – trees, 'db, dg, dp, dt, dw' - distance to buildings, grass, paved, trees, water, DSM – elevation, COH – cohesion index, LSI – landscape shape index, PLADJ – percentage of like adjacencies index.

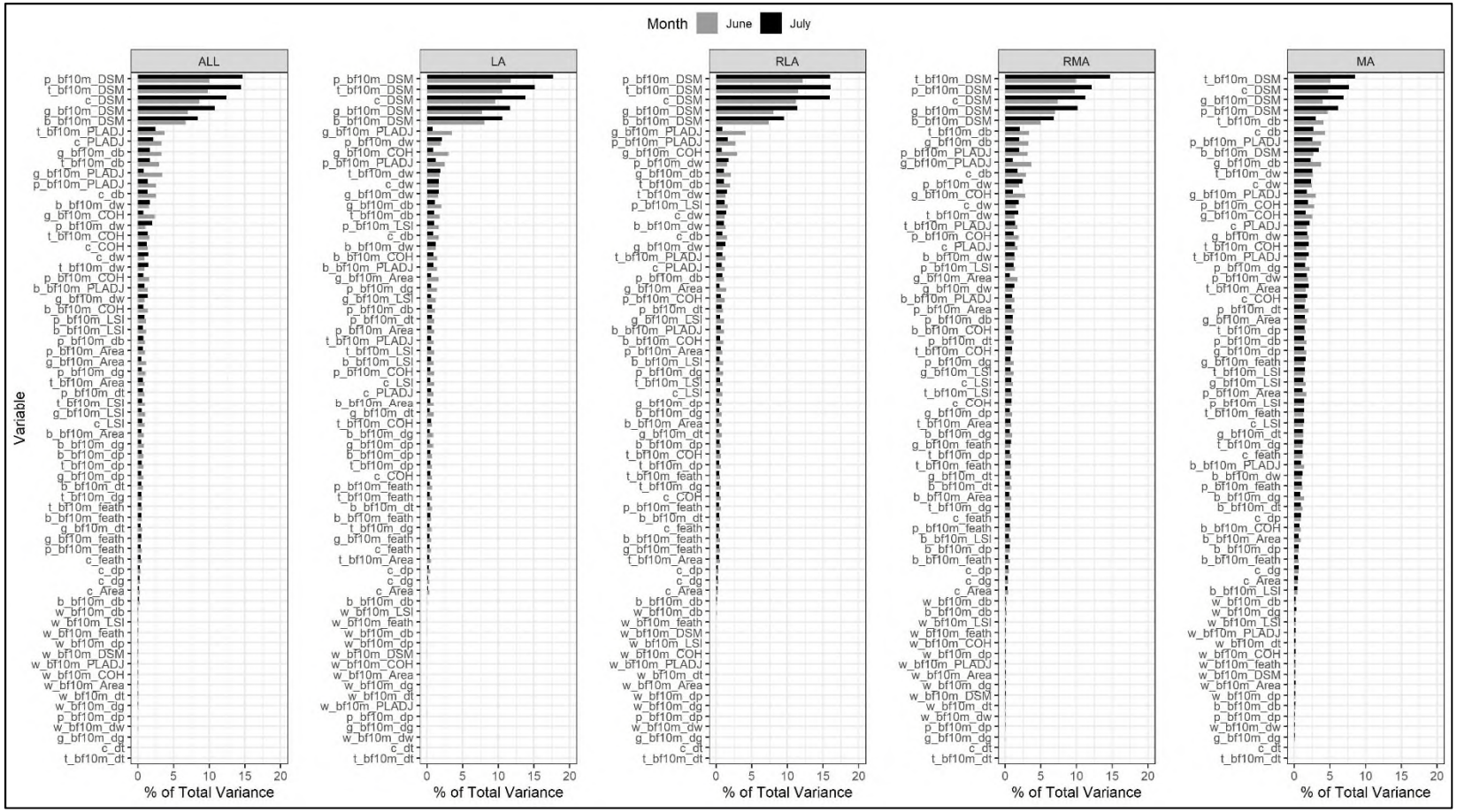

Figure_Apx C-6 Importance of spatial configuration descriptors of LST of four subtypes of trees in June and July ordered by the decreasing variable importance in June expressed as the amount of variance in LST explained by the RF models. 'bf10m' indicates properties of LC types in the 10m buffer zone around the core ('c') patches, 'b' – buildings, 'g' – grass, 'p' – paved, 't' – trees, 'db, dg, dp, dt, dw' - distance to buildings, grass, paved, trees, water, DSM – elevation, COH – cohesion index, LSI – landscape shape index, PLADJ – percentage of like adjacencies index.

Table_Apx C-2 Means and standard deviations (in brackets) of the selected most important descriptors of spatial configuration of urban form attributed to the coldest and hottest LC patches of different subtypes. (c) – core patch, (bf) – patches intersecting with the 10m buffer zone around (c). All means for C and H patches at a given date are statistically different at p<0.001.

Overall aggregation level of core LC			Least aggregated (LA)				Relatively less aggregated (RLA)				Relatively more aggregated (RMA)				Most aggregated (MA)			
DT	Descriptor	Core LC	June		July		June		July		June		July		June		July	
			C	H	C	H	C	H	C	H	C	H	C	H	C	H	C	H
Elevation	Elevation (c) [m]	Buildings	89 (22)	102 (51)	88 (19)	140 (20)	88 (21)	92 (51)	88 (18)	136 (21)	n/a	n/a	n/a	n/a	88 (21)	101 (47)	87 (18)	133 (16)
		Grass	85 (19)	107 (49)	84 (20)	134 (23)	83 (20)	101 (49)	82 (20)	130 (27)	81 (22)	94 (51)	81 (21)	122 (39)	81 (25)	101 (49)	82 (26)	125 (38)
		Paved	81 (18)	80 (51)	82 (18)	96 (53)	87 (21)	106 (51)	87 (19)	134 (29)	94 (53)	108 (48)	88 (24)	135 (23)	89 (25)	103 (48)	86 (21)	131 (21)
		Trees	87 (21)	135 (18)	88 (17)	137 (17)	88 (21)	136 (18)	87 (17)	138 (18)	85 (19)	132 (23)	85 (17)	136 (18)	85 (20)	120 (30)	85 (18)	132 (24)
Aggregation	PLADJ of trees (bf) [%]	Buildings	74 (7)	65 (7)	73 (7)	66 (6)	76 (7)	65 (8)	75 (7)	66 (8)	n/a	n/a	n/a	n/a	76 (9)	63 (10)	76 (8)	65 (10)
		Grass	77 (9)	65 (7)	76 (9)	67 (7)	81 (7)	66 (8)	80 (7)	67 (7)	83 (7)	68 (10)	82 (8)	69 (9)	82 (8)	69 (12)	81 (9)	70 (10)
		Paved	83 (7)	68 (8)	82 (7)	68 (7)	79 (7)	66 (7)	77 (8)	66 (7)	78 (12)	65 (8)	74 (10)	66 (8)	83 (9)	65 (12)	82 (11)	66 (12)
	COH of trees (bf) [%]	Buildings	92 (5)	86 (7)	92 (5)	87 (6)	92 (5)	84 (9)	91 (5)	85 (8)	n/a	n/a	n/a	n/a	90 (7)	79 (11)	90 (6)	81 (11)
		Grass	93 (5)	86 (7)	93 (5)	87 (7)	95 (4)	86 (7)	94 (4)	87 (7)	95 (4)	86 (9)	94 (5)	87 (8)	93 (5)	85 (12)	93 (7)	87 (9)
		Paved	94 (5)	88 (7)	95 (5)	88 (7)	93 (5)	87 (6)	92 (5)	87 (6)	91 (11)	84 (8)	90 (7)	85 (7)	93 (7)	82 (12)	93 (8)	82 (12)
	PLADJ of grass (bf) [%]	Trees	72 (16)	53 (12)	64 (17)	57 (13)	71 (15)	54 (10)	65 (16)	57 (11)	77 (13)	58 (12)	72 (14)	60 (13)	79 (11)	61 (15)	76 (12)	66 (16)
	COH of grass (bf) [%]	Trees	85 (13)	70 (13)	78 (16)	73 (12)	85 (12)	71 (10)	79 (14)	73 (11)	89 (10)	74 (11)	86 (12)	76 (12)	91 (8)	77 (14)	89 (9)	81 (13)
	PLADJ of paved (bf) [%]	Buildings	72 (5)	76 (5)	72 (5)	76 (4)	74 (6)	80 (5)	75 (7)	79 (5)	n/a	n/a	n/a	n/a	81 (7)	86 (5)	81 (6)	86 (4)
		Grass	72 (8)	78 (6)	72 (8)	77 (5)	74 (9)	78 (6)	74 (9)	77 (6)	73 (12)	78 (8)	73 (12)	78 (7)	67 (15)	81 (9)	68 (15)	80 (8)
		Trees	74 (9)	80 (6)	74 (7)	78 (6)	72 (8)	78 (5)	72 (7)	77 (5)	70 (12)	79 (6)	71 (11)	78 (6)	69 (15)	82 (8)	70 (15)	79 (9)
	LSI (c) [-]	Buildings	4.9 (1)	6.0 (0.8)	5.1 (1)	5.9 (0.7)	4 (0.9)	5.2 (1)	4.1 (1)	5.0 (0.9)	n/a	n/a	n/a	n/a	2.6 (0.6)	3.2 (0.9)	2.6 (0.6)	3.2 (0.9)
	LSI of buildings (bf) [-]	Buildings	5.0 (1)	6.0 (0.8)	5.1 (1)	5.9 (0.7)	4 (0.9)	5.3 (1)	4.2 (1)	5.1 (0.9)	n/a	n/a	n/a	n/a	2.5 (0.6)	3.3 (0.9)	2.5 (0.6)	3.2 (0.9)
		Paved	4.1 (1)	5.5 (1.1)	4.5 (1)	5.5 (1)	4.4 (1.1)	5.7 (0.9)	4.7 (1.1)	5.7 (0.9)	3.7 (1.2)	5.1 (1.3)	4.1 (1.4)	5.2 (1.1)	3.0 (1)	3.4 (1.2)	2.8 (1.2)	3.5 (1.1)
Distance	Distance to water (c) [m]	Buildings	257 (209)	483 (315)	252 (193)	569 (363)	274 (227)	457 (268)	276 (208)	565 (331)	n/a	n/a	n/a	n/a	279 (198)	455 (305)	276 (170)	527 (316)
		Grass	269 (202)	517 (316)	268 (197)	587 (336)	237 (195)	482 (319)	239 (197)	555 (360)	182 (190)	428 (326)	183 (193)	510 (369)	137 (176)	398 (334)	154 (199)	468 (370)
		Paved	118 (150)	410 (264)	135 (164)	443 (289)	235 (212)	506 (323)	245 (206)	571 (353)	326 (319)	498 (321)	278 (210)	567 (350)	176 (173)	443 (288)	188 (168)	516 (305)
		Trees	233 (199)	572 (315)	247 (190)	571 (329)	232 (212)	573 (351)	238 (200)	582 (371)	182 (203)	537 (353)	183 (183)	555 (369)	159 (184)	513 (400)	163 (180)	559 (426)
	Distance to buildings (c) [m]	Grass	19 (36)	8 (8)	18 (35)	8 (8)	34 (42)	10 (12)	33 (42)	9 (11)	70 (62)	18 (38)	69 (65)	15 (20)	98 (71)	42 (74)	97 (76)	32 (42)
		Paved	94 (73)	8 (23)	81 (74)	8 (22)	35 (50)	4 (8)	27 (46)	5 (10)	34 (32)	5 (10)	33 (77)	5 (12)	99 (77)	10 (21)	98 (94)	10 (19)
		Trees	47 (75)	8 (16)	40 (84)	8 (15)	37 (56)	7 (12)	29 (53)	7 (11)	65 (66)	11 (18)	55 (64)	11 (15)	88 (63)	25 (37)	81 (61)	29 (35)
	Distance of trees (bf) to buildings [m]	Grass	19 (31)	7 (7)	18 (30)	7 (7)	34 (39)	9 (10)	33 (40)	9 (9)	67 (58)	16 (31)	67 (61)	14 (15)	90 (65)	33 (61)	90 (69)	27 (37)
		Paved	90 (69)	9 (17)	79 (69)	8 (13)	35 (47)	6 (4)	27 (42)	6 (5)	34 (32)	6 (9)	29 (59)	7 (9)	91 (69)	11 (16)	89 (76)	12 (18)
		Trees	47 (75)	8 (16)	40 (84)	8 (15)	37 (56)	7 (11)	30 (52)	8 (11)	65 (64)	12 (18)	55 (62)	12 (14)	86 (60)	28 (35)	80 (58)	30 (32)
	Distance of grass (bf) to buildings [m]	Grass	19 (36)	8 (7)	18 (35)	8 (7)	34 (41)	10 (11)	33 (42)	9 (10)	70 (61)	18 (37)	69 (65)	16 (19)	97 (69)	44 (73)	96 (72)	33 (41)
		Paved	91 (69)	10 (20)	78 (70)	10 (20)	37 (49)	7 (8)	28 (45)	7 (9)	36 (31)	7 (8)	36 (77)	8 (10)	100 (76)	14 (23)	102 (97)	15 (23)
		Trees	47 (68)	9 (15)	40 (79)	9 (14)	38 (54)	8 (11)	30 (51)	8 (10)	65 (63)	12 (17)	55 (62)	12 (14)	85 (59)	28 (41)	79 (58)	29 (33)

Table_Apx C-3 Ordinary kriging results for LST in the three towns at 2m and 100m resolution observed on 6th June and 8th July 2013. Major range is indicative of spatial auto-correlation distance of LST values.

Dataset	**BD**	**LT JUN 100m**	**MK**	**BD**	**LT JUL 100m**	**MK**	**BD**	**LT JUN 2m**	**MK**	**BD**	**LT JUL 2m**	**MK**
Function	Exp	Exp	Exp	Exp	Exp	Exp	Exp	Exp	Exp	Exp	Exp	Exp
Major range [m]	1100	1000	1100	900	1050	1100	300	520	400	250	450	350
Nugget	0	0	0	0	0	0	0.1	0	0.08	0.5	0	0.11
Partial sill	4.7	4.34	6.6	2.7	3.6	4.85	3.25	3.2	3.7	1.5	2.54	2.3
Lag	100	100	100	100	100	100	10	10	10	10	10	10
No of Lags	30	30	30	30	30	30	100	100	100	100	100	100
RMSE	0.07	0.07	0.08	0.06	0.06	0.07	0.34	0.23	0.42	0.52	0.19	0.41

(a)

c_dsm_mn		LA				RLA				MA		
		C	M-C	M-H	H	C	M-C	M-H	H	C	M-C	M-H
LA	M-C	**	NA	NA	NA	NA	NA	NA	NA	NA	NA	NA
	M-H	***	***	NA	NA	NA	NA	NA	NA	NA	NA	NA
	H	***	***	***	NA	NA	NA	NA	NA	NA	NA	NA
RLA	C	ns	*	***	***	NA	NA	NA	NA	NA	NA	NA
	M-C	ns	ns	***	***	ns	NA	NA	NA	NA	NA	NA
	M-H	***	***	***	ns	***	***	NA	NA	NA	NA	NA
	H	***	**	***	***	**	ns	***	NA	NA	NA	NA
MA	C	ns	ns	***	***	ns	ns	***	ns	NA	NA	NA
	M-C	ns	ns	***	***	ns	ns	***	ns	ns	NA	NA
	M-H	***	**	**	ns	**	*	ns	ns	*	**	NA
	H	***	***	**	ns	***	***	ns	ns	***	***	ns

(b)

c_dsm_mn		LA				RLA				MA		
		C	M-C	M-H	H	C	M-C	M-H	H	C	M-C	M-H
LA	M-C	***	NA	NA	NA	NA	NA	NA	NA	NA	NA	NA
	M-H	***	***	NA	NA	NA	NA	NA	NA	NA	NA	NA
	H	***	***	***	NA	NA	NA	NA	NA	NA	NA	NA
RLA	C	ns	*	***	***	NA	NA	NA	NA	NA	NA	NA
	M-C	***	***	***	***	***	NA	NA	NA	NA	NA	NA
	M-H	***	***	***	***	***	***	NA	NA	NA	NA	NA
	H	***	***	***	***	***	***	***	NA	NA	NA	NA
MA	C	ns	ns	***	***	ns	*	***	***	NA	NA	NA
	M-C	***	*	**	***	***	ns	***	***	ns	NA	NA
	M-H	**	*	ns	***	**	ns	ns	***	ns	ns	NA
	H	***	***	***	***	***	***	***	**	***	***	***

(c)

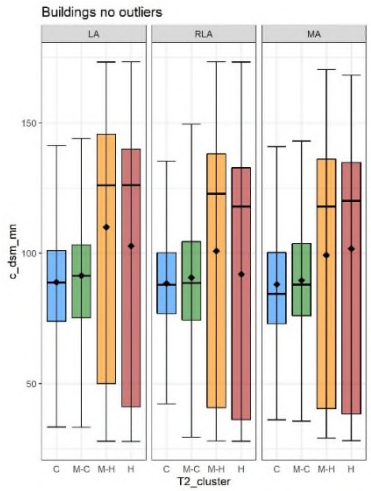

(d)

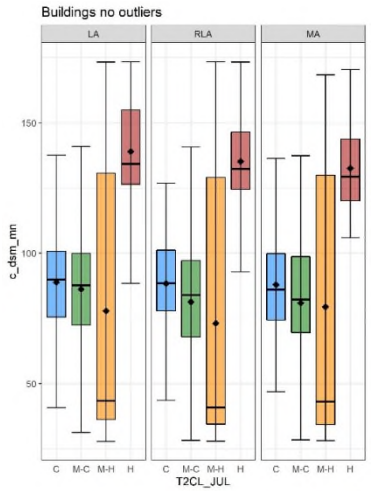

Figure_Apx C-7 Results of the ANOVA (a, b) and boxplots (c, d) for elevation (dsm) of the core patches of buildings in June (a, c) and July (b, d). Boxplots represent elevation values associated with the coldest (C), medium-cold (M-C), medium-hot (M-H) and the hottest (H) Tier 2 clusters within each Tier 1 cluster: LA – Least aggregated, RLA – Relatively less aggregated, MA – Most aggregated.

(a)

c_dsm_mn		LA				RLA				RMA				MA		
		C	M-C	M-H	H	C	M-C	M-H	H	C	M-C	M-H	H	C	M-C	M-H
LA	M-C	ns	NA	NA	NA	NA	NA	NA	NA	NA	NA	NA	NA	NA	NA	NA
	M-H	***	***	NA	NA	NA	NA	NA	NA	NA	NA	NA	NA	NA	NA	NA
	H	***	***	***	NA	NA	NA	NA	NA	NA	NA	NA	NA	NA	NA	NA
RLA	C	***	***	***	***	NA	NA	NA	NA	NA	NA	NA	NA	NA	NA	NA
	M-C	***	***	***	***	ns	NA	NA	NA	NA	NA	NA	NA	NA	NA	NA
	M-H	***	***	***	***	***	***	NA	NA	NA	NA	NA	NA	NA	NA	NA
	H	***	***	***	***	***	***	***	NA	NA	NA	NA	NA	NA	NA	NA
RMA	C	***	***	***	***	***	***	***	***	NA	NA	NA	NA	NA	NA	NA
	M-C	***	**	***	***	ns	**	***	***	***	NA	NA	NA	NA	NA	NA
	M-H	*	***	***	***	***	***	***	***	***	***	NA	NA	NA	NA	NA
	H	***	***	**	***	***	***	*	***	***	***	***	NA	NA	NA	NA
MA	C	***	***	***	***	***	**	***	***	ns	***	***	***	NA	NA	NA
	M-C	***	**	***	***	ns	ns	***	***	ns	ns	**	***	ns	NA	NA
	M-H	***	***	***	***	***	***	ns	***	***	***	ns	*	***	***	NA
	H	***	***	ns	*	***	***	***	ns	***	***	***	**	***	***	***

(b)

c_dsm_mn		LA				RLA				RMA				MA		
		C	M-C	M-H	H	C	M-C	M-H	H	C	M-C	M-H	H	C	M-C	M-H
LA	M-C	***	NA	NA	NA	NA	NA	NA	NA	NA	NA	NA	NA	NA	NA	NA
	M-H	***	***	NA	NA	NA	NA	NA	NA	NA	NA	NA	NA	NA	NA	NA
	H	***	***	***	NA	NA	NA	NA	NA	NA	NA	NA	NA	NA	NA	NA
RLA	C	***	***	***	***	NA	NA	NA	NA	NA	NA	NA	NA	NA	NA	NA
	M-C	***	***	***	***	***	NA	NA	NA	NA	NA	NA	NA	NA	NA	NA
	M-H	***	***	*	***	***	***	NA	NA	NA	NA	NA	NA	NA	NA	NA
	H	***	***	***	***	***	***	***	NA	NA	NA	NA	NA	NA	NA	NA
RMA	C	***	ns	***	***	***	***	***	***	NA	NA	NA	NA	NA	NA	NA
	M-C	***	***	***	***	*	***	***	***	*	NA	NA	NA	NA	NA	NA
	M-H	***	***	ns	***	***	***	***	***	***	***	NA	NA	NA	NA	NA
	H	***	***	***	***	***	***	***	***	***	***	***	NA	NA	NA	NA
MA	C	***	ns	***	***	ns	***	***	***	ns	ns	***	***	NA	NA	NA
	M-C	***	ns	***	***	***	*	***	***	ns	*	***	***	ns	NA	NA
	M-H	***	ns	***	***	**	ns	***	***	*	*	***	***	ns	ns	NA
	H	***	***	***	**	***	***	***	ns	***	***	***	ns	***	***	***

(c)

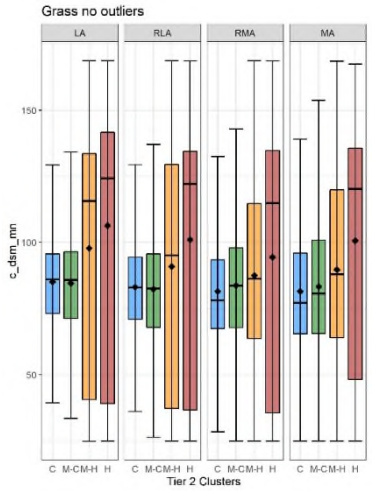

(d)

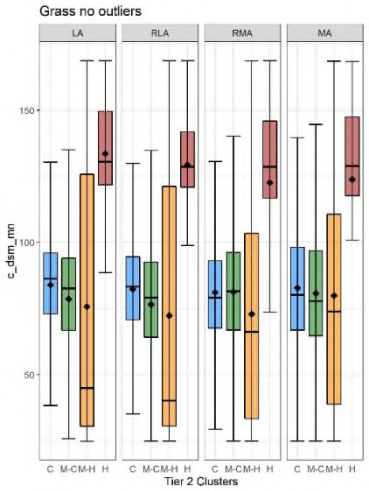

Figure_Apx C-8 Results of the ANOVA (a, b) and boxplots (c, d) for elevation (dsm) of the core patches of grass in June (a, c) and July (b, d). Boxplots represent elevation values associated with the coldest (C), medium-cold (M-C), medium-hot (M-H) and the hottest (H) Tier 2 clusters within each Tier 1 cluster: LA – Least aggregated, RLA – Relatively less aggregated, RMA – Relatively more aggregated, MA – Most aggregated.

(a) (b)

c_dsm_mn		LA				RLA				RMA				MA		
		C	M-C	M-H	H	C	M-C	M-H	H	C	M-C	M-H	H	C	M-C	M-H
LA	M-C	ns	NA	NA	NA	NA	NA	NA	NA	NA	NA	NA	NA	NA	NA	NA
	M-H	***	***	NA	NA	NA	NA	NA	NA	NA	NA	NA	NA	NA	NA	NA
	H	***	***	ns	NA	NA	NA	NA	NA	NA	NA	NA	NA	NA	NA	NA
RLA	C	***	***	***	***	NA	NA	NA	NA	NA	NA	NA	NA	NA	NA	NA
	M-C	***	***	***	***	***	NA	NA	NA	NA	NA	NA	NA	NA	NA	NA
	M-H	***	***	***	***	***	***	NA	NA	NA	NA	NA	NA	NA	NA	NA
	H	***	***	***	***	***	***	***	NA	NA	NA	NA	NA	NA	NA	NA
RMA	C	**	**	***	ns	*	*	ns	**	NA	NA	NA	NA	NA	NA	NA
	M-C	***	***	***	***	***	ns	***	***	ns	NA	NA	NA	NA	NA	NA
	M-H	***	***	***	***	***	***	***	***	*	***	NA	NA	NA	NA	NA
	H	***	***	***	***	***	***	***	ns	**	***	***	NA	NA	NA	NA
MA	C	***	***	***	***	ns	ns	*	***	ns	ns	***	***	NA	NA	NA
	M-C	**	*	***	***	**	***	***	***	*	***	***	***	*	NA	NA
	M-H	***	***	***	***	ns	ns	**	***	ns	ns	***	***	ns	**	NA
	H	***	***	***	***	***	***	***	***	ns	***	ns	**	***	***	***

c_dsm_mn		LA				RLA				RMA				MA		
		C	M-C	M-H	H	C	M-C	M-H	H	C	M-C	M-H	H	C	M-C	M-H
LA	M-C	ns	NA	NA	NA	NA	NA	NA	NA	NA	NA	NA	NA	NA	NA	NA
	M-H	***	***	NA	NA	NA	NA	NA	NA	NA	NA	NA	NA	NA	NA	NA
	H	***	***	***	NA	NA	NA	NA	NA	NA	NA	NA	NA	NA	NA	NA
RLA	C	***	***	***	***	NA	NA	NA	NA	NA	NA	NA	NA	NA	NA	NA
	M-C	***	***	***	***	***	NA	NA	NA	NA	NA	NA	NA	NA	NA	NA
	M-H	***	***	***	***	***	***	NA	NA	NA	NA	NA	NA	NA	NA	NA
	H	***	***	***	***	***	***	***	NA	NA	NA	NA	NA	NA	NA	NA
RMA	C	***	***	***	***	ns	***	***	***	NA	NA	NA	NA	NA	NA	NA
	M-C	ns	*	***	***	***	***	***	***	***	NA	NA	NA	NA	NA	NA
	M-H	*	*	***	***	***	***	***	***	*	ns	NA	NA	NA	NA	NA
	H	***	***	***	***	***	***	***	**	***	***	***	NA	NA	NA	NA
MA	C	**	**	***	***	ns	ns	***	***	*	*	*	***	NA	NA	NA
	M-C	ns	ns	***	***	***	***	***	***	***	ns	ns	***	**	NA	NA
	M-H	***	***	*	***	***	***	ns	***	***	***	***	***	***	***	NA
	H	***	***	***	***	***	***	***	***	***	***	***	***	***	***	***

(c)

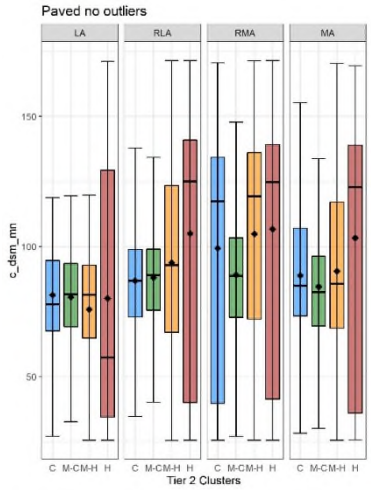

(d)

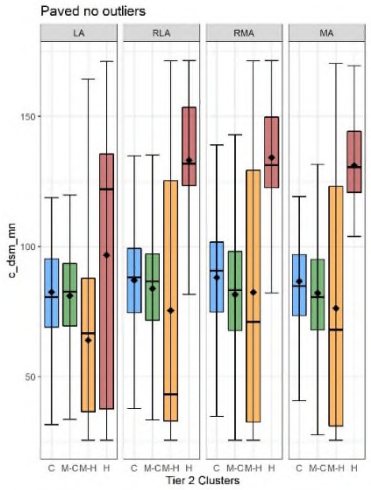

Figure_Apx C-9 Results of the ANOVA (a, b) and boxplots (c, d) for elevation (dsm) of the core patches of paved in June (a, c) and July (b, d). Boxplots represent elevation values associated with the coldest (C), medium-cold (M-C), medium-hot (M-H) and the hottest (H) Tier 2 clusters within each Tier 1 cluster: LA – Least aggregated, RLA – Relatively less aggregated, RMA – Relatively more aggregated, MA – Most aggregated.

(a)

c_dsm_mn		LA				RLA				RMA				MA		
		C	M-C	M-H	H	C	M-C	M-H	H	C	M-C	M-H	H	C	M-C	M-H
LA	M-C	***	NA	NA	NA	NA	NA	NA	NA	NA	NA	NA	NA	NA	NA	NA
	M-H	***	***	NA	NA	NA	NA	NA	NA	NA	NA	NA	NA	NA	NA	NA
	H	***	***	***	NA	NA	NA	NA	NA	NA	NA	NA	NA	NA	NA	NA
RLA	C	ns	***	***	***	NA	NA	NA	NA	NA	NA	NA	NA	NA	NA	NA
	M-C	***	***	***	***	***	NA	NA	NA	NA	NA	NA	NA	NA	NA	NA
	M-H	***	***	**	***	***	***	NA	NA	NA	NA	NA	NA	NA	NA	NA
	H	***	***	***	*	***	***	***	NA	NA	NA	NA	NA	NA	NA	NA
RMA	C	*	***	***	***	***	***	***	***	NA	NA	NA	NA	NA	NA	NA
	M-C	*	***	***	***	ns	***	***	***	***	NA	NA	NA	NA	NA	NA
	M-H	***	***	***	***	***	***	***	***	***	***	NA	NA	NA	NA	NA
	H	***	***	***	***	***	***	***	***	***	***	***	NA	NA	NA	NA
MA	C	ns	***	***	***	***	***	***	***	ns	***	***	***	NA	NA	NA
	M-C	**	*	***	***	*	ns	***	***	***	ns	***	***	***	NA	NA
	M-H	***	***	***	***	***	***	***	***	***	***	**	***	***	***	NA
	H	***	***	*	***	***	***	ns	***	***	***	***	***	***	***	***

(b)

c_dsm_mn		LA				RLA				RMA				MA		
		C	M-C	M-H	H	C	M-C	M-H	H	C	M-C	M-H	H	C	M-C	M-H
LA	M-C	***	NA	NA	NA	NA	NA	NA	NA	NA	NA	NA	NA	NA	NA	NA
	M-H	***	***	NA	NA	NA	NA	NA	NA	NA	NA	NA	NA	NA	NA	NA
	H	***	***	***	NA	NA	NA	NA	NA	NA	NA	NA	NA	NA	NA	NA
RLA	C	***	*	***	***	NA	NA	NA	NA	NA	NA	NA	NA	NA	NA	NA
	M-C	***	ns	***	***	***	NA	NA	NA	NA	NA	NA	NA	NA	NA	NA
	M-H	***	***	***	***	***	***	NA	NA	NA	NA	NA	NA	NA	NA	NA
	H	***	***	***	ns	***	***	***	NA	NA	NA	NA	NA	NA	NA	NA
RMA	C	***	***	***	***	***	***	***	***	NA	NA	NA	NA	NA	NA	NA
	M-C	***	ns	***	***	***	ns	***	***	***	NA	NA	NA	NA	NA	NA
	M-H	***	***	***	***	***	***	***	***	***	***	NA	NA	NA	NA	NA
	H	***	***	***	ns	***	***	***	***	***	***	***	NA	NA	NA	NA
MA	C	***	ns	***	***	**	ns	***	***	ns	ns	***	***	NA	NA	NA
	M-C	*	ns	***	***	ns	ns	***	***	***	ns	***	***	*	NA	NA
	M-H	***	***	***	***	***	***	***	***	***	***	***	***	***	***	NA
	H	***	***	***	ns	***	***	***	*	***	***	***	ns	***	***	***

(c)

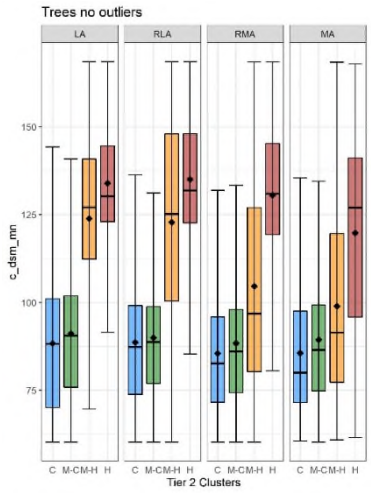

(d)

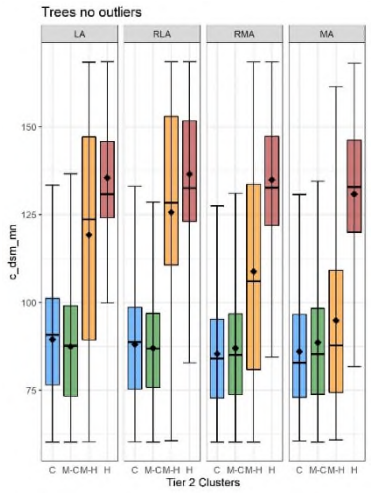

Figure_Apx C-10 Results of the ANOVA (a, b) and boxplots (c, d) for elevation (dsm) of the core patches of trees in June (a, c) and July (b, d). Boxplots represent elevation values associated with the coldest (C), medium-cold (M-C), medium-hot (M-H) and the hottest (H) Tier 2 clusters within each Tier 1 cluster: LA – Least aggregated, RLA – Relatively less aggregated, RMA – Relatively more aggregated, MA – Most aggregated.

(a)

t_bf10m_PLADJ		LA				RLA				MA		
		C	M-C	M-H	H	C	M-C	M-H	H	C	M-C	M-H
LA	M-C	***	NA	NA	NA	NA	NA	NA	NA	NA	NA	NA
	M-H	***	***	NA	NA	NA	NA	NA	NA	NA	NA	NA
	H	***	***	***	NA	NA	NA	NA	NA	NA	NA	NA
RLA	C	***	***	***	***	NA	NA	NA	NA	NA	NA	NA
	M-C	***	***	ns	***	***	NA	NA	NA	NA	NA	NA
	M-H	***	***	*	***	***	ns	NA	NA	NA	NA	NA
	H	***	***	***	ns	***	***	***	NA	NA	NA	NA
MA	C	***	***	***	***	ns	***	***	***	NA	NA	NA
	M-C	***	***	*	***	***	ns	ns	***	***	NA	NA
	M-H	***	**	ns	***	***	ns	ns	***	***	ns	NA
	H	***	***	***	ns	***	***	***	ns	***	***	***

(b)

t_bf10m_PLADJ		LA				RLA				MA		
		C	M-C	M-H	H	C	M-C	M-H	H	C	M-C	M-H
LA	M-C	***	NA	NA	NA	NA	NA	NA	NA	NA	NA	NA
	M-H	***	***	NA	NA	NA	NA	NA	NA	NA	NA	NA
	H	***	ns	***	NA	NA	NA	NA	NA	NA	NA	NA
RLA	C	***	***	***	***	NA	NA	NA	NA	NA	NA	NA
	M-C	***	**	***	***	***	NA	NA	NA	NA	NA	NA
	M-H	***	***	***	***	***	***	NA	NA	NA	NA	NA
	H	***	ns	***	ns	***	**	***	NA	NA	NA	NA
MA	C	***	***	***	***	*	***	***	***	NA	NA	NA
	M-C	***	***	ns	***	***	ns	ns	***	***	NA	NA
	M-H	***	*	ns	**	***	ns	ns	**	***	ns	NA
	H	***	ns	***	ns	***	*	***	ns	***	**	*

(c)

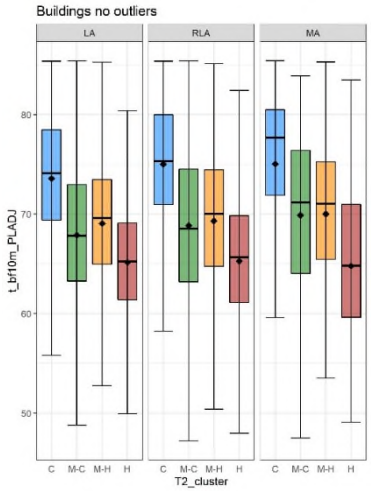

(d)

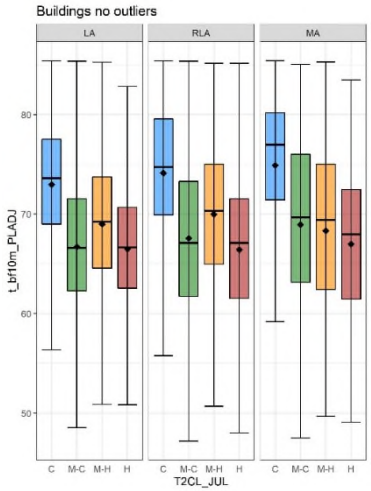

Figure_Apx C-11 Results of the ANOVA (a, b) and boxplots (c, d) for PLADJ of trees located in the neighbourhood to core building patches in June (a, c) and July (b, d). Boxplots represent elevation values associated with the coldest (C), medium-cold (M-C), medium-hot (M-H) and the hottest (H) Tier 2 clusters within each Tier 1 cluster: LA – Least aggregated, RLA – Relatively less aggregated, MA – Most aggregated.

(a)

t_bf10m_PLADJ		LA				RLA				RMA				MA		
		C	M-C	M-H	H	C	M-C	M-H	H	C	M-C	M-H	H	C	M-C	M-H
LA	M-C	***	NA	NA	NA	NA	NA	NA	NA	NA	NA	NA	NA	NA	NA	NA
	M-H	***	***	NA	NA	NA	NA	NA	NA	NA	NA	NA	NA	NA	NA	NA
	H	***	***	***	NA	NA	NA	NA	NA	NA	NA	NA	NA	NA	NA	NA
RLA	C	***	***	***	***	NA	NA	NA	NA	NA	NA	NA	NA	NA	NA	NA
	M-C	***	***	***	***	***	NA	NA	NA	NA	NA	NA	NA	NA	NA	NA
	M-H	***	***	***	***	***	***	NA	NA	NA	NA	NA	NA	NA	NA	NA
	H	***	***	***	***	***	***	***	NA	NA	NA	NA	NA	NA	NA	NA
RMA	C	***	***	***	***	***	***	***	***	NA	NA	NA	NA	NA	NA	NA
	M-C	***	***	***	***	***	***	***	***	***	NA	NA	NA	NA	NA	NA
	M-H	***	***	***	***	***	***	***	***	***	***	NA	NA	NA	NA	NA
	H	***	*	ns	***	***	***	***	***	***	***	***	NA	NA	NA	NA
MA	C	***	***	***	***	**	***	***	***	*	***	***	***	NA	NA	NA
	M-C	***	***	***	***	***	***	***	***	***	**	***	***	***	NA	NA
	M-H	*	***	***	***	***	***	***	***	***	***	***	***	***	***	NA
	H	***	***	**	***	***	***	ns	***	***	***	***	*	***	***	***

(b)

t_bf10m_PLADJ		LA				RLA				RMA				MA		
		C	M-C	M-H	H	C	M-C	M-H	H	C	M-C	M-H	H	C	M-C	M-H
LA	M-C	***	NA	NA	NA	NA	NA	NA	NA	NA	NA	NA	NA	NA	NA	NA
	M-H	***	***	NA	NA	NA	NA	NA	NA	NA	NA	NA	NA	NA	NA	NA
	H	***	***	***	NA	NA	NA	NA	NA	NA	NA	NA	NA	NA	NA	NA
RLA	C	***	***	***	***	NA	NA	NA	NA	NA	NA	NA	NA	NA	NA	NA
	M-C	***	***	***	***	***	NA	NA	NA	NA	NA	NA	NA	NA	NA	NA
	M-H	***	***	***	***	***	***	NA	NA	NA	NA	NA	NA	NA	NA	NA
	H	***	ns	***	***	***	***	***	NA	NA	NA	NA	NA	NA	NA	NA
RMA	C	***	***	***	***	***	***	***	***	NA	NA	NA	NA	NA	NA	NA
	M-C	***	***	***	***	***	***	***	***	***	NA	NA	NA	NA	NA	NA
	M-H	***	***	***	***	***	*	***	***	***	***	NA	NA	NA	NA	NA
	H	***	***	*	***	***	***	***	***	***	***	***	NA	NA	NA	NA
MA	C	***	***	***	***	***	***	***	***	*	***	***	***	NA	NA	NA
	M-C	***	***	***	***	***	***	***	***	***	***	***	***	***	NA	NA
	M-H	ns	***	***	***	***	***	***	***	***	***	***	***	***	***	NA
	H	***	***	***	***	***	*	**	***	***	***	ns	***	***	***	***

(c)

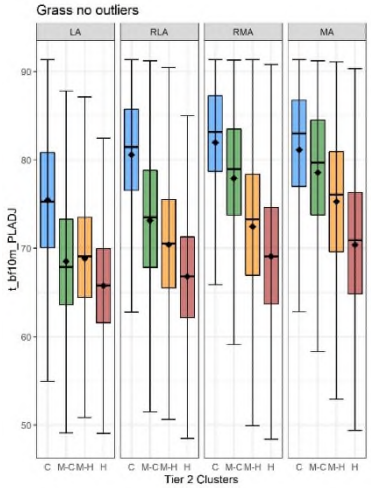

(d)

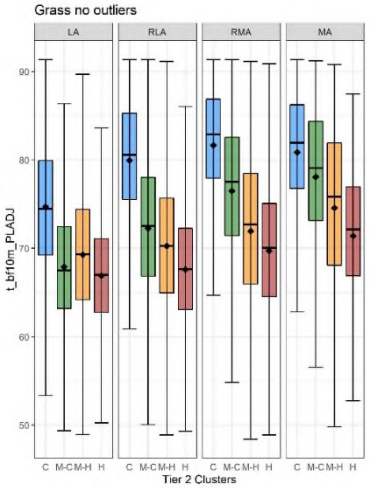

Figure_Apx C-12 Results of the ANOVA (a, b) and boxplots (c, d) for PLADJ of trees located in the neighbourhood to core grass patches in June (a, c) and July (b, d). Boxplots represent elevation values associated with the coldest (C), medium-cold (M-C), medium-hot (M-H) and the hottest (H) Tier 2 clusters within each Tier 1 cluster: LA – Least aggregated, RLA – Relatively less aggregated, RMA – Relatively more aggregated, MA – Most aggregated.

(a)

t_bf10m_PLADJ		LA				RLA				RMA				MA		
		C	M-C	M-H	H	C	M-C	M-H	H	C	M-C	M-H	H	C	M-C	M-H
LA	M-C	***	NA	NA	NA	NA	NA	NA	NA	NA	NA	NA	NA	NA	NA	NA
	M-H	***	***	NA	NA	NA	NA	NA	NA	NA	NA	NA	NA	NA	NA	NA
	H	***	***	***	NA	NA	NA	NA	NA	NA	NA	NA	NA	NA	NA	NA
RLA	C	***	***	***	***	NA	NA	NA	NA	NA	NA	NA	NA	NA	NA	NA
	M-C	***	***	***	***	***	NA	NA	NA	NA	NA	NA	NA	NA	NA	NA
	M-H	***	***	***	ns	***	***	NA	NA	NA	NA	NA	NA	NA	NA	NA
	H	***	***	***	***	***	***	***	NA	NA	NA	NA	NA	NA	NA	NA
RMA	C	**	**	***	***	ns	***	***	***	NA	NA	NA	NA	NA	NA	NA
	M-C	***	***	*	***	***	***	***	***	***	NA	NA	NA	NA	NA	NA
	M-H	***	***	***	***	***	***	***	***	***	***	NA	NA	NA	NA	NA
	H	***	***	***	***	***	***	***	***	***	***	***	NA	NA	NA	NA
MA	C	*	***	***	***	***	***	***	***	***	***	***	***	NA	NA	NA
	M-C	***	ns	***	***	**	***	***	***	*	***	***	***	***	NA	NA
	M-H	***	***	ns	***	***	**	***	***	***	ns	***	***	***	***	NA
	H	***	***	***	***	***	***	***	ns	***	***	***	**	***	***	***

(b)

t_bf10m_PLADJ		LA				RLA				RMA				MA		
		C	M-C	M-H	H	C	M-C	M-H	H	C	M-C	M-H	H	C	M-C	M-H
LA	M-C	***	NA	NA	NA	NA	NA	NA	NA	NA	NA	NA	NA	NA	NA	NA
	M-H	***	***	NA	NA	NA	NA	NA	NA	NA	NA	NA	NA	NA	NA	NA
	H	***	***	***	NA	NA	NA	NA	NA	NA	NA	NA	NA	NA	NA	NA
RLA	C	***	***	***	***	NA	NA	NA	NA	NA	NA	NA	NA	NA	NA	NA
	M-C	***	***	***	*	***	NA	NA	NA	NA	NA	NA	NA	NA	NA	NA
	M-H	***	***	***	ns	***	ns	NA	NA	NA	NA	NA	NA	NA	NA	NA
	H	***	***	***	***	***	***	***	NA	NA	NA	NA	NA	NA	NA	NA
RMA	C	***	***	***	***	***	***	***	***	NA	NA	NA	NA	NA	NA	NA
	M-C	***	***	***	***	***	***	***	***	***	NA	NA	NA	NA	NA	NA
	M-H	***	***	***	***	***	***	***	***	***	ns	NA	NA	NA	NA	NA
	H	***	***	***	***	***	***	***	ns	***	***	***	NA	NA	NA	NA
MA	C	*	***	***	***	***	***	***	***	***	***	***	***	NA	NA	NA
	M-C	***	***	***	***	***	***	***	***	ns	***	***	***	***	NA	NA
	M-H	***	***	ns	***	***	***	***	***	***	ns	*	***	***	***	NA
	H	***	***	***	*	***	***	***	ns	***	***	***	ns	***	***	***

(c)

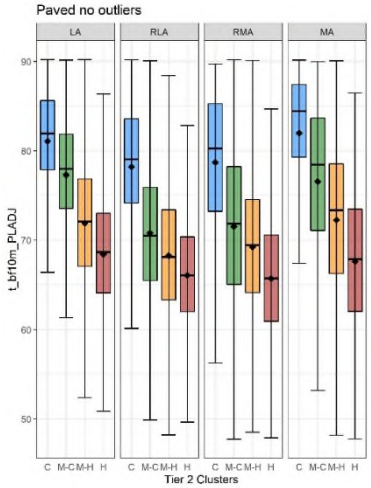

(d)

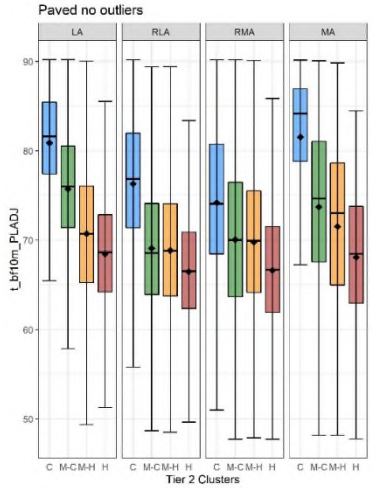

Figure_Apx C-13 Results of the ANOVA (a, b) and boxplots (c, d) for PLADJ of trees located in the neighbourhood to core paved patches in June (a, c) and July (b, d). Boxplots represent elevation values associated with the coldest (C), medium-cold (M-C), medium-hot (M-H) and the hottest (H) Tier 2 clusters within each Tier 1 cluster: LA – Least aggregated, RLA – Relatively less aggregated, RMA – Relatively more aggregated, MA – Most aggregated.

(a)

t_bf10m_COH		LA				RLA				MA		
		C	M-C	M-H	H	C	M-C	M-H	H	C	M-C	M-H
LA	M-C	***	NA	NA	NA	NA	NA	NA	NA	NA	NA	NA
	M-H	***	***	NA	NA	NA	NA	NA	NA	NA	NA	NA
	H	***	***	***	NA	NA	NA	NA	NA	NA	NA	NA
RLA	C	ns	***	***	***	NA	NA	NA	NA	NA	NA	NA
	M-C	***	*	***	***	***	NA	NA	NA	NA	NA	NA
	M-H	***	ns	**	***	***	*	NA	NA	NA	NA	NA
	H	***	***	***	***	***	***	***	NA	NA	NA	NA
MA	C	*	***	*	***	ns	***	**	***	NA	NA	NA
	M-C	***	***	***	ns	***	***	***	**	***	NA	NA
	M-H	***	***	***	ns	***	***	***	ns	***	ns	NA
	H	***	***	***	***	***	***	***	***	***	***	***

(b)

t_bf10m_COH		LA				RLA				MA		
		C	M-C	M-H	H	C	M-C	M-H	H	C	M-C	M-H
LA	M-C	***	NA	NA	NA	NA	NA	NA	NA	NA	NA	NA
	M-H	***	***	NA	NA	NA	NA	NA	NA	NA	NA	NA
	H	***	***	***	NA	NA	NA	NA	NA	NA	NA	NA
RLA	C	ns	***	***	***	NA	NA	NA	NA	NA	NA	NA
	M-C	***	**	***	ns	***	NA	NA	NA	NA	NA	NA
	M-H	***	***	ns	***	***	***	NA	NA	NA	NA	NA
	H	***	***	***	***	***	***	***	NA	NA	NA	NA
MA	C	*	***	ns	***	ns	***	ns	***	NA	NA	NA
	M-C	***	***	***	***	***	**	***	ns	***	NA	NA
	M-H	***	***	***	***	***	**	***	ns	***	ns	NA
	H	***	***	***	***	***	***	***	***	***	***	*

(c)

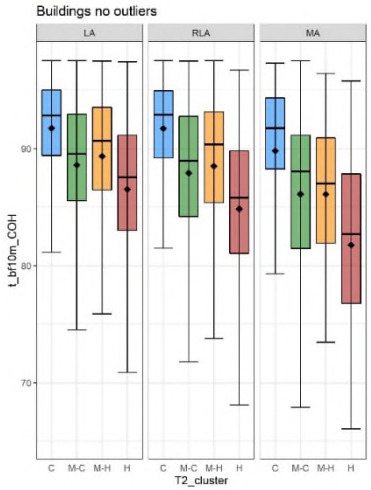

(d)

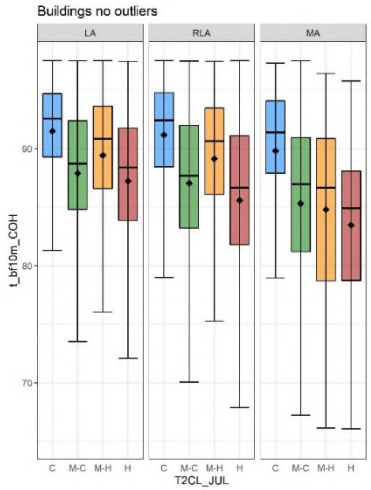

Figure_Apx C-14 Results of the ANOVA (a, b) and boxplots (c, d) for COHESION of trees located in the neighbourhood to core building patches in June (a, c) and July (b, d). Boxplots represent elevation values associated with the coldest (C), medium-cold (M-C), medium-hot (M-H) and the hottest (H) Tier 2 clusters within each Tier 1 cluster: LA – Least aggregated, RLA – Relatively less aggregated, MA – Most aggregated.

(a)

t_bf10m_COH		LA				RLA				RMA				MA		
		C	M-C	M-H	H	C	M-C	M-H	H	C	M-C	M-H	H	C	M-C	M-H
LA	M-C	***	NA	NA	NA	NA	NA	NA	NA	NA	NA	NA	NA	NA	NA	NA
	M-H	***	***	NA	NA	NA	NA	NA	NA	NA	NA	NA	NA	NA	NA	NA
	H	***	***	***	NA	NA	NA	NA	NA	NA	NA	NA	NA	NA	NA	NA
RLA	C	***	***	***	***	NA	NA	NA	NA	NA	NA	NA	NA	NA	NA	NA
	M-C	***	***	***	***	***	NA	NA	NA	NA	NA	NA	NA	NA	NA	NA
	M-H	***	***	***	***	***	***	NA	NA	NA	NA	NA	NA	NA	NA	NA
	H	***	***	***	**	***	***	***	NA	NA	NA	NA	NA	NA	NA	NA
RMA	C	***	***	***	***	ns	***	***	***	NA	NA	NA	NA	NA	NA	NA
	M-C	***	***	***	***	***	***	***	***	***	NA	NA	NA	NA	NA	NA
	M-H	***	***	***	***	***	***	ns	***	***	***	NA	NA	NA	NA	NA
	H	***	***	***	***	***	***	***	ns	***	***	***	NA	NA	NA	NA
MA	C	***	***	***	***	***	***	***	***	***	***	***	***	NA	NA	NA
	M-C	**	***	***	***	***	***	***	***	***	ns	***	***	***	NA	NA
	M-H	***	***	***	***	***	ns	***	***	***	***	***	***	***	***	NA
	H	***	***	***	ns	***	***	***	ns	***	***	***	ns	***	***	***

(b)

t_bf10m_COH		LA				RLA				RMA				MA		
		C	M-C	M-H	H	C	M-C	M-H	H	C	M-C	M-H	H	C	M-C	M-H
LA	M-C	***	NA	NA	NA	NA	NA	NA	NA	NA	NA	NA	NA	NA	NA	NA
	M-H	***	***	NA	NA	NA	NA	NA	NA	NA	NA	NA	NA	NA	NA	NA
	H	***	***	***	NA	NA	NA	NA	NA	NA	NA	NA	NA	NA	NA	NA
RLA	C	***	***	***	***	NA	NA	NA	NA	NA	NA	NA	NA	NA	NA	NA
	M-C	***	***	***	***	***	NA	NA	NA	NA	NA	NA	NA	NA	NA	NA
	M-H	***	***	ns	***	***	***	NA	NA	NA	NA	NA	NA	NA	NA	NA
	H	***	***	***	ns	***	***	***	NA	NA	NA	NA	NA	NA	NA	NA
RMA	C	***	***	***	***	ns	***	***	***	NA	NA	NA	NA	NA	NA	NA
	M-C	***	***	***	***	***	***	***	***	***	NA	NA	NA	NA	NA	NA
	M-H	***	***	ns	***	***	***	ns	***	***	***	NA	NA	NA	NA	NA
	H	***	***	***	ns	***	***	***	ns	***	***	***	NA	NA	NA	NA
MA	C	***	***	***	***	**	***	***	***	***	***	***	***	NA	NA	NA
	M-C	**	***	***	***	***	***	***	***	***	*	***	***	***	NA	NA
	M-H	***	***	**	***	***	ns	*	***	***	***	**	***	***	***	NA
	H	***	*	***	ns	***	***	***	ns	***	***	***	ns	***	***	***

(c)

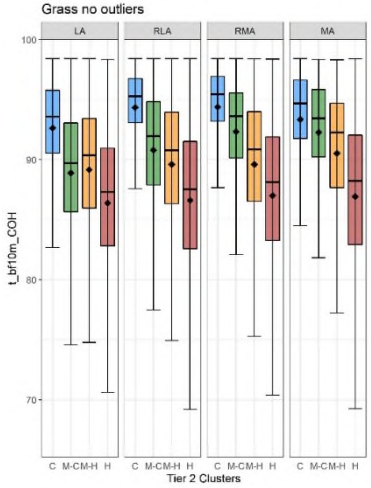

(d)

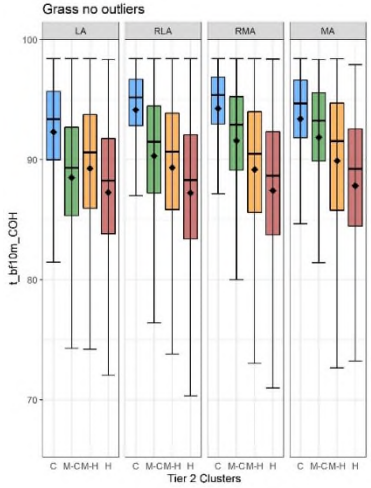

Figure_Apx C-15 Results of the ANOVA (a, b) and boxplots (c, d) for COHESION of trees located in the neighbourhood to core grass patches in June (a, c) and July (b, d). Boxplots represent elevation values associated with the coldest (C), medium-cold (M-C), medium-hot (M-H) and the hottest (H) Tier 2 clusters within each Tier 1 cluster: LA – Least aggregated, RLA – Relatively less aggregated, RMA – Relatively more aggregated, MA – Most aggregated.

(a)

t_bf10m_COH		LA				RLA				RMA				MA		
		C	M-C	M-H	H	C	M-C	M-H	H	C	M-C	M-H	H	C	M-C	M-H
LA	M-C	***	NA	NA	NA	NA	NA	NA	NA	NA	NA	NA	NA	NA	NA	NA
	M-H	***	***	NA	NA	NA	NA	NA	NA	NA	NA	NA	NA	NA	NA	NA
	H	***	***	***	NA	NA	NA	NA	NA	NA	NA	NA	NA	NA	NA	NA
RLA	C	***	***	***	***	NA	NA	NA	NA	NA	NA	NA	NA	NA	NA	NA
	M-C	***	***	***	***	***	NA	NA	NA	NA	NA	NA	NA	NA	NA	NA
	M-H	***	***	***	***	***	***	NA	NA	NA	NA	NA	NA	NA	NA	NA
	H	***	***	***	***	***	***	***	NA	NA	NA	NA	NA	NA	NA	NA
RMA	C	***	ns	**	***	ns	***	***	***	NA	NA	NA	NA	NA	NA	NA
	M-C	***	***	***	**	***	***	ns	***	***	NA	NA	NA	NA	NA	NA
	M-H	***	***	***	***	***	***	***	***	***	***	NA	NA	NA	NA	NA
	H	***	***	***	***	***	***	***	***	***	***	***	NA	NA	NA	NA
MA	C	*	**	***	***	***	***	***	***	ns	***	***	***	NA	NA	NA
	M-C	***	***	**	***	***	***	***	***	***	***	***	***	***	NA	NA
	M-H	***	***	***	***	***	***	*	**	***	*	ns	***	***	***	NA
	H	***	***	***	***	***	***	***	***	***	***	***	**	***	***	***

(b)

t_bf10m_COH		LA				RLA				RMA				MA		
		C	M-C	M-H	H	C	M-C	M-H	H	C	M-C	M-H	H	C	M-C	M-H
LA	M-C	***	NA	NA	NA	NA	NA	NA	NA	NA	NA	NA	NA	NA	NA	NA
	M-H	***	***	NA	NA	NA	NA	NA	NA	NA	NA	NA	NA	NA	NA	NA
	H	***	***	***	NA	NA	NA	NA	NA	NA	NA	NA	NA	NA	NA	NA
RLA	C	***	***	***	***	NA	NA	NA	NA	NA	NA	NA	NA	NA	NA	NA
	M-C	***	***	***	ns	***	NA	NA	NA	NA	NA	NA	NA	NA	NA	NA
	M-H	***	***	***	ns	***	*	NA	NA	NA	NA	NA	NA	NA	NA	NA
	H	***	***	***	***	***	***	***	NA	NA	NA	NA	NA	NA	NA	NA
RMA	C	***	***	ns	***	***	***	***	***	NA	NA	NA	NA	NA	NA	NA
	M-C	***	***	***	***	***	***	***	***	***	NA	NA	NA	NA	NA	NA
	M-H	***	***	***	**	***	***	***	***	***	*	NA	NA	NA	NA	NA
	H	***	***	***	***	***	***	***	***	***	***	***	NA	NA	NA	NA
MA	C	***	***	***	***	***	***	***	***	***	***	***	***	NA	NA	NA
	M-C	***	***	***	ns	***	ns	ns	***	***	***	*	***	***	NA	NA
	M-H	***	***	***	***	***	***	***	ns	***	ns	*	**	***	**	NA
	H	***	***	***	***	***	***	***	***	***	***	***	***	***	***	***

(c)

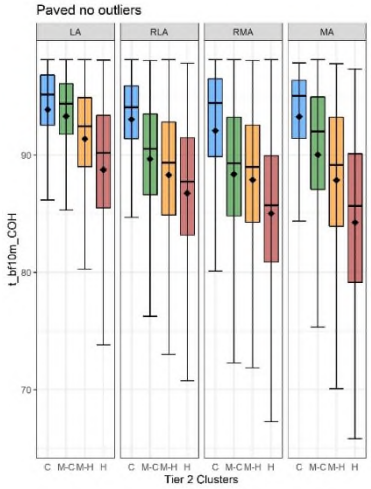

(d)

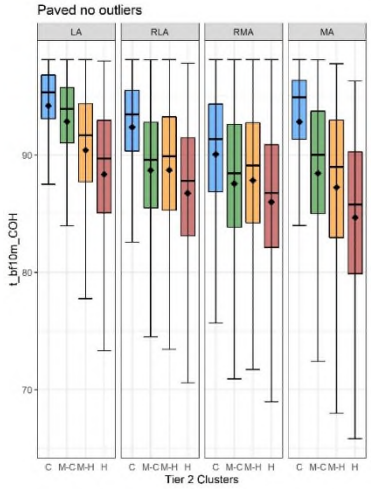

Figure_Apx C-16 Results of the ANOVA (a, b) and boxplots (c, d) for COHESION of trees located in the neighbourhood to core paved patches in June (a, c) and July (b, d). Boxplots represent elevation values associated with the coldest (C), medium-cold (M-C), medium-hot (M-H) and the hottest (H) Tier 2 clusters within each Tier 1 cluster: LA – Least aggregated, RLA – Relatively less aggregated, RMA – Relatively more aggregated, MA – Most aggregated.

(a)

g_bf10m_PLADJ		LA				RLA				RMA				MA		
		C	M-C	M-H	H	C	M-C	M-H	H	C	M-C	M-H	H	C	M-C	M-H
LA	M-C	***	NA	NA	NA	NA	NA	NA	NA	NA	NA	NA	NA	NA	NA	NA
	M-H	***	***	NA	NA	NA	NA	NA	NA	NA	NA	NA	NA	NA	NA	NA
	H	***	***	***	NA	NA	NA	NA	NA	NA	NA	NA	NA	NA	NA	NA
RLA	C	*	***	***	***	NA	NA	NA	NA	NA	NA	NA	NA	NA	NA	NA
	M-C	***	***	***	***	***	NA	NA	NA	NA	NA	NA	NA	NA	NA	NA
	M-H	***	***	ns	***	***	***	NA	NA	NA	NA	NA	NA	NA	NA	NA
	H	***	***	***	***	***	***	***	NA	NA	NA	NA	NA	NA	NA	NA
RMA	C	***	***	***	***	***	***	***	***	NA	NA	NA	NA	NA	NA	NA
	M-C	***	***	***	***	***	***	***	***	***	NA	NA	NA	NA	NA	NA
	M-H	***	***	***	***	***	***	***	***	***	***	NA	NA	NA	NA	NA
	H	***	***	**	***	***	ns	ns	***	***	***	***	NA	NA	NA	NA
MA	C	***	***	***	***	***	***	***	***	***	***	***	***	NA	NA	NA
	M-C	ns	***	***	***	**	***	***	***	***	***	***	***	***	NA	NA
	M-H	***	***	***	***	**	***	***	***	***	***	***	***	***	***	NA
	H	***	***	**	***	***	***	***	***	***	***	ns	***	***	***	***

(b)

g_bf10m_PLADJ		LA				RLA				RMA				MA		
		C	M-C	M-H	H	C	M-C	M-H	H	C	M-C	M-H	H	C	M-C	M-H
LA	M-C	***	NA	NA	NA	NA	NA	NA	NA	NA	NA	NA	NA	NA	NA	NA
	M-H	*	***	NA	NA	NA	NA	NA	NA	NA	NA	NA	NA	NA	NA	NA
	H	***	***	***	NA	NA	NA	NA	NA	NA	NA	NA	NA	NA	NA	NA
RLA	C	**	***	***	***	NA	NA	NA	NA	NA	NA	NA	NA	NA	NA	NA
	M-C	***	***	***	ns	***	NA	NA	NA	NA	NA	NA	NA	NA	NA	NA
	M-H	***	***	**	***	***	***	NA	NA	NA	NA	NA	NA	NA	NA	NA
	H	***	***	***	ns	***	ns	***	NA	NA	NA	NA	NA	NA	NA	NA
RMA	C	***	***	***	***	***	***	***	***	NA	NA	NA	NA	NA	NA	NA
	M-C	***	***	***	***	***	***	***	***	***	NA	NA	NA	NA	NA	NA
	M-H	*	***	***	***	ns	***	***	***	***	***	NA	NA	NA	NA	NA
	H	***	***	***	***	***	***	ns	***	***	***	***	NA	NA	NA	NA
MA	C	***	***	***	***	***	***	***	***	***	***	***	***	NA	NA	NA
	M-C	***	***	***	***	***	***	***	***	ns	***	***	***	***	NA	NA
	M-H	***	***	***	***	***	***	***	***	ns	***	***	***	***	*	NA
	H	*	***	***	***	ns	***	***	***	***	ns	ns	***	***	***	***

(c)

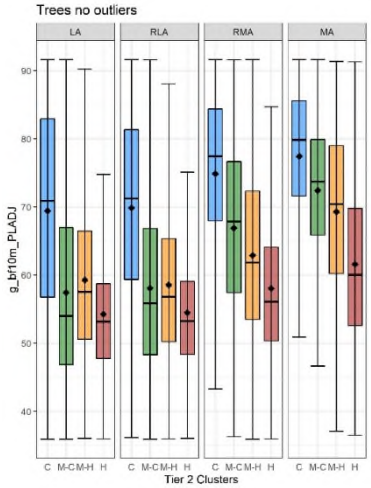

(d)

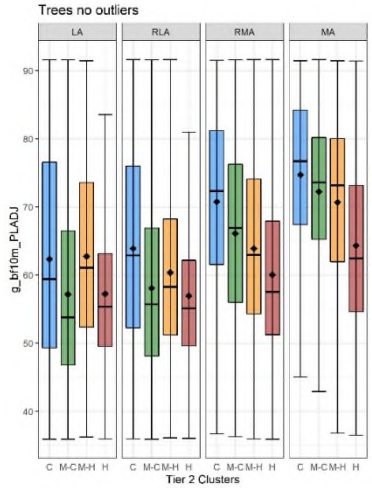

Figure_Apx C-17 Results of the ANOVA (a, b) and boxplots (c, d) for PLADJ of grass located in the neighbourhood to core tree patches in June (a, c) and July (b, d). Boxplots represent elevation values associated with the coldest (C), medium-cold (M-C), medium-hot (M-H) and the hottest (H) Tier 2 clusters within each Tier 1 cluster: LA – Least aggregated, RLA – Relatively less aggregated, RMA – Relatively more aggregated, MA – Most aggregated.

(a)

g_bf10m_COH		LA				RLA				RMA				MA		
		C	M-C	M-H	H	C	M-C	M-H	H	C	M-C	M-H	H	C	M-C	M-H
LA	M-C	***	NA	NA	NA	NA	NA	NA	NA	NA	NA	NA	NA	NA	NA	NA
	M-H	***	***	NA	NA	NA	NA	NA	NA	NA	NA	NA	NA	NA	NA	NA
	H	***	***	***	NA	NA	NA	NA	NA	NA	NA	NA	NA	NA	NA	NA
RLA	C	***	***	***	***	NA	NA	NA	NA	NA	NA	NA	NA	NA	NA	NA
	M-C	***	***	***	***	***	NA	NA	NA	NA	NA	NA	NA	NA	NA	NA
	M-H	***	***	***	***	***	***	NA	NA	NA	NA	NA	NA	NA	NA	NA
	H	***	*	***	**	***	***	***	NA	NA	NA	NA	NA	NA	NA	NA
RMA	C	***	***	***	***	***	***	***	***	NA	NA	NA	NA	NA	NA	NA
	M-C	***	***	***	***	***	***	***	***	***	NA	NA	NA	NA	NA	NA
	M-H	***	***	***	***	***	***	***	***	***	***	NA	NA	NA	NA	NA
	H	***	***	***	***	***	***	ns	***	***	***	***	NA	NA	NA	NA
MA	C	***	***	***	***	***	***	***	***	***	***	***	***	NA	NA	NA
	M-C	ns	***	***	***	***	***	***	***	***	***	***	***	***	NA	NA
	M-H	***	***	***	***	*	***	***	***	***	***	***	***	***	***	NA
	H	***	***	**	***	***	***	***	***	***	***	ns	***	***	***	***

(b)

g_bf10m_COH		LA				RLA				RMA				MA		
		C	M-C	M-H	H	C	M-C	M-H	H	C	M-C	M-H	H	C	M-C	M-H
LA	M-C	***	NA	NA	NA	NA	NA	NA	NA	NA	NA	NA	NA	NA	NA	NA
	M-H	ns	***	NA	NA	NA	NA	NA	NA	NA	NA	NA	NA	NA	NA	NA
	H	***	***	***	NA	NA	NA	NA	NA	NA	NA	NA	NA	NA	NA	NA
RLA	C	*	***	**	***	NA	NA	NA	NA	NA	NA	NA	NA	NA	NA	NA
	M-C	***	***	***	**	***	NA	NA	NA	NA	NA	NA	NA	NA	NA	NA
	M-H	***	***	***	***	***	***	NA	NA	NA	NA	NA	NA	NA	NA	NA
	H	***	***	***	*	***	ns	***	NA	NA	NA	NA	NA	NA	NA	NA
RMA	C	***	***	***	***	***	***	***	***	NA	NA	NA	NA	NA	NA	NA
	M-C	***	***	***	***	***	***	***	***	***	NA	NA	NA	NA	NA	NA
	M-H	*	***	**	***	ns	***	***	***	***	***	NA	NA	NA	NA	NA
	H	***	***	***	***	***	***	ns	***	***	***	***	NA	NA	NA	NA
MA	C	***	***	***	***	***	***	***	***	***	***	***	***	NA	NA	NA
	M-C	***	***	***	***	***	***	***	***	ns	***	***	***	***	NA	NA
	M-H	***	***	***	***	***	***	***	***	ns	***	***	***	***	*	NA
	H	*	***	**	***	ns	***	***	***	***	ns	ns	***	***	***	***

(c)

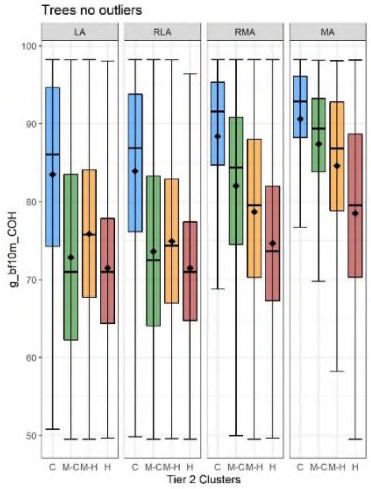

(d)

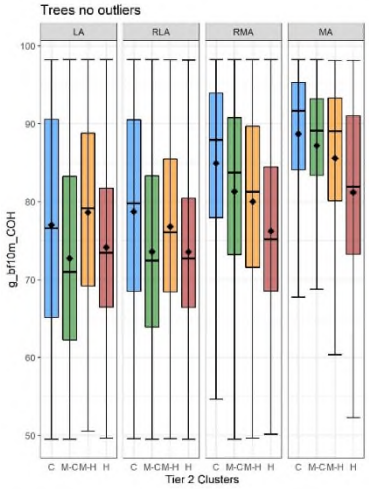

Figure_Apx C-18 Results of the ANOVA (a, b) and boxplots (c, d) for COHESION of grass located in the neighbourhood to core tree patches in June (a, c) and July (b, d). Boxplots represent elevation values associated with the coldest (C), medium-cold (M-C), medium-hot (M-H) and the hottest (H) Tier 2 clusters within each Tier 1 cluster: LA – Least aggregated, RLA – Relatively less aggregated, RMA – Relatively more aggregated, MA – Most aggregated.

(a)

p_bf10m_PLADJ		LA				RLA				MA		
		C	M-C	M-H	H	C	M-C	M-H	H	C	M-C	M-H
LA	M-C	***	NA	NA	NA	NA	NA	NA	NA	NA	NA	NA
	M-H	***	***	NA	NA	NA	NA	NA	NA	NA	NA	NA
	H	***	***	***	NA	NA	NA	NA	NA	NA	NA	NA
RLA	C	***	***	ns	***	NA	NA	NA	NA	NA	NA	NA
	M-C	***	***	***	ns	***	NA	NA	NA	NA	NA	NA
	M-H	***	***	***	***	***	**	NA	NA	NA	NA	NA
	H	***	***	***	***	***	***	***	NA	NA	NA	NA
MA	C	***	***	***	***	***	***	***	*	NA	NA	NA
	M-C	***	***	***	***	***	***	***	***	*	NA	NA
	M-H	***	***	***	***	***	***	***	***	*	ns	NA
	H	***	***	***	***	***	***	***	***	***	***	***

(b)

p_bf10m_PLADJ		LA				RLA				MA		
		C	M-C	M-H	H	C	M-C	M-H	H	C	M-C	M-H
LA	M-C	***	NA	NA	NA	NA	NA	NA	NA	NA	NA	NA
	M-H	***	***	NA	NA	NA	NA	NA	NA	NA	NA	NA
	H	***	***	***	NA	NA	NA	NA	NA	NA	NA	NA
RLA	C	***	***	***	***	NA	NA	NA	NA	NA	NA	NA
	M-C	***	***	***	ns	***	NA	NA	NA	NA	NA	NA
	M-H	***	***	***	ns	***	ns	NA	NA	NA	NA	NA
	H	***	***	***	***	***	***	***	NA	NA	NA	NA
MA	C	***	***	***	***	***	***	***	***	NA	NA	NA
	M-C	***	***	***	***	***	***	***	***	*	NA	NA
	M-H	***	***	***	***	***	***	***	***	ns	ns	NA
	H	***	***	***	***	***	***	***	***	***	***	***

(c)

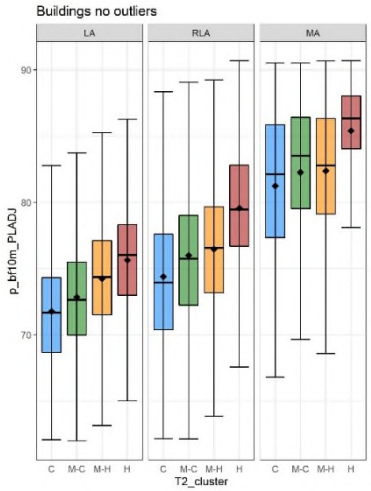

(d)

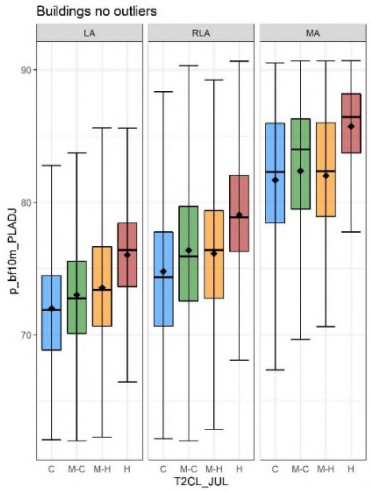

Figure_Apx C-19 Results of the ANOVA (a, b) and boxplots (c, d) for PLADJ of paved located in the neighbourhood to core building patches in June (a, c) and July (b, d). Boxplots represent elevation values associated with the coldest (C), medium-cold (M-C), medium-hot (M-H) and the hottest (H) Tier 2 clusters within each Tier 1 cluster: LA – Least aggregated, RLA – Relatively less aggregated, MA – Most aggregated.

(a)

p_bf10m_PLADJ		LA				RLA				RMA				MA		
		C	M-C	M-H	H	C	M-C	M-H	H	C	M-C	M-H	H	C	M-C	M-H
LA	M-C	***	NA	NA	NA	NA	NA	NA	NA	NA	NA	NA	NA	NA	NA	NA
	M-H	***	***	NA	NA	NA	NA	NA	NA	NA	NA	NA	NA	NA	NA	NA
	H	***	***	***	NA	NA	NA	NA	NA	NA	NA	NA	NA	NA	NA	NA
RLA	C	***	***	***	***	NA	NA	NA	NA	NA	NA	NA	NA	NA	NA	NA
	M-C	***	***	***	***	**	NA	NA	NA	NA	NA	NA	NA	NA	NA	NA
	M-H	***	***	*	***	***	***	NA	NA	NA	NA	NA	NA	NA	NA	NA
	H	***	***	***	***	***	***	***	NA	NA	NA	NA	NA	NA	NA	NA
RMA	C	***	***	***	***	ns	ns	***	***	NA	NA	NA	NA	NA	NA	NA
	M-C	***	***	*	***	***	***	**	***	***	NA	NA	NA	NA	NA	NA
	M-H	***	***	***	***	***	***	***	***	***	***	NA	NA	NA	NA	NA
	H	***	***	***	***	***	***	***	***	***	***	***	NA	NA	NA	NA
MA	C	***	***	***	***	***	***	***	***	***	***	***	***	NA	NA	NA
	M-C	***	***	ns	***	ns	*	ns	***	ns	**	***	***	***	NA	NA
	M-H	***	***	***	ns	***	***	***	ns	***	***	*	***	***	***	NA
	H	***	***	***	***	***	***	***	***	***	***	***	***	***	***	***

(b)

p_bf10m_PLADJ		LA				RLA				RMA				MA		
		C	M-C	M-H	H	C	M-C	M-H	H	C	M-C	M-H	H	C	M-C	M-H
LA	M-C	***	NA	NA	NA	NA	NA	NA	NA	NA	NA	NA	NA	NA	NA	NA
	M-H	***	***	NA	NA	NA	NA	NA	NA	NA	NA	NA	NA	NA	NA	NA
	H	***	***	***	NA	NA	NA	NA	NA	NA	NA	NA	NA	NA	NA	NA
RLA	C	***	***	***	***	NA	NA	NA	NA	NA	NA	NA	NA	NA	NA	NA
	M-C	***	***	***	***	ns	NA	NA	NA	NA	NA	NA	NA	NA	NA	NA
	M-H	***	***	*	***	***	***	NA	NA	NA	NA	NA	NA	NA	NA	NA
	H	***	***	***	ns	***	***	***	NA	NA	NA	NA	NA	NA	NA	NA
RMA	C	***	***	***	***	ns	ns	***	***	NA	NA	NA	NA	NA	NA	NA
	M-C	***	***	**	***	***	***	***	***	***	NA	NA	NA	NA	NA	NA
	M-H	***	***	***	***	***	***	***	***	***	***	NA	NA	NA	NA	NA
	H	***	***	***	***	***	***	***	***	***	***	***	NA	NA	NA	NA
MA	C	***	***	***	***	***	***	***	***	***	***	***	***	NA	NA	NA
	M-C	***	***	ns	***	*	***	ns	***	ns	*	***	***	***	NA	NA
	M-H	***	***	***	ns	***	***	***	ns	***	***	*	ns	***	***	NA
	H	***	***	***	***	***	***	***	***	***	***	***	***	***	***	***

(c)

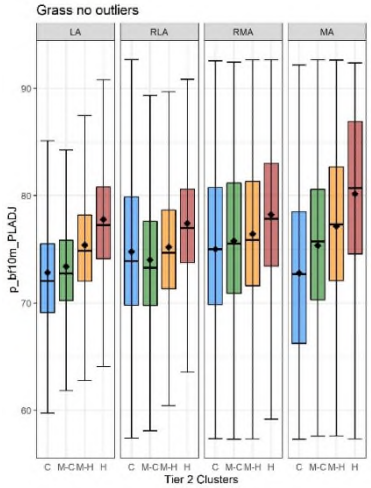

(d)

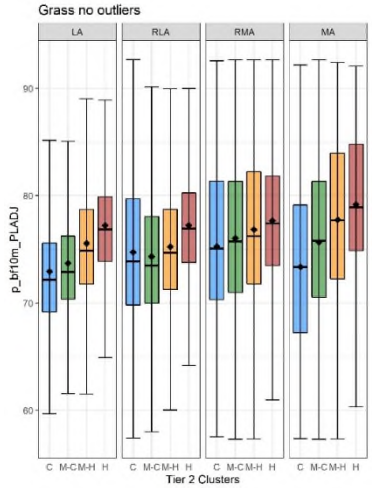

Figure_Apx C-20 Results of the ANOVA (a, b) and boxplots (c, d) for PLADJ of paved located in the neighbourhood to core grass patches in June (a, c) and July (b, d). Boxplots represent elevation values associated with the coldest (C), medium-cold (M-C), medium-hot (M-H) and the hottest (H) Tier 2 clusters within each Tier 1 cluster: LA – Least aggregated, RLA – Relatively less aggregated, RMA – Relatively more aggregated, MA – Most aggregated.

(a)

p_bf10m_PLADJ		LA				RLA				RMA				MA		
		C	M-C	M-H	H	C	M-C	M-H	H	C	M-C	M-H	H	C	M-C	M-H
LA	M-C	***	NA	NA	NA	NA	NA	NA	NA	NA	NA	NA	NA	NA	NA	NA
	M-H	***	***	NA	NA	NA	NA	NA	NA	NA	NA	NA	NA	NA	NA	NA
	H	***	***	***	NA	NA	NA	NA	NA	NA	NA	NA	NA	NA	NA	NA
RLA	C	***	***	***	***	NA	NA	NA	NA	NA	NA	NA	NA	NA	NA	NA
	M-C	***	***	***	***	***	NA	NA	NA	NA	NA	NA	NA	NA	NA	NA
	M-H	***	***	***	***	***	***	NA	NA	NA	NA	NA	NA	NA	NA	NA
	H	***	***	***	***	***	***	***	NA	NA	NA	NA	NA	NA	NA	NA
RMA	C	***	***	***	***	*	***	***	***	NA	NA	NA	NA	NA	NA	NA
	M-C	**	***	***	***	***	***	***	***	***	NA	NA	NA	NA	NA	NA
	M-H	***	***	***	***	***	***	ns	***	***	***	NA	NA	NA	NA	NA
	H	***	***	***	***	***	***	***	***	***	***	***	NA	NA	NA	NA
MA	C	***	***	***	***	ns	**	***	***	ns	***	***	***	NA	NA	NA
	M-C	***	***	**	***	***	***	***	ns	***	***	***	***	***	NA	NA
	M-H	***	***	***	ns	***	***	***	***	***	***	***	*	***	***	NA
	H	***	***	***	***	***	***	***	***	***	***	***	***	***	***	***

(b)

p_bf10m_PLADJ		LA				RLA				RMA				MA		
		C	M-C	M-H	H	C	M-C	M-H	H	C	M-C	M-H	H	C	M-C	M-H
LA	M-C	***	NA	NA	NA	NA	NA	NA	NA	NA	NA	NA	NA	NA	NA	NA
	M-H	***	***	NA	NA	NA	NA	NA	NA	NA	NA	NA	NA	NA	NA	NA
	H	***	***	*	NA	NA	NA	NA	NA	NA	NA	NA	NA	NA	NA	NA
RLA	C	***	***	***	***	NA	NA	NA	NA	NA	NA	NA	NA	NA	NA	NA
	M-C	***	***	***	***	***	NA	NA	NA	NA	NA	NA	NA	NA	NA	NA
	M-H	***	ns	***	***	***	***	NA	NA	NA	NA	NA	NA	NA	NA	NA
	H	***	***	ns	***	***	***	***	NA	NA	NA	NA	NA	NA	NA	NA
RMA	C	***	***	***	***	ns	***	***	***	NA	NA	NA	NA	NA	NA	NA
	M-C	**	***	***	***	***	**	***	***	***	NA	NA	NA	NA	NA	NA
	M-H	***	***	ns	ns	***	***	***	*	***	***	NA	NA	NA	NA	NA
	H	***	***	***	***	***	***	***	***	***	***	***	NA	NA	NA	NA
MA	C	***	***	***	***	ns	**	***	***	ns	***	***	***	NA	NA	NA
	M-C	***	***	ns	ns	***	***	***	***	***	***	ns	ns	***	NA	NA
	M-H	***	***	***	***	***	***	***	***	***	***	***	***	***	***	NA
	H	***	***	***	***	***	***	***	***	***	***	***	***	***	***	ns

(c)

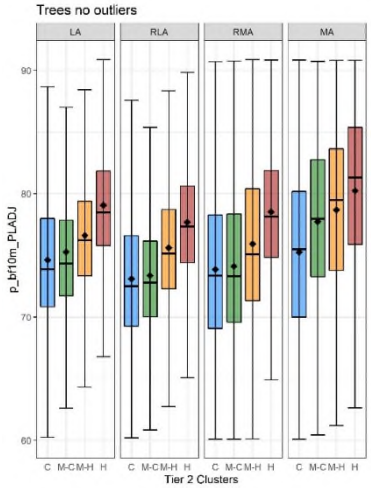

(d)

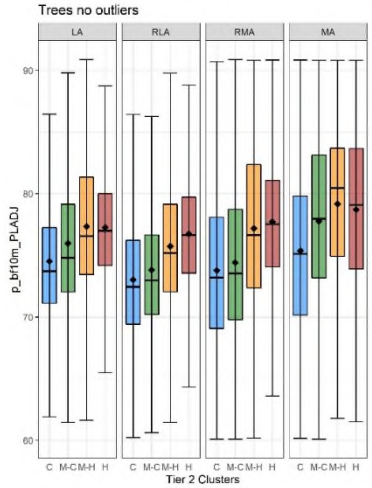

Figure_Apx C-21 Results of the ANOVA (a, b) and boxplots (c, d) for PLADJ of paved located in the neighbourhood to core tree patches in June (a, c) and July (b, d). Boxplots represent elevation values associated with the coldest (C), medium-cold (M-C), medium-hot (M-H) and the hottest (H) Tier 2 clusters within each Tier 1 cluster: LA – Least aggregated, RLA – Relatively less aggregated, RMA – Relatively more aggregated, MA – Most aggregated.

(a)

c_lsi_mn		LA				RLA				MA		
		C	M-C	M-H	H	C	M-C	M-H	H	C	M-C	M-H
LA	M-C	***	NA	NA	NA	NA	NA	NA	NA	NA	NA	NA
	M-H	***	***	NA	NA	NA	NA	NA	NA	NA	NA	NA
	H	***	***	***	NA	NA	NA	NA	NA	NA	NA	NA
RLA	C	***	***	***	***	NA	NA	NA	NA	NA	NA	NA
	M-C	***	***	***	***	***	NA	NA	NA	NA	NA	NA
	M-H	ns	***	***	***	***	***	NA	NA	NA	NA	NA
	H	***	***	***	***	***	***	***	NA	NA	NA	NA
MA	C	***	***	***	***	***	***	***	***	NA	NA	NA
	M-C	***	***	***	***	***	***	***	***	**	NA	NA
	M-H	***	***	***	***	***	***	***	***	***	***	NA
	H	***	***	***	***	***	***	***	***	***	***	**

(b)

c_lsi_mn		LA				RLA				MA		
		C	M-C	M-H	H	C	M-C	M-H	H	C	M-C	M-H
LA	M-C	***	NA	NA	NA	NA	NA	NA	NA	NA	NA	NA
	M-H	***	***	NA	NA	NA	NA	NA	NA	NA	NA	NA
	H	***	ns	***	NA	NA	NA	NA	NA	NA	NA	NA
RLA	C	***	***	***	***	NA	NA	NA	NA	NA	NA	NA
	M-C	***	***	***	***	***	NA	NA	NA	NA	NA	NA
	M-H	***	***	***	***	***	***	NA	NA	NA	NA	NA
	H	*	***	***	***	***	***	***	NA	NA	NA	NA
MA	C	***	***	***	***	***	***	***	***	NA	NA	NA
	M-C	***	***	***	***	***	***	***	***	***	NA	NA
	M-H	***	***	***	***	***	***	***	***	***	**	NA
	H	***	***	***	***	***	***	***	***	***	***	ns

(c)

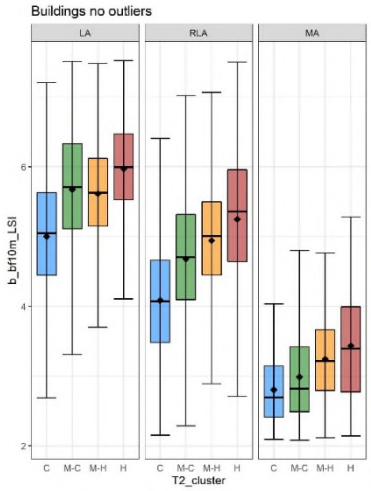

(d)

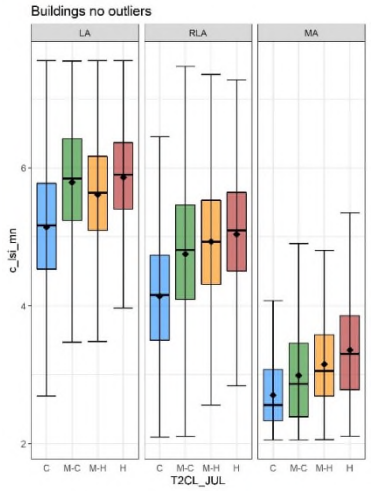

Figure_Apx C-22 Results of the ANOVA (a, b) and boxplots (c, d) for LSI of core building patches in June (a, c) and July (b, d). Boxplots represent elevation values associated with the coldest (C), medium-cold (M-C), medium-hot (M-H) and the hottest (H) Tier 2 clusters within each Tier 1 cluster: LA – Least aggregated, RLA – Relatively less aggregated, MA – Most aggregated.

(a)

b_bf10m_LSI		LA				RLA				MA		
		C	M-C	M-H	H	C	M-C	M-H	H	C	M-C	M-H
LA	M-C	***	NA	NA	NA	NA	NA	NA	NA	NA	NA	NA
	M-H	***	***	NA	NA	NA	NA	NA	NA	NA	NA	NA
	H	***	***	***	NA	NA	NA	NA	NA	NA	NA	NA
RLA	C	***	***	***	***	NA	NA	NA	NA	NA	NA	NA
	M-C	***	***	***	***	***	NA	NA	NA	NA	NA	NA
	M-H	ns	***	***	***	***	***	NA	NA	NA	NA	NA
	H	***	***	***	***	***	***	***	NA	NA	NA	NA
MA	C	***	***	***	***	***	***	***	***	NA	NA	NA
	M-C	***	***	***	***	***	***	***	***	*	NA	NA
	M-H	***	***	***	***	***	***	***	***	***	***	NA
	H	***	***	***	***	***	***	***	***	***	***	*

(b)

b_bf10m_LSI		LA				RLA				MA		
		C	M-C	M-H	H	C	M-C	M-H	H	C	M-C	M-H
LA	M-C	***	NA	NA	NA	NA	NA	NA	NA	NA	NA	NA
	M-H	***	***	NA	NA	NA	NA	NA	NA	NA	NA	NA
	H	***	ns	***	NA	NA	NA	NA	NA	NA	NA	NA
RLA	C	***	***	***	***	NA	NA	NA	NA	NA	NA	NA
	M-C	***	***	***	***	***	NA	NA	NA	NA	NA	NA
	M-H	***	***	***	***	***	***	NA	NA	NA	NA	NA
	H	ns	***	***	***	***	***	***	NA	NA	NA	NA
MA	C	***	***	***	***	***	***	***	***	NA	NA	NA
	M-C	***	***	***	***	***	***	***	***	***	NA	NA
	M-H	***	***	***	***	***	***	***	***	***	**	NA
	H	***	***	***	***	***	***	***	***	***	***	ns

(c)

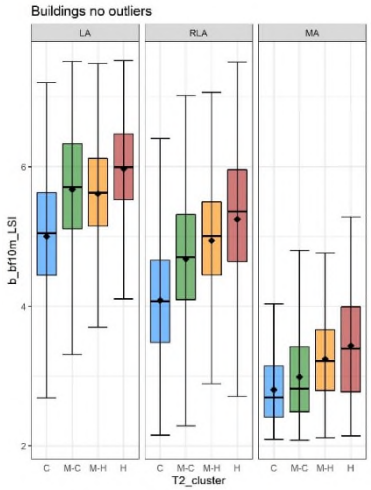

(d)

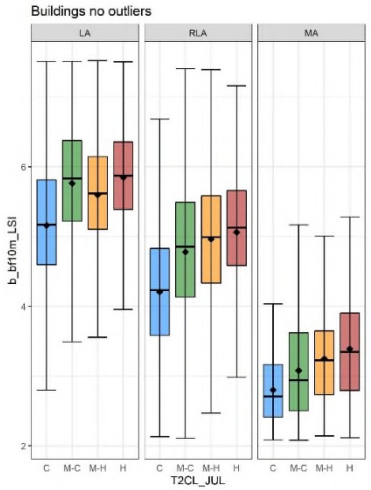

Figure_Apx C-23 Results of the ANOVA (a, b) and boxplots (c, d) for LSI of buildings located in neighbourhood of core building patches in June (a, c) and July (b, d). Boxplots represent elevation values associated with the coldest (C), medium-cold (M-C), medium-hot (M-H) and the hottest (H) Tier 2 clusters within each Tier 1 cluster: LA – Least aggregated, RLA – Relatively less aggregated, MA – Most aggregated.

(a)

b_bf10m_LSI		LA				RLA				RMA				MA		
		C	M-C	M-H	H	C	M-C	M-H	H	C	M-C	M-H	H	C	M-C	M-H
LA	M-C	***	NA	NA	NA	NA	NA	NA	NA	NA	NA	NA	NA	NA	NA	NA
	M-H	***	***	NA	NA	NA	NA	NA	NA	NA	NA	NA	NA	NA	NA	NA
	H	***	***	***	NA	NA	NA	NA	NA	NA	NA	NA	NA	NA	NA	NA
RLA	C	***	***	***	***	NA	NA	NA	NA	NA	NA	NA	NA	NA	NA	NA
	M-C	***	***	***	***	***	NA	NA	NA	NA	NA	NA	NA	NA	NA	NA
	M-H	***	***	***	***	***	***	NA	NA	NA	NA	NA	NA	NA	NA	NA
	H	***	***	***	***	***	***	***	NA	NA	NA	NA	NA	NA	NA	NA
RMA	C	*	***	***	***	***	***	***	***	NA	NA	NA	NA	NA	NA	NA
	M-C	ns	***	***	***	**	***	***	***	**	NA	NA	NA	NA	NA	NA
	M-H	***	*	***	***	***	***	***	***	***	***	NA	NA	NA	NA	NA
	H	***	***	***	***	***	ns	***	***	***	***	***	NA	NA	NA	NA
MA	C	***	***	***	***	***	***	***	***	ns	***	***	***	NA	NA	NA
	M-C	***	***	***	***	***	***	***	***	***	***	***	***	ns	NA	NA
	M-H	***	***	***	***	***	***	***	***	***	***	***	***	ns	ns	NA
	H	***	***	***	***	***	***	***	***	ns	***	***	***	ns	***	***

(b)

b_bf10m_LSI		LA				RLA				RMA				MA		
		C	M-C	M-H	H	C	M-C	M-H	H	C	M-C	M-H	H	C	M-C	M-H
LA	M-C	***	NA	NA	NA	NA	NA	NA	NA	NA	NA	NA	NA	NA	NA	NA
	M-H	***	***	NA	NA	NA	NA	NA	NA	NA	NA	NA	NA	NA	NA	NA
	H	***	***	***	NA	NA	NA	NA	NA	NA	NA	NA	NA	NA	NA	NA
RLA	C	***	***	***	***	NA	NA	NA	NA	NA	NA	NA	NA	NA	NA	NA
	M-C	***	***	ns	***	***	NA	NA	NA	NA	NA	NA	NA	NA	NA	NA
	M-H	***	***	ns	**	***	**	NA	NA	NA	NA	NA	NA	NA	NA	NA
	H	***	***	***	***	***	***	***	NA	NA	NA	NA	NA	NA	NA	NA
RMA	C	***	***	***	***	***	***	***	***	NA	NA	NA	NA	NA	NA	NA
	M-C	ns	***	***	***	***	***	***	***	*	NA	NA	NA	NA	NA	NA
	M-H	***	***	***	***	ns	***	***	***	***	***	NA	NA	NA	NA	NA
	H	***	***	***	***	***	***	***	***	***	***	***	NA	NA	NA	NA
MA	C	***	***	***	***	***	***	***	***	***	***	***	***	NA	NA	NA
	M-C	***	***	***	***	***	***	***	***	***	***	***	***	ns	NA	NA
	M-H	***	***	***	***	***	***	***	***	***	***	***	***	**	***	NA
	H	***	***	***	***	***	***	***	***	***	***	***	***	***	***	**

(c)

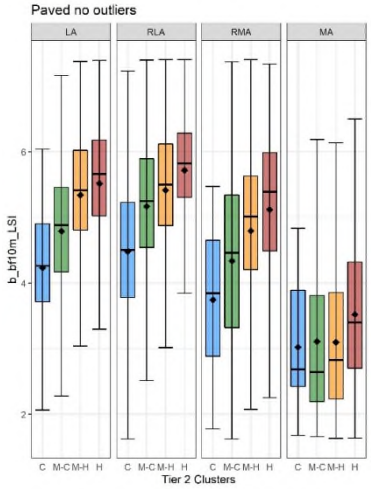

(d)

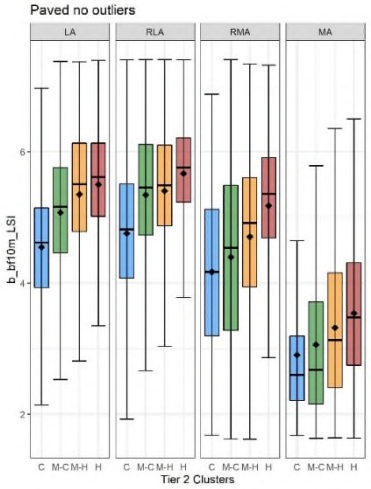

Figure_Apx C-24 Results of the ANOVA (a, b) and boxplots (c, d) for LSI of buildings located in the neighbourhood to core paved patches in June (a, c) and July (b, d). Boxplots represent elevation values associated with the coldest (C), medium-cold (M-C), medium-hot (M-H) and the hottest (H) Tier 2 clusters within each Tier 1 cluster: LA – Least aggregated, RLA – Relatively less aggregated, RMA – Relatively more aggregated, MA – Most aggregated.

(a)

c_dw_mn		LA				RLA				MA		
		C	M-C	M-H	H	C	M-C	M-H	H	C	M-C	M-H
LA	M-C	***	NA	NA	NA	NA	NA	NA	NA	NA	NA	NA
	M-H	***	***	NA	NA	NA	NA	NA	NA	NA	NA	NA
	H	***	***	ns	NA	NA	NA	NA	NA	NA	NA	NA
RLA	C	ns	***	***	***	NA	NA	NA	NA	NA	NA	NA
	M-C	***	***	***	***	***	NA	NA	NA	NA	NA	NA
	M-H	***	***	ns	ns	***	***	NA	NA	NA	NA	NA
	H	***	***	ns	ns	***	***	ns	NA	NA	NA	NA
MA	C	ns	ns	***	***	ns	*	***	***	NA	NA	NA
	M-C	*	ns	***	***	ns	**	***	***	ns	NA	NA
	M-H	***	***	*	*	***	*	ns	ns	***	***	NA
	H	***	***	ns	ns	***	***	ns	ns	***	***	ns

(b)

c_dw_mn		LA				RLA				MA		
		C	M-C	M-H	H	C	M-C	M-H	H	C	M-C	M-H
LA	M-C	***	NA	NA	NA	NA	NA	NA	NA	NA	NA	NA
	M-H	***	***	NA	NA	NA	NA	NA	NA	NA	NA	NA
	H	***	***	***	NA	NA	NA	NA	NA	NA	NA	NA
RLA	C	*	***	***	***	NA	NA	NA	NA	NA	NA	NA
	M-C	***	ns	***	***	***	NA	NA	NA	NA	NA	NA
	M-H	***	***	ns	***	***	***	NA	NA	NA	NA	NA
	H	***	***	***	ns	***	***	***	NA	NA	NA	NA
MA	C	*	ns	***	***	ns	ns	***	***	NA	NA	NA
	M-C	ns	*	***	***	ns	**	***	***	ns	NA	NA
	M-H	***	**	ns	***	***	ns	ns	***	*	***	NA
	H	***	***	***	ns	***	***	***	ns	***	***	***

(c)

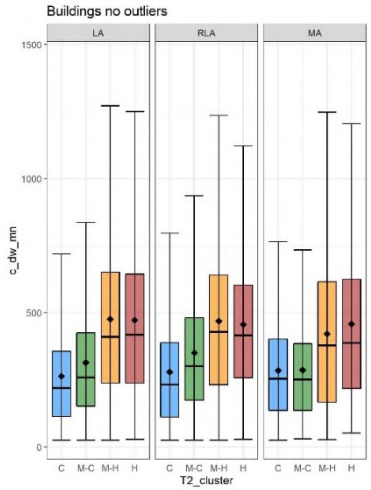

(d)

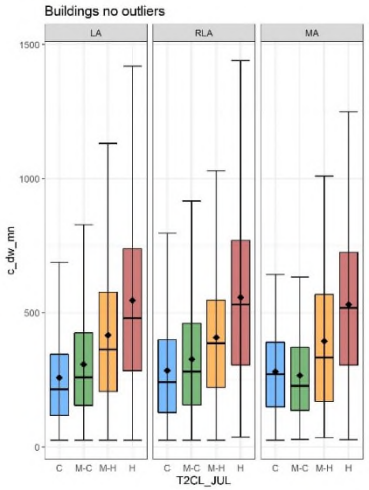

Figure_Apx C-25 Results of the ANOVA (a, b) and boxplots (c, d) for distance to water of core building patches in June (a, c) and July (b, d). Boxplots represent elevation values associated with the coldest (C), medium-cold (M-C), medium-hot (M-H) and the hottest (H) Tier 2 clusters within each Tier 1 cluster: LA – Least aggregated, RLA – Relatively less aggregated, MA – Most aggregated.

(a)

c_dw_mn		LA				RLA				RMA				MA		
		C	M-C	M-H	H	C	M-C	M-H	H	C	M-C	M-H	H	C	M-C	M-H
LA	M-C	***	NA	NA	NA	NA	NA	NA	NA	NA	NA	NA	NA	NA	NA	NA
	M-H	***	***	NA	NA	NA	NA	NA	NA	NA	NA	NA	NA	NA	NA	NA
	H	***	***	***	NA	NA	NA	NA	NA	NA	NA	NA	NA	NA	NA	NA
RLA	C	***	***	***	***	NA	NA	NA	NA	NA	NA	NA	NA	NA	NA	NA
	M-C	***	***	***	***	***	NA	NA	NA	NA	NA	NA	NA	NA	NA	NA
	M-H	***	***	***	***	***	***	NA	NA	NA	NA	NA	NA	NA	NA	NA
	H	***	***	**	***	***	***	***	NA	NA	NA	NA	NA	NA	NA	NA
RMA	C	***	***	***	***	***	***	***	***	NA	NA	NA	NA	NA	NA	NA
	M-C	***	***	***	***	*	***	***	***	***	NA	NA	NA	NA	NA	NA
	M-H	***	***	***	***	***	**	***	***	***	***	NA	NA	NA	NA	NA
	H	***	***	***	***	***	***	*	***	***	***	***	NA	NA	NA	NA
MA	C	***	***	***	***	***	***	***	***	***	***	***	***	NA	NA	NA
	M-C	***	***	***	***	***	***	***	***	***	***	***	***	***	NA	NA
	M-H	ns	***	***	***	***	ns	***	***	***	***	*	***	***	***	NA
	H	***	*	***	***	***	***	***	***	***	***	***	**	***	***	***

(b)

c_dw_mn		LA				RLA				RMA				MA		
		C	M-C	M-H	H	C	M-C	M-H	H	C	M-C	M-H	H	C	M-C	M-H
LA	M-C	***	NA	NA	NA	NA	NA	NA	NA	NA	NA	NA	NA	NA	NA	NA
	M-H	***	***	NA	NA	NA	NA	NA	NA	NA	NA	NA	NA	NA	NA	NA
	H	***	***	***	NA	NA	NA	NA	NA	NA	NA	NA	NA	NA	NA	NA
RLA	C	***	***	***	***	NA	NA	NA	NA	NA	NA	NA	NA	NA	NA	NA
	M-C	***	***	***	***	***	NA	NA	NA	NA	NA	NA	NA	NA	NA	NA
	M-H	***	***	***	***	***	***	NA	NA	NA	NA	NA	NA	NA	NA	NA
	H	***	***	***	***	***	***	***	NA	NA	NA	NA	NA	NA	NA	NA
RMA	C	***	***	***	***	***	***	***	***	NA	NA	NA	NA	NA	NA	NA
	M-C	***	***	***	***	***	***	***	***	***	NA	NA	NA	NA	NA	NA
	M-H	***	***	***	***	***	ns	***	***	***	***	NA	NA	NA	NA	NA
	H	***	***	***	***	***	***	***	***	***	***	***	NA	NA	NA	NA
MA	C	***	***	***	***	***	***	***	***	***	***	***	***	NA	NA	NA
	M-C	***	***	***	***	***	***	***	***	***	***	***	***	***	NA	NA
	M-H	ns	***	***	***	***	*	***	***	***	**	*	***	***	***	NA
	H	***	***	ns	***	***	***	*	***	***	***	***	**	***	***	***

(c)

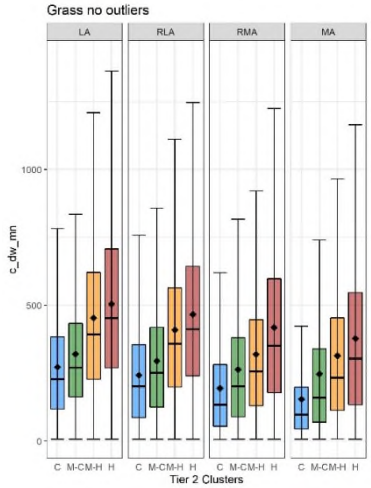

(d)

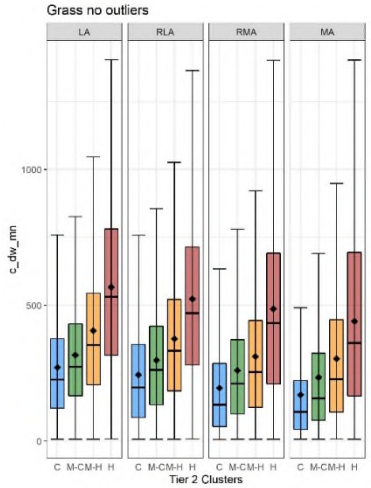

Figure_Apx C-26 Results of the ANOVA (a, b) and boxplots (c, d) for distance to water of core grass patches in June (a, c) and July (b, d). Boxplots represent elevation values associated with the coldest (C), medium-cold (M-C), medium-hot (M-H) and the hottest (H) Tier 2 clusters within each Tier 1 cluster: LA – Least aggregated, RLA – Relatively less aggregated, RMA – Relatively more aggregated, MA – Most aggregated.

(a)

c_dw_mn		LA				RLA				RMA				MA		
		C	M-C	M-H	H	C	M-C	M-H	H	C	M-C	M-H	H	C	M-C	M-H
LA	M-C	***	NA	NA	NA	NA	NA	NA	NA	NA	NA	NA	NA	NA	NA	NA
	M-H	***	***	NA	NA	NA	NA	NA	NA	NA	NA	NA	NA	NA	NA	NA
	H	***	***	***	NA	NA	NA	NA	NA	NA	NA	NA	NA	NA	NA	NA
RLA	C	***	***	***	***	NA	NA	NA	NA	NA	NA	NA	NA	NA	NA	NA
	M-C	***	***	ns	***	***	NA	NA	NA	NA	NA	NA	NA	NA	NA	NA
	M-H	***	***	***	***	***	***	NA	NA	NA	NA	NA	NA	NA	NA	NA
	H	***	***	***	***	***	***	***	NA	NA	NA	NA	NA	NA	NA	NA
RMA	C	***	***	ns	***	ns	ns	***	***	NA	NA	NA	NA	NA	NA	NA
	M-C	***	***	ns	***	***	ns	***	***	ns	NA	NA	NA	NA	NA	NA
	M-H	***	***	***	*	***	***	***	***	***	***	NA	NA	NA	NA	NA
	H	***	***	***	***	***	***	***	ns	***	***	***	NA	NA	NA	NA
MA	C	***	ns	***	***	***	***	***	***	***	***	***	***	NA	NA	NA
	M-C	***	***	***	***	ns	***	***	***	ns	***	***	***	***	NA	NA
	M-H	***	***	ns	***	***	ns	***	***	ns	ns	***	***	***	***	NA
	H	***	***	***	ns	***	***	***	***	***	***	ns	***	***	***	***

(b)

c_dw_mn		LA				RLA				RMA				MA		
		C	M-C	M-H	H	C	M-C	M-H	H	C	M-C	M-H	H	C	M-C	M-H
LA	M-C	***	NA	NA	NA	NA	NA	NA	NA	NA	NA	NA	NA	NA	NA	NA
	M-H	***	***	NA	NA	NA	NA	NA	NA	NA	NA	NA	NA	NA	NA	NA
	H	***	***	***	NA	NA	NA	NA	NA	NA	NA	NA	NA	NA	NA	NA
RLA	C	***	***	***	***	NA	NA	NA	NA	NA	NA	NA	NA	NA	NA	NA
	M-C	***	***	**	***	***	NA	NA	NA	NA	NA	NA	NA	NA	NA	NA
	M-H	***	***	***	***	***	***	NA	NA	NA	NA	NA	NA	NA	NA	NA
	H	***	***	***	***	***	***	***	NA	NA	NA	NA	NA	NA	NA	NA
RMA	C	***	***	***	***	***	**	***	***	NA	NA	NA	NA	NA	NA	NA
	M-C	***	***	**	***	***	ns	***	***	*	NA	NA	NA	NA	NA	NA
	M-H	***	***	***	***	***	***	ns	***	***	***	NA	NA	NA	NA	NA
	H	***	***	***	***	***	***	***	ns	***	***	***	NA	NA	NA	NA
MA	C	***	*	***	***	***	***	***	***	***	***	***	***	NA	NA	NA
	M-C	***	***	***	***	ns	***	***	***	*	***	***	***	***	NA	NA
	M-H	***	***	ns	***	***	ns	***	***	**	ns	***	***	***	***	NA
	H	***	***	***	***	***	***	***	*	***	***	***	*	***	***	***

(c)

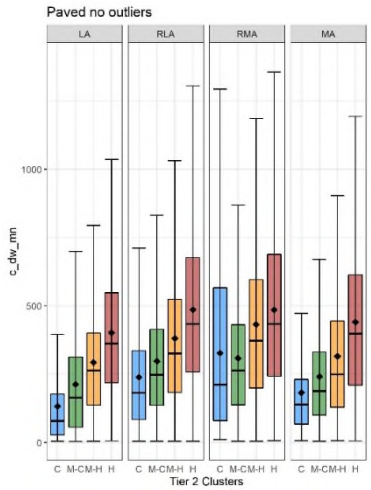

(d)

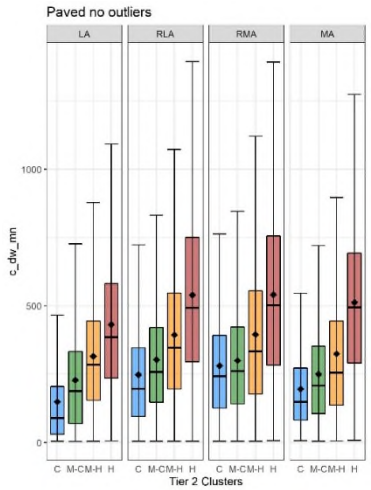

Figure_Apx C-27 Results of the ANOVA (a, b) and boxplots (c, d) for distance to water of core paved patches in June (a, c) and July (b, d). Boxplots represent elevation values associated with the coldest (C), medium-cold (M-C), medium-hot (M-H) and the hottest (H) Tier 2 clusters within each Tier 1 cluster: LA – Least aggregated, RLA – Relatively less aggregated, RMA – Relatively more aggregated, MA – Most aggregated.

(a)

c_dw_mn		LA				RLA				RMA				MA		
		C	M-C	M-H	H	C	M-C	M-H	H	C	M-C	M-H	H	C	M-C	M-H
LA	M-C	***	NA	NA	NA	NA	NA	NA	NA	NA	NA	NA	NA	NA	NA	NA
	M-H	***	***	NA	NA	NA	NA	NA	NA	NA	NA	NA	NA	NA	NA	NA
	H	***	***	***	NA	NA	NA	NA	NA	NA	NA	NA	NA	NA	NA	NA
RLA	C	ns	***	***	***	NA	NA	NA	NA	NA	NA	NA	NA	NA	NA	NA
	M-C	***	ns	***	***	***	NA	NA	NA	NA	NA	NA	NA	NA	NA	NA
	M-H	***	***	ns	***	***	***	NA	NA	NA	NA	NA	NA	NA	NA	NA
	H	***	***	***	ns	***	***	***	NA	NA	NA	NA	NA	NA	NA	NA
RMA	C	***	***	***	***	***	***	***	***	NA	NA	NA	NA	NA	NA	NA
	M-C	***	***	***	***	***	***	***	***	***	NA	NA	NA	NA	NA	NA
	M-H	***	***	***	***	***	***	***	***	***	***	NA	NA	NA	NA	NA
	H	***	***	***	***	***	***	***	***	***	***	***	NA	NA	NA	NA
MA	C	***	***	***	***	***	***	***	***	*	***	***	***	NA	NA	NA
	M-C	ns	***	***	***	**	***	***	***	***	ns	***	***	***	NA	NA
	M-H	***	ns	***	***	***	ns	***	***	***	***	***	***	***	***	NA
	H	***	***	ns	***	***	***	ns	***	***	***	***	*	***	***	***

(b)

c_dw_mn		LA				RLA				RMA				MA		
		C	M-C	M-H	H	C	M-C	M-H	H	C	M-C	M-H	H	C	M-C	M-H
LA	M-C	***	NA	NA	NA	NA	NA	NA	NA	NA	NA	NA	NA	NA	NA	NA
	M-H	***	***	NA	NA	NA	NA	NA	NA	NA	NA	NA	NA	NA	NA	NA
	H	***	***	***	NA	NA	NA	NA	NA	NA	NA	NA	NA	NA	NA	NA
RLA	C	**	***	***	***	NA	NA	NA	NA	NA	NA	NA	NA	NA	NA	NA
	M-C	***	**	***	***	***	NA	NA	NA	NA	NA	NA	NA	NA	NA	NA
	M-H	***	***	***	***	***	***	NA	NA	NA	NA	NA	NA	NA	NA	NA
	H	***	***	***	ns	***	***	***	NA	NA	NA	NA	NA	NA	NA	NA
RMA	C	***	***	***	***	***	***	***	***	NA	NA	NA	NA	NA	NA	NA
	M-C	*	***	***	***	***	***	***	***	***	NA	NA	NA	NA	NA	NA
	M-H	***	***	***	***	***	***	***	***	***	***	NA	NA	NA	NA	NA
	H	***	***	***	***	***	***	***	***	***	***	***	NA	NA	NA	NA
MA	C	***	***	***	***	***	***	***	***	**	***	***	***	NA	NA	NA
	M-C	**	***	***	***	ns	***	***	***	***	***	***	***	***	NA	NA
	M-H	***	ns	***	***	***	ns	***	***	***	***	***	***	***	***	NA
	H	***	***	***	*	***	***	ns	*	***	***	***	ns	***	***	***

(c)

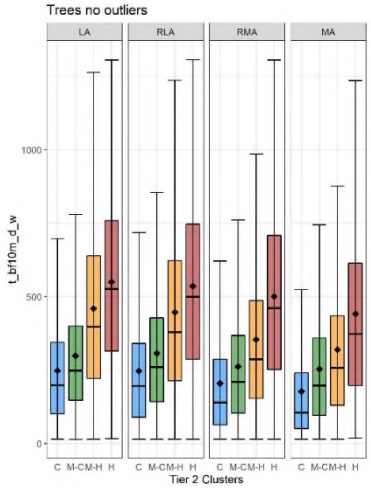

(d)

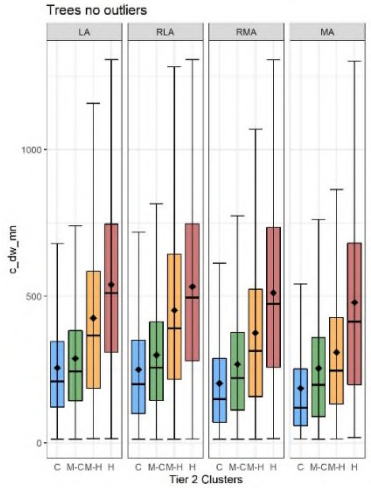

Figure_Apx C-28 Results of the ANOVA (a, b) and boxplots (c, d) for distance to water of core tree patches in June (a, c) and July (b, d). Boxplots represent elevation values associated with the coldest (C), medium-cold (M-C), medium-hot (M-H) and the hottest (H) Tier 2 clusters within each Tier 1 cluster: LA – Least aggregated, RLA – Relatively less aggregated, RMA – Relatively more aggregated, MA – Most aggregated.

(a)

c_db_mn		LA				RLA				RMA				MA		
		C	M-C	M-H	H	C	M-C	M-H	H	C	M-C	M-H	H	C	M-C	M-H
LA	M-C	***	NA	NA	NA	NA	NA	NA	NA	NA	NA	NA	NA	NA	NA	NA
	M-H	***	ns	NA	NA	NA	NA	NA	NA	NA	NA	NA	NA	NA	NA	NA
	H	***	*	*	NA	NA	NA	NA	NA	NA	NA	NA	NA	NA	NA	NA
RLA	C	***	***	***	***	NA	NA	NA	NA	NA	NA	NA	NA	NA	NA	NA
	M-C	***	***	***	***	***	NA	NA	NA	NA	NA	NA	NA	NA	NA	NA
	M-H	**	***	***	***	***	***	NA	NA	NA	NA	NA	NA	NA	NA	NA
	H	***	***	***	***	***	***	**	NA	NA	NA	NA	NA	NA	NA	NA
RMA	C	***	***	***	***	***	***	***	***	NA	NA	NA	NA	NA	NA	NA
	M-C	***	***	***	***	***	***	***	***	***	NA	NA	NA	NA	NA	NA
	M-H	***	***	***	***	***	***	***	***	***	***	NA	NA	NA	NA	NA
	H	***	***	***	***	***	***	***	***	***	***	***	NA	NA	NA	NA
MA	C	***	***	***	***	***	***	***	***	***	***	***	***	NA	NA	NA
	M-C	***	***	***	***	***	***	***	***	*	***	***	***	***	NA	NA
	M-H	***	***	***	***	***	***	***	***	***	***	***	***	***	***	NA
	H	***	***	***	***	ns	***	***	***	***	*	***	***	***	***	***

(b)

c_db_mn		LA				RLA				RMA				MA		
		C	M-C	M-H	H	C	M-C	M-H	H	C	M-C	M-H	H	C	M-C	M-H
LA	M-C	***	NA	NA	NA	NA	NA	NA	NA	NA	NA	NA	NA	NA	NA	NA
	M-H	***	***	NA	NA	NA	NA	NA	NA	NA	NA	NA	NA	NA	NA	NA
	H	***	ns	**	NA	NA	NA	NA	NA	NA	NA	NA	NA	NA	NA	NA
RLA	C	***	***	***	***	NA	NA	NA	NA	NA	NA	NA	NA	NA	NA	NA
	M-C	***	***	***	***	***	NA	NA	NA	NA	NA	NA	NA	NA	NA	NA
	M-H	ns	***	***	***	***	***	NA	NA	NA	NA	NA	NA	NA	NA	NA
	H	***	***	***	***	***	***	***	NA	NA	NA	NA	NA	NA	NA	NA
RMA	C	***	***	***	***	***	***	***	***	NA	NA	NA	NA	NA	NA	NA
	M-C	***	***	***	***	***	***	***	***	***	NA	NA	NA	NA	NA	NA
	M-H	***	***	***	***	***	***	***	***	***	***	NA	NA	NA	NA	NA
	H	***	***	***	***	***	***	***	***	***	***	***	NA	NA	NA	NA
MA	C	***	***	***	***	***	***	***	***	***	***	***	***	NA	NA	NA
	M-C	***	***	***	***	***	***	***	***	ns	***	***	***	***	NA	NA
	M-H	***	***	***	***	***	***	***	***	***	***	***	***	***	***	NA
	H	***	***	***	***	ns	***	***	***	***	ns	***	***	***	***	***

(c)

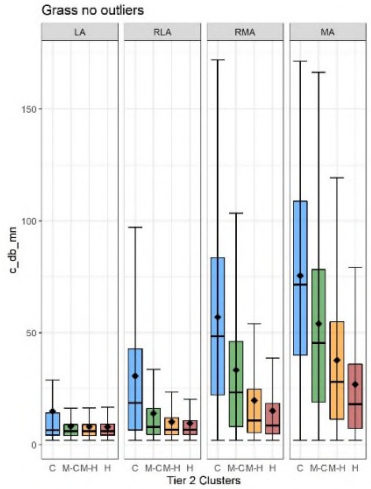

(d)

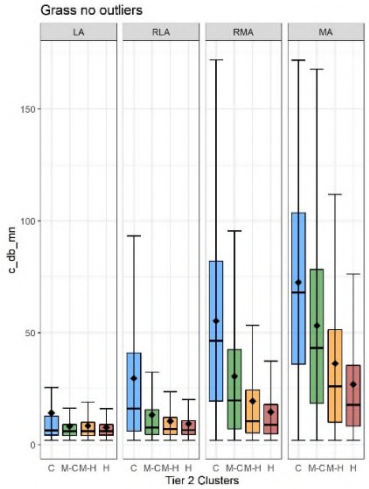

Figure_Apx C-29 Results of the ANOVA (a, b) and boxplots (c, d) for distance to buildings of core grass patches in June (a, c) and July (b, d). Boxplots represent elevation values associated with the coldest (C), medium-cold (M-C), medium-hot (M-H) and the hottest (H) Tier 2 clusters within each Tier 1 cluster: LA – Least aggregated, RLA – Relatively less aggregated, RMA – Relatively more aggregated, MA – Most aggregated.

(a) (b)

c_db_mn		LA				RLA				RMA				MA		
		C	M-C	M-H	H	C	M-C	M-H	H	C	M-C	M-H	H	C	M-C	M-H
LA	M-C	***	NA	NA	NA	NA	NA	NA	NA	NA	NA	NA	NA	NA	NA	NA
	M-H	***	***	NA	NA	NA	NA	NA	NA	NA	NA	NA	NA	NA	NA	NA
	H	***	***	***	NA	NA	NA	NA	NA	NA	NA	NA	NA	NA	NA	NA
RLA	C	***	ns	***	***	NA	NA	NA	NA	NA	NA	NA	NA	NA	NA	NA
	M-C	***	***	***	***	***	NA	NA	NA	NA	NA	NA	NA	NA	NA	NA
	M-H	***	***	***	***	***	***	NA	NA	NA	NA	NA	NA	NA	NA	NA
	H	***	***	***	***	***	***	***	NA	NA	NA	NA	NA	NA	NA	NA
RMA	C	***	*	***	***	*	***	***	***	NA	NA	NA	NA	NA	NA	NA
	M-C	***	***	***	***	***	***	***	***	***	NA	NA	NA	NA	NA	NA
	M-H	***	***	***	ns	***	***	***	***	***	***	NA	NA	NA	NA	NA
	H	***	***	***	***	***	***	***	ns	***	***	***	NA	NA	NA	NA
MA	C	ns	***	***	***	***	***	***	***	***	***	***	***	NA	NA	NA
	M-C	***	***	***	***	***	***	***	***	ns	***	***	***	***	NA	NA
	M-H	***	***	***	***	***	***	***	***	***	***	***	***	***	***	NA
	H	***	***	***	ns	***	***	ns	***	***	***	ns	***	***	***	***

(c)

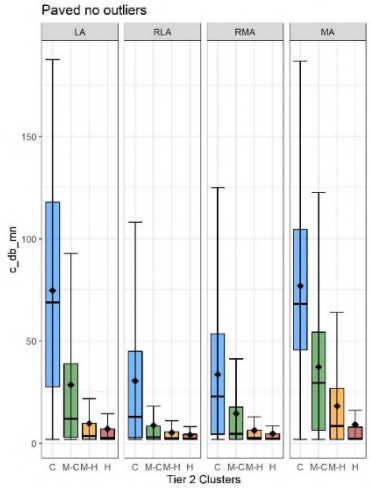

c_db_mn		LA				RLA				RMA				MA		
		C	M-C	M-H	H	C	M-C	M-H	H	C	M-C	M-H	H	C	M-C	M-H
LA	M-C	***	NA	NA	NA	NA	NA	NA	NA	NA	NA	NA	NA	NA	NA	NA
	M-H	***	***	NA	NA	NA	NA	NA	NA	NA	NA	NA	NA	NA	NA	NA
	H	***	***	***	NA	NA	NA	NA	NA	NA	NA	NA	NA	NA	NA	NA
RLA	C	***	**	***	***	NA	NA	NA	NA	NA	NA	NA	NA	NA	NA	NA
	M-C	***	***	***	**	***	NA	NA	NA	NA	NA	NA	NA	NA	NA	NA
	M-H	***	***	***	**	***	***	NA	NA	NA	NA	NA	NA	NA	NA	NA
	H	***	***	***	***	***	***	***	NA	NA	NA	NA	NA	NA	NA	NA
RMA	C	***	*	***	***	ns	***	***	***	NA	NA	NA	NA	NA	NA	NA
	M-C	***	***	*	***	***	***	***	***	***	NA	NA	NA	NA	NA	NA
	M-H	***	***	***	*	***	ns	***	***	***	***	NA	NA	NA	NA	NA
	H	***	***	***	***	***	***	*	ns	***	***	***	NA	NA	NA	NA
MA	C	**	***	***	***	***	***	***	***	***	***	***	***	NA	NA	NA
	M-C	***	***	***	***	***	***	***	***	***	***	***	***	***	NA	NA
	M-H	***	***	***	***	*	***	***	***	ns	***	***	***	***	***	NA
	H	***	***	***	ns	***	ns	ns	**	***	***	ns	*	***	***	***

(d)

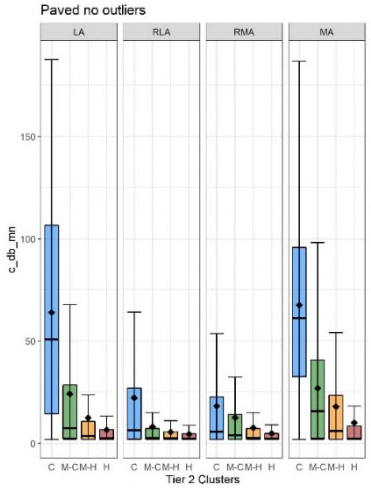

Figure_Apx C-30 Results of the ANOVA (a, b) and boxplots (c, d) for distance to buildings r of core paved patches in June (a, c) and July (b, d). Boxplots represent elevation values associated with the coldest (C), medium-cold (M-C), medium-hot (M-H) and the hottest (H) Tier 2 clusters within each Tier 1 cluster: LA – Least aggregated, RLA – Relatively less aggregated, RMA – Relatively more aggregated, MA – Most aggregated.

(a)

c_db_mn		LA				RLA				RMA				MA		
		C	M-C	M-H	H	C	M-C	M-H	H	C	M-C	M-H	H	C	M-C	M-H
LA	M-C	***	NA	NA	NA	NA	NA	NA	NA	NA	NA	NA	NA	NA	NA	NA
	M-H	***	**	NA	NA	NA	NA	NA	NA	NA	NA	NA	NA	NA	NA	NA
	H	***	***	*	NA	NA	NA	NA	NA	NA	NA	NA	NA	NA	NA	NA
RLA	C	ns	***	***	***	NA	NA	NA	NA	NA	NA	NA	NA	NA	NA	NA
	M-C	***	ns	**	***	***	NA	NA	NA	NA	NA	NA	NA	NA	NA	NA
	M-H	***	***	ns	*	***	***	NA	NA	NA	NA	NA	NA	NA	NA	NA
	H	***	***	ns	ns	***	***	ns	NA	NA	NA	NA	NA	NA	NA	NA
RMA	C	***	***	***	***	***	***	***	***	NA	NA	NA	NA	NA	NA	NA
	M-C	***	***	***	***	***	***	***	***	***	NA	NA	NA	NA	NA	NA
	M-H	***	***	***	***	***	***	***	***	***	***	NA	NA	NA	NA	NA
	H	***	***	***	***	***	***	***	***	***	***	***	NA	NA	NA	NA
MA	C	***	***	***	***	***	***	***	***	***	***	***	***	NA	NA	NA
	M-C	***	***	***	***	***	***	***	***	ns	***	***	***	***	NA	NA
	M-H	***	***	***	***	***	***	***	***	***	***	***	***	***	***	NA
	H	ns	***	***	***	ns	***	***	***	***	ns	***	***	***	***	***

(b)

c_db_mn		LA				RLA				RMA				MA		
		C	M-C	M-H	H	C	M-C	M-H	H	C	M-C	M-H	H	C	M-C	M-H
LA	M-C	***	NA	NA	NA	NA	NA	NA	NA	NA	NA	NA	NA	NA	NA	NA
	M-H	***	**	NA	NA	NA	NA	NA	NA	NA	NA	NA	NA	NA	NA	NA
	H	***	***	***	NA	NA	NA	NA	NA	NA	NA	NA	NA	NA	NA	NA
RLA	C	ns	***	***	***	NA	NA	NA	NA	NA	NA	NA	NA	NA	NA	NA
	M-C	***	ns	***	***	***	NA	NA	NA	NA	NA	NA	NA	NA	NA	NA
	M-H	***	***	ns	***	***	***	NA	NA	NA	NA	NA	NA	NA	NA	NA
	H	***	***	***	ns	***	***	***	NA	NA	NA	NA	NA	NA	NA	NA
RMA	C	***	***	***	***	***	***	***	***	NA	NA	NA	NA	NA	NA	NA
	M-C	***	***	***	***	*	***	***	***	***	NA	NA	NA	NA	NA	NA
	M-H	ns	***	***	***	**	***	***	***	***	***	NA	NA	NA	NA	NA
	H	***	***	ns	***	***	***	ns	***	***	***	***	NA	NA	NA	NA
MA	C	***	***	***	***	***	***	***	***	***	***	***	***	NA	NA	NA
	M-C	***	***	***	***	***	***	***	***	***	***	***	***	***	NA	NA
	M-H	***	***	***	***	***	***	***	***	ns	***	***	***	***	***	NA
	H	***	***	***	***	***	***	***	***	***	**	***	***	***	***	***

(c)

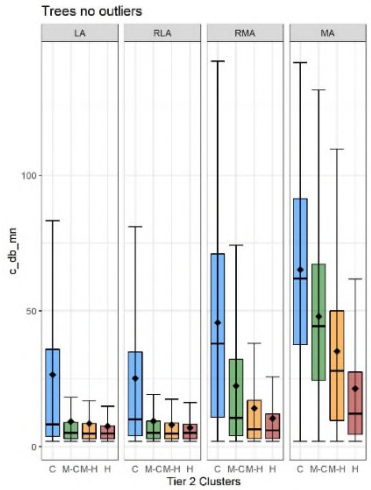

(d)

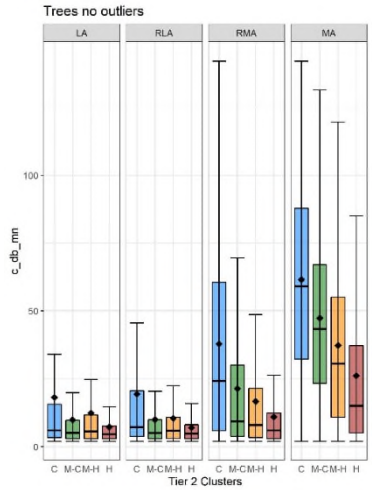

Figure_Apx C-31 Results of the ANOVA (a, b) and boxplots (c, d) for distance to buildings of core tree patches in June (a, c) and July (b, d). Boxplots represent elevation values associated with the coldest (C), medium-cold (M-C), medium-hot (M-H) and the hottest (H) Tier 2 clusters within each Tier 1 cluster: LA – Least aggregated, RLA – Relatively less aggregated, RMA – Relatively more aggregated, MA – Most aggregated.

(a)

t_bf10m_d_b		LA				RLA				RMA				MA		
		C	M-C	M-H	H	C	M-C	M-H	H	C	M-C	M-H	H	C	M-C	M-H
LA	M-C	***	NA	NA	NA	NA	NA	NA	NA	NA	NA	NA	NA	NA	NA	NA
	M-H	***	ns	NA	NA	NA	NA	NA	NA	NA	NA	NA	NA	NA	NA	NA
	H	***	***	***	NA	NA	NA	NA	NA	NA	NA	NA	NA	NA	NA	NA
RLA	C	***	***	***	***	NA	NA	NA	NA	NA	NA	NA	NA	NA	NA	NA
	M-C	**	***	***	***	***	NA	NA	NA	NA	NA	NA	NA	NA	NA	NA
	M-H	***	***	***	***	***	***	NA	NA	NA	NA	NA	NA	NA	NA	NA
	H	***	***	***	***	***	***	***	NA	NA	NA	NA	NA	NA	NA	NA
RMA	C	***	***	***	***	***	***	***	***	NA	NA	NA	NA	NA	NA	NA
	M-C	***	***	***	***	***	***	***	***	***	NA	NA	NA	NA	NA	NA
	M-H	***	***	***	***	***	***	***	***	***	***	NA	NA	NA	NA	NA
	H	ns	***	***	***	***	ns	***	***	***	***	***	NA	NA	NA	NA
MA	C	***	***	***	***	***	***	***	***	***	***	***	***	NA	NA	NA
	M-C	***	***	***	***	***	***	***	***	***	***	***	***	***	NA	NA
	M-H	***	***	***	***	***	***	***	***	***	*	***	***	***	***	NA
	H	***	***	***	***	***	***	***	***	***	***	***	***	***	***	***

(b)

t_bf10m_d_b		LA				RLA				RMA				MA		
		C	M-C	M-H	H	C	M-C	M-H	H	C	M-C	M-H	H	C	M-C	M-H
LA	M-C	***	NA	NA	NA	NA	NA	NA	NA	NA	NA	NA	NA	NA	NA	NA
	M-H	***	**	NA	NA	NA	NA	NA	NA	NA	NA	NA	NA	NA	NA	NA
	H	***	ns	**	NA	NA	NA	NA	NA	NA	NA	NA	NA	NA	NA	NA
RLA	C	***	***	***	***	NA	NA	NA	NA	NA	NA	NA	NA	NA	NA	NA
	M-C	***	***	***	***	***	NA	NA	NA	NA	NA	NA	NA	NA	NA	NA
	M-H	***	***	***	***	***	***	NA	NA	NA	NA	NA	NA	NA	NA	NA
	H	***	***	***	***	***	***	***	NA	NA	NA	NA	NA	NA	NA	NA
RMA	C	***	***	***	***	***	***	***	***	NA	NA	NA	NA	NA	NA	NA
	M-C	***	***	***	***	*	***	***	***	***	NA	NA	NA	NA	NA	NA
	M-H	***	***	***	***	***	***	***	***	***	***	NA	NA	NA	NA	NA
	H	***	***	***	***	***	*	***	***	***	***	***	NA	NA	NA	NA
MA	C	***	***	***	***	***	***	***	***	***	***	***	***	NA	NA	NA
	M-C	***	***	***	***	***	***	***	***	***	***	***	***	***	NA	NA
	M-H	***	***	***	***	***	***	***	***	***	**	***	***	***	***	NA
	H	***	***	***	***	**	***	***	***	***	***	***	***	***	***	***

(c)

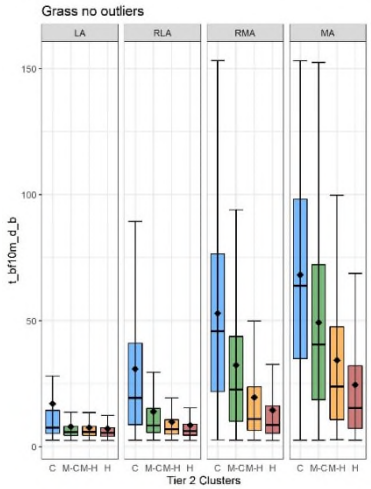

(d)

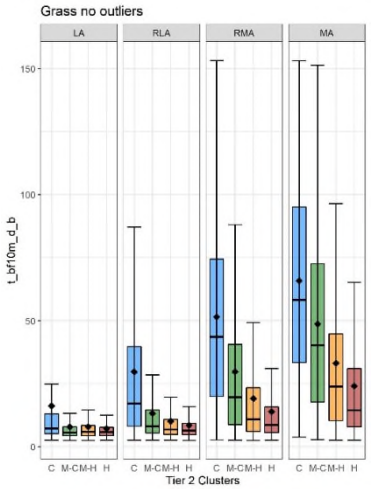

Figure_Apx C-32 Results of the ANOVA (a, b) and boxplots (c, d) for distance to buildings of tree patches located in the neighbourhood of core grass patches in June (a, c) and July (b, d). Boxplots represent elevation values associated with the coldest (C), medium-cold (M-C), medium-hot (M-H) and the hottest (H) Tier 2 clusters within each Tier 1 cluster: LA – Least aggregated, RLA – Relatively less aggregated, RMA – Relatively more aggregated, MA – Most aggregated.

(a)

t_bf10m_d_b		LA				RLA				RMA				MA		
		C	M-C	M-H	H	C	M-C	M-H	H	C	M-C	M-H	H	C	M-C	M-H
LA	M-C	***	NA	NA	NA	NA	NA	NA	NA	NA	NA	NA	NA	NA	NA	NA
	M-H	***	***	NA	NA	NA	NA	NA	NA	NA	NA	NA	NA	NA	NA	NA
	H	***	***	***	NA	NA	NA	NA	NA	NA	NA	NA	NA	NA	NA	NA
RLA	C	***	***	***	***	NA	NA	NA	NA	NA	NA	NA	NA	NA	NA	NA
	M-C	***	***	ns	***	***	NA	NA	NA	NA	NA	NA	NA	NA	NA	NA
	M-H	***	***	***	***	***	***	NA	NA	NA	NA	NA	NA	NA	NA	NA
	H	***	***	***	***	***	***	***	NA	NA	NA	NA	NA	NA	NA	NA
RMA	C	***	**	***	***	ns	***	***	***	NA	NA	NA	NA	NA	NA	NA
	M-C	***	***	***	***	***	***	***	***	***	NA	NA	NA	NA	NA	NA
	M-H	***	***	***	***	***	***	***	***	***	***	NA	NA	NA	NA	NA
	H	***	***	***	***	***	***	***	*	***	***	***	NA	NA	NA	NA
MA	C	ns	***	***	***	***	***	***	***	***	***	***	***	NA	NA	NA
	M-C	***	***	***	***	***	***	***	***	*	***	***	***	***	NA	NA
	M-H	***	***	***	***	***	***	***	***	***	***	***	***	***	***	NA
	H	***	***	*	**	***	**	*	***	***	***	ns	***	***	***	***

(b)

t_bf10m_d_b		LA				RLA				RMA				MA		
		C	M-C	M-H	H	C	M-C	M-H	H	C	M-C	M-H	H	C	M-C	M-H
LA	M-C	***	NA	NA	NA	NA	NA	NA	NA	NA	NA	NA	NA	NA	NA	NA
	M-H	***	***	NA	NA	NA	NA	NA	NA	NA	NA	NA	NA	NA	NA	NA
	H	***	***	***	NA	NA	NA	NA	NA	NA	NA	NA	NA	NA	NA	NA
RLA	C	***	*	***	***	NA	NA	NA	NA	NA	NA	NA	NA	NA	NA	NA
	M-C	***	***	***	***	***	NA	NA	NA	NA	NA	NA	NA	NA	NA	NA
	M-H	***	***	***	ns	***	***	NA	NA	NA	NA	NA	NA	NA	NA	NA
	H	***	***	***	ns	***	***	**	NA	NA	NA	NA	NA	NA	NA	NA
RMA	C	***	ns	***	***	ns	***	***	***	NA	NA	NA	NA	NA	NA	NA
	M-C	***	***	***	***	***	***	***	***	***	NA	NA	NA	NA	NA	NA
	M-H	***	***	***	***	***	ns	***	***	***	***	NA	NA	NA	NA	NA
	H	***	***	***	ns	***	***	ns	ns	***	***	***	NA	NA	NA	NA
MA	C	*	***	***	***	***	***	***	***	***	***	***	***	NA	NA	NA
	M-C	***	***	***	***	***	***	***	***	***	***	***	***	***	NA	NA
	M-H	***	*	***	***	**	***	***	***	*	***	***	***	***	***	NA
	H	***	***	ns	***	***	ns	***	***	***	***	ns	***	***	***	***

(c)

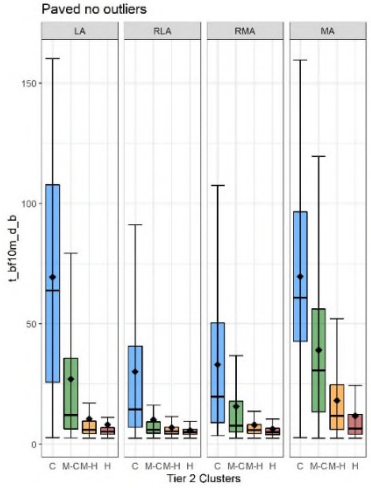

(d)

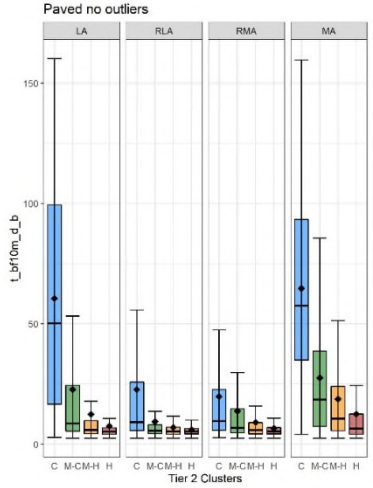

Figure_Apx C-33 Results of the ANOVA (a, b) and boxplots (c, d) for distance to buildings of tree patches located in the neighbourhood of core paved patches in June (a, c) and July (b, d). Boxplots represent elevation values associated with the coldest (C), medium-cold (M-C), medium-hot (M-H) and the hottest (H) Tier 2 clusters within each Tier 1 cluster: LA – Least aggregated, RLA – Relatively less aggregated, RMA – Relatively more aggregated, MA – Most aggregated.

(a)

t_bf10m_d_b		LA				RLA				RMA				MA		
		C	M-C	M-H	H	C	M-C	M-H	H	C	M-C	M-H	H	C	M-C	M-H
LA	M-C	***	NA	NA	NA	NA	NA	NA	NA	NA	NA	NA	NA	NA	NA	NA
	M-H	***	ns	NA	NA	NA	NA	NA	NA	NA	NA	NA	NA	NA	NA	NA
	H	***	***	***	NA	NA	NA	NA	NA	NA	NA	NA	NA	NA	NA	NA
RLA	C	ns	***	***	***	NA	NA	NA	NA	NA	NA	NA	NA	NA	NA	NA
	M-C	***	***	***	***	***	NA	NA	NA	NA	NA	NA	NA	NA	NA	NA
	M-H	***	***	***	***	***	*	NA	NA	NA	NA	NA	NA	NA	NA	NA
	H	***	ns	**	***	***	***	***	NA	NA	NA	NA	NA	NA	NA	NA
RMA	C	***	***	***	***	***	***	***	***	NA	NA	NA	NA	NA	NA	NA
	M-C	ns	***	***	***	ns	***	***	***	***	NA	NA	NA	NA	NA	NA
	M-H	***	***	***	***	***	***	***	***	***	***	NA	NA	NA	NA	NA
	H	***	***	***	***	***	***	***	***	***	***	***	NA	NA	NA	NA
MA	C	***	***	***	***	***	***	***	***	***	***	***	***	NA	NA	NA
	M-C	***	***	***	***	***	***	***	***	ns	***	***	***	***	NA	NA
	M-H	***	***	***	***	***	***	***	***	***	***	***	***	***	***	NA
	H	**	***	***	***	**	***	***	***	***	***	***	***	***	***	***

(b)

t_bf10m_d_b		LA				RLA				RMA				MA		
		C	M-C	M-H	H	C	M-C	M-H	H	C	M-C	M-H	H	C	M-C	M-H
LA	M-C	***	NA	NA	NA	NA	NA	NA	NA	NA	NA	NA	NA	NA	NA	NA
	M-H	***	***	NA	NA	NA	NA	NA	NA	NA	NA	NA	NA	NA	NA	NA
	H	***	***	***	NA	NA	NA	NA	NA	NA	NA	NA	NA	NA	NA	NA
RLA	C	***	***	***	***	NA	NA	NA	NA	NA	NA	NA	NA	NA	NA	NA
	M-C	***	***	ns	***	***	NA	NA	NA	NA	NA	NA	NA	NA	NA	NA
	M-H	***	***	***	***	***	***	NA	NA	NA	NA	NA	NA	NA	NA	NA
	H	***	*	***	***	***	***	***	NA	NA	NA	NA	NA	NA	NA	NA
RMA	C	***	***	***	***	***	***	***	***	NA	NA	NA	NA	NA	NA	NA
	M-C	***	***	***	***	***	***	***	***	***	NA	NA	NA	NA	NA	NA
	M-H	***	***	***	***	ns	***	***	***	***	***	NA	NA	NA	NA	NA
	H	ns	***	***	***	***	***	***	***	***	***	***	NA	NA	NA	NA
MA	C	***	***	***	***	***	***	***	***	***	***	***	***	NA	NA	NA
	M-C	***	***	***	***	***	***	***	***	***	***	***	***	***	NA	NA
	M-H	***	***	***	***	***	***	***	***	ns	***	***	***	***	***	NA
	H	***	***	***	***	***	***	***	***	***	***	***	***	***	***	***

(c)

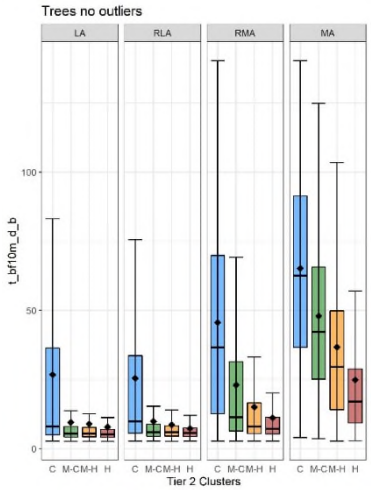

(d)

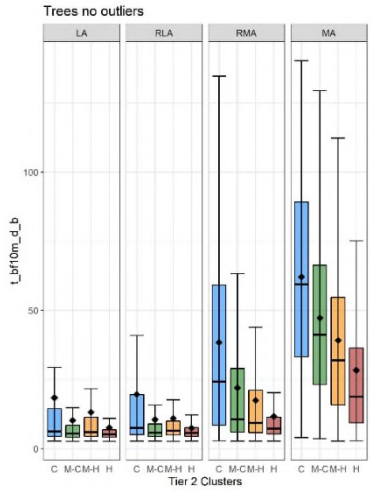

Figure_Apx C-34 Results of the ANOVA (a, b) and boxplots (c, d) for distance to buildings of tree patches located in the neighbourhood of core tree patches in June (a, c) and July (b, d). Boxplots represent elevation values associated with the coldest (C), medium-cold (M-C), medium-hot (M-H) and the hottest (H) Tier 2 clusters within each Tier 1 cluster: LA – Least aggregated, RLA – Relatively less aggregated, RMA – Relatively more aggregated, MA – Most aggregated.

(a)

g_bf10m_d_b		LA				RLA				RMA				MA		
		C	M-C	M-H	H	C	M-C	M-H	H	C	M-C	M-H	H	C	M-C	M-H
LA	M-C	***	NA	NA	NA	NA	NA	NA	NA	NA	NA	NA	NA	NA	NA	NA
	M-H	***	***	NA	NA	NA	NA	NA	NA	NA	NA	NA	NA	NA	NA	NA
	H	***	**	***	NA	NA	NA	NA	NA	NA	NA	NA	NA	NA	NA	NA
RLA	C	***	***	***	***	NA	NA	NA	NA	NA	NA	NA	NA	NA	NA	NA
	M-C	***	***	***	***	***	NA	NA	NA	NA	NA	NA	NA	NA	NA	NA
	M-H	ns	***	***	***	***	***	NA	NA	NA	NA	NA	NA	NA	NA	NA
	H	***	***	***	***	***	***	***	NA	NA	NA	NA	NA	NA	NA	NA
RMA	C	***	***	***	***	***	***	***	***	NA	NA	NA	NA	NA	NA	NA
	M-C	***	***	***	***	***	***	***	***	***	NA	NA	NA	NA	NA	NA
	M-H	***	***	***	***	***	***	***	***	***	***	NA	NA	NA	NA	NA
	H	***	***	***	***	***	***	***	***	***	***	***	NA	NA	NA	NA
MA	C	***	***	***	***	***	***	***	***	***	***	***	***	NA	NA	NA
	M-C	***	***	***	***	***	***	***	***	ns	***	***	***	***	NA	NA
	M-H	***	***	***	***	***	***	***	***	***	***	***	***	***	***	NA
	H	***	***	***	***	**	***	***	***	***	ns	***	***	***	***	***

(b)

g_bf10m_d_b		LA				RLA				RMA				MA		
		C	M-C	M-H	H	C	M-C	M-H	H	C	M-C	M-H	H	C	M-C	M-H
LA	M-C	***	NA	NA	NA	NA	NA	NA	NA	NA	NA	NA	NA	NA	NA	NA
	M-H	***	***	NA	NA	NA	NA	NA	NA	NA	NA	NA	NA	NA	NA	NA
	H	***	**	***	NA	NA	NA	NA	NA	NA	NA	NA	NA	NA	NA	NA
RLA	C	***	***	***	***	NA	NA	NA	NA	NA	NA	NA	NA	NA	NA	NA
	M-C	***	***	***	***	***	NA	NA	NA	NA	NA	NA	NA	NA	NA	NA
	M-H	***	***	***	***	***	***	NA	NA	NA	NA	NA	NA	NA	NA	NA
	H	ns	***	***	***	***	***	***	NA	NA	NA	NA	NA	NA	NA	NA
RMA	C	***	***	***	***	***	***	***	***	NA	NA	NA	NA	NA	NA	NA
	M-C	***	***	***	***	***	***	***	***	***	NA	NA	NA	NA	NA	NA
	M-H	***	***	***	***	***	***	***	***	***	***	NA	NA	NA	NA	NA
	H	***	***	***	***	***	***	***	***	***	***	***	NA	NA	NA	NA
MA	C	***	***	***	***	***	***	***	***	***	***	***	***	NA	NA	NA
	M-C	***	***	***	***	***	***	***	***	***	***	***	***	ns	NA	NA
	M-H	***	***	***	***	***	***	***	***	***	***	***	***	***	***	NA
	H	***	***	***	***	***	***	***	***	***	ns	***	***	***	***	***

(c)

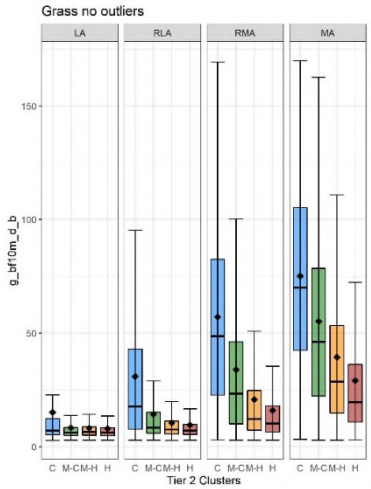

(d)

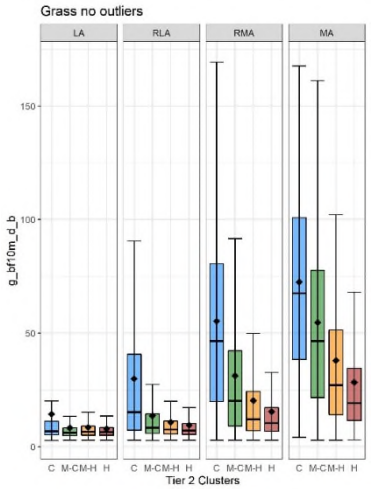

Figure_Apx C-35 Results of the ANOVA (a, b) and boxplots (c, d) for distance to buildings of grass patches located in the neighbourhood of core grass patches in June (a, c) and July (b, d). Boxplots represent elevation values associated with the coldest (C), medium-cold (M-C), medium-hot (M-H) and the hottest (H) Tier 2 clusters within each Tier 1 cluster: LA – Least aggregated, RLA – Relatively less aggregated, RMA – Relatively more aggregated, MA – Most aggregated.

(a)

g_bf10m_d_b		LA				RLA				RMA				MA		
		C	M-C	M-H	H	C	M-C	M-H	H	C	M-C	M-H	H	C	M-C	M-H
LA	M-C	***	NA	NA	NA	NA	NA	NA	NA	NA	NA	NA	NA	NA	NA	NA
	M-H	***	***	NA	NA	NA	NA	NA	NA	NA	NA	NA	NA	NA	NA	NA
	H	***	***	***	NA	NA	NA	NA	NA	NA	NA	NA	NA	NA	NA	NA
RLA	C	***	*	***	***	NA	NA	NA	NA	NA	NA	NA	NA	NA	NA	NA
	M-C	***	***	ns	***	***	NA	NA	NA	NA	NA	NA	NA	NA	NA	NA
	M-H	***	***	***	ns	***	***	NA	NA	NA	NA	NA	NA	NA	NA	NA
	H	***	***	***	***	***	***	***	NA	NA	NA	NA	NA	NA	NA	NA
RMA	C	***	**	***	***	*	***	***	***	NA	NA	NA	NA	NA	NA	NA
	M-C	***	***	***	***	***	***	***	***	***	NA	NA	NA	NA	NA	NA
	M-H	***	***	**	***	***	*	***	***	***	***	NA	NA	NA	NA	NA
	H	***	***	***	***	***	***	***	***	***	***	***	NA	NA	NA	NA
MA	C	ns	***	***	***	***	***	***	***	***	***	***	***	NA	NA	NA
	M-C	***	***	***	***	***	***	***	***	ns	***	***	***	***	NA	NA
	M-H	***	ns	***	***	**	***	***	***	***	***	***	***	***	***	NA
	H	***	***	ns	**	***	ns	***	***	***	***	ns	***	***	***	***

(b)

g_bf10m_d_b		LA				RLA				RMA				MA		
		C	M-C	M-H	H	C	M-C	M-H	H	C	M-C	M-H	H	C	M-C	M-H
LA	M-C	***	NA	NA	NA	NA	NA	NA	NA	NA	NA	NA	NA	NA	NA	NA
	M-H	***	***	NA	NA	NA	NA	NA	NA	NA	NA	NA	NA	NA	NA	NA
	H	***	***	***	NA	NA	NA	NA	NA	NA	NA	NA	NA	NA	NA	NA
RLA	C	***	ns	***	***	NA	NA	NA	NA	NA	NA	NA	NA	NA	NA	NA
	M-C	***	***	***	ns	***	NA	NA	NA	NA	NA	NA	NA	NA	NA	NA
	M-H	***	***	***	ns	***	***	NA	NA	NA	NA	NA	NA	NA	NA	NA
	H	***	***	***	**	***	***	*	NA	NA	NA	NA	NA	NA	NA	NA
RMA	C	***	ns	***	***	ns	***	***	***	NA	NA	NA	NA	NA	NA	NA
	M-C	***	***	***	***	***	***	***	***	***	NA	NA	NA	NA	NA	NA
	M-H	***	***	***	**	***	ns	***	***	***	***	NA	NA	NA	NA	NA
	H	***	***	***	**	***	***	*	ns	***	***	***	NA	NA	NA	NA
MA	C	***	***	***	***	***	***	***	***	***	***	***	***	NA	NA	NA
	M-C	***	***	***	***	***	***	***	***	***	***	***	***	***	NA	NA
	M-H	***	ns	***	***	ns	***	***	***	ns	***	***	***	***	***	NA
	H	***	***	ns	***	***	**	***	***	***	*	*	***	***	***	***

(c)

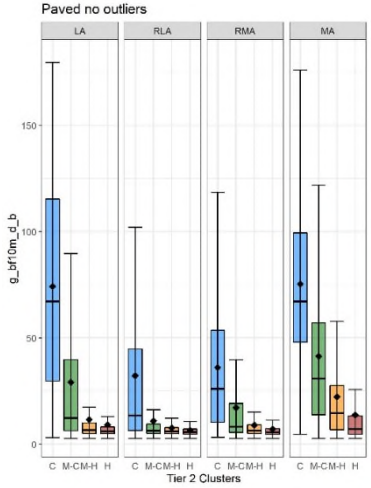

(d)

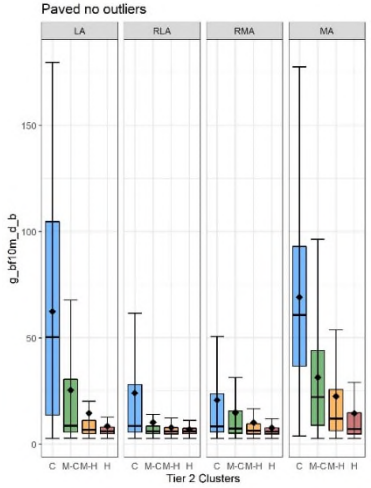

Figure_Apx C-36 Results of the ANOVA (a, b) and boxplots (c, d) for distance to buildings of grass patches located in the neighbourhood of core paved patches in June (a, c) and July (b, d). Boxplots represent elevation values associated with the coldest (C), medium-cold (M-C), medium-hot (M-H) and the hottest (H) Tier 2 clusters within each Tier 1 cluster: LA – Least aggregated, RLA – Relatively less aggregated, RMA – Relatively more aggregated, MA – Most aggregated.

(a)

g_bf10m_d_b		LA				RLA				RMA				MA		
		C	M-C	M-H	H	C	M-C	M-H	H	C	M-C	M-H	H	C	M-C	M-H
LA	M-C	***	NA	NA	NA	NA	NA	NA	NA	NA	NA	NA	NA	NA	NA	NA
	M-H	***	ns	NA	NA	NA	NA	NA	NA	NA	NA	NA	NA	NA	NA	NA
	H	***	***	***	NA	NA	NA	NA	NA	NA	NA	NA	NA	NA	NA	NA
RLA	C	ns	***	***	***	NA	NA	NA	NA	NA	NA	NA	NA	NA	NA	NA
	M-C	***	***	***	***	***	NA	NA	NA	NA	NA	NA	NA	NA	NA	NA
	M-H	***	***	***	***	***	ns	NA	NA	NA	NA	NA	NA	NA	NA	NA
	H	***	**	ns	***	***	***	***	NA	NA	NA	NA	NA	NA	NA	NA
RMA	C	***	***	***	***	***	***	***	***	NA	NA	NA	NA	NA	NA	NA
	M-C	***	***	***	***	***	***	***	***	***	NA	NA	NA	NA	NA	NA
	M-H	***	***	***	***	***	***	***	***	***	***	NA	NA	NA	NA	NA
	H	***	***	***	***	***	***	***	***	***	***	***	NA	NA	NA	NA
MA	C	***	***	***	***	***	***	***	***	***	***	***	***	NA	NA	NA
	M-C	***	***	***	***	***	***	***	***	ns	***	***	***	***	NA	NA
	M-H	***	***	***	***	***	***	***	***	***	***	***	***	***	***	NA
	H	ns	***	***	***	ns	***	***	***	***	ns	***	***	***	***	***

(b)

g_bf10m_d_b		LA				RLA				RMA				MA		
		C	M-C	M-H	H	C	M-C	M-H	H	C	M-C	M-H	H	C	M-C	M-H
LA	M-C	***	NA	NA	NA	NA	NA	NA	NA	NA	NA	NA	NA	NA	NA	NA
	M-H	***	***	NA	NA	NA	NA	NA	NA	NA	NA	NA	NA	NA	NA	NA
	H	***	***	***	NA	NA	NA	NA	NA	NA	NA	NA	NA	NA	NA	NA
RLA	C	**	***	***	***	NA	NA	NA	NA	NA	NA	NA	NA	NA	NA	NA
	M-C	***	**	***	***	***	NA	NA	NA	NA	NA	NA	NA	NA	NA	NA
	M-H	***	***	ns	***	***	***	NA	NA	NA	NA	NA	NA	NA	NA	NA
	H	***	ns	***	***	***	***	***	NA	NA	NA	NA	NA	NA	NA	NA
RMA	C	***	***	***	***	***	***	***	***	NA	NA	NA	NA	NA	NA	NA
	M-C	***	***	***	***	***	***	***	***	***	NA	NA	NA	NA	NA	NA
	M-H	**	***	***	***	ns	***	***	***	***	***	NA	NA	NA	NA	NA
	H	***	***	**	***	***	***	ns	***	***	***	***	NA	NA	NA	NA
MA	C	***	***	***	***	***	***	***	***	***	***	***	***	NA	NA	NA
	M-C	***	***	***	***	***	***	***	***	***	***	***	***	***	NA	NA
	M-H	***	***	***	***	***	***	***	***	ns	***	***	***	***	***	NA
	H	***	***	***	***	***	***	***	***	***	***	***	***	***	***	***

(c)

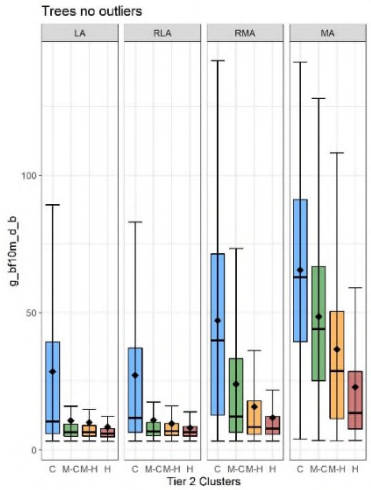

(d)

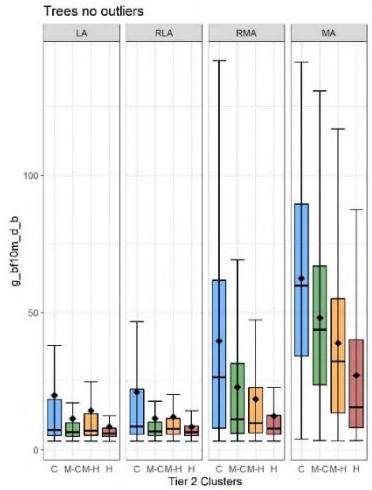

Figure_Apx C-37 Results of the ANOVA (a, b) and boxplots (c, d) for distance to buildings of grass patches located in the neighbourhood of core tree patches in June (a, c) and July (b, d). Boxplots represent elevation values associated with the coldest (C), medium-cold (M-C), medium-hot (M-H) and the hottest (H) Tier 2 clusters within each Tier 1 cluster: LA – Least aggregated, RLA – Relatively less aggregated, RMA – Relatively more aggregated, MA – Most aggregated.

Appendix D Supplementary Materials to Chapter 5

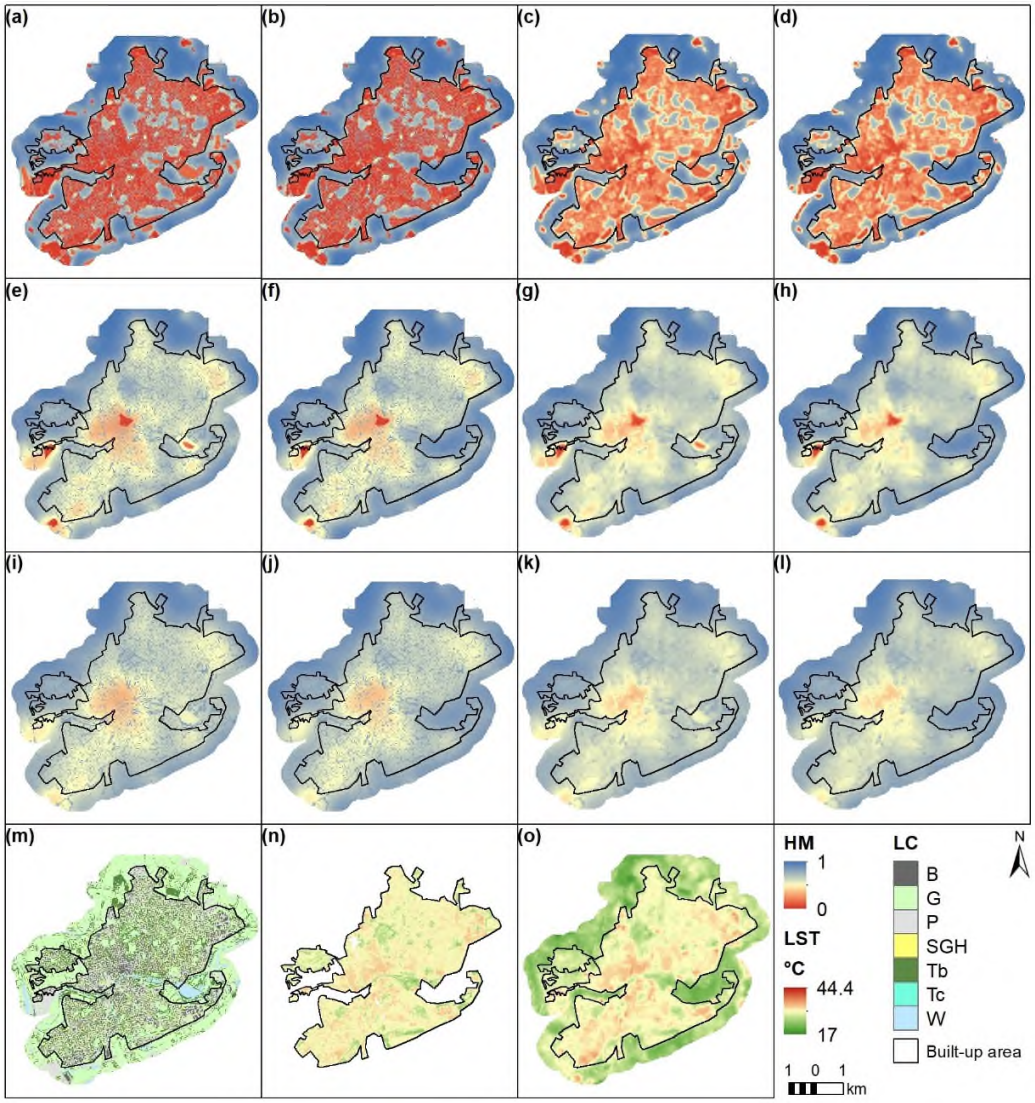

Figure_Apx D-1 Heat mitigation index maps at 2m and 30m resolution for Bedford at various vegetation cooling distance and cooling feature settings. (a) 100m, V, 2m; (b) 100m V&W, 2m; (c) 100m, V, 30m; (d) 100m, V&W, 30m; (d) 200m, V, 2m; (e) 200m V&W, 2m; (f) 200m, V, 30m; (g) 200m, V&W, 30m; (h) 300m, V, 2m; (i) 300m V&W, 2m; (j) 300m, V, 30m; (k) 300m, V&W, 30m. Land cover map is shown in image (m) and land surface temperature in image (n) for 2m and (o) 30m resolution. V – vegetation, V&W – vegetation and water.

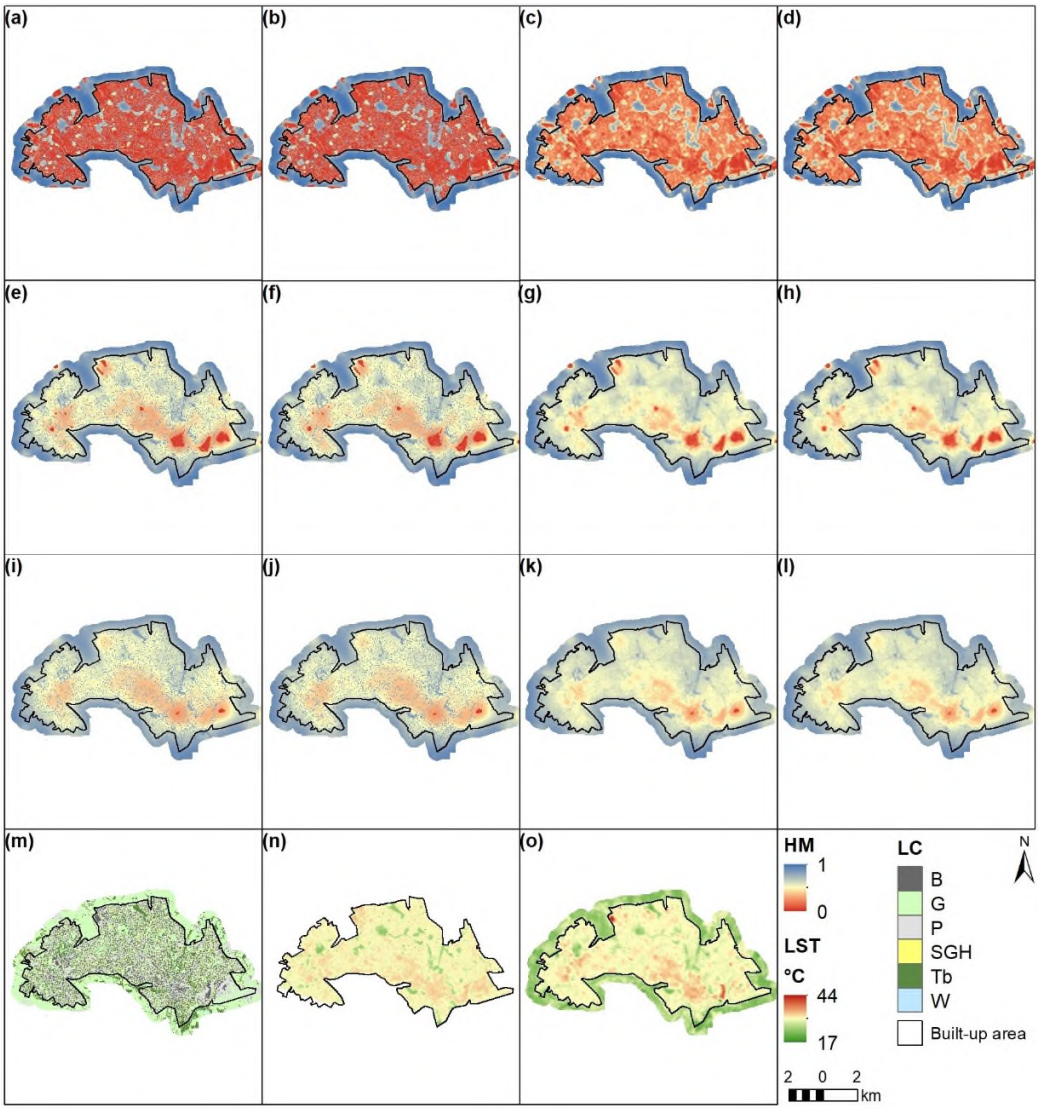

Figure_Apx D-2 Heat mitigation index maps at 2m and 30m resolution for Luton at various vegetation cooling distance and cooling feature settings. (a) 100m, V, 2m; (b) 100m V&W, 2m; (c) 100m, V, 30m; (d) 100m, V&W, 30m; (d) 200m, V, 2m; (e) 200m V&W, 2m; (f) 200m, V, 30m; (g) 200m, V&W, 30m; (h) 300m, V, 2m; (i) 300m V&W, 2m; (j) 300m, V, 30m; (k) 300m, V&W, 30m. Land cover map is shown in image (m) and land surface temperature in image (n) for 2m and (o) 30m resolution. V – vegetation, V&W – vegetation and water.

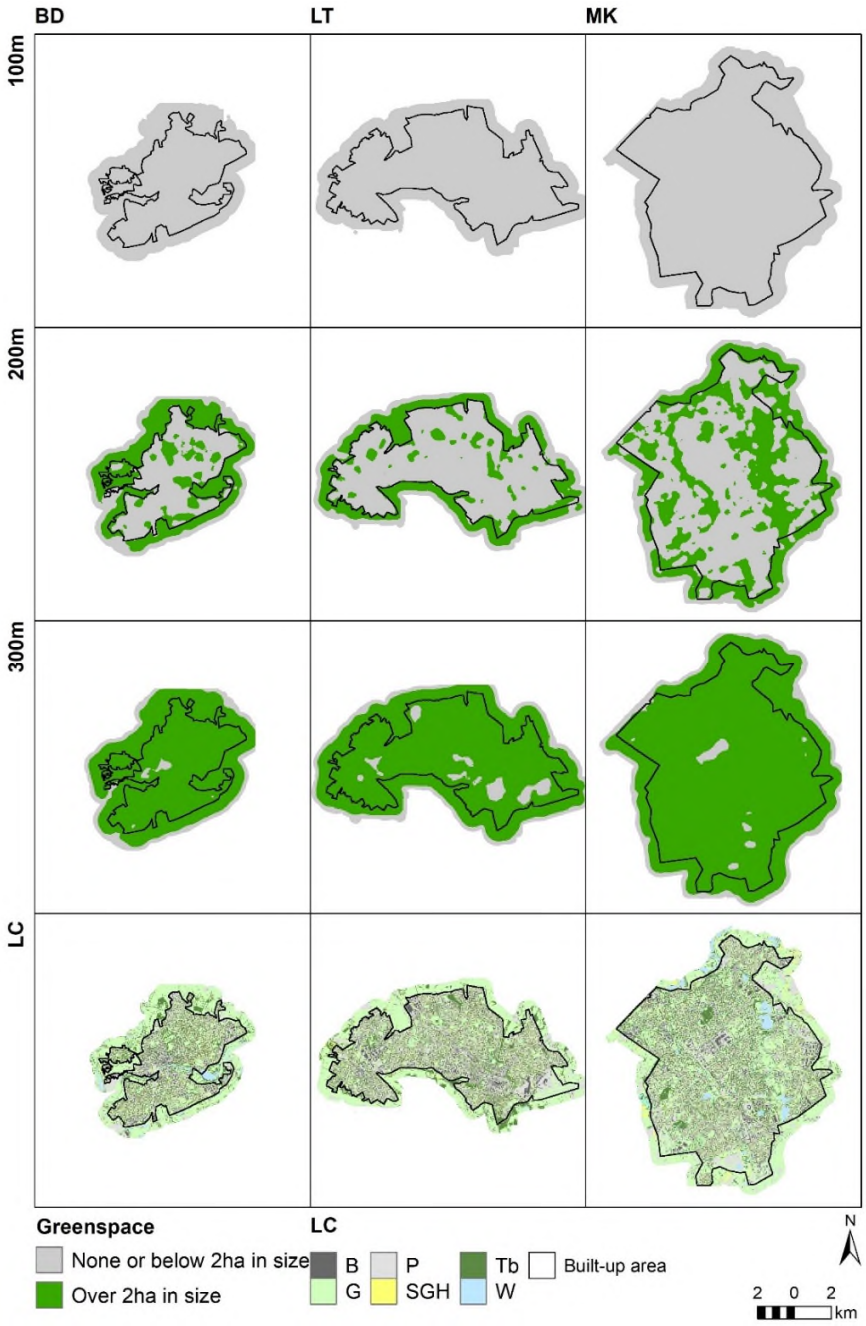

Figure_Apx D-3 Differing definitions of large greenspaces resulting from varied cooling distance setting (100m, 200m 300m) of the InVEST 3.8.7 Urban Cooling model across three towns (BD – Bedford, LT – Luton, MK – Milton Keynes). Land cover (LC) definitions are given in description of Table 1.

Table_Apx D-1 Heat mitigation means and standard deviations (in brackets) estimated for Bedford - BD, Luton - LT and Milton Keynes - MK for Urban Cooling model outputs at two spatial resolutions: 2m and resampled to 30m, assessed for two different sets of cooling features (V – vegetation or W&V – water and vegetation) and at three different cooling distances away from large greenspaces (>2ha in size).

Town	Resolution [m]	Cooling features	LST [°C]	Cooling distance		
				100m	200m	300m
BD	2m	W&V	30.43 (2)	0.37 (0.34)	0.63 (0.14)	0.65 (0.12)
		V		0.36 (0.34)	0.62 (0.15)	0.63 (0.13)
	30m	W&V	28.48 (3.18)	0.56 (0.31)	0.71 (0.14)	0.71 (0.11)
		V		0.52 (0.3)	0.68 (0.14)	0.68 (0.11)
LT	2m	W&V	30.9 (1.83)	0.29 (0.32)	0.55 (0.17)	0.57 (0.15)
		V		0.29 (0.32)	0.55 (0.17)	0.57 (0.15)
	30m	W&V	29.23 (2.81)	0.39 (0.28)	0.6 (0.15)	0.61 (0.12)
		V		0.39 (0.28)	0.6 (0.15)	0.61 (0.12)
MK	2m	W&V	27.83 (1.89)	0.42 (0.35)	0.64 (0.14)	0.65 (0.12)
		V		0.4 (0.35)	0.62 (0.15)	0.63 (0.13)
	30m	W&V	26.98 (2.56)	0.46 (0.26)	0.65 (0.11)	0.66 (0.08)
		V		0.43 (0.25)	0.63 (0.11)	0.64 (0.08)

Table_Apx D-2 Heat mitigation means and standard deviations (in brackets) returned by the InVEST 3.8.7 Urban Cooling models for different types of land cover in all three towns for three different cooling distances of large vegetation patches and at two spatial resolutions – 2m and 30m. Statistics for land surface temperature (LST) are also given. B – buildings, G – grass, P – paved, SGH – short trees/tall grass/hedge, Tb – broadleaf trees, Tc – coniferous trees, W – water. BD – Bedford, LT – Luton, MK – Milton Keynes.

LC	Town	Cooling features	Cooling distance						LST	
			100m		200m		300m			
		Sp. res.	2m	30m	2m	30m	2m	30m	2m	30m
B	BD	V	0.26 (0.18)	0.13 (0.21)	0.58 (0.12)	0.53 (0.13)	0.6 (0.09)	0.56 (0.1)	31.28 (1.94)	31.82 (1.15)
		V&W	0.27 (0.18)	0.13 (0.22)	0.59 (0.12)	0.55 (0.13)	0.62 (0.09)	0.58 (0.1)	31.28 (1.94)	31.82 (1.15)
	LT	V	0.2 (0.12)	0.08 (0.14)	0.5 (0.14)	0.45 (0.15)	0.54 (0.1)	0.49 (0.1)	31.11 (2.21)	31.85 (1.18)
		V&W	0.2 (0.12)	0.08 (0.14)	0.5 (0.14)	0.46 (0.15)	0.54 (0.1)	0.49 (0.1)	31.11 (2.21)	31.85 (1.18)
	MK	V	0.23 (0.14)	0.11 (0.18)	0.56 (0.12)	0.52 (0.12)	0.59 (0.08)	0.55 (0.08)	28.92 (2.25)	29.52 (1.07)
		V&W	0.24 (0.15)	0.11 (0.19)	0.58 (0.12)	0.54 (0.12)	0.6 (0.08)	0.57 (0.09)	28.92 (2.25)	29.52 (1.07)
G	BD	V	0.7 (0.25)	0.47 (0.27)	0.75 (0.12)	0.62 (0.11)	0.73 (0.1)	0.62 (0.1)	27.31 (2.92)	29.42 (1.94)
		V&W	0.73 (0.25)	0.48 (0.28)	0.77 (0.12)	0.63 (0.11)	0.76 (0.1)	0.64 (0.1)	27.31 (2.92)	29.42 (1.94)
	LT	V	0.6 (0.29)	0.4 (0.25)	0.68 (0.14)	0.55 (0.11)	0.67 (0.11)	0.55 (0.1)	27.7 (2.86)	29.87 (2.01)
		V&W	0.6 (0.29)	0.41 (0.26)	0.68 (0.14)	0.56 (0.12)	0.67 (0.11)	0.56 (0.1)	27.7 (2.86)	29.87 (2.01)
	MK	V	0.58 (0.24)	0.5 (0.27)	0.67 (0.09)	0.61 (0.1)	0.66 (0.07)	0.61 (0.09)	26.26 (2.28)	27.02 (1.83)
		V&W	0.6 (0.24)	0.53 (0.28)	0.69 (0.09)	0.64 (0.11)	0.68 (0.07)	0.63 (0.09)	26.26 (2.28)	27.02 (1.83)
P	BD	V	0.3 (0.22)	0.13 (0.23)	0.6 (0.14)	0.55 (0.12)	0.62 (0.1)	0.57 (0.1)	30.28 (2.26)	31.19 (1.38)
		V&W	0.31 (0.23)	0.14 (0.24)	0.62 (0.14)	0.57 (0.12)	0.64 (0.1)	0.6 (0.1)	30.28 (2.26)	31.19 (1.38)
	LT	V	0.23 (0.16)	0.09 (0.18)	0.53 (0.14)	0.48 (0.14)	0.56 (0.1)	0.51 (0.11)	30.25 (2.13)	31.48 (1.25)
		V&W	0.23 (0.16)	0.09 (0.18)	0.53 (0.14)	0.48 (0.14)	0.56 (0.1)	0.51 (0.11)	30.25 (2.13)	31.48 (1.25)
	MK	V	0.30 (0.2)	0.17 (0.27)	0.59 (0.11)	0.55 (0.12)	0.61 (0.08)	0.57 (0.09)	27.81 (2.21)	28.57 (1.5)
		V&W	0.31 (0.21)	0.18 (0.28)	0.61 (0.12)	0.57 (0.13)	0.63 (0.08)	0.59 (0.1)	27.81 (2.21)	28.57 (1.5)
SGH	BD	V	0.44 (0.25)	0.38 (0.28)	0.65 (0.11)	0.61 (0.13)	0.66 (0.09)	0.62 (0.12)	29.44 (2.65)	30.3 (1.69)
		V&W	0.46 (0.27)	0.39 (0.28)	0.67 (0.11)	0.63 (0.12)	0.68 (0.09)	0.64 (0.11)	29.44 (2.65)	30.3 (1.69)
	LT	V	0.33 (0.21)	0.32 (0.25)	0.59 (0.11)	0.55 (0.14)	0.6 (0.09)	0.56 (0.13)	29.68 (2.09)	30.82 (1.53)
		V&W	0.33 (0.21)	0.32 (0.25)	0.59 (0.11)	0.55 (0.14)	0.6 (0.09)	0.56 (0.13)	29.68 (2.09)	30.82 (1.53)
	MK	V	0.40 (0.22)	0.40 (0.29)	0.63 (0.08)	0.61 (0.12)	0.63 (0.07)	0.61 (0.12)	27.3 (2.22)	27.86 (1.64)
		V&W	0.42 (0.23)	0.42 (0.3)	0.65 (0.09)	0.63 (0.12)	0.65 (0.07)	0.63 (0.11)	27.3 (2.22)	27.86 (1.64)

LC	Town	Cooling features	Cooling distance						LST	
			100m		200m		300m			
		Spatial resolution	2m	30m	2m	30m	2m	30m	2m	30m
Tb	BD	V	0.56 (0.26)	0.72 (0.24)	0.70 (0.11)	0.78 (0.1)	0.70 (0.1)	0.78 (0.1)	28.04 (3.23)	29.79 (2.1)
		V&W	0.59 (0.27)	0.73 (0.24)	0.72 (0.12)	0.78 (0.1)	0.72 (0.1)	0.78 (0.09)	28.04 (3.23)	29.79 (2.1)
	LT	V	0.45 (0.25)	0.72 (0.24)	0.64 (0.12)	0.77 (0.12)	0.64 (0.11)	0.77 (0.12)	28.6 (2.77)	30.11 (2.18)
		V&W	0.45 (0.25)	0.72 (0.24)	0.64 (0.12)	0.77 (0.12)	0.64 (0.11)	0.77 (0.12)	28.6 (2.77)	30.11 (2.18)
	MK	V	0.5 (0.22)	0.73 (0.24)	0.67 (0.08)	0.78 (0.1)	0.67 (0.07)	0.78 (0.1)	26.34 (2.5)	26.96 (1.85)
		V&W	0.53 (0.23)	0.73 (0.23)	0.69 (0.09)	0.78 (0.1)	0.69 (0.07)	0.78 (0.09)	26.34 (2.5)	26.96 (1.85)
Tc	BD	V	0.7 (0.21)	0.79 (0.13)	0.75 (0.1)	0.81 (0.06)	0.74 (0.08)	0.81 (0.06)	26.08 (2.84)	28.26 (2.11)
		V&W	0.75 (0.21)	0.8 (0.13)	0.78 (0.09)	0.81 (0.06)	0.77 (0.07)	0.81 (0.06)	26.08 (2.84)	28.26 (2.11)
	MK	V	0.52 (0.21)	0.74 (0.21)	0.67 (0.08)	0.78 (0.1)	0.67 (0.07)	0.78 (0.1)	26.47 (2.3)	26.86 (1.79)
		V&W	0.54 (0.21)	0.75 (0.21)	0.68 (0.08)	0.78 (0.1)	0.69 (0.07)	0.78 (0.09)	26.47 (2.3)	26.86 (1.79)
	BD	V	0.41 (0.26)	0.29 (0.25)	0.63 (0.14)	0.56 (0.13)	0.65 (0.09)	0.56 (0.11)	24.48 (2.28)	24.89 (2.07)
		V&W	0.82 (0.18)	0.65 (0.26)	0.79 (0.1)	0.67 (0.14)	0.76 (0.09)	0.65 (0.13)	24.48 (2.28)	24.89 (2.07)
W	LT	V	0.57 (0.23)	0.51 (0.28)	0.65 (0.1)	0.6 (0.13)	0.63 (0.08)	0.58 (0.12)	27.67 (2.54)	26.8 (2.91)
		V&W	0.57 (0.23)	0.56 (0.28)	0.65 (0.1)	0.61 (0.13)	0.63 (0.08)	0.59 (0.12)	27.67 (2.54)	26.8 (2.91)
	MK	V	0.31 (0.22)	0.25 (0.22)	0.52 (0.17)	0.49 (0.16)	0.58 (0.09)	0.54 (0.09)	22.83 (2.58)	22.74 (2.01)
		V&W	0.79 (0.17)	0.79 (0.19)	0.76 (0.08)	0.75 (0.09)	0.73 (0.06)	0.71 (0.08)	22.83 (2.58)	22.74 (2.01)

Table_Apx D-3 OLS regression statistics between heat mitigation index and land surface temperature at 2m and 30m spatial resolution across Bedford (BD), Luton (LT) and Milton Keynes (MK).

Town	Cooling	Cooling	Sp. Res	Rsq	Adj. Rsq	SE	Intercept	b	SE a	SE b	t value a	t value b	Prob t a	Prob t b	f statistic
BD	100m	V	2m	0.24	0.24	1.75	31.45	-2.87	0.00	0.00	32261	-1450	0.00	0.00	2102379
			30m	0.48	0.48	2.29	32.28	-7.29	0.02	0.03	1652	-228	0.00	0.00	51856
		W&V	2m	0.28	0.28	1.71	31.56	-3.08	0.00	0.00	32931	-1621	0.00	0.00	2628327
			30m	0.63	0.63	1.94	32.97	-8.05	0.02	0.03	1943	-306	0.00	0.00	93892
	200m	V	2m	0.16	0.16	1.84	33.81	-5.48	0.00	0.00	11033	-1134	0.00	0.00	1286748
			30m	0.44	0.44	2.37	38.61	-14.86	0.05	0.07	778	-210	0.00	0.00	43954
		W&V	2m	0.18	0.18	1.81	34.21	-5.99	0.00	0.00	10895	-1235	0.00	0.00	1526390
			30m	0.59	0.59	2.03	40.59	-17.11	0.04	0.06	925	-283	0.00	0.00	80073
	300m	V	2m	0.12	0.12	1.88	33.88	-5.47	0.00	0.01	9410	-979	0.00	0.00	957845
			30m	0.46	0.46	2.34	41.54	-19.11	0.06	0.09	677	-217	0.00	0.00	46941
		W&V	2m	0.14	0.14	1.86	34.39	-6.13	0.00	0.01	9043	-1062	0.00	0.00	1126840
			30m	0.58	0.58	2.05	43.86	-21.71	0.06	0.08	783	-279	0.00	0.00	77795
LT	100m	V	2m	0.24	0.24	1.59	31.70	-2.81	0.00	0.00	53360	-2031	0.00	0.00	4124672
			30m	0.64	0.64	1.84	32.19	-7.86	0.01	0.02	2890	-388	0.00	0.00	150887
		W&V	2m	0.25	0.25	1.58	31.70	-2.83	0.00	0.00	53478	-2053	0.00	0.00	4215599
			30m	0.64	0.64	1.83	32.20	-7.85	0.01	0.02	2904	-391	0.00	0.00	152986
	200m	V	2m	0.19	0.19	1.64	33.42	-4.60	0.00	0.00	21959	-1740	0.00	0.00	3027020
			30m	0.63	0.63	1.87	37.87	-14.66	0.03	0.04	1501	-379	0.00	0.00	143534
		W&V	2m	0.19	0.19	1.64	33.44	-4.63	0.00	0.00	21951	-1754	0.00	0.00	3077919
			30m	0.63	0.63	1.87	37.87	-14.63	0.03	0.04	1502	-379	0.00	0.00	143805
	300m	V	2m	0.14	0.14	1.70	33.47	-4.54	0.00	0.00	17823	-1416	0.00	0.00	2004458
			30m	0.63	0.63	1.85	40.67	-19.06	0.03	0.05	1272	-384	0.00	0.00	147763
		W&V	2m	0.14	0.14	1.70	33.50	-4.58	0.00	0.00	17775	-1428	0.00	0.00	2040157
			30m	0.63	0.63	1.85	40.69	-19.06	0.03	0.05	1273	-385	0.00	0.00	148322
MK	100m	V	2m	0.31	0.31	1.57	29.05	-3.04	0.00	0.00	55879	-3089	0.00	0.00	9544094
			30m	0.30	0.30	2.33	29.25	-5.65	0.01	0.02	2259	-233	0.00	0.00	54064
		W&V	2m	0.33	0.33	1.54	29.12	-3.09	0.00	0.00	56226	-3248	0.00	0.00	10551109
			30m	0.48	0.48	2.01	30.02	-6.80	0.01	0.02	2650	-343	0.00	0.00	117488
	200m	V	2m	0.22	0.22	1.67	31.60	-6.06	0.00	0.00	19956	-2445	0.00	0.00	5975877
			30m	0.22	0.22	2.44	34.09	-11.53	0.04	0.06	871	-193	0.00	0.00	37298
		W&V	2m	0.24	0.24	1.64	31.93	-6.42	0.00	0.00	19713	-2593	0.00	0.00	6724289
			30m	0.44	0.44	2.07	37.18	-15.69	0.03	0.05	1111	-320	0.00	0.00	102082
	300m	V	2m	0.18	0.18	1.71	31.79	-6.28	0.00	0.00	17036	-2162	0.00	0.00	4672386
			30m	0.26	0.26	2.39	37.56	-16.83	0.05	0.08	723	-212	0.00	0.00	44803
		W&V	2m	0.20	0.20	1.69	32.21	-6.76	0.00	0.00	16534	-2286	0.00	0.00	5225048
			30m	0.45	0.45	2.06	40.68	-20.85	0.04	0.06	929	-323	0.00	0.00	104460

Table_Apx D-4 OLS regression statistics between heat mitigation index and land surface temperature at 2m and 30m spatial resolution for individual LC classes in Bedford

LC	Cooling distance	Cooling features	Sp. Res	Rsq	Adj.	SE	Intercept	b	SE a	SE b	t value a	t value	Prob t a	Prob t	f
B	100m	V	2m	0.12	0.12	1.07	32.06	-1.91	0.00	0.00	26475	-389	0.00	0.00	151219
			30m	0.48	0.48	1.39	33.24	-7.58	0.04	0.12	874	-64	0.00	0.00	4144
		W&V	2m	0.14	0.14	1.06	32.08	-1.93	0.00	0.00	26606	-411	0.00	0.00	168792
			30m	0.52	0.52	1.34	33.29	-7.59	0.04	0.11	912	-69	0.00	0.00	4767
	200m	V	2m	0.19	0.19	1.03	33.88	-3.87	0.00	0.01	7896	-495	0.00	0.00	244906
			30m	0.50	0.50	1.37	37.53	-10.94	0.10	0.16	386	-67	0.00	0.00	4443
		W&V	2m	0.18	0.18	1.04	33.92	-3.82	0.00	0.01	7605	-483	0.00	0.00	233084
			30m	0.50	0.50	1.37	37.74	-11.05	0.10	0.17	377	-67	0.00	0.00	4466
	300m	V	2m	0.15	0.15	1.06	34.31	-4.44	0.01	0.01	5914	-436	0.00	0.00	189733
			30m	0.52	0.52	1.35	40.08	-14.71	0.13	0.21	307	-69	0.00	0.00	4736
		W&V	2m	0.14	0.14	1.06	34.31	-4.29	0.01	0.01	5616	-413	0.00	0.00	170585
			30m	0.50	0.50	1.37	40.32	-14.73	0.14	0.22	290	-66	0.00	0.00	4413
G	100m	V	2m	0.26	0.26	1.67	31.10	-3.61	0.00	0.00	12041	-754	0.00	0.00	567788
			30m	0.40	0.40	2.25	32.46	-7.34	0.04	0.06	727	-123	0.00	0.00	15151
		W&V	2m	0.29	0.29	1.64	31.23	-3.75	0.00	0.00	12122	-808	0.00	0.00	653223
			30m	0.49	0.49	2.08	33.23	-8.09	0.04	0.06	776	-147	0.00	0.00	21532
	200m	V	2m	0.11	0.11	1.83	33.07	-5.90	0.01	0.01	3970	-444	0.00	0.00	197356
			30m	0.40	0.40	2.26	38.56	-15.05	0.09	0.12	413	-122	0.00	0.00	14989
		W&V	2m	0.14	0.14	1.80	33.65	-6.67	0.01	0.01	4024	-513	0.00	0.00	262964
			30m	0.50	0.50	2.06	40.54	-17.13	0.09	0.11	453	-150	0.00	0.00	22480
	300m	V	2m	0.06	0.06	1.88	32.51	-4.98	0.01	0.02	3378	-325	0.00	0.00	105521
			30m	0.38	0.38	2.29	39.93	-17.28	0.11	0.15	368	-118	0.00	0.00	13880
		W&V	2m	0.09	0.09	1.86	33.25	-5.99	0.01	0.02	3368	-392	0.00	0.00	153684
			30m	0.48	0.48	2.11	42.43	-20.03	0.11	0.14	397	-143	0.00	0.00	20421
P	100m	V	2m	0.15	0.15	1.27	31.49	-2.32	0.00	0.00	30906	-606	0.00	0.00	366664
			30m	0.36	0.36	1.81	32.08	-6.16	0.03	0.08	1121	-80	0.00	0.00	6430
		W&V	2m	0.17	0.17	1.26	31.52	-2.36	0.00	0.00	31138	-653	0.00	0.00	426111
			30m	0.44	0.44	1.71	32.25	-6.42	0.03	0.07	1201	-94	0.00	0.00	8746
	200m	V	2m	0.18	0.18	1.25	33.90	-4.92	0.00	0.01	8313	-680	0.00	0.00	462553
			30m	0.33	0.33	1.86	35.88	-9.47	0.08	0.13	462	-75	0.00	0.00	5565
		W&V	2m	0.19	0.19	1.25	33.96	-4.88	0.00	0.01	8200	-684	0.00	0.00	467654
			30m	0.40	0.40	1.76	36.64	-10.40	0.08	0.12	487	-87	0.00	0.00	7591
	300m	V	2m	0.16	0.16	1.27	34.35	-5.50	0.01	0.01	6572	-614	0.00	0.00	376892
			30m	0.40	0.40	1.76	39.12	-14.28	0.10	0.16	378	-87	0.00	0.00	7546
		W&V	2m	0.15	0.15	1.27	34.40	-5.40	0.01	0.01	6414	-607	0.00	0.00	369008
			30m	0.48	0.48	1.64	40.29	-15.64	0.10	0.15	402	-102	0.00	0.00	10307
SGH	100m	V	2m	0.12	0.12	1.59	31.11	-2.16	0.00	0.01	8719	-282	0.00	0.00	79595
			30m	0.57	0.57	1.74	32.92	-7.99	0.06	0.12	536	-66	0.00	0.00	4347
		W&V	2m	0.14	0.14	1.57	31.18	-2.28	0.00	0.01	8732	-305	0.00	0.00	92827
			30m	0.68	0.68	1.50	33.19	-8.19	0.05	0.10	633	-84	0.00	0.00	6989
	200m	V	2m	0.09	0.09	1.62	32.74	-3.99	0.01	0.02	3065	-234	0.00	0.00	54721
			30m	0.50	0.50	1.87	40.90	-17.54	0.20	0.31	202	-57	0.00	0.00	3306
		W&V	2m	0.11	0.11	1.60	33.06	-4.42	0.01	0.02	3027	-258	0.00	0.00	66776
			30m	0.64	0.63	1.61	41.97	-18.62	0.17	0.25	248	-75	0.00	0.00	5657
	300m	V	2m	0.07	0.07	1.63	32.73	-3.90	0.01	0.02	2749	-208	0.00	0.00	43235
			30m	0.50	0.50	1.89	43.11	-20.75	0.24	0.37	176	-57	0.00	0.00	3198

LC	Cooling distance	Cooling features	Sp. Res	Rsq	Adj.	SE	Intercept	b	SE a	SE b	t value a	t value	Prob t a	Prob t	f
		W&V	2m	0.09	0.09	1.62	33.16	-4.47	0.01	0.02	2657	-233	0.00	0.00	54117
			30m	0.60	0.60	1.69	44.18	-21.71	0.21	0.31	206	-70	0.00	0.00	4835
Tb	100m	V	2m	0.05	0.05	2.04	31.20	-1.97	0.01	0.01	5835	-280	0.00	0.00	78191
			30m	0.60	0.60	2.04	33.36	-9.49	0.05	0.08	675	-120	0.00	0.00	14352
		W&V	2m	0.06	0.06	2.04	31.27	-2.04	0.01	0.01	5788	-289	0.00	0.00	83520
			30m	0.70	0.70	1.75	33.87	-9.88	0.04	0.07	791	-151	0.00	0.00	22832
	200m	V	2m	0.04	0.04	2.05	33.08	-4.25	0.01	0.02	2553	-257	0.00	0.00	65869
			30m	0.54	0.54	2.18	42.69	-20.88	0.14	0.20	305	-106	0.00	0.00	11307
		W&V	2m	0.05	0.05	2.05	33.31	-4.50	0.01	0.02	2476	-264	0.00	0.00	69602
			30m	0.66	0.66	1.87	44.40	-22.67	0.12	0.16	368	-138	0.00	0.00	18974
	300m	V	2m	0.04	0.04	2.06	33.08	-4.22	0.01	0.02	2407	-242	0.00	0.00	58411
			30m	0.53	0.53	2.21	45.08	-24.35	0.17	0.23	271	-104	0.00	0.00	10746
		W&V	2m	0.04	0.04	2.05	33.42	-4.63	0.01	0.02	2275	-249	0.00	0.00	61990
			30m	0.62	0.62	1.98	46.94	-26.32	0.15	0.21	310	-126	0.00	0.00	15913
Tc	100m	V	2m	0.02	0.02	2.09	30.17	-2.41	0.09	0.12	324	-21	0.00	0.00	435
			30m	0.36	0.35	2.27	31.91	-8.32	0.57	0.78	56	-11	0.00	0.00	113
		W&V	2m	0.03	0.03	2.08	30.55	-2.86	0.10	0.12	317	-24	0.00	0.00	580
			30m	0.51	0.51	1.97	33.46	-9.88	0.52	0.67	64	-15	0.00	0.00	217
	200m	V	2m	0.02	0.02	2.09	31.96	-4.59	0.19	0.24	166	-19	0.00	0.00	370
			30m	0.38	0.38	2.23	39.73	-18.26	1.23	1.63	32	-11	0.00	0.00	126
		W&V	2m	0.02	0.02	2.09	32.54	-5.28	0.21	0.25	158	-21	0.00	0.00	432
			30m	0.59	0.59	1.82	45.06	-24.32	1.12	1.42	40	-17	0.00	0.00	293
	300m	V	2m	0.02	0.02	2.09	31.70	-4.25	0.20	0.25	159	-17	0.00	0.00	301
			30m	0.38	0.37	2.23	42.22	-21.92	1.46	1.96	29	-11	0.00	0.00	124
		W&V	2m	0.02	0.02	2.09	32.38	-5.08	0.22	0.27	149	-19	0.00	0.00	360
			30m	0.55	0.55	1.90	48.22	-28.88	1.41	1.82	34	-16	0.00	0.00	251
W	100m	V	2m	0.07	0.07	1.99	25.53	-2.21	0.01	0.03	2067	-68	0.00	0.00	4596
			30m	0.03	0.03	2.24	23.84	1.50	0.11	0.22	224	7	0.00	0.00	47
		W&V	2m	0.07	0.07	1.99	26.24	-2.06	0.02	0.03	1217	-67	0.00	0.00	4491
			30m	0.48	0.48	1.63	31.69	-8.81	0.19	0.23	166	-39	0.00	0.00	1499
	200m	V	2m	0.17	0.17	1.89	28.61	-6.67	0.03	0.06	832	-111	0.00	0.00	12282
			30m	0.02	0.02	2.25	23.03	2.29	0.26	0.40	90	6	0.00	0.00	33
		W&V	2m	0.06	0.06	2.01	27.24	-3.49	0.04	0.06	684	-60	0.00	0.00	3610
			30m	0.47	0.47	1.65	36.48	-15.14	0.32	0.40	114	-38	0.00	0.00	1422
	300m	V	2m	0.11	0.11	1.94	28.35	-6.15	0.04	0.07	720	-90	0.00	0.00	8024
			30m	0.00	0.00	2.27	25.05	-0.91	0.40	0.61	63	-1	0.00	0.14	2
		W&V	2m	0.05	0.05	2.02	27.16	-3.49	0.04	0.06	645	-55	0.00	0.00	3011
			30m	0.40	0.40	1.75	37.25	-16.78	0.39	0.51	95	-33	0.00	0.00	1084

Table_Apx D-5 OLS regression statistics between heat mitigation index and land surface temperature at 2m and 30m spatial resolution for individual LC classes in Luton

LC	Cooling distance	Cooling features	Sp. Res	Rsq	Adj. Rsq	SE	Intercept a	b	SE a	SE b	t value a	t value b	Prob t a	Prob t b	f statistic
B	100m	V	2m	0.08	0.08	1.14	32.04	-2.32	0.00	0.01	34986	-412	0.00	0.00	169706
			30m	0.32	0.32	1.82	33.26	-10.53	0.04	0.16	881	-66	0.00	0.00	4344
		W&V	2m	0.08	0.08	1.14	32.04	-2.33	0.00	0.01	35031	-417	0.00	0.00	174085
			30m	0.32	0.32	1.82	33.26	-10.48	0.04	0.16	883	-66	0.00	0.00	4344
	200m	V	2m	0.34	0.34	0.96	33.99	-4.70	0.00	0.00	15528	-1024	0.00	0.00	1048442
			30m	0.42	0.42	1.68	36.05	-9.89	0.06	0.12	576	-82	0.00	0.00	6767
		W&V	2m	0.34	0.34	0.96	33.99	-4.70	0.00	0.00	15506	-1024	0.00	0.00	1049101
			30m	0.42	0.42	1.68	36.06	-9.88	0.06	0.12	575	-82	0.00	0.00	6755
	300m	V	2m	0.22	0.22	1.04	34.48	-5.35	0.00	0.01	9897	-771	0.00	0.00	594931
			30m	0.35	0.35	1.79	37.97	-12.85	0.10	0.18	381	-70	0.00	0.00	4918
		W&V	2m	0.23	0.23	1.04	34.50	-5.39	0.00	0.01	9851	-774	0.00	0.00	598881
			30m	0.35	0.35	1.78	38.02	-12.91	0.10	0.18	380	-70	0.00	0.00	4939
G	100m	V	2m	0.32	0.32	1.66	31.67	-4.46	0.00	0.00	16670	-1120	0.00	0.00	1254211
			30m	0.59	0.59	1.84	32.20	-7.54	0.03	0.04	1159	-180	0.00	0.00	32393
		W&V	2m	0.32	0.32	1.65	31.69	-4.49	0.00	0.00	16776	-1139	0.00	0.00	1298204
			30m	0.59	0.59	1.84	32.21	-7.54	0.03	0.04	1157	-180	0.00	0.00	32385
	200m	V	2m	0.09	0.09	1.92	32.74	-5.19	0.01	0.01	5692	-510	0.00	0.00	259892
			30m	0.58	0.58	1.85	38.36	-15.59	0.06	0.09	625	-177	0.00	0.00	31416
		W&V	2m	0.09	0.09	1.91	32.83	-5.33	0.01	0.01	5729	-528	0.00	0.00	278525
			30m	0.58	0.58	1.85	38.40	-15.63	0.06	0.09	624	-177	0.00	0.00	31505
	300m	V	2m	0.03	0.03	1.98	31.64	-3.21	0.01	0.01	4793	-274	0.00	0.00	74937
			30m	0.54	0.54	1.94	39.95	-18.37	0.08	0.11	525	-163	0.00	0.00	26642
		W&V	2m	0.03	0.03	1.98	31.74	-3.37	0.01	0.01	4799	-288	0.00	0.00	82925
			30m	0.54	0.54	1.94	40.02	-18.44	0.08	0.11	524	-163	0.00	0.00	26723
P	100m	V	2m	0.13	0.13	1.17	31.69	-2.47	0.00	0.00	53122	-818	0.00	0.00	669911
			30m	0.29	0.29	1.79	31.93	-7.27	0.02	0.07	1518	-97	0.00	0.00	9423
		W&V	2m	0.13	0.13	1.16	31.70	-2.49	0.00	0.00	53241	-835	0.00	0.00	696582
			30m	0.29	0.29	1.79	31.93	-7.24	0.02	0.07	1522	-97	0.00	0.00	9463
	200m	V	2m	0.25	0.25	1.08	33.57	-4.35	0.00	0.00	19140	-1239	0.00	0.00	1534545
			30m	0.36	0.36	1.70	35.15	-9.19	0.04	0.08	788	-113	0.00	0.00	12876
		W&V	2m	0.25	0.25	1.08	33.58	-4.37	0.00	0.00	19150	-1245	0.00	0.00	1550847
			30m	0.36	0.36	1.70	35.16	-9.18	0.04	0.08	788	-114	0.00	0.00	12909
	300m	V	2m	0.19	0.19	1.12	34.06	-5.08	0.00	0.00	13478	-1042	0.00	0.00	1085690
			30m	0.42	0.42	1.63	37.71	-13.34	0.06	0.10	633	-127	0.00	0.00	16217
		W&V	2m	0.19	0.19	1.12	34.09	-5.11	0.00	0.00	13467	-1050	0.00	0.00	1102326
			30m	0.42	0.42	1.63	37.74	-13.37	0.06	0.10	633	-128	0.00	0.00	16297
SGH	100m	V	2m	0.12	0.12	1.44	31.48	-2.09	0.00	0.01	13349	-359	0.00	0.00	129224
			30m	0.64	0.64	1.26	32.31	-7.89	0.03	0.09	960	-92	0.00	0.00	8539
		W&V	2m	0.12	0.12	1.44	31.49	-2.11	0.00	0.01	13371	-365	0.00	0.00	133014
			30m	0.64	0.64	1.26	32.30	-7.86	0.03	0.09	960	-92	0.00	0.00	8522
	200m	V	2m	0.08	0.08	1.47	32.52	-3.12	0.01	0.01	5355	-290	0.00	0.00	84011
			30m	0.61	0.61	1.30	38.64	-15.27	0.10	0.17	373	-88	0.00	0.00	7720
		W&V	2m	0.08	0.08	1.47	32.55	-3.16	0.01	0.01	5350	-293	0.00	0.00	86117
			30m	0.61	0.61	1.30	38.65	-15.27	0.10	0.17	373	-88	0.00	0.00	7734
	300m	V	2m	0.05	0.05	1.50	32.27	-2.61	0.01	0.01	4815	-223	0.00	0.00	49790
			30m	0.57	0.57	1.37	40.06	-17.46	0.13	0.22	308	-81	0.00	0.00	6505

LC	Cooling distance	Cooling features	Sp. Res	Rsq	Adj. Rsq	SE	Intercept a	b	SE a	SE b	t value a	t value b	Prob t a	Prob t b	f statistic
		W&V	2m	0.05	0.05	1.50	32.30	-2.65	0.01	0.01	4799	-226	0.00	0.00	51156
			30m	0.57	0.57	1.37	40.09	-17.49	0.13	0.22	308	-81	0.00	0.00	6525
Tb	100m	V	2m	0.04	0.04	2.14	31.35	-1.72	0.00	0.01	7118	-297	0.00	0.00	88305
			30m	0.72	0.72	1.46	32.81	-9.30	0.03	0.05	1238	-182	0.00	0.00	33205
		W&V	2m	0.04	0.04	2.14	31.37	-1.74	0.00	0.01	7116	-300	0.00	0.00	90238
			30m	0.73	0.73	1.45	32.81	-9.27	0.03	0.05	1239	-182	0.00	0.00	33255
	200m	V	2m	0.03	0.03	2.15	32.51	-3.10	0.01	0.01	3653	-272	0.00	0.00	74166
			30m	0.71	0.71	1.50	40.83	-19.21	0.07	0.11	573	-175	0.00	0.00	30580
		W&V	2m	0.03	0.03	2.15	32.53	-3.12	0.01	0.01	3642	-274	0.00	0.00	74842
			30m	0.71	0.71	1.50	40.86	-19.22	0.07	0.11	573	-175	0.00	0.00	30637
	300m	V	2m	0.03	0.03	2.15	32.45	-3.02	0.01	0.01	3458	-252	0.00	0.00	63457
			30m	0.69	0.69	1.55	42.58	-21.88	0.08	0.13	502	-167	0.00	0.00	27952
		W&V	2m	0.03	0.03	2.15	32.47	-3.04	0.01	0.01	3444	-253	0.00	0.00	63950
			30m	0.69	0.69	1.54	42.64	-21.94	0.08	0.13	502	-168	0.00	0.00	28077
Tc	100m	V	2m												
			30m												
		W&V	2m												
			30m												
	200m	V	2m												
			30m												
		W&V	2m												
			30m												
	300m	V	2m												
			30m												
		W&V	2m												
			30m												
W	100m	V	2m	0.15	0.15	2.68	28.82	-4.00	0.05	0.08	627	-50	0.00	0.00	2542
			30m	0.49	0.49	1.82	32.03	-8.32	0.53	0.94	60	-9	0.00	0.00	78
		W&V	2m	0.25	0.25	2.52	29.70	-5.22	0.05	0.08	634	-69	0.00	0.00	4806
			30m	0.56	0.55	1.71	32.42	-8.38	0.51	0.84	64	-10	0.00	0.00	100
	200m	V	2m	0.04	0.04	2.86	29.36	-4.26	0.11	0.18	259	-23	0.00	0.00	535
			30m	0.61	0.61	1.59	40.91	-20.66	1.19	1.83	34	-11	0.00	0.00	127
		W&V	2m	0.05	0.05	2.83	30.00	-5.22	0.11	0.18	261	-28	0.00	0.00	810
			30m	0.64	0.63	1.54	41.12	-20.69	1.15	1.75	36	-12	0.00	0.00	140
	300m	V	2m	0.00	0.00	2.91	27.04	-0.41	0.12	0.20	228	-2	0.00	0.04	4
			30m	0.60	0.59	1.63	44.01	-26.08	1.52	2.40	29	-11	0.00	0.00	118
		W&V	2m	0.00	0.00	2.91	27.39	-1.00	0.12	0.20	225	-5	0.00	0.00	24
			30m	0.62	0.61	1.58	44.40	-26.46	1.48	2.33	30	-11	0.00	0.00	129

Table_Apx D-6 OLS regression statistics between heat mitigation index and land surface temperature at 2m and 30m spatial resolution for individual LC classes in Milton Keynes.

LC	Cooling	Cooling	Sp. Res	Rsq	Adj. Rsq	SE	Intercept	b	SE a	SE b	t value a	t value b	Prob t a	Prob t b	f
B	100m	V	2m	0.08	0.08	1.03	29.70	-1.65	0.00	0.00	38155	-443	0.00	0.00	195954
			30m	0.28	0.28	1.92	30.89	-8.48	0.04	0.13	862	-64	0.00	0.00	4100
		W&V	2m	0.09	0.09	1.02	29.72	-1.71	0.00	0.00	38472	-490	0.00	0.00	239828
			30m	0.29	0.29	1.90	30.86	-8.18	0.03	0.12	889	-66	0.00	0.00	4331
	200m	V	2m	0.17	0.17	0.98	31.49	-3.77	0.00	0.01	10931	-701	0.00	0.00	491411
			30m	0.27	0.27	1.92	34.66	-10.18	0.09	0.16	377	-64	0.00	0.00	4052
		W&V	2m	0.16	0.16	0.98	31.40	-3.50	0.00	0.01	10946	-672	0.00	0.00	452023
			30m	0.27	0.27	1.92	34.58	-9.81	0.09	0.16	378	-63	0.00	0.00	3983
	300m	V	2m	0.14	0.14	1.00	32.10	-4.71	0.00	0.01	7505	-610	0.00	0.00	372047
			30m	0.26	0.26	1.94	37.21	-14.12	0.14	0.23	270	-61	0.00	0.00	3676
		W&V	2m	0.12	0.12	1.01	31.85	-4.10	0.00	0.01	7565	-559	0.00	0.00	312291
			30m	0.24	0.24	1.97	36.73	-12.94	0.14	0.22	269	-58	0.00	0.00	3325
G	100m	V	2m	0.24	0.24	1.60	28.66	-3.26	0.00	0.00	20027	-1304	0.00	0.00	1700712
			30m	0.35	0.35	1.84	29.53	-5.62	0.03	0.04	1108	-132	0.00	0.00	17540
		W&V	2m	0.27	0.27	1.56	28.81	-3.37	0.00	0.00	20149	-1418	0.00	0.00	2012127
			30m	0.43	0.43	1.73	29.93	-6.08	0.03	0.04	1173	-155	0.00	0.00	24045
	200m	V	2m	0.14	0.14	1.69	31.13	-6.70	0.00	0.01	7067	-946	0.00	0.00	894403
			30m	0.32	0.32	1.88	35.87	-14.28	0.08	0.12	456	-123	0.00	0.00	15147
		W&V	2m	0.17	0.17	1.66	31.51	-7.03	0.00	0.01	7408	-1071	0.00	0.00	1146189
			30m	0.41	0.41	1.75	37.26	-15.87	0.07	0.10	508	-151	0.00	0.00	22890
	300m	V	2m	0.09	0.09	1.74	30.91	-6.41	0.01	0.01	5911	-752	0.00	0.00	564823
			30m	0.29	0.29	1.92	37.75	-17.35	0.10	0.15	377	-115	0.00	0.00	13321
		W&V	2m	0.12	0.12	1.72	31.34	-6.81	0.01	0.01	6169	-859	0.00	0.00	738367
			30m	0.37	0.37	1.81	39.09	-18.77	0.09	0.14	418	-138	0.00	0.00	19047
P	100m	V	2m	0.17	0.17	1.37	28.96	-2.33	0.00	0.00	46316	-1170	0.00	0.00	1369686
			30m	0.27	0.27	1.89	29.54	-5.78	0.02	0.05	1558	-109	0.00	0.00	11884
		W&V	2m	0.19	0.19	1.35	29.00	-2.35	0.00	0.00	46613	-1260	0.00	0.00	1586887
			30m	0.31	0.31	1.84	29.62	-5.85	0.02	0.05	1625	-119	0.00	0.00	14267
	200m	V	2m	0.16	0.16	1.37	31.22	-4.84	0.00	0.00	12878	-1121	0.00	0.00	1256639
			30m	0.24	0.24	1.93	33.40	-9.43	0.06	0.09	590	-100	0.00	0.00	10086
		W&V	2m	0.17	0.17	1.37	31.32	-4.86	0.00	0.00	12961	-1166	0.00	0.00	1358965
			30m	0.28	0.28	1.87	33.90	-10.01	0.06	0.09	614	-112	0.00	0.00	12568
	300m	V	2m	0.13	0.13	1.40	31.82	-5.74	0.00	0.01	9690	-1003	0.00	0.00	1006163
			30m	0.30	0.30	1.85	36.94	-14.96	0.08	0.13	468	-117	0.00	0.00	13603
		W&V	2m	0.14	0.14	1.39	31.85	-5.59	0.00	0.01	9832	-1025	0.00	0.00	1051176
			30m	0.33	0.33	1.81	37.21	-14.98	0.08	0.12	493	-125	0.00	0.00	15736
SGH	100m	V	2m	0.13	0.13	1.53	28.69	-2.07	0.00	0.00	13569	-484	0.00	0.00	233993
			30m	0.41	0.41	1.70	29.94	-6.54	0.04	0.09	714	-72	0.00	0.00	5119
		W&V	2m	0.16	0.16	1.50	28.78	-2.21	0.00	0.00	13661	-537	0.00	0.00	288347
			30m	0.47	0.47	1.62	30.08	-6.62	0.04	0.08	763	-80	0.00	0.00	6457
	200m	V	2m	0.07	0.07	1.58	30.01	-3.52	0.01	0.01	4674	-342	0.00	0.00	116691
			30m	0.40	0.40	1.72	38.30	-17.39	0.16	0.25	239	-69	0.00	0.00	4786
		W&V	2m	0.09	0.09	1.56	30.40	-4.05	0.01	0.01	4651	-396	0.00	0.00	156857
			30m	0.45	0.45	1.64	38.61	-17.48	0.15	0.23	263	-78	0.00	0.00	6015
	300m	V	2m	0.05	0.05	1.60	29.75	-3.08	0.01	0.01	4239	-274	0.00	0.00	75161
			30m	0.37	0.37	1.76	40.19	-20.30	0.20	0.31	203	-65	0.00	0.00	4273

LC	Cooling	Cooling	Sp. Res	Rsq	Adj. Rsq	SE	Intercept	b	SE a	SE b	t value a	t value b	Prob t a	Prob t b	f
		W&V	2m	0.06	0.06	1.59	30.16	-3.63	0.01	0.01	4130	-320	0.00	0.00	102372
			30m	0.41	0.41	1.71	40.29	-19.92	0.18	0.28	219	-71	0.00	0.00	5039
Tb	100m	V	2m	0.08	0.08	1.77	28.58	-2.24	0.00	0.00	10635	-636	0.00	0.00	404612
			30m	0.51	0.51	1.75	30.43	-8.11	0.03	0.05	1011	-148	0.00	0.00	21988
		W&V	2m	0.09	0.09	1.76	28.72	-2.40	0.00	0.00	10526	-677	0.00	0.00	458678
			30m	0.57	0.57	1.63	30.65	-8.21	0.03	0.05	1096	-168	0.00	0.00	28333
	200m	V	2m	0.06	0.06	1.79	30.37	-4.39	0.01	0.01	4782	-542	0.00	0.00	293463
			30m	0.48	0.48	1.81	40.30	-20.85	0.10	0.15	398	-139	0.00	0.00	19288
		W&V	2m	0.07	0.07	1.78	30.80	-4.93	0.01	0.01	4577	-576	0.00	0.00	331797
			30m	0.55	0.55	1.67	41.14	-21.60	0.09	0.13	446	-162	0.00	0.00	26102
	300m	V	2m	0.05	0.05	1.80	30.31	-4.31	0.01	0.01	4561	-509	0.00	0.00	258852
			30m	0.48	0.48	1.80	42.56	-24.19	0.12	0.17	363	-139	0.00	0.00	19408
		W&V	2m	0.06	0.06	1.79	30.76	-4.87	0.01	0.01	4293	-535	0.00	0.00	285733
			30m	0.53	0.53	1.71	43.32	-24.70	0.11	0.16	394	-155	0.00	0.00	24078
Tc	100m	V	2m	0.05	0.05	1.74	28.29	-1.93	0.01	0.01	3982	-209	0.00	0.00	43674
			30m	0.51	0.50	1.62	30.61	-7.90	0.07	0.13	424	-62	0.00	0.00	3796
		W&V	2m	0.06	0.06	1.73	28.44	-2.12	0.01	0.01	3900	-225	0.00	0.00	50697
			30m	0.58	0.58	1.49	30.89	-8.13	0.07	0.11	464	-71	0.00	0.00	5085
	200m	V	2m	0.03	0.03	1.76	29.28	-3.11	0.02	0.02	1929	-161	0.00	0.00	25901
			30m	0.48	0.48	1.66	39.85	-20.04	0.23	0.34	172	-58	0.00	0.00	3389
		W&V	2m	0.04	0.04	1.75	29.65	-3.57	0.02	0.02	1821	-173	0.00	0.00	29939
			30m	0.55	0.55	1.55	40.73	-20.87	0.21	0.31	190	-67	0.00	0.00	4485
	300m	V	2m	0.03	0.03	1.76	29.14	-2.93	0.02	0.02	1865	-147	0.00	0.00	21736
			30m	0.46	0.46	1.69	41.37	-22.29	0.27	0.40	155	-56	0.00	0.00	3146
		W&V	2m	0.03	0.03	1.76	29.50	-3.37	0.02	0.02	1731	-156	0.00	0.00	24348
			30m	0.50	0.50	1.63	42.07	-22.77	0.26	0.37	163	-61	0.00	0.00	3709
W	100m	V	2m	0.05	0.05	1.96	23.24	-2.00	0.00	0.01	6055	-176	0.00	0.00	30972
			30m	0.12	0.12	2.40	21.52	4.12	0.08	0.21	266	20	0.00	0.00	385
		W&V	2m	0.04	0.04	1.97	24.39	-2.09	0.01	0.01	2212	-154	0.00	0.00	23722
			30m	0.61	0.61	1.59	32.01	-11.66	0.14	0.18	224	-66	0.00	0.00	4320
	200m	V	2m	0.09	0.09	1.92	24.48	-3.59	0.01	0.02	3150	-237	0.00	0.00	56223
			30m	0.23	0.23	2.25	19.00	7.28	0.14	0.26	135	29	0.00	0.00	815
		W&V	2m	0.00	0.00	2.00	23.83	-1.46	0.02	0.03	1127	-52	0.00	0.00	2726
			30m	0.56	0.56	1.71	41.70	-24.76	0.32	0.42	128	-58	0.00	0.00	3410
	300m	V	2m	0.02	0.02	1.98	24.70	-3.61	0.02	0.03	1504	-121	0.00	0.00	14670
			30m	0.24	0.24	2.23	15.12	13.33	0.27	0.46	57	29	0.00	0.00	857
		W&V	2m	0.00	0.00	2.01	23.10	-0.51	0.02	0.03	978	-15	0.00	0.00	236
			30m	0.39	0.39	2.01	41.37	-25.37	0.45	0.61	92	-41	0.00	0.00	1718

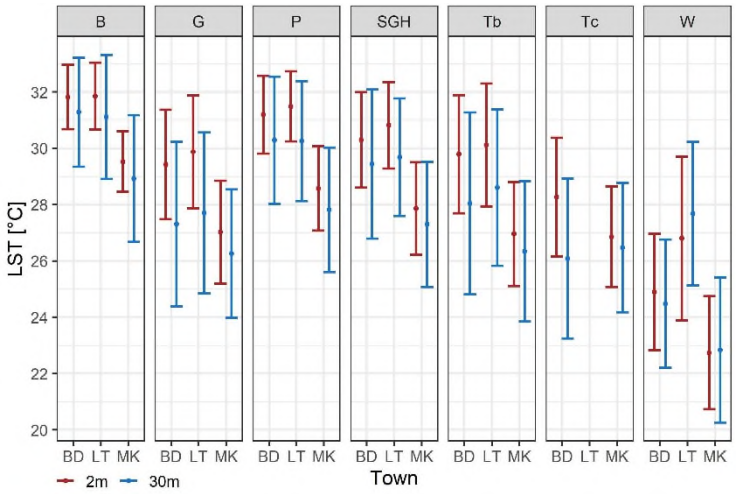

Figure_Apx D-4 Means (points) and standard deviations (whiskers) of land surface temperature in each LC type across Bedford - BD, Luton - LT and Milton Keynes - MK and at two spatial resolutions: 2m and 30m. B – buildings, G – grass, P – paved, SGH – short trees/tall grass/hedge, Tb – broadleaf trees, Tc – coniferous trees, W – water